Thermodynamic Investigations of Metalloproteins:

Metal as Probe and Protein as Probe

by

Claire Jarvis Parker Siburt

Department of Chemistry
Duke University

Date:_____

Approved:

_____
Dr. Alvin L. Crumbliss, Supervisor

_____
Dr. Richard A. Palmer

_____
Dr. Michael C. Fitzgerald

_____
Dr. David C. Richardson

Dissertation submitted in partial fulfillment of
the requirements for the degree of
Doctor of Philosophy
in the
Department of Chemistry
in the Graduate School
of Duke University

2010

ABSTRACT

Thermodynamic Investigations of Metalloproteins:

Metal as Probe and Protein as Probe

by

Claire Jarvis Parker Siburt

Department of Chemistry
Duke University

Date:_____

Approved:

_____
Dr. Alvin L. Crumbliss, Supervisor

_____
Dr. Richard A. Palmer

_____
Dr. Michael C. Fitzgerald

_____
Dr. David C. Richardson

An abstract of a dissertation submitted in partial fulfillment of
the requirements for the degree of
Doctor of Philosophy
in the
Department of Chemistry
in the Graduate School
of Duke University

2010

Abstract

In this dissertation several metalloproteins, both metal transport proteins and the classic metalloprotein hemoglobin, are investigated using a variety of biophysical and electrochemical techniques. In each case, thermodynamic measurements provide insight into the role and mode of action of the metalloprotein under investigation. In Chapters 2 and 3, we focus on the thermodynamic properties of the metal while bound by the protein. In Chapter 4, we focus on the thermodynamic properties of the protein with and without the metal. In Chapter 5, we utilize both the metal and the protein as our probe.

In Chapter 2, we probe the thermodynamic properties of the heme-bound iron to elucidate the structure-function relationships underlying two important physiological responses of hemoglobin (Hb): the Root Effect of hemoglobin from certain fish and the different nitrite reactivities of hemoglobins from clams. Hemoglobins of some fish exhibit significantly lowered oxygen affinity at low pH, allowing for proton-mediated release of O_2. This phenomenon, known as the Root Effect, serves as a proton-driven pump delivering O_2 to the swim bladders and eyes of the fish. The clam, *L. pectinata*, expresses functionally distinct Hb I that transports H_2S and Hb II that transports O_2. These two hemoglobins differ widely in their reactivity with nitrite, a reactant of great importance to the study of vasodilation in humans. The structural basis of the extreme pH-sensitivity of the Root Effect Hbs and the extreme reactivities of the *Lucina* Hbs with

nitrite are debated. Focusing on the metal as the probe, we investigate the reduction potentials of these Hbs using spectroelectrochemistry and compare our findings with oxygen binding studies performed by our collaborators. In both cases, our data strongly suggest that steric hindrance is the determining factor governing the respective physiological response of each hemoglobin.

In Chapter 3, we again use the metal as the probe to determine the reduction potential of titanium bound by transferrin (Tf). Tf is the human iron transport protein that can also bind titanium. To address the possible mechanisms of titanium transport through the hypothesized redox-mediated Fe_2-Tf transport pathway, a modified spectroelectrochemistry (SEC) method was developed to measure the electrochemical properties of metalloproteins with very negative potentials. However, the reduction potential of Ti_2-Tf is far too negative to access with our system. As an alternative approach, the redox properties of several model titanium and iron compounds were characterized in order to develop a linear free energy relationship (LFER) allowing us to estimate the reduction potential of Ti_2-Tf to be ca. -900 mV vs. NHE. Our results indicate that the reduction potential of Ti_2-Tf is too low to be reduced by biological reducing agents and suggest that transferrin-mediated titanium transport follows a different mechanism than iron transport.

In Chapter 4, our focus shifts to the thermodynamic properties of the protein. Some pathogenic Gram-negative bacteria such as *N. gonorrhoeae* steal iron from their

human host by expressing a receptor (TbpA/TbpB), which binds the human iron transport protein transferrin (Tf). Once iron crosses the outer membrane, ferric binding protein (FbpA) transports it across the periplasm to the cytosol. Focusing on the protein, we investigated the protein-protein interactions involved in this transport process and the roles that TbpA and TbpB play with the use of an H/D exchange and mass spectrometry based method termed SUPREX. We report herein the first direct measurement of periplasmic FbpA binding to the outer membrane protein TbpA and we demonstrate that both TbpA and TbpB individually can deferrate Tf without energy supplied from TonB, resulting in sequestration by apo-FbpA.

In Chapter 5 we extend our investigation of the *N. gonorrhoeae* iron uptake system by using the metal as the probe in one case and the protein as the probe in another case. TbpA, the β-barrel receptor protein that is required for utilization of Fe_2-Tf as an iron source, has a plug domain which we hypothesize binds iron and interacts with FbpA on the periplasmic side of the outer membrane. Utilizing SUPREX to monitor the thermodynamic properties of protein folding, we investigate 1) the possible interactions between the TbpA-plug and FbpA and 2) the ability of the TbpA-plug to bind iron.

Focusing on the metal as the probe, we designed an experimental apparatus to investigate the possible thermodynamic effects of the TbpA/TbpB receptor on the release of iron from Tf. We report the use of a competitive iron chelator and equilibrium

dialysis allows for the spectroscopic monitoring of iron release from Tf in the absence of FbpA, but in the presence of opaque bacterial membrane preparations containing the receptor.

Dedication

To Michael, the love of my life and my best friend,

and

To Mom and Dad…

Thank you

Contents

List of Tables

List of Figures

List of Symbols and Commonly Used Abbreviations

(g)	gas
(s)	solid
A	absorbance
A_m	absorbance of the mediator
A_{ox}	absorbance of the oxidize species
A_p	absorbance of the protein
apo	without metal present
A_{red}	absorbance of the reduced species
Bis-Tris	2-(Bis-2(hydroxyethyl)imino)-2-(hydroxymethyl)-1,3-propanediol
CD	circular dichroism
CDTA	1,2-cyclohexylenedinitrilotetraacetic acid
CIT	citrate
CV	cyclic voltammetry
D	diffusion coefficient
D_{ano}	diffusion coefficient calculate from the anodic peak data
D_{cat}	diffusion coefficient calculate from the cathodic peak data
ΔA	change in the absorbance
$\Delta\Delta G$	change in the Gibss free energy
ΔE_p	peak to peak separation

ΔG	Gibbs free energy
deoxy	deoxygenated sample
DI H_2O	deionized water
DMT1	divalent metal transporter 1
dSEC	discontinuous spectroelectrochemistry
DTPA	diethylenetriaminepentaacetic acid
$E_{1/2}$	redox potential
E_{app}	applied potential
EDTA	ethylenediaminetetraacetic acid
eq	equilibrium
F	Faraday's constant
FbpA	ferric binding protein A
FepA	ferric enterobactin receptor
FhuA	ferrichrome receptor
GdmCl	guandinium chloride
H/D	hydrogen and deuterium
Hb	hemoglobin
HbA_o	adult human hemoglobin
HBED	N,N'-di(2-hydroxybenzyl)-ethylenediamine-N,N'-diacetic acid
Hbs	hemoglobins

HbS	Sickle cell hemoglobin
Hepes	4-(2-hydroxyethyl)-1-piperazineethanesulfonic acid
holo	iron bound
hr	hour
HRP	horse radish peroxidase
I_a	anodic current
I_c	cathodic current
IHP	inositol hexaphosphate
LFER	linear free energy relationship
M	metal
MALDI-MS	matrix assissted laser desorption ionization mass spectrometry
Mb	myoglobin
MES	2-(*N*-morpholino)ethanesulfonic acid
min	minutes
MOPS	3-(N-morpholino)propanesulfonic acid
n_{50}	slope at the $E_{1/2}$ or log P_{50}
NAPHTHOL	2,3-dihydroxynaphthlene
NHE	normal hydrogen electrode
OTTLE	optically transparent thin layer electrode
ox	oxidize species

oxy	oxygenated species
P_{50}	pressure at which 50% of the sample is oxygenated
P_{O2}	pressure of oxygen
R	ideal gas constant
red	reduced speices
s	seconds
SEC	spectroelectrochemistry
SUPREX	stability of unpurified proteins through rates of H/D exchange
swMb	sperm whale myoglobin
T	tiron
T	temperature
TbpA	transferrin binding protein A
TbpA-plug	plug domain of transferrin binding protein A
TbpB	transferrin binding protein B
Tf	transferrin
TFA	trifluoroacetic acid
TfR	human transferrin receptor
UV	ultra violet
vis	visible

Acknowledgements

First, I would like to recognize the many scientists that have contributed to this work. I have enjoyed our collaborations and have learned enormous amounts from each of you. Katherine Weaver, Petra Rouhlac, Cindi Cornelissen, Jennifer Noto, and Michael Fitzgerald are acknowledged for their hard work, training, and helpful discussions regarding our iron uptake studies. I am also grateful for the hard work, insight, time, and friendship of Patrick DeArmond and Michael MacIntyre. Celia Bonaventura is recognized for her interesting perspective on hemoglobin and the opportunity to collaborate. Similarly, Anne Valentine and her students are recognized for their interesting questions regarding titanium and for the opportunity to collaborate. I am grateful to Sara Brandt and Kirsten Bazemore for their hard work, perseverance, and humor and I recognize Emily Lin for her enormous investment of time, effort, and thought as well as her friendship. To Bo and Arnav I enjoyed working and learning with each of you. To Jared and Kassy, thank you for your guidance, support, leadership, example, and friendship. To Esther and James, I enjoyed our time together and I wish each of you the best of luck.

Second, I would like to acknowledge the people with whom I have shared five years of special moments.

I would like to acknowledge Dr. Crumbliss (Boss) for his guidance and support. His scientific expertise and insight paved the way for the completion of this work and

the effort and time he has invested in me are humbling. I appreciate his willingness to serve as my scientific and professional mentor and I aspire to display the wisdom, patience, and professionalism he does. I thank him for the many opportunities and encouragement he has afforded me. I have truly enjoyed working and learning by your side.

Michael, my best friend and husband, deserves more gratitude than I could ever express in writing. His love, support, encouragement, counsel, and patience are endless and he never ceases to amaze me. He is my rock and my inspiration and I thank him for his hard work, steadfastness, high expectations, insight, and perspective. I love you and I can't wait for our next adventure.

Esther, Sarah, and Jenn have been by my side every step of the way and for that I am grateful. I have never had as close of friends as each of you and I will forever cherish our time together.

Finally, I would like to acknowledge my family whose love and support have made me who I am today. To Mom and Dad, thank you for your endless encouragement, guidance, and insight. To Beverly, Grandpa, Susie, Paul, and Grandma, thank you for believing in me. I am so grateful each of you are apart of my life. To John, Mark, Scott, Kennedy, and Grant, I am so proud of each of you. To Linda and Caroline thank you for being the best aunts a girl could have. To Hannah, I am honored to be the

second doctor in the family. I love each of you and am so proud to carry the name Jarvis Parker Siburt.

1. Introduction

This dissertation reports the biophysical investigations of a series of metalloproteins. Employing a variety of methods, we have in some instances found it to be advantageous to use the metal as the probe and in some instances there are distinct advantages to use the protein as the probe to investigate inter- and intra-molecular interactions. In all cases we have made thermodynamic measurements to address specific physiological questions.

1.1 Metal as Probe

In order to make thermodynamic measurements of metalloproteins using a metal probe, the fundamental chemistry of the metal must be understood. One metal examined in detail in this dissertation is iron. Iron is a Lewis acid, which forms five and six coordinate complexes with electron donating Lewis base ligands. The fully aquated form of the ferric iron (Fe^{3+}) readily undergoes hydrolysis leading to the formation of insoluble iron hydroxides (Equations 1.1-1.3).[1-3]

$$[Fe(H_2O)_6]^{3+} \leftrightarrows [Fe(H_2O)_5(OH)]^{2+} + H^+ \quad (1.1)$$

$$[Fe(H_2O)_5(OH)]^{2+} \leftrightarrows [Fe(H_2O)_4(OH)_2]^{1+} + H^+ \quad (1.2)$$

$$[Fe(H_2O)_4(OH)_2]^{1+} \leftrightarrows [Fe(H_2O)_3]_{(s)} + H^+ \quad (1.3)$$

The resulting low solubility of iron must be overcome in order to make this necessary metal bioavailable.

Another important chemical property of iron is the existence of multiple stable oxidation states. In biology the most common oxidation states of iron are Fe^{3+} and Fe^{2+}.[3] The ability to cycle between the ferric (Fe^{3+}) and ferrous (Fe^{2+}) ions provides a range of possible reactions in a biological setting. In aqueous solution, the redox potential of the reduction reaction in which the hexaaquoferric iron is reduced to the hexaaquoferrous ion is +0.771 V (Equation 1.4).[3]

$$[Fe(H_2O)_6]^{3+} + e^- \leftrightarrows [Fe(H_2O)_6]^{2+} \qquad (1.4)$$

The redox potential of a reaction is a measure of how easy or difficult the given reduction reaction is relative to the reduction reaction in which two protons are reduced and form molecular hydrogen (Equation 1.5).

$$2H^+ + 2e^- \leftrightarrows H_2 \qquad (1.5)$$

For the half reactions described in Equations 1.4 and 1.5, the positive and large value of +0.771 V indicates that in an electrochemical cell connecting the two reactions, electrons would flow from the hydrogen half reaction and toward the iron half reaction. Said another way, $[Fe(H_2O)_6]^{3+}$ will be reduced spontaneously by H_2 because it is easier to reduce $[Fe(H_2O)_6]^{3+}$ than the protons.

Uncontrolled, the redox cycling of aqueous iron ions can produce reactive oxygen species through a series of reactions known as the Haber Weiss cycle (Equations 1.6 and 1.7).[4] In this cycle, Fe^{3+} reacts with superoxide to produce Fe^{2+}. Then in the

Fenton reaction, Fe^{2+} reacts with hydrogen peroxide restoring the ferric ion, but producing the deleterious hydroxyl radical.

$$Fe^{3+} + O_2^{-\cdot} \rightarrow Fe^{2+} + O_2 \quad (1.6)$$

$$Fe^{2+} + H_2O_2 \rightarrow Fe^{3+} + OH^- + OH^\cdot \quad (1.7)$$

Iron is able to participate in these reactions because the reduction potential of each half reaction is in the correct range to produce a positive cell potential and therefore spontaneously reacts (i.e. $\Delta G = -n\Im E < 0$).

Iron chelators prevent hydrolysis by replacing the H_2O ligands in the first coordination shell around the iron and alter the reduction potential of the metal making it easier or harder to reduce the metal.[5] The identities of the specific ligands in the first coordination shell dictate the reduction potential of the metal, while the atoms in the second coordination shell fine tune the reduction potential.[1, 6, 7] The second coordination shell consists of atoms that are not directly bound to the metal, but are close enough to affect the electronic environment of the metal and the dielectric constant surrounding the metal.[1, 8] As shown in Figure 1.1, the redox potentials of iron complexes vary over 2 V.

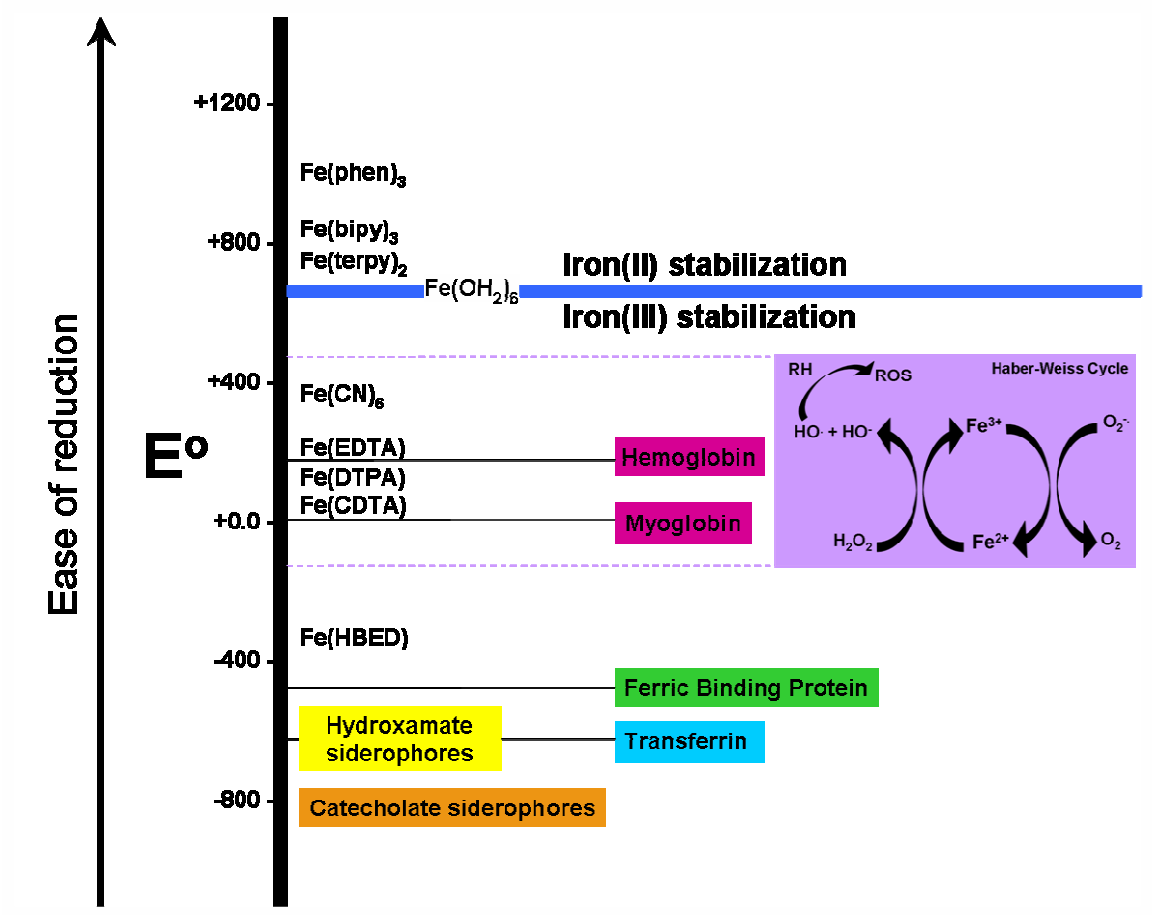

Figure 1.1: Scale of iron complexes showing the wide range of reduction potentials, E^o, reported in mV vs. NHE.[1, 2, 7-10]

Iron chelators that stabilize the Fe^{2+} oxidation state relative to the hexaaquo complex raise the reduction potential, while Fe^{3+} stabilizing chelators lower the reduction potential.

Biological iron chelators, whether they are small molecules or proteins, act as Lewis bases, donating electron density to the iron and forming coordinate-covalent bonds. By forming coordination complexes with the iron ion, biological chelators combat both deleterious properties of this necessary iron: insoluble hydroxide formation

and radical oxygen production.[7] Biological ligands prevent iron hydrolysis by replacing the H_2O ligands in the first coordination shell. Some biological chelators, such as siderophores and iron transport proteins, solubilize the iron and provide a molecular signature that can be recognized by a cell. These two functions increase the bioavailability of this necessary nutrient.

Most biological ligands alter the reduction potential of the iron by stabilizing Fe^{3+}. As shown in Figure 1.1, many biological chelators substantially lower the reduction potential of iron making the iron complex unable to participate in the Haber Weiss cycle described above (Equations 1.6 and 1.7). By lowering the reduction potential of iron, biological chelators protect the biological system from the production of reactive oxygen species.

We are also interested in titanium metalloproteins. Titanium is another redox active metal which we can use as a probe in our thermodynamic investigations of metalloproteins. Like iron, titanium is a Lewis acid, which is prone to hydrolysis and is therefore effectively insoluble in aqueous solution.[3] The most common oxidation states of titanium are Ti^{4+} and Ti^{3+}.[3] The ionic radius of hexacoordinate Ti^{4+} is similar to hexacoordinate high spin Fe^{3+} and therefore the charge density of the Ti^{4+} ion is higher than Fe^{3+}.[3] Consequently, Ti^{4+} not only forms hydroxides in aqueous solvent, but readily forms oxo-species.[3] The high charge density of the Ti^{4+} ion also makes it a harder acid than Fe^{3+}. The Hard Soft Acid Base principle correlates the thermodynamic

strength of a ligand-metal interaction with the polarizability of the electron clouds, predicting that hard acids such as Fe^{3+} and Ti^{4+} will bind tightly with hard bases such as highly electronegative non-polarizable charged oxygen ligands like those found in carboxylic acids.[11] Therefore, it is expected that Ti^{4+} will bind to carboxylate oxygens more tightly than Fe^{3+}. Carboxylate containing chelators, as well as chelators containing other donor groups, alter the redox potential of Ti^{4+} in a similar manner as they do with Fe^{3+}.

By using analytical techniques to measure the reduction potential of either titanium or iron in the active site of a metalloprotein, we can investigate the influence of the ligands present in the first and second coordination shells on the reactivity of the metal. Using the metal as the probe in this way we can gain insight on the ability of the metalloprotein to participate in redox chemistry. In this dissertation we utilize the redox activity of iron (Equation 1.8) as a probe to study the thermodynamic properties of a series of hemoglobins (Hbs) with various small molecule (O_2 and H_2S) transport functions (Equation 1.9).

$$\text{deoxy-Hb}(Fe^{2+}) \leftrightarrows \text{met-Hb}(Fe^{3+}) + ne^- \qquad (1.8)$$

$$\text{deoxy-Hb}(Fe^{2+}) + nO_2 \leftrightarrows \text{oxy-Hb}(Fe^{2+}) + O_2 \qquad (1.9)$$

We utilize the redox activity of titanium as a probe to study titanium bound in the active site of transferrin (Tf) and evaluate how titanium might exit from that site. In order to

measure the reduction potential of iron and titanium bound by hemoglobin (Hb) and Tf, respectively, we use spectroelectrochemistry (SEC) and cyclic voltammetry (CV).

1.2 Protein as Probe

Another handle on metalloprotein characterization is the protein. Rather than focus on the metal, the thermodynamic properties of the protein can also be used as the probe to elucidate detailed information about the function and mechanism of action of a metalloprotein. The protein structure modulates the reactivity of the bound metal and in the case of metal transport proteins, the protein-metal interactions can vary widely as the metal is passed from one protein to another.[6, 12, 13] Here we briefly review some of the properties of proteins that can be used as probes for protein function in our thermodynamic studies.

Proteins are made of unique sequences of covalently bound amino acids (primary structure) that form into α-helices, β-sheets, and less structured loops. These stretches of secondary structure along the amino acid sequence are stabilized by hydrogen bonds and fold into higher order tertiary structures such as globules, lobes connected by hinges, and β-barrels, to name a few.[14] The tertiary structures are commonly referred to as the protein fold. Finally, multiple proteins can form larger complex proteins, where the interactions between individual proteins are known as quaternary structure.[14] Each structural level, as well as the chemical function of a

given protein can be used to monitor the thermodynamic properties of the protein and the reactions in which it participates.

When focusing on the protein as the probe in a reaction, the small molecule, the metal, or another protein that interacts with the protein under investigation is called the ligand. Ligand binding studies that monitor a change in the protein (e.g. absorbance spectrum) as a function of ligand concentration are common in thermodynamic investigations. Here we discuss some studies of this nature such as oxygen binding to Hb and iron binding to Tf. We also discuss studies incorporating other ligands such as antibodies, which are used in conjunction with mutated proteins to identify important epitopes (surfaces or facades of the folded protein).

Changes in the structure of a protein caused by ligand binding can be monitored with a variety of techniques. As a general principle, each technique focuses on a particular level of protein structure (1^{o} - 4^{o}). For example, the common spectroscopic technique fluorimetry is used to monitor the tyrosine and tryptophan residues in a protein as changes in the local environment around the fluorescent residue occur.[15] Another spectroscopic technique, circular dichroism, is used to monitor the change in 2^{o} structure of a protein because plane-polarized light interacts differentially with α-helices, β-sheets, and the less structure loops.[16]

In this dissertation, we have elected to monitor changes in the tertiary structure of the metalloproteins of interest. By probing the thermodynamic properties of the

folding and unfolding behavior of a given protein, information can be gleaned about the stability of a given protein fold. As well, the effects of a potential ligand on the protein fold can be investigated.[17] In this work we use the protein as probe to identify protein-protein and protein-metal interactions of metalloproteins involved in iron transport in bacteria.

1.3 Statement of Objectives

The thermodynamic properties of both metals and proteins provide a handle that can be used to investigate specific biological questions. In Chapter 2, we utilize SEC to measure the redox potential of iron in order to understand the structure-function relationships of clam and fish Hbs. In Chapter 3, we explore the limits of SEC in studying the redox potential of Tf bound titanium and probe the redox potential of low molecular weight titanium complexes in an attempt to address the pathway through which titanium enters the human cell. In Chapter 4, we shift our emphasis to the protein. Using the protein as our probe, we monitor the thermodynamics of protein folding to elucidate the protein-protein interactions involved in iron acquisition from the human host by pathogenic *N. gonorrhoeae*. In the final chapter (Chapter 5), we utilize both the protein and the metal to further explore the details of iron transport across the bacterial outer membrane.

2. Thermodynamic Investigation of Hemoglobins from Root Effect Fish and *Lucina pectinata*

2.1 Introduction

Traditionally, hemoglobin (Hb) is defined as the respiratory protein which reversibly binds oxygen in the lungs and delivers it to the tissues where the partial oxygen pressure (P_{O2}) is low (Equation 1.9). Functional and structural homologues of Hb are found in many species of vertebrates and invertebrates. Recently the definition of Hb has been expanded to include other functions and the number of hemoglobins (Hbs) identified has increased rapidly. Over 600 primary structures of Hbs have been determined and Hbs have been reported for organisms of all kingdoms.[18] The structure and function of the Hb (and often times Hbs) of a particular species have evolved to provide specific functions for the organism. In this chapter, we discuss the Hbs from several different species, each with their own structure-function relationships that determine a specific physiological purpose.

As the field of natural Hbs has exploded in recent times, research leading to the development of cell free Hbs has also grown. The approaches of producing cell free Hbs able to deliver oxygen as artificial blood substitutes, include genetic engineering of natural Hbs, *in vitro* chemical alteration of natural Hbs, and creation of synthetic oxygen carriers.[19-21] The difficulty with all of these approaches is maintaining control over the oxygen affinity and side reactions in which the Hb substitute can participate.[22] Together with the widening variation in structures and functions observed in nature, the

Hb field has been reignited with a focus on the underlying factors that control Hb function.

In this chapter we use iron as the probe for our thermodynamic studies of various Hbs and utilize spectroelectrochemistry (SEC) to characterize the redox behavior of the heme-bound iron. The redox behavior of a particular Hb is determined by the first and second coordination shells around the iron. In all Hbs the first coordination shell is constant (four ligands from the heme and one from the proximal histidine). However, the second coordination shell consisting of the globin chain, the protein fold, and the binding pocket vary from Hb to Hb and differentially affect O_2 transport and electron transfer. We present two investigations in which we are interested in the role of thermodynamic properties of the metal and the role of steric hindrance in the heme pocket. In both cases, the Hbs under investigation provide important physiological functions for the respective organism. Before turning to these specific case studies, we begin with a brief review of Hb structure, oxygen binding, and redox behavior.

2.1.1 Hemoglobin Structure and Function

2.1.1.1 Human Hemoglobin A_o

Human hemoglobin (HbA_o) is one the most studied Hbs and significant structural information is available. As well, a substantial amount of information regarding the transport of oxygen and the other reactions in which HbA_o participates

has been reported. It is not within the scope of this chapter to review the extensive body of work surrounding the structure and function relationships of HbA_o. Rather, we briefly summarize the relevant structural features of HbA_o that are required to set the stage for the investigations reported herein.

HbA_o is composed of four subunits, two α-subunits with 141 amino acids each and two β-subunits with 146 amino acids each. Each of the four subunits holds one heme molecule that is composed of a protoporphyrin IX ring complexed to an iron ion. The heme is coordinated to the iron through four nitrogen atoms, while the protein subunit provides a fifth ligand, histidine, to the first coordination shell of the iron. Figure 2.1 depicts the tetrameric structure of HbA_o with the four heme groups present.

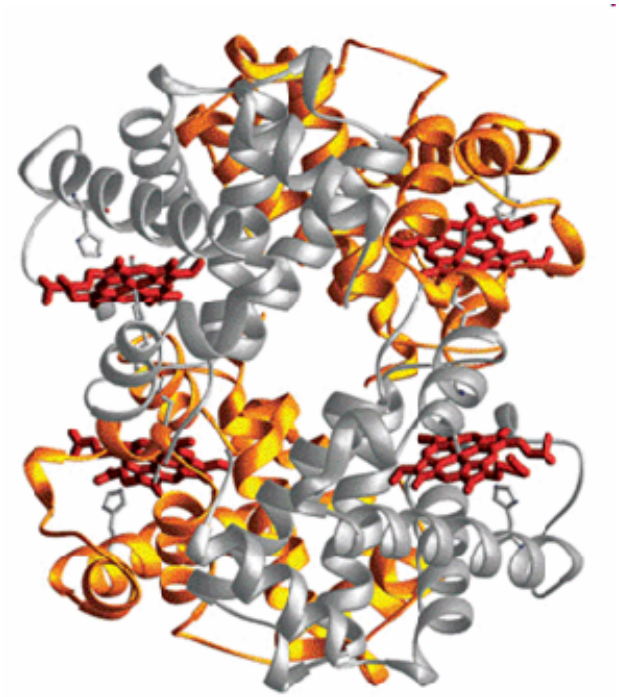

Figure 2.1: Ribbon diagram of HbA_o. Reproduced with permission from reference [22].

The four subunits are held together with hydrogen bonds, salt bridges, and hydrophobic interactions. These connections can communicate information between the monomers. The cavity in the center of the tetramer is positively charged and is the site where allosteric effectors such as polyanions can bind and alter the oxygen affinity of the protein (see Section 2.1.1.3).

Upon binding of O_2 a number of changes occur in the structure of the protein. These changes affect the ability of each monomer to bind O_2. It is beyond the scope of this chapter to discuss the specifics of all of the changes that have been identified. Rather, we defer to the classical designations of "R-state" and "T-state" put forth by

Monod, Wymann, and Changeux, where "R-state" refers to the high oxygen affinity conformer and "T-state" refers to the low affinity conformer.[23]

2.1.1.2 Ligand Binding

The fact that the stability of one monomer binding to oxygen is affected by the oxygen binding status of the other monomers is known as cooperativity. This cooperative behavior is observed for Hb as the binding of each oxygen molecule is made progressively easier by the binding of the previous oxygen molecule. Many models for cooperative ligand binding have been reported.[23-28] For the purposes of this chapter, we will use a two state model, in which the R-state and T-state conformations can be achieved without intermediates.

Herein oxygen binding data will be analyzed using a modified version of the Hill relationship. The classical Hill Equation,

$$\frac{Y}{1-Y} = K(X)^n \qquad (2.1)$$

relates the fraction of sites filled (Y) to the binding constant (K) as a function of added ligand (X), where n denotes the order of the reaction. For the Hb system, the concentration of oxy-Hb represents the number of sites filled and the amount of ligand added is measured as P_{O2} (Equation 1.9). The modified version of the Hill equation used herein is described by Equation 2.2, where P_{O2} is the applied oxygen pressure and n is a measure of cooperativity.

$$\log\left(\frac{[oxy-Hb]}{[deoxy-Hb]}\right) = \log P_{50} + n\log P_{O_2} \qquad (2.2)$$

As shown in Figure 2.2, when the Log([oxy-Hb]/[deoxy-Hb]) is plotted as a function of Log P_{O2}, Log P_{50} refers to the log of the applied pressure at which 50% of the sample is oxygenated and 50% is in the deoxygenated form.

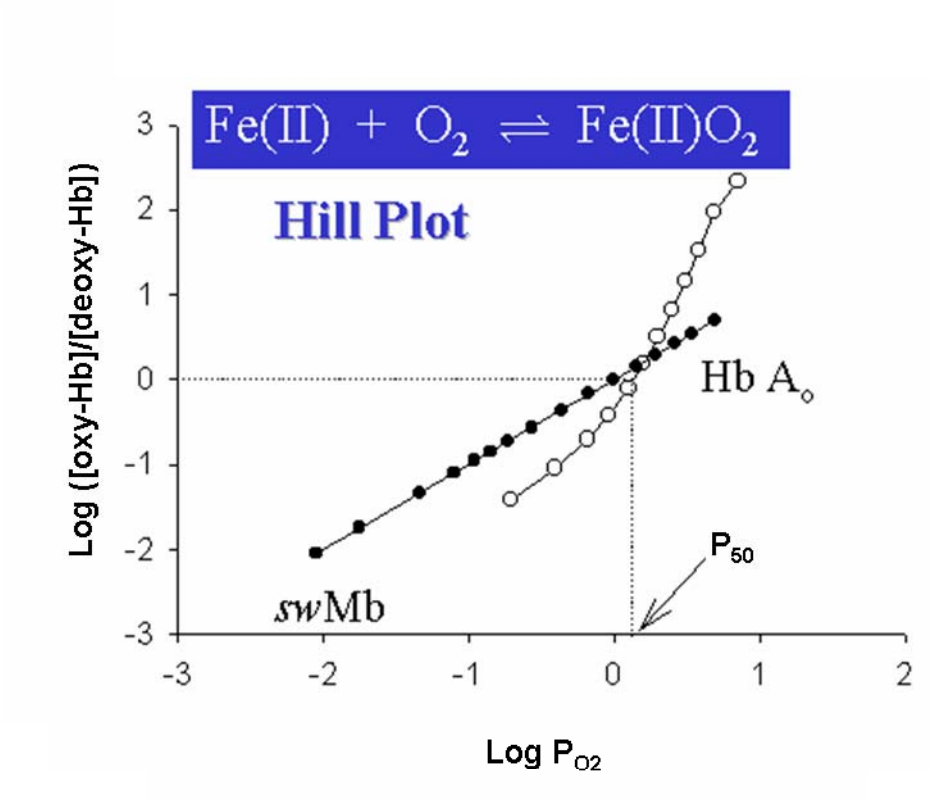

Figure 2.2: Representative Hill plot of sperm whale Mb (swMb) and HbA$_o$. Figure modified from reference [8].

Myoglobin (Mb), another respiratory protein functions as an O_2 storage protein. Mb consists of one monomeric polypeptide and binds only one oxygen molecule. Mb shows a linear response to changes in applied P_{O2} using the Hill analysis (Figure 2.2). The linear behavior reflects the non-cooperative nature of the heme monomer and the

unity slope reflects the single oxygen binding site. We introduce Mb here for a comparison to Hb. In this chapter we use swMb as a calibrant for our SEC method.

HbA_o shows a sigmoidal response using the Hill analysis. The non-linear response (Figure 2.2) indicates the cooperative nature of HbA_o binding to four molecules of diatomic oxygen. Further discussion of the Hill plot and its use in this chapter are discussed in Section 2.1.2.

2.1.1.3 Allosteric Effectors

The ease of ligand (e.g. O_2) binding or oxygen affinity is a thermodynamic concept that is described by the equilibrium constant of the oxygenation reaction (Figure 2.2). Using the two state model, the protein is in equilibrium between the oxy-Hb R-state and the deoxy-Hb T-state. Allosteric effectors can alter this equilibrium by stabilizing or destabilizing one form of the protein over the other. Effectors are divided into to two categories heterotrophic and homotrophic. Homotrophic effectors bind to the protein at the ligand binding site while heterotrophic effectors bind to the protein at a site different than the ligand binding site.

In this chapter we utilize the heterotrophic effector phosphate, which has been shown to stabilize the T-state of HbA_o.[25] The poly-anionic phosphate ion binds in the positively charged cavity of the of the tetrameric HbA_o.[29] By stabilizing the T-state of HbA_o, phosphate allosterically decreases oxygen affinity and decreases cooperativity. In

our studies of Root Effect Hbs, which will be introduced in Section 2.1.3, we use 0.2 M phosphate buffer to allosterically induce the Hbs under investigation into the T-state conformation. Using these conditions we can control the thermodynamic properties of the reactions being studied and isolate the factors determining reactivity.

2.1.2 Redox Behavior of Hemoglobins

2.1.2.1 Anaerobic Oxidation

Taking a ferrocentric view of Hb, the changes in the heme environment of the iron are similar for both the anaerobic oxidation reaction (Equation 1.8) and the oxygenation reaction (Equation 1.9). Figure 2.3 compares these two reactions with emphasis on the iron.

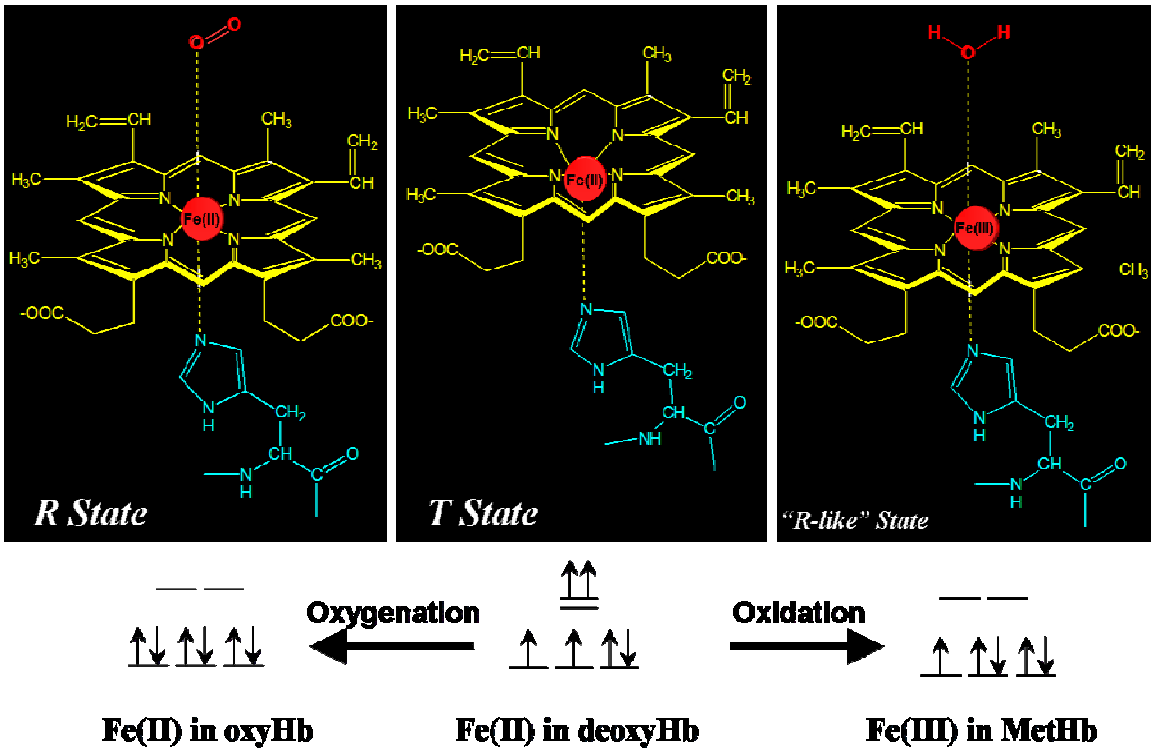

Figure 2.3: Ferrocentric view of Hb. The environment around the iron changes in similar ways during the oxygenation and anaerobic oxidation of Hb.

As shown in Figure 2.3, deoxy-Hb, in the low O_2 affinity T-state conformation, involves a five coordinate Fe(II) ion that lies slightly out of the plane of the heme and has a high spin d^6 electron configuration. Upon oxygenation, the Fe(II) ion binds O_2 becoming six coordinate, moves into the plane of the heme, and changes spin state to low spin. Similar changes occur upon anaerobic oxidation. The oxidized iron (now Fe(III)) moves into the plane of the heme and a spin state change occurs, although the electron configuration is now low spin d^5. The coordination number also increases to six as it does during the oxygenation, because during anaerobic oxidation a water molecule already present in the heme-pocket binds to the Fe(III).[30]

The similarities between anaerobic oxidation and oxygenation can also be seen by comparing the Nernst plot with the Hill plot (Figure 2.4). The Nernst equation,

$$E_{app} = E_{1/2} + \frac{RT}{nF}\log\left(\frac{[ox]}{[red]}\right) \tag{2.3}$$

relates the potential (E_{app}) applied to the system with the concentrations of the oxidized and reduced forms of Hb. Similar to the Hill plot for oxygen binding, a modified version of Equation 2.3 can be used to create a Nernst plot for anaerobic oxidation. Figure 2.4 shows the similarities between the resulting Nernst plot and the Hill plot discussed in Section 2.1.1.2.

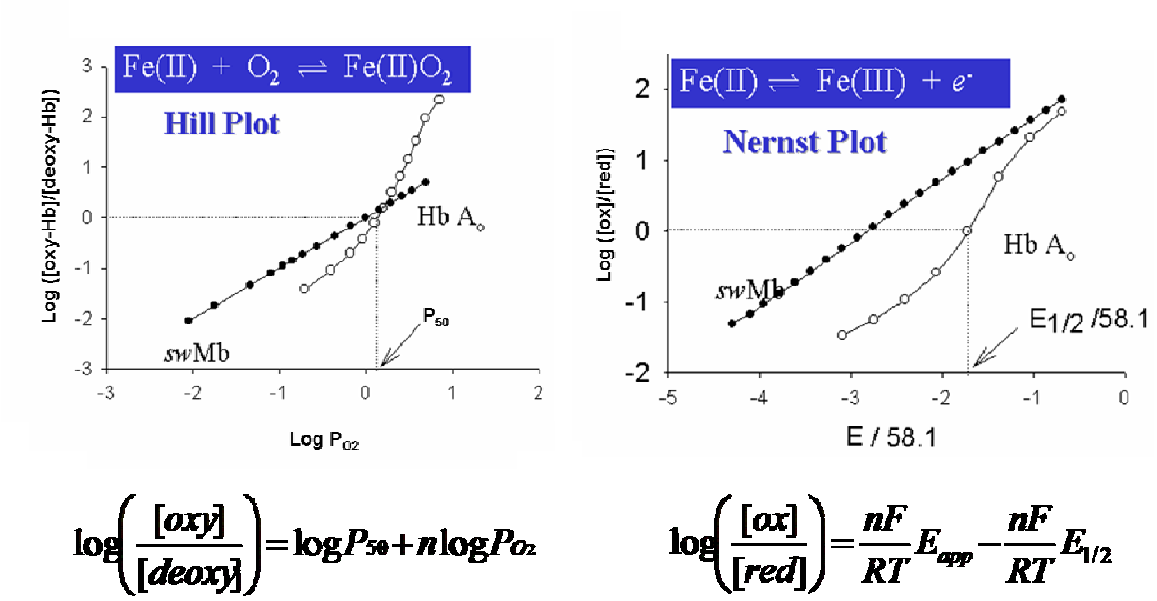

$$\log\left(\frac{[oxy]}{[deoxy]}\right) = \log P_{50} + n\log P_{O_2} \qquad \log\left(\frac{[ox]}{[red]}\right) = \frac{nF}{RT}E_{app} - \frac{nF}{RT}E_{1/2}$$

Figure 2.4: Comparison of the Hill plot with the Nernst Plot. The modified version of Equation 2.3 and Equation 2.2 are printed as part of the figure of ease of comparison. Figure modified from reference [8].

As can be seen in Figure 2.4, the monomeric swMb responds linearly to changes in Log P_{O2}. Similarly, swMb responds to externally applied potential in a linear fashion. Both trends indicate the lack of cooperativity in a monomeric system. For linear Hill and Nernst plots, the n-value or slope of the line represents the number of O_2 ligands bound and the number of electrons transferred respectively. On the other hand, HbA_o, the classic cooperative tetrameric Hb, displays a sigmoidal shape on both the Hill plot and the Nernst plot. This sigmoidal shape indicates the increasing ease of oxygenation or oxidation as subsequent subunits react. For cooperative systems an n_{50} value is defined as the slope of the plot at the $E_{1/2}$ for the Nernst plot or Log P_{50} for the Hill plot. Here the n_{50} value does not represent the order of the reaction, but it can be related to the degree of cooperativity exhibited by the system.[31] It should be noted that heterogeneous mixtures of heme-active sites can also cause the Nernst behavior to deviate from linearity. Extensive work has been reported regarding the interpretation of the shape of the Nernst and Hill plots. The reader is referred to an excellent review by Taboy et al.[13]

In addition to the shape of the Nernst and Hill plots, the relative position of the $E_{1/2}$ and Log P_{50} can be correlated to one another. The P_{50} value is the pressure at which 50% of the sample is oxygenated and 50% is deoxygenated. Correspondingly, the $E_{1/2}$ value is the applied potential at which 50% of the sample is oxidized and 50% is reduced. A large and positive Log P_{50} value indicates that the sample is difficult to

oxygenate. A large and positive $E_{1/2}$ value indicates that the sample is difficult to oxidize. The general principle that Log P_{50} value increases as $E_{1/2}$ value increases is shown graphically in Figure 2.5.

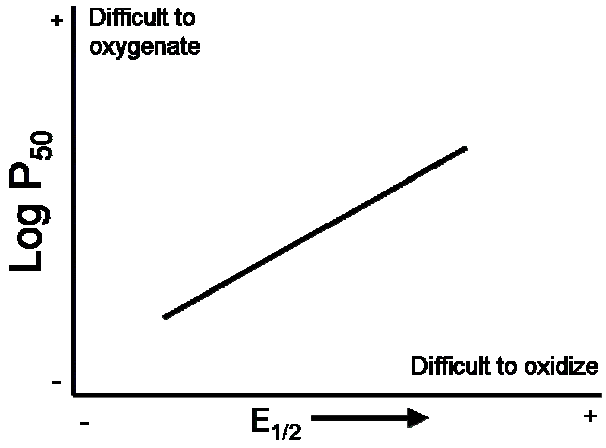

Figure 2.5: General correlation between Log P_{50} values and $E_{1/2}$ values of a generic Hb.

Comparing the Log P_{50} values of swMb and HbA_o, in Figure 2.4, it can be seen that swMb has a higher oxygen affinity than HbA_o. A similar trend is seen in the Nernst plot (Figure 2.4). swMb has a lower $E_{1/2}$ than HbA_o meaning that swMb is more easily oxidized than is HbA_o. It should be noted here that the Hill plots for swMb and HbA_o intersect close to the Log P_{50} values of each species. The Hill plots for human Mb and HbA_o do not intersect, ensuring human Mb serves as the O_2 storage protein and HbA_o serves as the O_2 transporter.

Given the similarities between anaerobic oxidation and oxygenation, anaerobic oxidation is a good model for the thermodynamic properties underlying the

oxygenation of Hb. However, anaerobic oxidation also provides a distinct advantage over traditional thermodynamic measurements of Hb: the ability to measure the underlying thermodynamic properties without the complication of a chemical reactant entering the heme pocket. Anaerobic oxidation, measured using the method of spectroelectrochemistry (SEC), has been used to isolate the thermodynamic properties of Hbs from many different species and engineered Hbs. As well, the effects of chemical environment such as allosteric effectors or pH have been investigated using SEC.[13, 19, 29, 31-34] Important to our investigations herein, low concentrations of the allosteric effector phosphate (see Section 2.1.1.3) stabilize the T-state of Hb and raise the $E_{1/2}$ value, indicating a the heme-bound iron is harder to oxidize.[29] Here we utilize SEC to investigate the role of the thermodynamic properties of the heme-bound iron in determining the physiological function of various Hbs. We also control the SEC conditions such as the presence of allosteric effector in order to isolate various conformations of the Hbs under investigation.

2.1.2.2 Spectroelectrochemistry

SEC is a method to accurately measure the redox properties of metalloproteins. For a detailed review of the method of metalloprotein SEC the reader is referred to references.[13, 32] A brief description of the SEC method is provided here as an introduction. The experimental details and calculations associated with the data

analysis are described in detail in the Methods and Materials section of this chapter (Section 2.2).

In SEC the absorption spectra of a metalloprotein is used to monitor the reduction or oxidation of the protein as an external potential is applied to the sample. The concentrations of the oxidized and reduced species of the metalloprotein are calculated from the absorbance data and analyzed as a function of the applied potential using a modified version of the Nernst equation (Equation 2.3) as depicted in Figure 2.4.

SEC allows for accurate measurement of each species when the UV-vis spectrum of the oxidized and reduced forms of the metalloprotein are significantly different, and is more advantageous than monitoring the current of the electrochemical reaction as is done in CV. The heterogeneous electron transfer between the solid electrode surface and the metal center of the protein is slow, making current readings unreliable. As well, the heterogeneous electron transfer vital to CV has been shown to alter the hydrogen bonding network on the distal side of the heme pocket of, thus complicating structural interpretations of Hb data.[35] SEC incorporates a small molecule mediator to shuttle electrons between the solid electrode surface and the protein, minimizing the difficulties of heterogeneous electron transfer to the protein. An ideal mediator should: 1) have a known $E_{1/2}$ within the potential range of the analyte, 2) have fast homo- and heterogeneous electron transfer rates with known stoichiometry, 3) be stable in both redox forms, and 4) not interfere optically or physically with the analyte.[36, 37] The

choice of mediator for the SEC study of Hbs will be discussed in the Materials and Methods section of this chapter (Section 2.2).

For the Hbs under investigation in this chapter, we have elected to use UV-vis spectroscopy as part of our SEC method because the UV-vis spectral properties of oxy-Hb, deoxy-Hb, and met-Hb are well defined. The principles of SEC could however be applied to any spectroscopic detection system (e.g. fluorescence, IR, etc.) Generally, we used the Soret bands (430 nm ϵ= 133,000 M^{-1} cm^{-1} for deoxy-HbA_o and 406 nm ϵ= 162,000 M^{-1} cm^{-1} for met-HbA_o) as our specific spectral handles because these wavelengths change the largest amount during the redox reaction.[38] The molar absorptivities listed above are for HbA_o and vary depending on the specific Hb structure under investigation. Here we explore the electrochemical properties of Hbs from multiple species in order to investigate two physiologically important phenomena: the varied functions of Hbs from *Lucina pectinata* and the factors determining the Root Effect of some fish Hbs.

2.1.3 Hemoglobins from Fish Exhibiting the Root Effect

Here we investigate Hbs from various fish that off load oxygen in a heightened response to changes in pH. This phenomenon is known as the Root Effect.[39] We measured the effect of changes in pH on the redox potential of the heme-bound iron in an effort to elucidate the underlying factors that control the Root Effect. The Root Effect

is an exaggerated version of the more general Bohr Effect, so we begin this section with a survey of the Bohr Effect.

2.1.3.1 Bohr Effect

The deoxygenation of all Hbs is sensitive to changes in pH. As pH is decreased more O_2 is released. Generally this trend, called the Bohr Effect, is explained by protons acting as allosteric effectors and shifting the conformation of Hb from the high O_2 affinity R-state to the low O_2 affinity T-state.[37]

As discussed in Section 2.1.2.1, anaerobic oxidation serves as a good model for the thermodynamic changes associated with oxygenation of Hbs. Similar to the Bohr Effect, a "Redox Bohr Effect" has been observed for HbA_o in that the measured redox potential ($E_{1/2}$) of HbA_o increases as pH decreases in a similar manner to the decrease in oxygen affinity over the same pH range.[37] In 1987, Colletta et al attributed the similar pH-sensitivities of oxidation and oxygenation of Trout Hb to the same ionizable groups.[40]

2.1.3.2 Root Effect

Some fish, represented here by *Cyprinus caprio* (Carp) and *Leiostomus xanthurus* (Spot), exhibit a heightened sensitivity to pH and unload O_2 in acidic conditions to a dramatic extent compared to HbA_o.[39, 41] This phenomenon is called the Root Effect

and allows Hb to serve as an O_2 pump for Root Effect fish.[42] Through this acid-controlled mechanism, O_2 is pumped into the swim bladders and eyes of the fish against high O_2 pressures.[33, 42, 43]

The nature of this increased pH-sensitivity of Root Effect Hbs is contested and has been studied for many years. A good review of the progress made towards understanding the biochemistry and biophysics underlying the Root Effect can be found in reference [33]. In brief, both Spot Hb and Carp Hb are tetrameric Hbs that bind and release oxygen cooperatively. Both are highly sensitive to acidic conditions. The reduced cooperativity and reduced oxygen affinity at low pH seen in these Root Effect Hbs are usually attributed to an alteration in the balance between R-state and T-state conformations of the respective Hb. In 1996, Mylvaganam et al. reported the crystal structure of Spot Hb-CO (PDB code 1SPG), and demonstrated that a positive cluster of amino acid residues located at the interface between the β-chains are protonated at low pH.[42] With this increase in charge, the β-β interface is destabilized and the tetramer shifts from R-state to T-state. The shift to the T-state conformation alleviates some of the charge repulsion, because in the T-state conformer the β-chains are further apart. In addition to identifying specific residues in this positive cluster that destabilizes the R-state, Mylvaganam et al. also identified residues that stabilize the T-state, a complementary and long standing explanation for the Root Effect.[42]

Recent reports from the Bonaventura and Crumbliss laboratories, on Root Effect Hbs have suggested that steric hindrance towards the entering ligand, rather than thermodynamic arguments (shifts in conformer populations) is the cause of the Root Effect.[33] SEC was used to measure the redox behavior of the Spot Hb, a Root Effect fish, in the absence of allosteric effects.[33, 43] Unlike Trout Hb and HbA_o, the pH sensitivity of the redox potentials of Spot Hb does not mimic the sensitivity of the corresponding oxygenation properties. Said another way, recent studies of Spot Hb demonstrate the lack of a "Redox Root Effect" under the conditions used.[33, 43] Given that these preliminary data showed the lack of a "Redox Root Effect" we question whether thermodynamic arguments can fully explain the Root Effect.

2.1.3.3 Statement of Objectives

In collaboration with Dr. Celia Bonaventura, Duke University Marine Laboratory (DUML), our objective is to determine the underlying factors that control the Root Effect in Spot and Carp Hbs. As part of our approach we investigated the effect of pH on the $E_{1/2}$ of two Root Effect Hbs (Carp and Spot) and HbA_o in two different buffer systems at various pH values. We hypothesized that the Hbs from the three species would exhibit similar changes in reduction potential as a function of pH. Investigating the effect of pH on reduction potential allowed us to probe the thermodynamic properties of these Hbs without the complexity of O_2 binding, as anaerobic oxidation has been shown to be a

good alternative method to investigate the factors that influence thermodynamic properties of oxygenation. We performed our experiments in two different buffer systems: Hepes buffer and phosphate buffer. By including the allosteric effector phosphate in some experiments, the conformation of the Hbs under investigation was shifted to the low oxygen affinity, hard to oxidize T-state. Controlling the thermodynamic properties of the Hbs in this way, increased the range of conformations for which we can evaluate the factors that may determine the structure-function relationships leading to the Root Effect. Oxygen binding studies performed by our collaborators at the DUML are presented here for comparison.

2.1.4 Hemoglobins from *Lucina pectinata*

In a separate investigation, we examine two Hbs from *Lucina pectinata* that exhibit distinct physiological functions: one transports O_2 while one transports H_2S.[44-48] These Hbs have been shown to react at extremely fast and extremely slow rates with nitrite, a physiologically important chemical oxidant.[49] We measured the redox potential of the heme-bound iron in an effort to elucidate the underlying factors that control the reactivity of these Hbs. We begin with a survey of the *Lucina pectinata* Hbs and a brief review of the reactions of Hb with nitrite and its derivatives. Then we return to the divergent rates of nitrite-induced oxidation exhibited by the *Lucina pectinata* Hbs.

2.1.4.1 *Lucina pectinata* Hemoglobins

Enormous structural and functional diversity exists among invertebrate Hbs.[50] The multiple Hbs of *Lucina pectinata*, a clam that hosts symbiotic bacteria, exemplify how the differences among invertebrate Hbs allow the organism to meet widely varying physiological demands.

Lucina pectinata is a large tropical clam that lives in the sulfide-rich mud of mangrove swamps. The presence of high (mM) levels of functionally distinct Hbs in its gills provides adaptive advantages for the clam and its symbiotic bacteria.[45-48] The bacterial symbionts thrive and supply metabolic by-products to the clam only when supplied with both O_2 and H_2S. The clam contributes to the symbiosis by producing high levels of structurally distinct Hbs in its gills to perform both O_2 and H_2S transport functions.[45] *Lucina* Hb I which transports H_2S to the clam's symbiotic bacteria is a monomer and has a relatively open heme pocket.[44] Conversely, *Lucina* Hb II transports O_2 even in the presence of high levels of H_2S. *Lucina* Hb II exists as a monomer, but can polymerize at high protein concentrations. Even in the polymeric form however, Hb II binds oxygen non-cooperatively.[44-48]

As depicted in Figure 2.6, the amino acid residues surrouding heme of Hb II are closer to the heme-bound iron compared to the heme pocket constituents in Hb I. The distal side of the heme pocket of both Hb I and Hb II consists of a glutamine instead of

the histidine found in human HbA_0. Three phenylalanines complete the heme pocket of Hb I, while that of Hb II consists of two phenylalanines and a tyrosine.[44]

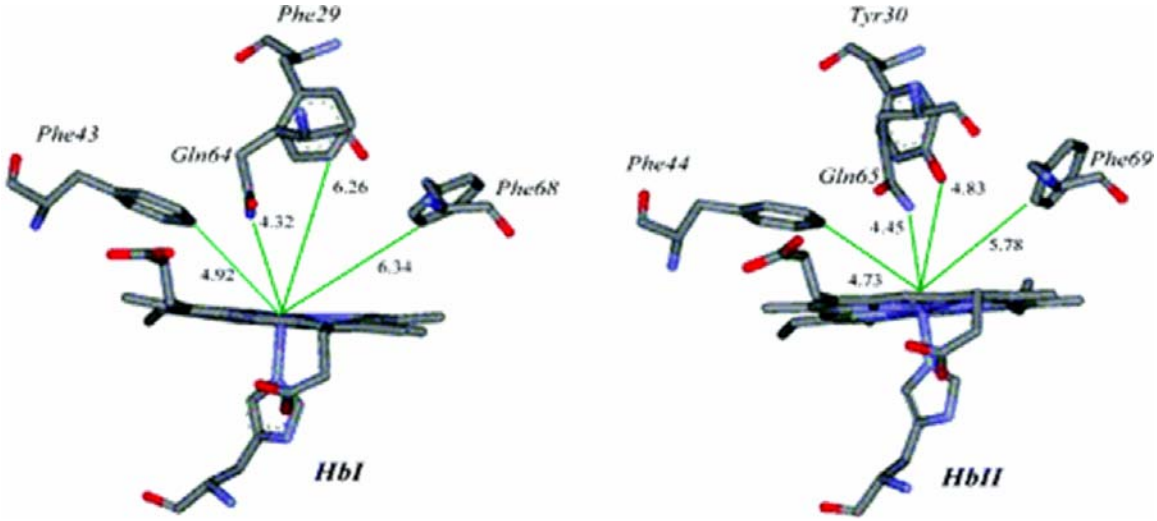

Figure 2.6: Heme pocket active sites of *Lucina pectinata* Hb I (PDB code 1EBT) and Hb II (PDB code 2OLP). The distances calculated from the distal residues to the heme iron demonstrate that the heme pocket of Hb I is more open (has a larger volume) than that of Hb II. These stereo diagrams and distance calculations created by our collaborators were previously published in Biochemistry 2007, 46, 10451-10460 have been reproduced here with permission.[44]

Although, these two Hbs function as transporters of different molecules, both can bind oxygen, albeit with different reaction rates. The rates of oxygen binding by the two Hbs have been correlated to the differences in heme pocket geometry.[45] The more open heme pocket of *Lucina* Hb I binds oxygen very quickly, while the more closed binding site of *Lucina* Hb II leads to slow O_2 binding.[44]

In addition to oxygen, the reactions of Hb I and Hb II with other small molecules have been explored and correlated to heme pocket architecture. In 1990, Kraus suggested that the differences in the amino acid residues of the heme pocket may be

responsible for the very different reactions of Hb I and Hb II reacting with H_2S.[45] More recently, our collaborators explored the reaction of these Hbs with NO and H_2O_2 and showed that unlike Hb I, Hb II is slow to react with NO and resists oxidation by H_2O_2.[44] In an attempt to engineer Hb I into Hb II, Walleska et al. substituted Phe(B10) with Tyr(B10). However, this mutation was not sufficient to change the behavior of Hb I to match that of Hb II.[44] Walleska et al. suggested that heme pocket architecture and solvent exposure might explain the variations between Hb I and Hb II, rather than just the identity of the ligands present in the pocket.[44] In 2008, our collaborators published the crystal structure of oxy-Hb II and showed that not only is the heme pocket of Hb II more narrow than Hb I, but that the tyrosine residue present in Hb II and absent in Hb I, forms a hydrogen bond to the bound oxygen molecule.[46]

2.1.4.2 Reactions of Nitrite and Hemoglobin

Nitrite (NO_2^-) can oxidize the Fe^{2+} heme of both oxy- and deoxy-Hbs. The following equations describe the overall reactions of Hb with nitrite, both of which follow complicated mechanisms that are currently under intense investigation (Equations 2.4 and 2.5).[51-58]

$$\text{Oxy-Hb}(Fe^{2+}) + NO_2^- \rightarrow \text{met-Hb}(Fe^{3+}) + NO_3^- \qquad (2.4)$$

$$\text{Deoxy-Hb}(Fe^{2+}) + NO_2^- \rightarrow \text{met-Hb}(Fe^{3+}) + NO \qquad (2.5)$$

HbA_o specifically, has been assigned the function of a nitrite reductase. Although the physiological role of the nitrite reductase activity of HbA_o is controversial, nitrite as been suggested as a storage source of nitric oxide (NO).[59-66] NO is a signaling molecule which affects blood pressure regulation and is therefore of great physiological and pharmacological importance.[67] Further, NO can also react both with Fe^{3+} and Fe^{2+} heme.[67, 68] In the case of Fe^{2+}, NO binds to deoxy-Hb as a ligand and NO reacts with oxy-Hb to produce met-Hb(Fe^{3+}) and nitrate.[69] Thus, the reaction of either nitrite or NO with functioning ferrous-Hb yields ferric-Hb (met-Hb) that cannot transport oxygen. The persistence of met-Hb can cause a condition is known as methemoglobinemia.[19, 70]

Given the potential Hb-dependent vasoactivity and methemoglobinemia caused by the redox reaction of Hb with nitrite, it is important to understand the redox properties of Hb. Further, when designing cell free Hb substitutes the possible redox reactions with nitrite and other small molecules that a new Hb might participate in must be considered. In fact, the nitrite reductase activity of blood substitutes and the subsequent deleterious effect on blood pressure is a major problem with the cell free Hbs being developed currently. The ability to control the redox reactions of these Hbs remains elusive.[67]

The redox reactions of Hbs have been studied for over 150 years.[71] However, the main focus of these studies has been and remains the thermodynamic properties

governing these reactions. As recently as 2008, Grubina et al. attributed the abnormal nitrite reductase activity of HbS (sickle cell) to a balance between allosteric effectors, another thermodynamic argument.[71] Here we report a different view of the regulation of Hb's nitrite reductase function. Later in this chapter, we will assert that steric hindrance of the heme pocket rather than conformational thermodynamics are the primary factor determining the rate of reaction between Hb and the chemical oxidant nitrite.

2.1.4.3 Unusual Reaction of *Lucina pectinata* Hemoglobins with Nitrite

Although nitrite-induced oxidation is a common feature of all Hbs previously studied [72], *Lucina* Hb I and II react with nitrite in opposite and extreme ways. Our collaborators have shown that air-equilibrated samples of *Lucina* Hb I are more rapidly oxidized by nitrite than any previously studied Hb, while samples of *Lucina* Hb II showed an unprecedented resistance to nitrite-induced oxidation.[49] *Lucina* Hb I had a half-time for nitrite-induced oxidation of 19 s, roughly ½ that for horse Mb (37 s), which was in turn ½ that for stripped HbA_o under the same conditions (74 s). The genetically modified form of *Lucina* Hb I (Phe to Tyr at B10) had a half-time for nitrite-induced oxidation of 50 s, approximately 2.5 times longer than that of *Lucina* Hb I under these conditions. Conversely, air-equilibrated solutions of *Lucina* Hb II strongly resisted nitrite-induced oxidation. Spectral analysis 500 s after rapid mixing showed Hb II to be

less than 5% oxidized. These kinetic results are catalogued in Table 2.6 in the Section 2.4.1.3.[49]

Manual mixing methods confirmed the results of the rapid-mixing experiments.[49] Air-equilibrated *Lucina* Hb I was oxidized rapidly (too fast to measure by manual mixing) after addition of nitrite. In contrast, *Lucina* Hb II stayed in its ferrous (un-oxidized) state for hours, even in the presence of 100-fold excess of nitrite.[49]

Oxygen was found to play a key role in the strong resistance of *Lucina* Hb II to nitrite oxidation.[49] After one hour of incubation, a solution of air-equilibrated *Lucina* Hb II with 100-fold excess nitrite was still largely in its ferrous state, with < 10% metHb. When all O_2 was removed by repetitive degassing and N_2 flushing, the normal reaction of nitrite with deoxy-Hb II occurred, generating a combination of met-Hb and Hb-NO. The active site of *Lucina* Hb II was thus shown to be available for nitrite reaction when deoxygenated, but was "clammed up" and essentially unreactive with nitrite when exposed to air. It should be noted that deoxygenation of *Lucina* Hb II in the absence of nitrite did not induce heme oxidation.[49]

2.1.4.4 Statement of Objectives

In collaboration with Dr. Celia Bonaventura (DUML), Robert Henkens, Walleska De Jesus-Bonilla, Juan Lopez-Garriga, Yiping Jia, and Abdu I. Alayash (FDA), we have further examined the *Lucina pectinata* Hbs. Our objective was to measure the

thermodynamic properties ($E_{1/2}$ and P_{50} values) of these Hbs in order to determine the biophysical cause of the very different reactivities of these Hbs with nitrite. We hypothesized that the reactivity of these Hbs is controlled by steric hindrance rather than the reduction potential or oxygen affinity. The author's role in this collaboration was to use SEC to measure the reduction potentials of Hb I, Hb II, and a mutant of Hb I (see Section 2.1.4.1). The results (and methods) of oxygen binding studies performed by our collaborators at the DUML are included here to provide a context for the electrochemical investigation.

2.1.5 Statement of Goals

Here we present two cases in which we use iron as the probe for our thermodynamic studies of various Hbs. In both cases, our goal is to utilize SEC to characterize the redox behavior of the heme-bound iron as part of an approach to determine in the underlying factors that control Hb reactivity and function. The results presented here are important not only for our understanding of how structure-function relationships dictate physiological function, but also have implications for the design of new Hb-based blood substitutes.

2.2 Materials and Methods

2.2.1 Isolation and Purification of Protein Samples

All Hb and Mb samples were provided by Dr. Celia Bonaventura. The following is a brief description of how the samples were prepared for our use. Hbs were stripped of effectors by chromatographic procedures. HbA_o was isolated and purified from adult human blood using stripped Hb and fast-phase liquid chromatography as the final purification step.[73] The isolation of different types of Hbs from *Lucina pectinata* was performed as previously described with minor modifications.[44, 74] The recombinant form of *Lucina* Hb I (Hb I Phe→B10Tyr) was prepared as previously described.[44] Spot Hb was isolated from blood samples of Spot caught near Beaufort, NC, while Carp Hb was the generous gift of Dr. Robert Noble. The fish and clam Hb samples tended to oxidize readily and were treated with sodium dithionite (Merck) to reduce all oxidized heme sites and subjected to Sephadex G-25 chromatography to remove the reductant prior to functional analysis.

2.2.2 Spectroelectrochemistry

The anaerobic redox behaviors of various Hbs were investigated using published SEC methods developed in the Crumbliss laboratory.[13, 31] SEC utilizes a short optical pathlength, created by an optically transparent thin layer electrode (OTTLE) cell prepared in-house.[75] The variations in UV-vis spectra of the protein-metal complex

are measured, while applying an increasingly negative potential.[76] The change in absorbance corresponds to a change in concentration of oxidized and reduced species.[13] Equilibrium at each applied potential (E_{app}) was determined by stabilization in absorbance spectrum. The amount of time for the spectrum to stabilize depends on the specific Hb sample. For the Root Effect Hbs (Carp Hb and Spot Hb) this stabilization occurred within ~20 min at each potential. Samples of *Lucina pectinata* Hbs required much longer times to reach equilibrium (~1 hr). Following the Nernst equation (Equation 2.3), the equilibrium absorbance data are plotted as a function of the applied potential, E_{app}, to determine both the midpoint potential, $E_{1/2}$, and the number of electrons, n, transferred during a redox reaction.

In order to calculate the concentration of the oxidized and reduced species at a particular E_{app}, one must know the absorbance of the fully oxidized and fully reduced systems. We assume for the systems under investigation here that each analyte is fully oxidized at 350 mV vs. NHE and assign A_{ox} (fully oxidized absorbance) as the absorbance value observed after the system reaches equilibrium at that applied potential. A similar assumption is made for the fully reduced absorbance (A_{red}), when the system reaches equilibrium at a very low potential (value depends on species). Using the conservation relationship (where [ox] and [red] represent the oxidized and reduced forms of Hb respectively),

$$[Hb]_{total} = [ox] + [red] \tag{2.6}$$

and Beer's Law

$$[deoxy - Hb] = \frac{Abs_{red}}{\varepsilon b} \tag{2.7}$$

$$[met - Hb] = \frac{Abs_{ox}}{\varepsilon b} \tag{2.8}$$

the concentration of oxidized and reduced Hb species at any applied potential can be calculated using Equations 2.9 and 2.10.

$$[ox] = (A - A_{red}) \tag{2.9}$$

$$[red] = (A_{ox} - A) \tag{2.10}$$

As shown in Figure 2.4, the Nernst equation can be modified to relate the experimental absorbance to the applied potential:

$$\log\left(\frac{[ox]}{[red]}\right) = \left(\frac{nF}{RT}\right)E_{app} - \left(\frac{nF}{RT}\right)E_{1/2} \tag{2.11}$$

Incorporating Equations 2.9 and 2.10 into Equation 2.11, Nernst plots, reported herein were created by plotting the $\log\left(\frac{[A - A_{red}]}{[A_{ox} - A]}\right)$ as a function of E_{app} as shown in Equation 2.12.

$$\log\left(\frac{[A - A_{red}]}{[A_{ox} - A]}\right) = \left(\frac{nF}{RT}\right)E_{app} - \left(\frac{nF}{RT}\right)E_{1/2} \tag{2.12}$$

The heterogeneous electron transfer reaction between a soluble metalloprotein and the solid electrode requires an electron shuttle called a mediator (Figure 2.7).[77]

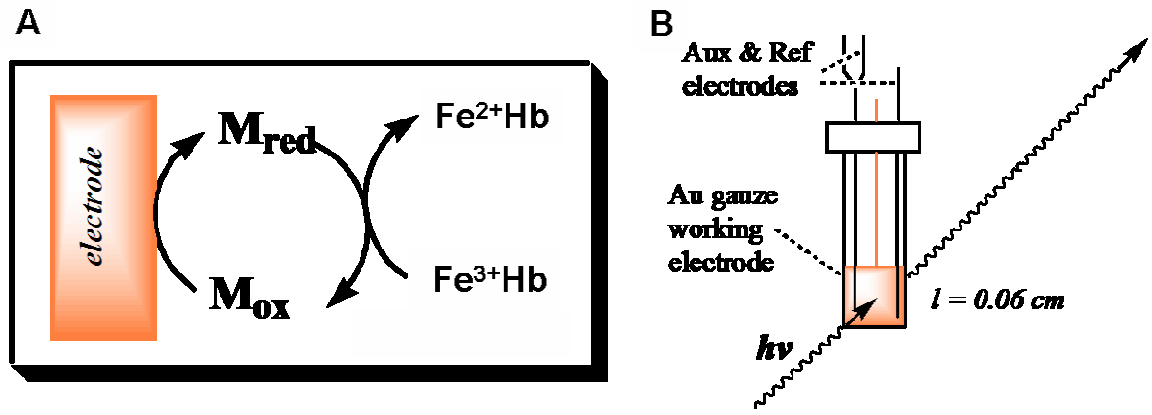

Figure 2.7: A) A mediator serves as an electron shuttle, transferring electrons between the solid electrode and the soluble protein. B) The OTTLE cell is built in-house to provide anaerobic conditions and a short pathlength for each SEC experiment.[13, 78]

In all SEC experiments reported in this chapter, hexaammineruthenium(III) chloride, $Ru(NH_3)_6Cl_3$, served as our electrochemical mediator. This cationic mediator is ideal for electrochemical investigations of Hbs, because the mediator does not act as an allosteric effector, thus altering the thermodynamic properties of the analyte.[13]

UV-vis spectra were taken on a CARY BIO 100 UV-vis spectrophotometer and a cell temperature of 20°C was maintained using a circulating water bath. Applied potentials in all SEC studies were controlled with an EG & G Princeton Applied Research model 363 potentiostat and samples were allowed to equilibrate for at least 15 min at each E_{app}. Full oxidation and deoxygenation were ensured by exposure to a large positive E_{app} for at least 1 hr and an anaerobic environment was maintained using $Ar_{(g)}$. A Ag/AgCl reference electrode (BAS) and platinum working and auxiliary electrodes were used for all experiments. Salt bridges were manufactured in-house using 0.1 M KCl in the respective buffer system. All potentials are reported vs. NHE.

2.2.3 Oxygen Binding Studies

Oxygen binding studies were performed by members of Dr. Celia Bonaventura research group at the DUML and carried out as follows. Oxygen binding affinities were measured using tonometry and UV-vis spectroscopy.[79] Deoxygenation of 3 mL Hb samples in large volume tonometers was achieved by repetitive pump-purge cycles of N_2 and vacuum at 20°C. A gastight syringe was used to inject measured volumes of room air through the rubber septum of the tonometer containing the Hb sample. After each addition, the tonometers were rotated in a water bath for 10 min before an absorbance spectrum was measured. At each equilibration step the P_{O2} was calculated and changes in the visible absorption spectrum were measured at three wavelengths on an HP-diode array spectrophotometer. The concentrations determined from the three wavelengths were averaged and used to calculate the corresponding fractional O_2 saturation.

2.3 Thermodynamic Investigations of Root Effect Hemoglobins

2.3.1 Results

2.3.1.1 Spectroelectrochemistry Control Experiments

Sperm whale myoglobin (swMb) provided by Dr. Bonaventura served as a standard for the SEC technique and equipment. The electrochemical behavior of swMb was tested under the following conditions: 0.21 mM swMb, 0.05 M Hepes buffer, 0.2 M

KCl, pH = 7.1, 1.2 mM $Ru(NH_3)_6Cl_3$, and 20°C. The average $E_{1/2}$ value of four determinations was 23 $\pm$ 3 mV and the average n_{50} value was 1.04 $\pm$ 0.08. These data correspond to previous studies of swMb using our method of SEC and confirms the Nernst behavior of swMb is non-cooperative.[29]

2.3.1.2 Electrochemical Investigations in Hepes Buffer

Figure 2.8 displays the change in absorbance spectra with applied potential for Carp Hb in Hepes buffer at pH 7. This plot is representative of all the experiments performed in Hepes buffer.

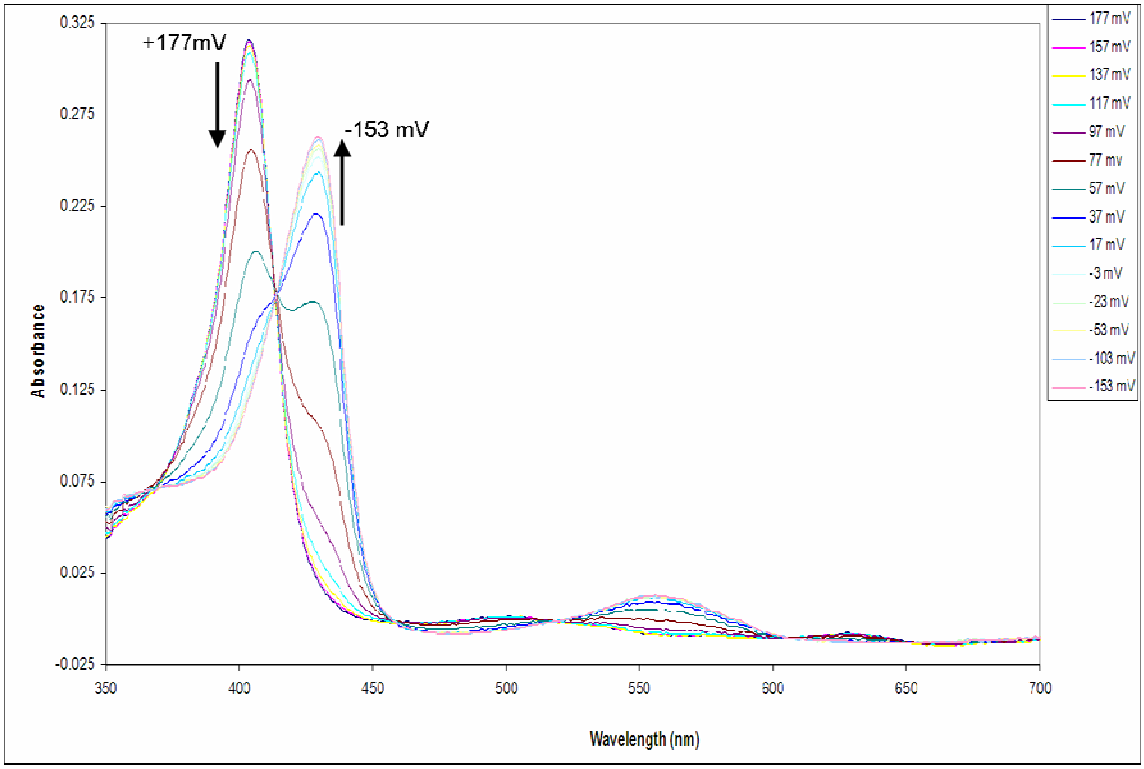

Figure 2.8: UV-vis absorbance spectra as a function of E_{app} of Carp Hb. Conditions: 0.07 mM Hb, 0.05 M Hepes buffer, pH 7, no added electrolyte, 1 mM $Ru(NH_3)_6Cl_3$, and 20°C. Potentials reported vs. NHE.

A stable baseline and six easily identifiable isosbestic points (located near 370, 415, 455, 515, 605, 650 nm) are characteristic of a clean reaction with two absorbing species in solution and no occurrence of side reactions. Absorbance data were collected at 405 and 430 nm for each experiment. Figures 2.9 and 2.10 show the Nernst plots for the sets of experiments for Carp Hb and HbA_o as a function of pH respectively. The deviation from the characteristic sigmoidal shape observed in the HbA_o Nernst plot is due to the lack of background electrolyte in the sample.

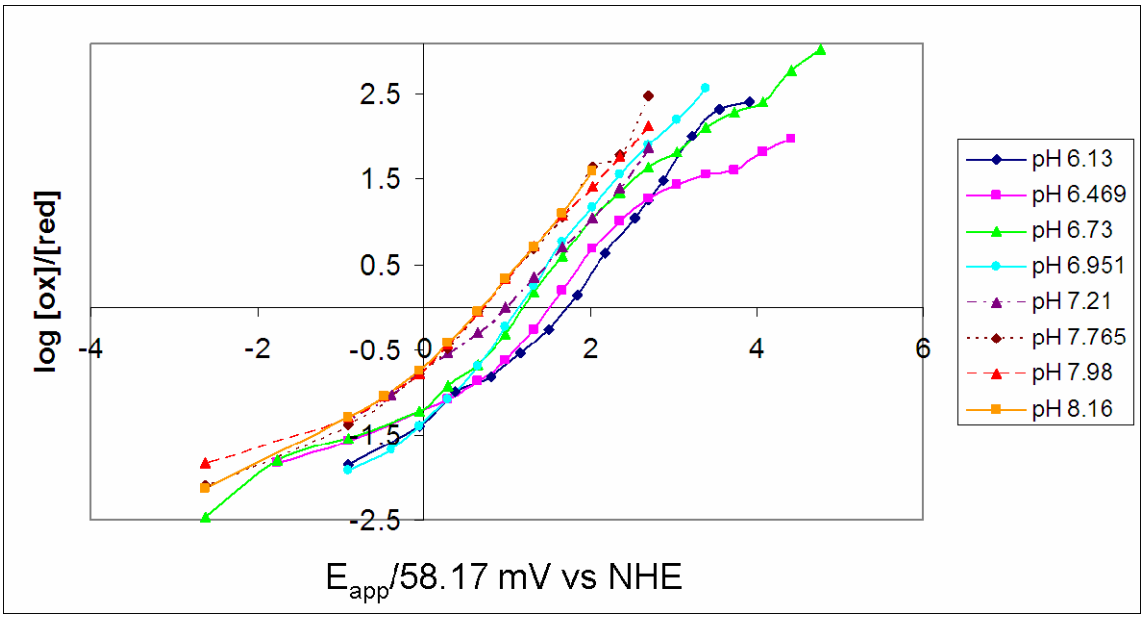

Figure 2.9: Nernst plots of Carp Hb at various pH values measured at 430 nm. Conditions: 0.03 mM - 0.09 mM Hb, 0.05 M Hepes buffer, no added electrolyte, 1 mM $Ru(NH_3)_6Cl_3$, and 20°C.

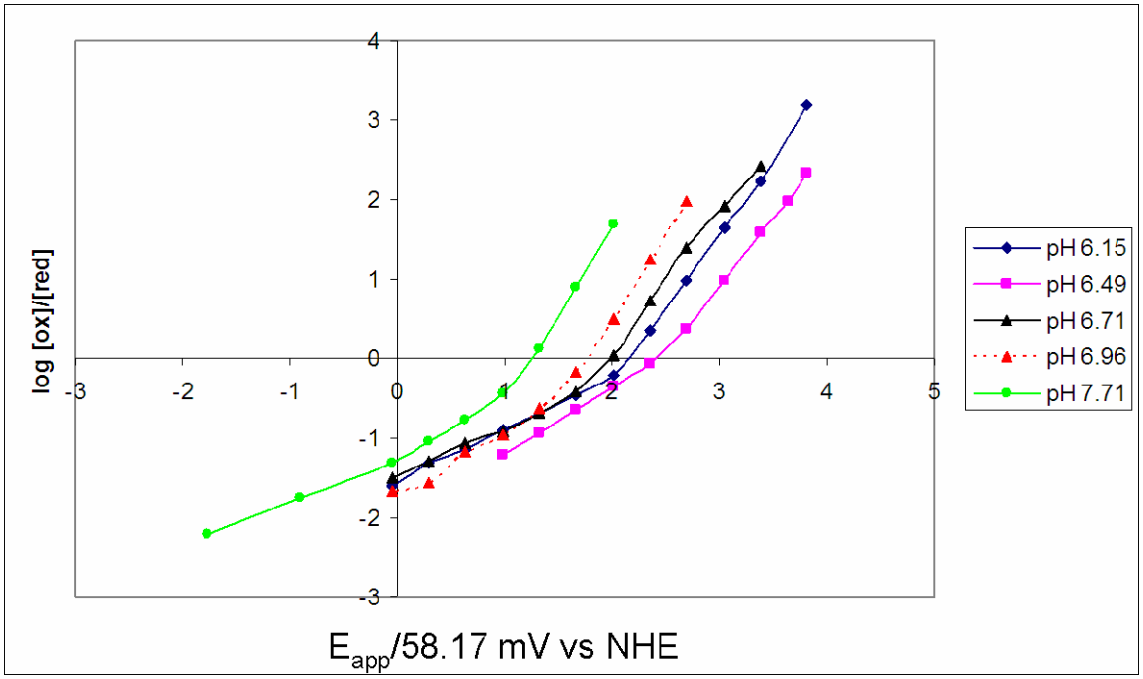

Figure 2.10: Nernst plots of HbA$_o$ at various pH values measured at 430 nm. Conditions: 0.03 mM - 0.09 mM Hb, 0.05 M Hepes buffer, no added electrolyte, 1 mM $Ru(NH_3)_6Cl_3$, and 20°C.

In addition to Carp Hb, Spot Hb also exhibits the Root Effect. As described in Section 2.1.3, preliminary results on the effect of pH on in the $E_{1/2}$ of Spot fish were reported by Kraiter and Crumbliss.[33, 43] Here we include Kraiter's data for Spot Hb in Hepes buffer at various pHs with no anionic effectors for comparison with the data collected by the author for Carp Hb and HbA$_o$ under the same conditions. Figure 2.11 depicts a representative Nernst plot for Spot Hb, Carp Hb, and HbA$_o$ in Hepes buffer at pH 7.

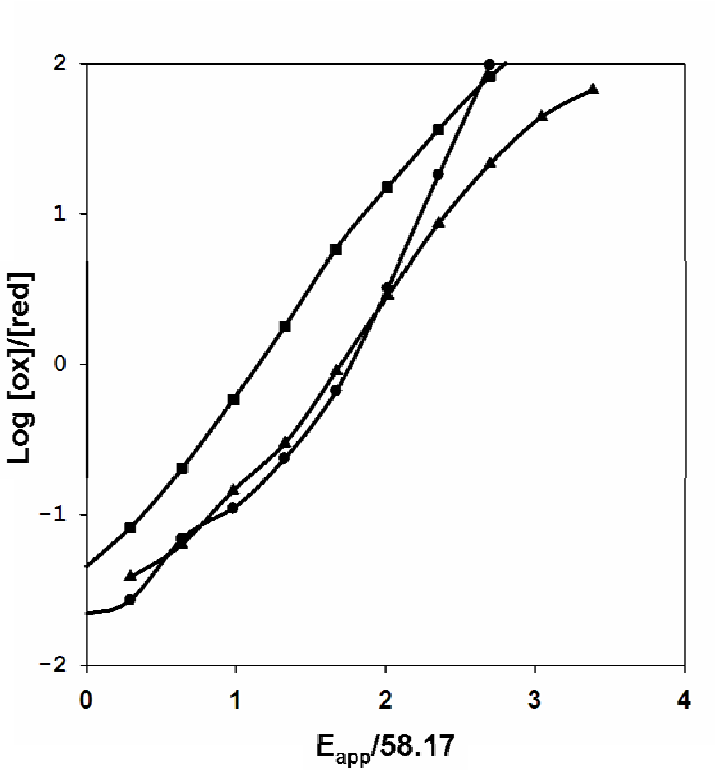

Figure 2.11: Nernst plots of Carp Hb (squares), Spot Hb (triangles), and HbA_o (circles) at pH 7 measured at 430 nm. E_{app} reported as mV vs. NHE. Conditions: 0.03 mM - 0.09 mM Hb, 0.05 M Hepes buffer, no added electrolyte, 1 mM $Ru(NH_3)_6Cl_3$, and 20°C. Spot Hb data was obtained from reference [43].

The slope at the $E_{1/2}$ of HbA_o, the oxidation n_{50} value, is 2.0 while Spot and Carp Hbs exhibit mid-point slopes of ~1.5.

2.3.1.3 Oxygen Binding Studies in Hepes Buffer

Oxygen binding studies on the Spot, Carp, and HbA_o Hbs under the same conditions as the SEC experiments were performed at the DUML by members of Dr. Celia Bonaventura laboratory. Figure 2.12 depicts the Hill plots of each Hb at pH 7 in Hepes buffer.

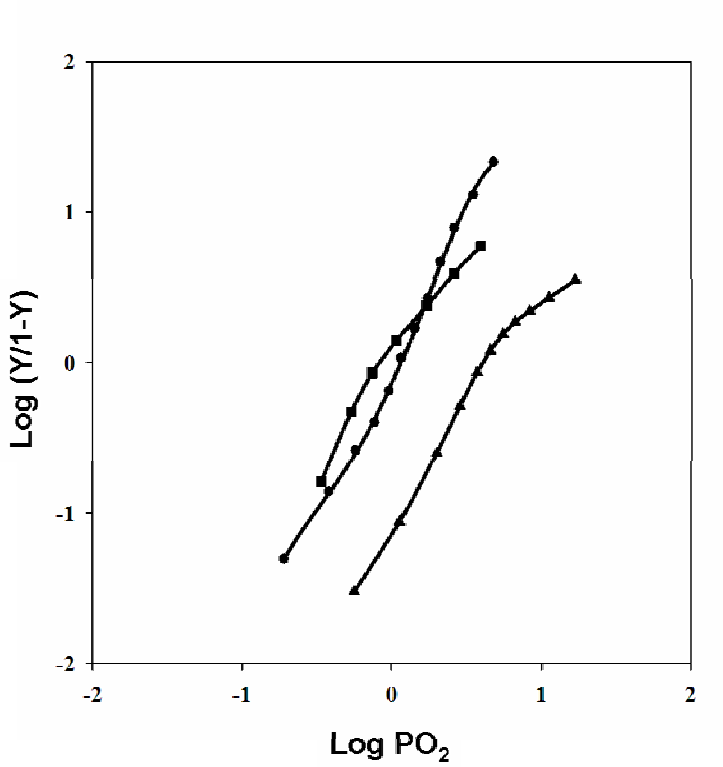

Figure 2.12: Hill plots for oxygen binding of Carp Hb (squares), Spot Hb (triangles), and HbA_o (circles) pH 7. Conditions: 0.03 mM - 0.09 mM Hb, 0.05 M Hepes buffer, no added electrolyte, and 20°C. Data collected at the DUML under the supervision of Dr. Bonaventura.[49]

The slope at the Log P_{50} of HbA_o, the oxygenation n_{50} value, is 2.7, indicative of significant cooperativity in the O_2 binding process. The n_{50} values for the Hill plots of Carp Hb and Spot Hb are similar to that of HbA_o.

2.3.1.4 pH Trends in Hepes Buffer

The oxidation and oxygenation behavior of the three Hbs were studied at various pH values in Hepes buffer. Figure 2.13 shows the Log P_{50} values and the $E_{1/2}$ values for the three Hb species as a function of pH in panels A and B respectively.

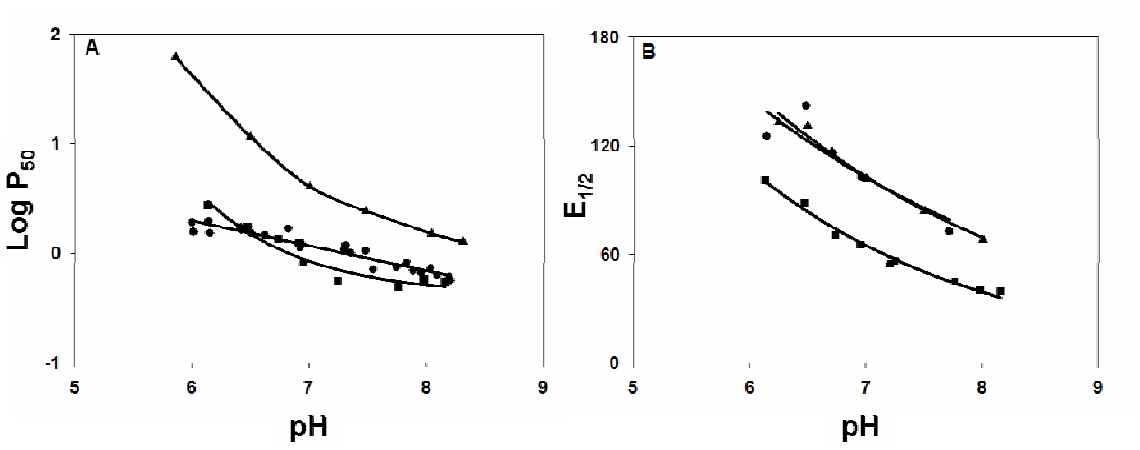

Figure 2.13: A) Oxygen affinity (Log P_{50}) values as a function of pH for Carp Hb (squares), Spot Hb (triangles), and HbA_o (circles), in Hepes buffer. Conditions 0.03 mM - 0.09 mM Hb, 0.05 M Hepes buffer, no added electrolyte, and 20°C. Data collected under the supervision of Dr. Celia Bonaventura at the DUML.[49] B) Redox potentials ($E_{1/2}$ reported as mV vs. NHE) of Carp Hb (squares), Spot Hb (triangles) and HbA_o (circles) as a function of pH determined by SEC. Spot Hb data was obtained from reference [43]. Conditions: 0.03 mM - 0.09 mM Hb, 0.05 M Hepes buffer, no added electrolyte, 1 mM $Ru(NH_3)_6Cl_3$, and 20°C. Each data point is the average $E_{1/2}$ value calculated from the oxidized species (405 nm) and reduced species (430 nm) in the same trial. The error associated with each data point calculated using this method is ~5 mV for these samples.

The results of the oxygenation and oxidation studies of the three Hbs in Hepes buffer at pH 6.5 and pH 7 specifically are tabulated in Table 2.1.

Table 2.1: Oxygen affinities (Log P_{50}) and the reduction potentials ($E_{1/2}$) in mV vs. NHE for Spot, Carp, and HbA_o Hbs at pH 6.5 and 7 in Hepes buffer.

Hbs in Hepes	Log P_{50}# pH 6.5	Log P_{50}# pH 7	$E_{1/2}$* pH 6.5	$E_{1/2}$* pH 7.0
Spot	1.05	0.6	131	102
Carp	0.35	-0.1	88.5	65.5
HbA_o	0.2	0.1	142	102.5

Reference: [49]

* This work

2.3.1.5 Oxidation and Oxygenation Studies in Phosphate Buffer

The oxidation and oxygenation properties of the three Hbs were also studied in phosphate buffer at two pH values (6.5 and 7). These data are summarized below in Table 2.2. Phosphate is an allosteric effector that stabilizes the T-state of these tetrameric Hbs (Spot Hb, Carp Hb and HbA_o). As expected, in the presence of phosphate the $E_{1/2}$ values for all of the Hbs are larger than in the absence of phosphate (compare Tables 2.1 and 2.2). As the pH is changed from pH 6.5 and 7 in phosphate buffer, the $E_{1/2}$ values for the three Hbs changed less than 15 mV.

Table 2.2: Oxygen affinities (Log P_{50}) and the reduction potentials ($E_{1/2}$) in mV vs. NHE for Spot, Carp, and HbA_o Hbs at pH 6.5 and 7 in phosphate buffer. Conditions: 0.2 M phosphate buffer, no added electrolyte, and 20°C. For SEC, 1 mM $Re(NH_3)_6Cl_3$ was used as a mediator and reported $E_{1/2}$ values of are the average of the $E_{1/2}$ values calculated from the oxidized species (405 nm) and reduced species (430 nm) in the same trial. The error associated with each average $E_{1/2}$ is less than 5 mV.

Hbs in Phosphate	Log P_{50}# pH 6.5	Log P_{50}# pH 7	$E_{1/2}$* pH 6.5	$E_{1/2}$* pH 7.0
Spot	2.5	1.5	152	148.5
Carp	1.37	0.85	133	120
HbA_o	1	0.87	151.5	144

Reference: [49]

* This work

2.3.1.6 Summary of Results

The bar graphs shown in Figure 2.14 illustrate the Log P_{50} and $E_{1/2}$ values at pH 6.5 and 7 in Hepes buffer and phosphate buffer for Spot Hb, Carp Hb, and HbA_o.

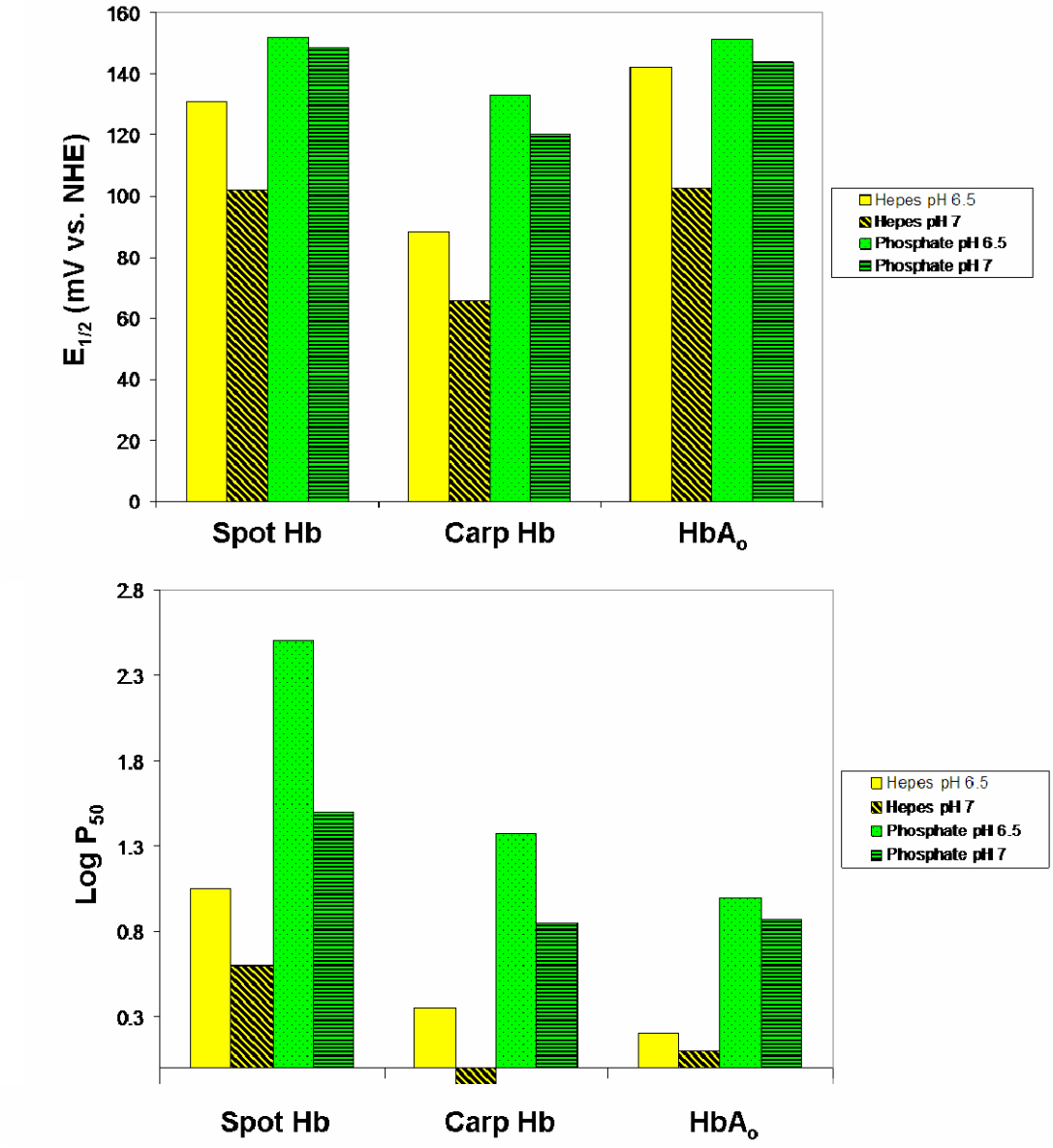

Figure 2.14: Summary of oxygenation (Log P_{50}) [49] and oxidation ($E_{1/2}$) results for Spot Hb, Carp Hb, and HbA_o in two buffers at two pH values. Identical data are also tabulated in Tables 2.1 and 2.2.

2.3.2 Discussion

2.3.2.1 Oxygenation

As shown in Figure 2.12 and Table 2.1, Carp Hb and HbA_0 showed similar Log P_{50} values, while Spot Hb showed significantly lower oxygen affinity (higher $LogP_{50}$ value) in 0.05 M Hepes buffer at pH 7 without anionic effectors. All three Hill plots show some sigmoidal character, indicative of cooperative oxygen binding. However, the Hill plots for the Carp and Spot Hbs deviate from the sigmoidal shape near full oxygenation of the sample. This decrease in cooperativity reflects the difficulty of completely oxygenating Root effect Hbs at and below pH 7.

The oxygen affinities (Log P_{50} values) of the three Hbs in Hepes buffer were affected in dramatically different ways by changes in pH (Figure 2.13, panel A). The oxygen affinities of Carp and Spot Hbs are much more sensitive to changes in pH compared to HbA_o. This phenomenon known as the Root Effect is depicted in Figure 2.13, panel A, where the slope of the curves fit to the Spot Hb and Carp Hb data is steep between pH 6 and pH 7 compared to the gradual change of the HbA_o data as a function of the same pH variation (the Bohr Effect).

The oxygen affinities of the three Hbs were also measured in phosphate buffer (Table 2.2). All three Hbs showed lower oxygen affinities (larger Log P_{50} values) in the presence of the anion effector as expected (Figure 2.14, bottom panel). The change in oxygen affinity for each of these Hbs in phosphate buffer as the pH is reduced from 7 to 6.5 is also tabulated in Table 2.2 and Figure 2.14. Spot Hb and Carp Hb were much more

sensitive to changes in pH under these conditions compared to the relatively small change in oxygen affinity for HbA_o as the pH is changed (Table 2.2 and Figure 2.14).

The oxygen binding studies performed by our collaborators demonstrate again that Spot and Carp Hbs exhibit the Root Effect and provide a context for the anaerobic oxidation studies performed by the author.[49]

2.3.2.2 Anaerobic Oxidation

Carp Hb, Spot Hb, and HbA_o were studied using SEC at different pHs in the presence and absence of allosteric effector. As shown in Figure 2.8 (which is representative of all of the SEC data for these systems), Carp Hb exhibited expected behavior, characteristic of only two species (reduced and oxidized Hb) in solution and no absorbance contribution from the mediator. Further, as expected, the Nernst plots at all pH values for Carp Hb showed a basic sigmoidal trend and the $E_{1/2}$ values decreased as a function of increasing pH (Figure 2.9). As shown in Figure 2.10, the Nernst plots of HbA_o did not exhibit the ideal sigmoidal shape due to the lack of electrolyte in the sample. However, as expected the $E_{1/2}$ values decrease as a function of increasing pH. For ease of comparison, Figure 2.11 displays a representative Nernst plot for Carp Hb, Spot Hb, and HbA_o in Hepes buffer at pH 7. The Spot Hb data are reproduced from references [33, 43]. All three Hbs display some level of sigmoidal shape indicative of

cooperative redox reactions and at pH 7, Spot Hb and HbA_o are more easily reduced than Carp Hb.

As shown in Figure 2.13 panel B, the reduction potentials ($E_{1/2}$) of all three Hbs in Hepes buffer decrease ~60 mV, as pH is increased from 6 to 8.5. These trends indicate that Hbs from all three species have the same level of sensitivity to changes in environmental pH, with respect to reduction potential. The specific $E_{1/2}$ values at pH 6.5 and 7 in Hepes buffer are tabulated in Table 2.1. The similarity of these responses is interesting given that the change in O_2 affinity as pH is increased is dramatically different for Root Effect Hbs compared to HbA_o.

A decrease in reduction potential at higher pH values means the heme-bound iron is more easily reduced in lower pH environments. Deoxy-Fe(II)-Hb is the product of this reduction and is a model for the low oxygen affinity T-state conformation of Hb. This ease of reduction at low pH values, termed the Redox Bohr Effect, is consistent with the observation that the Hb of any species unloads its O_2 as the pH is decreased (the Bohr Effect).

The influence of pH on the $E_{1/2}$ of each species was also observed in conditions of 0.2 M phosphate buffer (Table 2.2). Two pH values (pH 6.5 and pH 7) were used to represent the biological range of interest. All three Hbs in the presence of inorganic phosphate were more easily reduced compared to the studies in Hepes buffer (Figure 2.14). This indicates a shift toward the T-state caused by the presence of the allosteric

effector and can be seen by the more positive reduction potentials reported in Table 2.2 compared to those reported in Table 2.1, as graphed in Figure 2.14.

Also shown in Figure 2.14 and tabulated in Table 2.2, all three Hb samples in the phosphate buffer had a more positive reduction potential at pH 6.5 than at pH 7. This finding is consistent with the studies performed in Hepes buffer (also Figure 2.14) and with the Redox Bohr Effect. Similar to the behavior in Hepes buffer, in phosphate buffer there is also not a dramatic difference observed between species, when comparing the pH sensitivity of the respective reduction potentials. For each species, a change of only 3 - 13 mV was seen for the $E_{1/2}$ value as pH was decreased in presence of the anionic effector.

Regardless of buffer, HbA_o and the Hbs from representative Root Effect fish (Spot and Carp) show the same pH-sensitivity when measuring reduction potential ($E_{1/2}$). Therefore, we do not observe a Redox Root Effect. It follows that the observed pH-sensitivity of anaerobic oxidation potentials is not consistent with the heightened pH-sensitivity observed for oxygen affinity of Root Effect Hbs.

2.3.2.3 Analysis of Cooperativity

For systems that behave in a non-Nernstian fashion, the n-value derived from the slope of the sigmoidal Nernst plot reflects the cooperativity of the system (see Section

2.1.2). Figure 2.15 shows the n-value calculated at the $E_{1/2}$ (termed the n_{50} value) as a function of pH for Carp Hb, Spot Hb, and HbA_o.

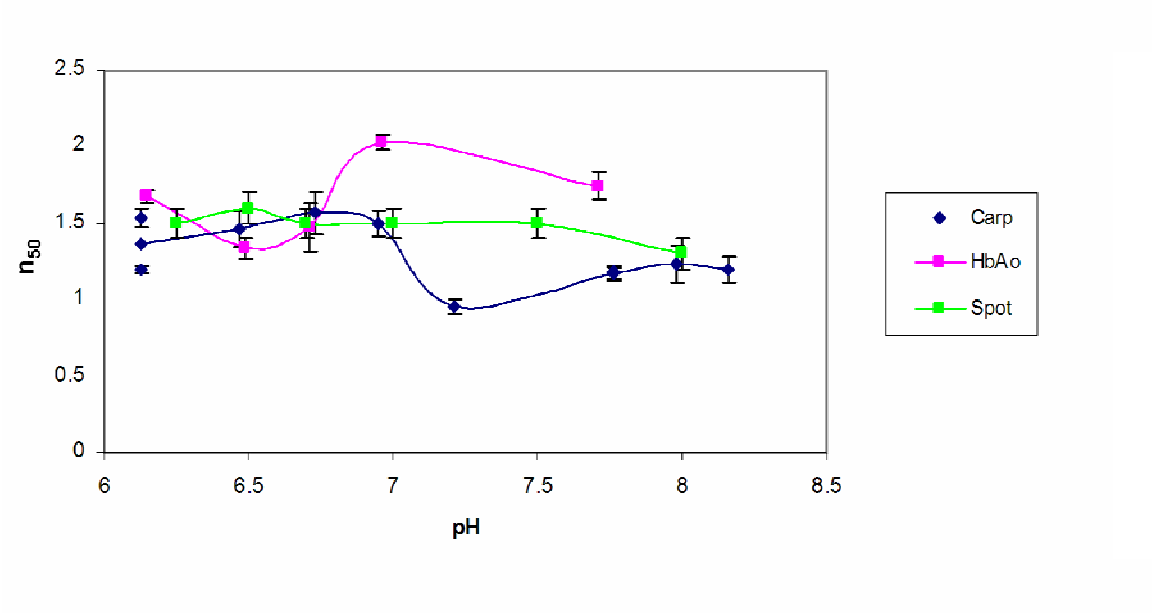

Figure 2.15: Dependence of n_{50} values for oxidation as a function of pH for HbA_o, Spot Hb, and Carp Hb in Hepes buffer. Spot Hb data were reproduced from reference [43]. n_{50} values shown are the average of data collected at two different wavelengths in one experiment. Error bars indicated the difference between two calculated values. Spline curves included between data points to aid visualization.

An increase in cooperativity is seen for Carp Hb around pH 7, while a decrease in cooperativity is observed at pH 6.5 for HbA_o. The fact that the shift in the cooperativity of the oxidation reaction, occurs at a higher pH for Carp Hb (between pH 6.9 and 7.2) compared to HbA_o (between 6.1 and 6.4) is consistent with the fact that the oxygenation reaction of Carp Hb is more sensitive to changes in pH around pH 7 compared to HbA_o.

Although the $E_{1/2}$ values do not show a difference in pH-sensitivity between species in Hepes buffer (slopes in Figure 2.13), the change in cooperativity of the electron transfer reaction (Nernst n-value) may indicate a conformational change in the protein that changes the extent of cooperation between the hemes. The $E_{1/2}$ value is an average of the reduction potentials of each monomer subunit. Measurement of this parameter may not be sensitive enough to determine a shift in populations of conformers. Interestingly, as shown in Figure 2.15, the level of cooperativity exhibited by Spot Hb remains constant across all pH values studies.

Figure 2.16 shows the relationship between pH and the n_{50} values for each species in a 0.2 M phosphate buffer.

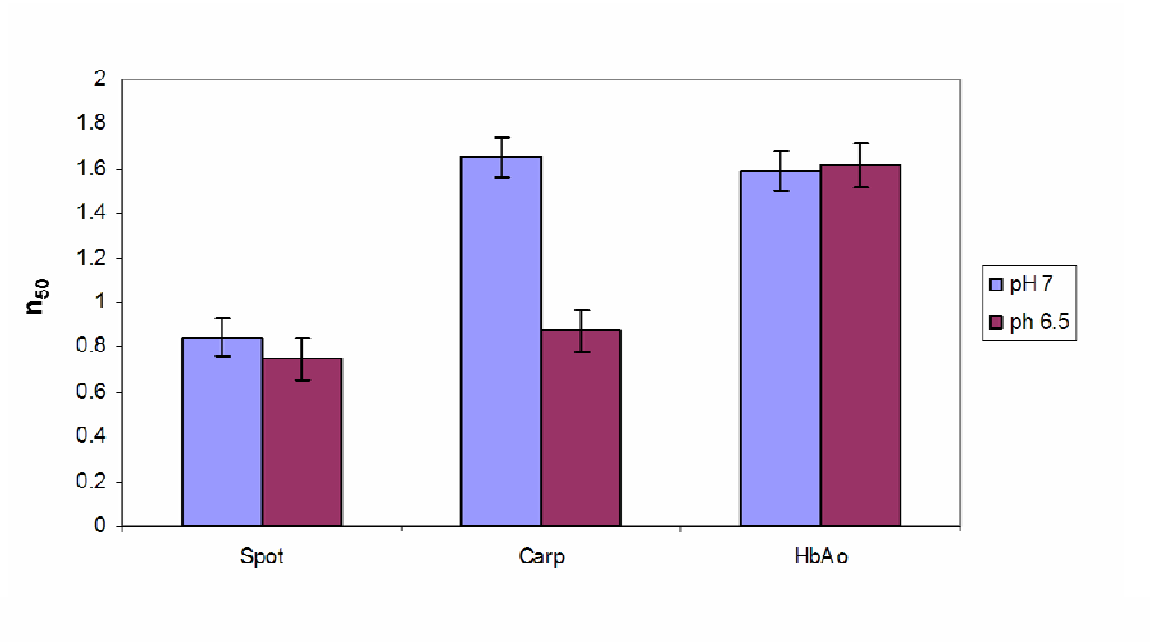

Figure 2.16: Average n_{50} values for each Hb species in phosphate buffer at pH 6.5 and pH 7. Error bars indicate the difference between the n_{50} values calculated from difference wavelengths in one experiment.

The cooperativity (n_{50} value) of Spot Hb is not affected by changes in pH in either buffer system. As expected however, the presence of phosphate does decrease the cooperativity of Spot Hb (compare Spot Hb n_{50} values in Figure 2.15 and 2.16) consistent with allosteric stabilization of the T-state. In the presence of phosphate the cooperativity of HbA_o is also decreased and, consistent with allosteric T-state stabilization, the cooperativity of the oxidation process is less sensitive to changes in pH (compare HbA_o n_{50} values in Figure 2.15 and 2.16). Interestingly, the cooperativity of Carp Hb responds in opposite directions to changes in pH when phosphate is present or not. As seen in Figure 2.15, the n_{50} value of Carp Hb increases upon acidification in the absence of allosteric effector. However, in the presence of phosphate (Figure 2.16), the n_{50} value decreases upon acidification.

In order to better understand the differential changes in cooperativity of the Hbs we also calculated another parameter that reflects the cooperativity of a Hb, the n_{max} value. The n_{max} value denotes the largest slope of the Nernst plot and is not set at a particular E_{app}.[13] The n_{max} values, shown in Figure 2.17, for each Hb in phosphate buffer show similar trends as the n_{50} values (Figure 2.16).

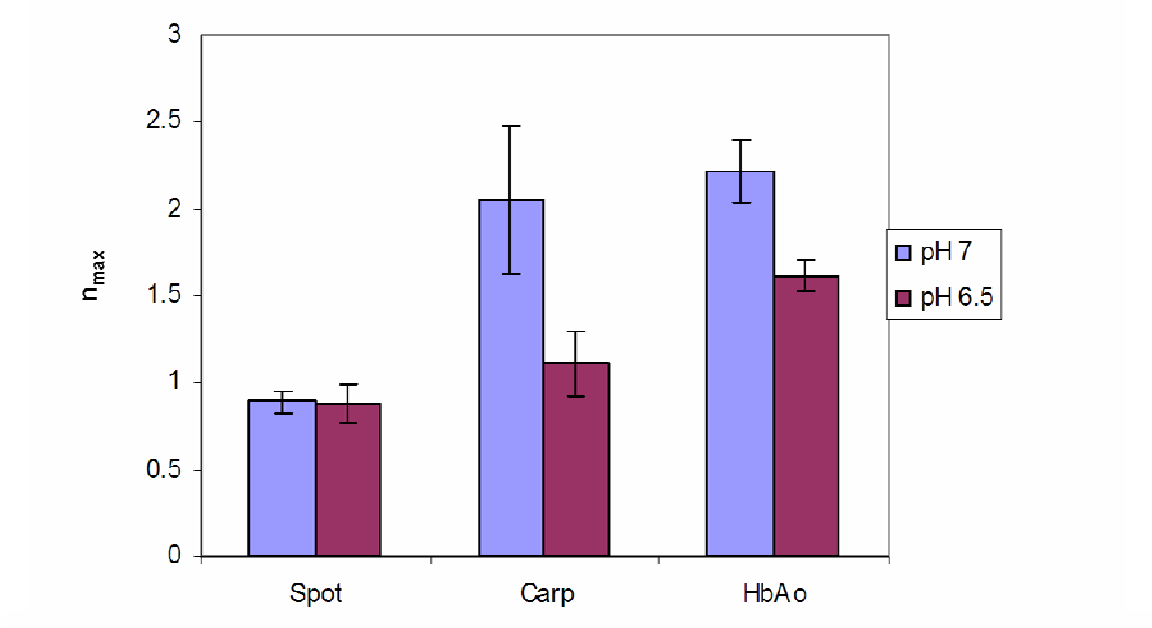

Figure 2.17: Average n_{max} values for each Hb species in phosphate buffer at pH 7 and pH 6.5. Error bars indicate the difference between the n_{max} calculated from difference wavelengths in one trial.

Like the n_{50} value, the n_{max} value of Spot Hb in phosphate buffer is not affected by changes in pH. The n_{max} value of HbA_o does respond to acidification, where as the n_{50} value does not. The lack of a response in n_{50} value is likely due to the lack of a background electrolyte in the OTTLE cell which alters the ideal sigmoidal behavior of HbA_o. When examining the effect of allosteric effector on the n-values of HbA_o (Figure 2.15 and 2.17), we observe that upon acidification the cooperativity of HbA_o is decreased regardless of the presence of phosphate.

Now we return to the opposite responses of the n_{50} value of Carp Hb to changes in pH when phosphate is present or absent. The n_{max} values of Carp Hb in phosphate buffer decrease upon acidification, similar to the n_{50} values in the presence of allosteric

effector (note the n_{50} values and the n_{max} values are derived from the same data sets in phosphate buffer). The data presented in Figures 2.15 - 2.17 suggests that the presence of phosphate significantly impacts the cooperativity of the oxidation process for Carp Hb.

The data presented in this section suggest that Carp Hb, HbA_o and Spot Hb respond differently to changes in pH, when measuring the cooperativity of the redox reaction. These electrochemical observations are consistent with the observation that decreases in pH drastically affect the deoxygenation of Carp Hb, while HbA_o is only affected minimally. Interestingly, Spot Hb may show an intermediate response when compared to HbA_o and Carp Hb.

However, the differences observed for the cooperativity of the redox reaction for the three Hbs are subtle interpretations of complicated electrochemical data and do not fully explain the significantly different responses to changes in pH observed for the oxygenation reactions of these Hbs. As well, the n-values reported here for the oxidation process may reflect any heterogeneity between the active sites of each Hb in addition to cooperativity between the sites. Although insight can be gleaned by studying the cooperativity of the redox reaction regarding the thermodynamic changes in a Hb, these arguments do not completely explain the Root Effect. For a more quantitative perspective on the effect of pH on oxygenation and anaerobic oxidation we now turn to free energy comparisons.

2.3.2.4 Free Energies of Oxygenation and Oxidation

Another way to examine the effect of pH on the oxygenation and oxidation processes of Hbs is to calculate the change in free energy (ΔΔG) of both reactions as a function of pH. That is ΔΔG is defined as the difference in the ΔG of oxygenation or oxidation at two different pH values. By calculating the change in free energy (ΔΔG) for oxidation and for oxygenation, the pH-sensitivities of the two processes can be compared quantitatively.

In order to calculate ΔΔG for oxygenation, we will first review the significance of the Log P_{50} value. The equilibrium constant K for the oxygenation reaction shown in Equation 2.13 is described below in Equation 2.14.

$$Hb + O_2 \leftrightarrows HbO_2 \tag{2.13}$$

$$K = \frac{[HbO_2]}{[Hb]P_{O_2}} \tag{2.14}$$

By definition the pressure at which 50% of the Hb is oxygenated and 50% is deoxygenated is the P_{50}. This relationship is shown in Equation 2.15.

$$K = \frac{1}{P_{50}} \tag{2.15}$$

Using the Gibbs Free Energy equation (Equation 2.16), we can relate P_{50} to the free energy (ΔG) associated with the oxygenation reaction as shown in Equation 2.17.

$$\Delta G = -RT(\ln K) \tag{2.16}$$

$$\Delta G = RT(\ln P_{50}) \tag{2.17}$$

To calculate the ΔΔG as a function of changes in pH we must calculate the difference between the ΔG value at one pH and the ΔG value at another pH. Here we have chosen to examine the effect of changing the pH from 7 to 6.5. This pH range will be used consistently for comparing the oxygenation and oxidation reactions in both buffer systems (Hepes buffer and phosphate buffer). The modified version of Equation 2.17, which allows the calculation of the ΔΔG value for the effect of changes in pH on the oxygenation process, is shown in Equation 2.18.

$$\Delta\Delta G = RT(\ln P_{50}{}^{pH\,6.5} - \ln P_{50}{}^{pH\,7.0}) \tag{2.18}$$

Notice that the reported values of $\log P_{50}$ must be converted to $\ln P_{50}$ values. For Equations 2.16-2.18 the temperature, T, equals 293 K and the ideal gas constant, R, is -8.314 $JK^{-1}mol^{-1}$. The reported values of ΔG and ΔΔG have been converted to units of kcal (1 cal = 4.814 J) and have been multiplied by four to describe the Hb tetramer rather than just one heme.[25] ΔG and ΔΔG values are reported using the absolute value of for ease of comparison.

In order to calculate ΔΔG for anaerobic oxidation, we used Equation 2.19 to relate $E_{1/2}$ for each oxidation reaction (Equation 2.20).

$$\Delta G = -nFE_{1/2} \tag{2.19}$$

$$\text{Fe(III)-heme} + e^- \leftrightarrows \text{Fe(II)-heme} \tag{2.20}$$

The modified version of Equation 2.19, which allows the calculation of the ΔΔG value for the effect of changes in pH (from 7 to 6.5) on the anaerobic oxidation process is shown in Equation 2.21.

$$\Delta\Delta G = -nF(E_{1/2}{}^{pH\,6.5} - E_{1/2}{}^{pH\,7.0}) \qquad (2.21)$$

An n-value of 4 is used to calculate the ΔΔG for the anaerobic oxidation the tetramer instead of just one heme.

Table 2.3 tabulates the oxygen affinities (Log P_{50}) and reduction potentials ($E_{1/2}$) of each Hb in Hepes buffer at pH 6.5 and 7 (the same information as in Table 2.1) with the corresponding ΔG and ΔΔG values (for the change in pH). Using Equation 2.22 below, the percent change in the free energy of the respective process (at pH 6.5) was calculated and is also included in Table 2.3.

$$\%change = \frac{\Delta\Delta G}{\Delta G^{pH\,6.5}} x100 \qquad (2.22)$$

Table 2.3: Thermodynamic parameters of Carp Hb, Spot Hb, and HbA_o in Hepes buffer.

	Anaerobic Oxidation					
Hbs in Hepes	$E_{1/2}$* pH 6.5	-ΔG (kcal) pH 6.5	$E_{1/2}$* pH 7.0	-ΔG (kcal) pH 7	ΔΔG (kcal)	% Change in ΔG
Spot	131	12.1	102	9.4	2.7	22
Carp	88.5	8.2	65.5	6.0	2.1	26
HbA_o	142	13.1	102.5	9.5	3.6	28

	Oxygenation					
Hbs in Hepes	Log P_{50}# pH 6.5	ΔG (kcal) pH 6.5	Log P_{50}# pH 7	ΔG (kcal) pH 7	ΔΔG (kcal)	% Change in ΔG
Spot	1.05	5.6	0.6	3.2	2.4	43
Carp	0.35	1.9	-0.1	0.5	2.4	129
HbA_o	0.2	1.0	0.1	0.5	0.5	50

Reference: [49]

* This work

In Hepes buffer, the free energy of the anaerobic oxidation of each Hb changes ~25% when the pH varies from 7 to 6.5 (Table 2.3). This shows that the effect of pH variation on the free energy (ΔG) associated with the anaerobic oxidation process is similar. Said another way, the pH-sensitivity of the heme-bound iron in each species is similar.

Conversely, the pH-sensitivity of the oxygenation of each species is quite different. As shown in Table 2.3, the free energy of the oxygenation reaction changes 43% for Spot Hb, 129% for Carp Hb, and 50% for HbA_o as a function of variation in pH. *These data suggest that thermodynamic properties of the heme-bound iron cannot account for the heightened sensitivity of the Root Effect Hbs observed for the oxygenation process under these conditions.*

The thermodynamic data for the oxygenation and oxidation of the Hbs in phosphate in buffer was also converted to free energy terms (Table 2.4).

Table 2.4: Thermodynamic parameters of Carp Hb, Spot Hb, and HbA_o in phosphate buffer.

	Anaerobic Oxidation					
Hbs in Phosphate	$E_{1/2}$* pH 6.5	-ΔG (kcal) pH 6.5	$E_{1/2}$* pH 7.0	-ΔG (kcal) pH 7	ΔΔG (kcal)	% Change in ΔG
Spot	152	14.0	148.5	13.7	0.3	2
Carp	133	12.3	120	11.1	1.2	10
HbA_o	151.5	14.0	144	13.3	0.7	5

	Oxygenation					
Hbs in Phosphate	Log P_{50}# pH 6.5	-ΔG (kcal) pH 6.5	Log P_{50}# pH 7	-ΔG (kcal) pH 7	ΔΔG (kcal)	% Change in ΔG
Spot	2.5	13.4	1.5	8.0	5.4	40
Carp	1.37	7.3	0.85	4.6	2.8	40
HbA_o	1	5.4	0.87	4.7	0.7	13

Reference: [49]

* This work

First we will compare the effect of the phosphate buffer on the free energy (ΔG values) of each process. Then we will return to our discussion of the pH-sensitivity of each process. For an alternative view of the free energy values, the ΔG values from Tables 2.3 and 2.4 are presented using bar graphs in Figure 2.18.

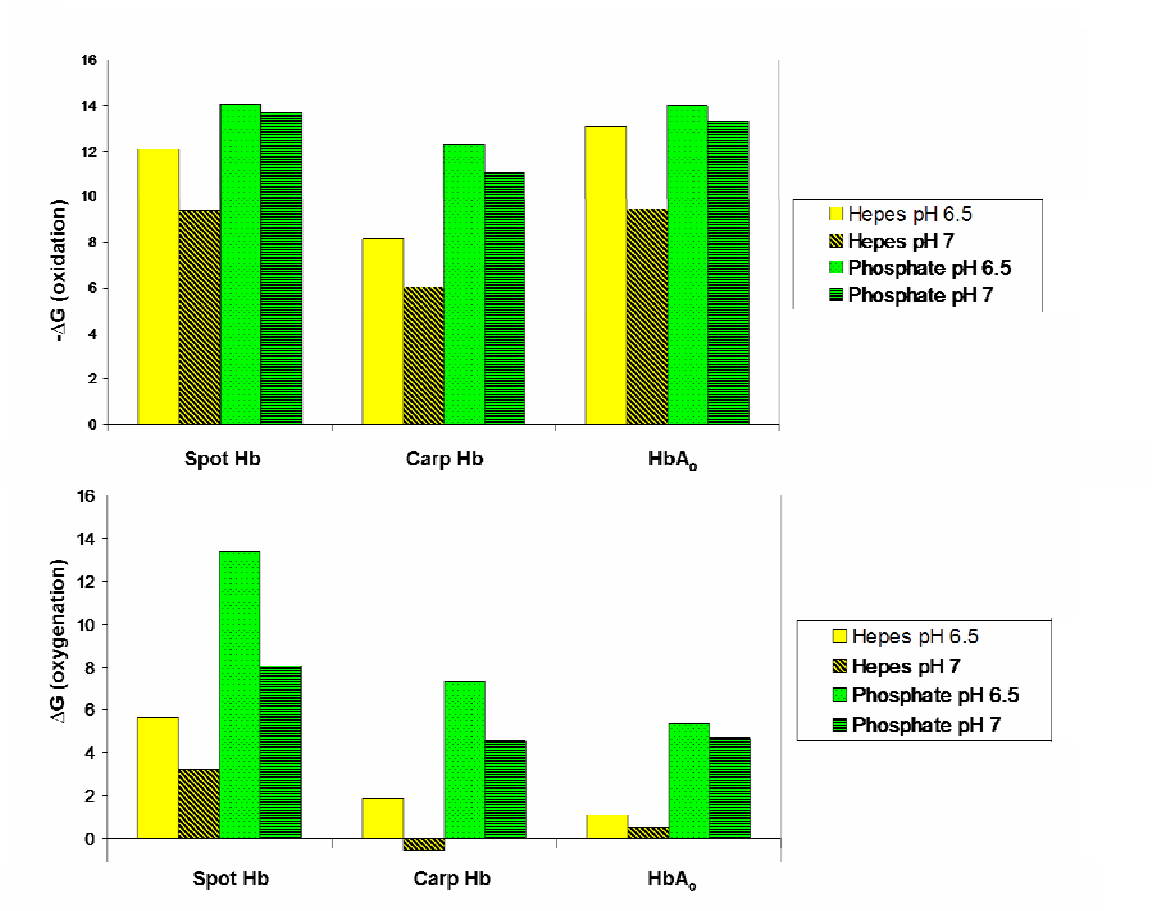

Figure 2.18: Comparison of ΔG values for anaerobic oxidation and oxygenation of Spot Hb, Carp Hb, and HbA_o in Hepes buffer and phosphate buffer at pH 6.5 and 7. The absolute values for ΔG of anaerobic oxidation are ploted for ease of comparison.

In phosphate buffer the Log P_{50} values and therefore the corresponding ΔG values for oxygenation are larger and more positive than those calculated for the data collected in Hepes buffer (Figure 2.19 and Tables 2.3 and 2.4). Phosphate has been shown to allosterically stabilize the low affinity T-state. The larger Log P_{50} values correspond to the increased energy requirement necessary to bind O_2 in the low affinity T-state.

The $E_{1/2}$ values measured in phosphate buffer are also larger and more positive than those measured in Hepes buffer (Table 2.3 and 2.4). Following the derivation discussed above, the $E_{1/2}$ values in phosphate buffer correspond to larger and more negative ΔG values compared to those for the Hepes buffer data. The absolute values of ΔG of anaerobic oxidation are presented in Figure 2.18. Larger and more negative ΔG values reflect the stabilization of the T-state by the phosphate effector, because T-state is easier to reduce (higher $E_{1/2}$).

Returning to the pH-sensitivity of each process, we see that in phosphate buffer the percent change in the free energy of the anaerobic oxidation process as a function of a 0.5 unit variation in pH is about ~5% for all three Hbs investigated (Table 2.4). The heme-bound iron ions of each Hb respond similarly to changes in pH. However, this observed response (5% change in ΔG of anaerobic oxidation) shows the Hbs are relatively insensitive to changes in pH when phosphate is present compared to the pH-sensitivity (~25%) observed in Hepes buffer (compared Tables 2.3 and 2.4). This differential response confirms that phosphate stabilizes the T-state of all three Hbs, making the anaerobic oxidation of each one less sensitive to pH variation.

Following the same trend, the presence of phosphate makes the oxygenation process of each Hb less sensitive to changes in pH. Comparing the percent change of ΔG for the oxygenation of each Hb as a function of pH (comparing between Tables 2.3 and 2.4), the pH-sensitivity of each Hb (oxygenation reaction) is dampened when phosphate

is present. In phosphate buffer, ΔG values for the oxygenation of Carp and Spot Hbs change 40% upon decreasing pH. In Hepes buffer, the change in ΔG is slightly higher for Spot (43%) and is dramatically different for Carp (130%). In phosphate buffer, the change in ΔG for HbA_o is 13%, while in Hepes buffer ΔG changes 50%. Similar to the oxidation data, this differential response in oxygenation to changes in pH whether phosphate is present or not, confirms that phosphate stabilizes the T-state of all three Hbs, making the oxygenation of each Hb less sensitive to pH variations.

Finally, by comparing the pH-sensitivity of the oxygenation process in the presence of phosphate with the pH-sensitivity of the anaerobic oxidation process in the presence of phosphate (Table 2.4), we see again that the oxygenation process is more sensitive to changes in pH than is the oxidation process. In phosphate buffer, the percent change in ΔG for the oxidation process is ~5%, for all three Hbs. However, the percent change in ΔG for the oxygenation process of Carp and Spot Hbs is 40% and for HbA_o is 13%. In all three cases, the oxygenation process is more sensitive to pH variation than the oxidation process. Further, the heightened pH-sensitivity of the Root Effect Hbs observed for the oxygenation process compared to the pH-sensitivity of HbA_o (the Bohr Effect) can not be explained by the thermodynamic properties of the heme-bound iron. Said another way, a Redox Bohr Effect is observed, however a Redox Root Effect is not observed.

2.3.2.5 Conclusions

The pH-sensitivity of the anaerobic oxidation process is similar for all three Hbs studies in phosphate buffer or Hepes buffer. Therefore, a Redox Root Effect was not observed in either Hepes buffer or phosphate buffer. It follows that the thermodynamic properties of the heme-bound iron cannot fully explain the observed difference in pH-sensitivity of the oxygenation process for Spot and Carp Hb compared to HbA_o. Additional factors must be considered when trying to explain the observed Root Effect for oxygen binding. For oxygen binding to occur, the oxygen molecule must enter the heme pocket prior to interacting with the heme. Given that the thermodynamic propensity of the heme-bound iron to be oxidized does not account for the entering ligand, we suggest that the steric hindrance of the heme pocket encountered by the entering ligand is the underlying factor causing the Root Effect.

2.4 Thermodynamic Investigations of Lucina pectinata Hemoglobins

2.4.1 Results

2.4.1.1 Oxygen Binding Studies

Representative Hill plots of oxygen binding by *Lucina* Hb I, *Lucina* Hb II and HbA_o are shown in Figure 2.19. *Lucina* Hbs I and II both have a higher oxygen affinity than HbA_o. Consistent with its monomeric structure, *Lucina* Hb I exhibited a Hill plot with unity slope. Although non-cooperative oxygen binding by both *Lucina* Hbs I and II

was previously reported [45], under our conditions some cooperativity was observed for *Lucina* Hb II. In our studies Hill plot slopes (n-values) at 20% saturation for *Lucina* Hb II were typically about 2, with lower values for partially oxidized samples. The Hill plots for *Lucina* Hb II consistently had slopes of unity above 60% saturation.

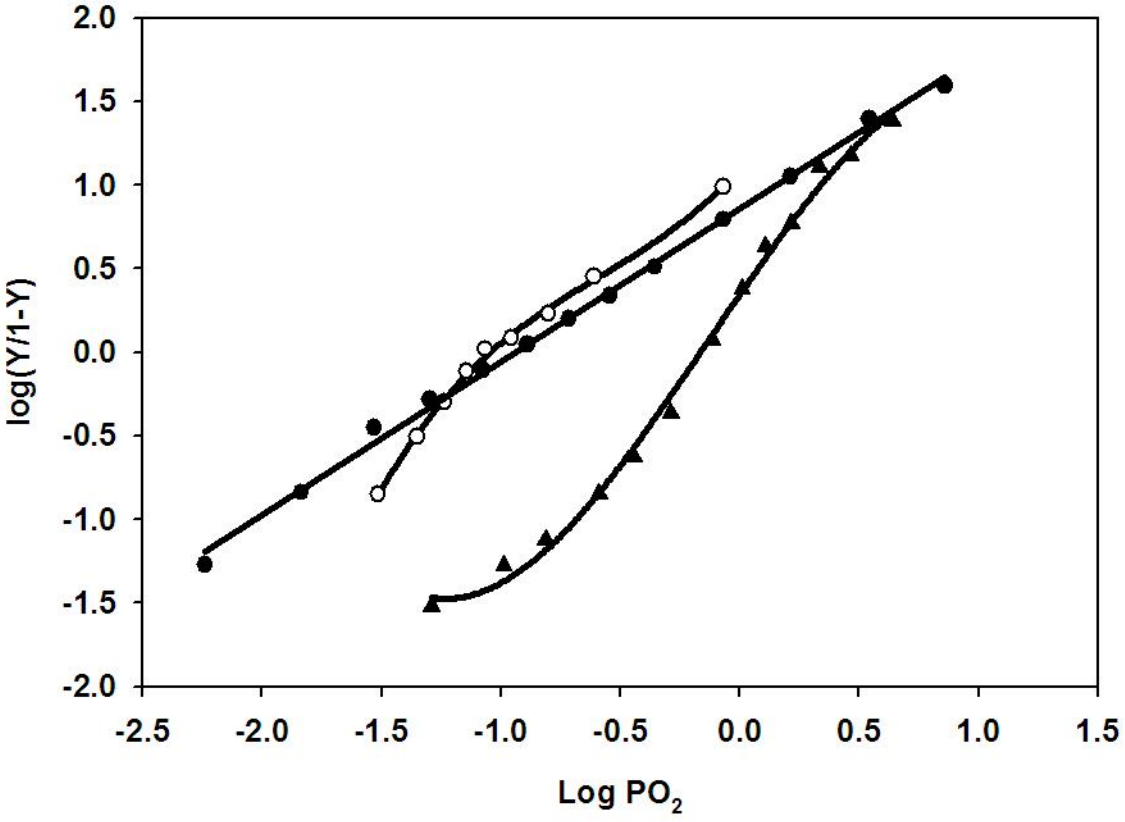

Figure 2.19: Hill plot of oxygen binding for *Lucina* Hb I (closed circles), *Lucina* Hb II (open circles), and HbA_o (closed triangles). Conditions: 0.05 M Bis-Tris buffer, pH 7.5, 20°C.[80]

Hill plots for oxygen binding by genetically engineered *Lucina* Hb I with Phe(B10)→Tyr(B10), show an increased oxygen affinity relative to native *Lucina* Hb I

(data not shown).[80] The oxygen tension required for half-saturation (Log P_{50} value) of the engineered Hb (see Section 2.1.4.1) is listed in Table 2.6 (Section 2.4.1.3) for comparison with the native *Lucina* Hbs.

2.4.1.2 Electrochemical Investigations

The anaerobic oxidation potentials of the normal and engineered forms of *Lucina* Hbs (see Section 2.1.4.1) were determined using SEC methods for obtaining accurate Nernst plots of the oxidation process. Figure 2.20 shows the spectral changes as a function of E_{app} for Hb I. Hb I required longer times (~30 min) to achieve equilibrium at each E_{app} relative to other species (normally ~15 min). However, Hb I yielded very clean isosbestic points and a stable baseline indicating a direct conversion between the oxidized and reduced forms of the protein.

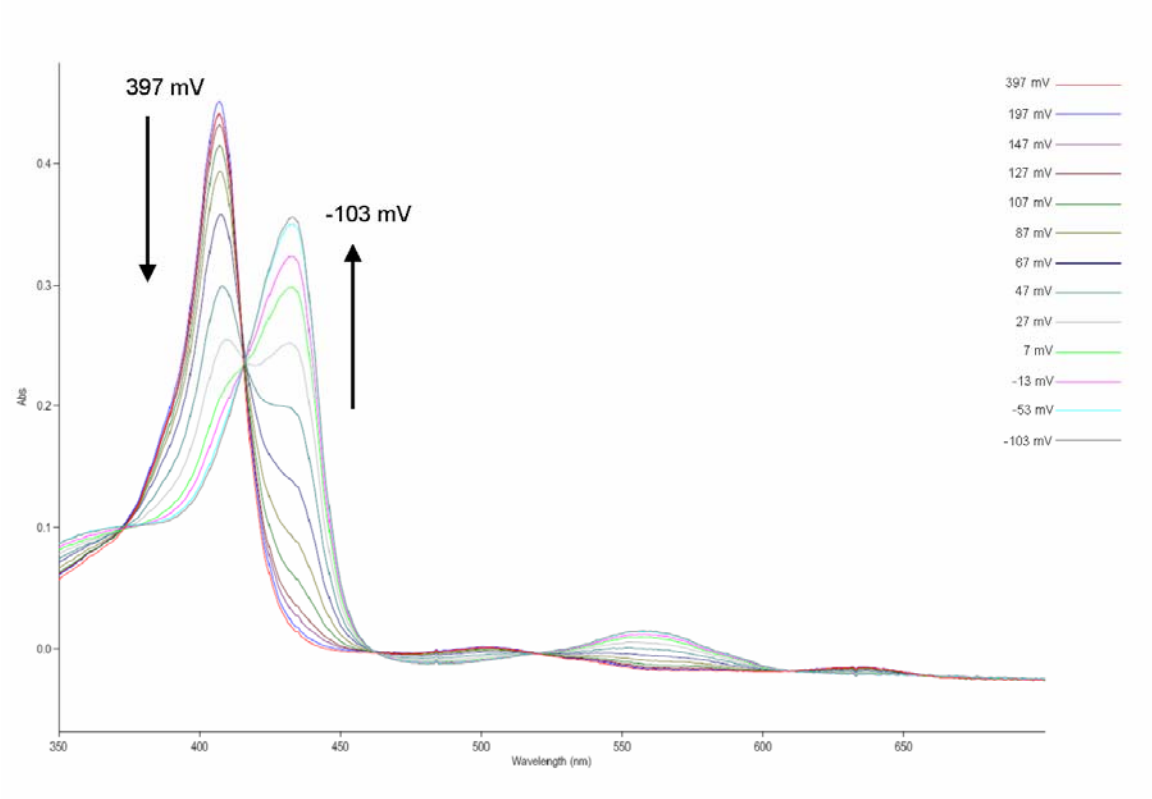

Figure 2.20: Spectral changes of *Lucina* Hb I as a function of E_{app}. E_{app} shown in the legend are vs. NHE. Conditions: 0.1 mM Hb, 50 mM Bis-Tris buffer, no additional salt, pH 7.5, at 20°C with 0.1 M KCl salt bridges.

Hb II required about an hour to come to equilibrium at each potential, compared to the usual 15 min for Carp Hb or swMb. Figure 2.21 shows spectral changes of Hb II as a function of E_{app}. The isosbestic point at 416 nm between the two Soret bands is not ideal, but the baseline is stable and the other isosbestic points are clean.

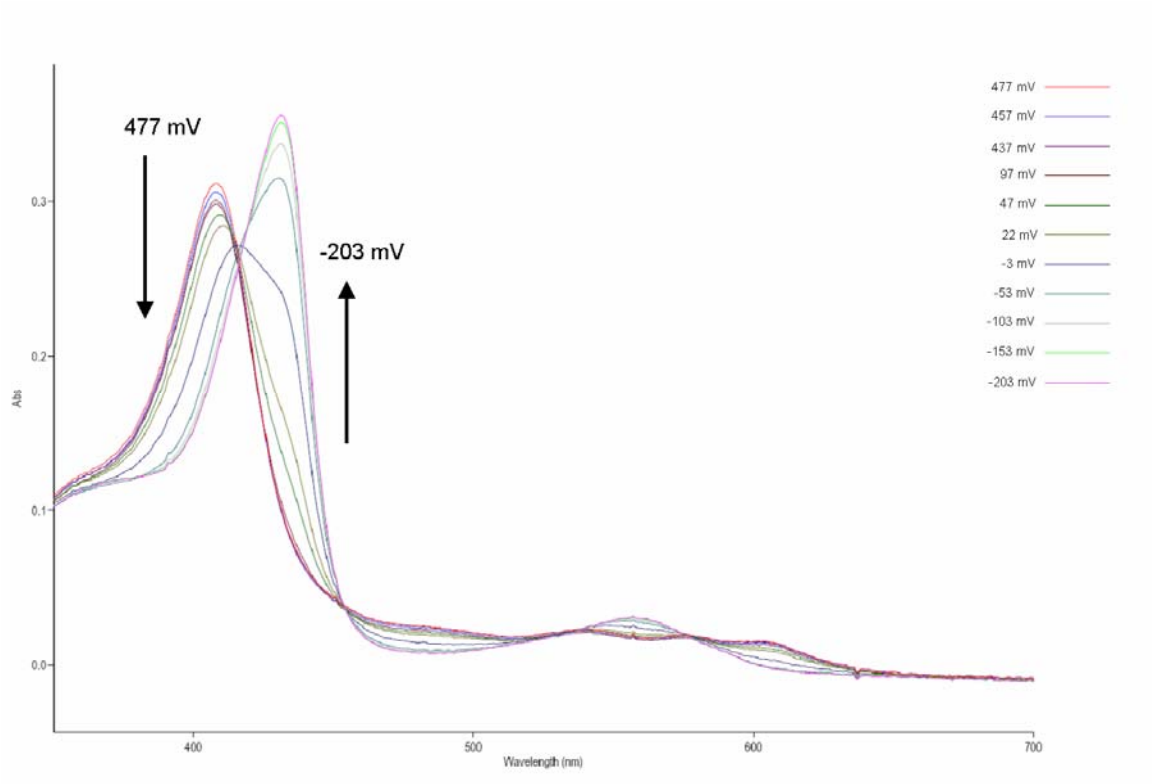

Figure 2.21: Spectra of Clam Hb II at various E_{app}. E_{app} shown in the legend are vs. NHE. Conditions: 0.1 mM Hb, 50 mM Bis-Tris buffer, no additional salt, pH 7.5, at 20°C with 0.1 M KCl salt bridges.

Nernst plots obtained for the *Lucina* Hbs are shown in Figure 2.22. Both *Lucina* Hb I and *Lucina* Hb II are more readily oxidized than HbA_o. Under the experimental conditions of this study, *Lucina* Hb II was more easily oxidized than *Lucina* Hb I. The Nernst plots for both *Lucina* Hbs I and II have mid-point slopes (n_{50} values) of near unity.

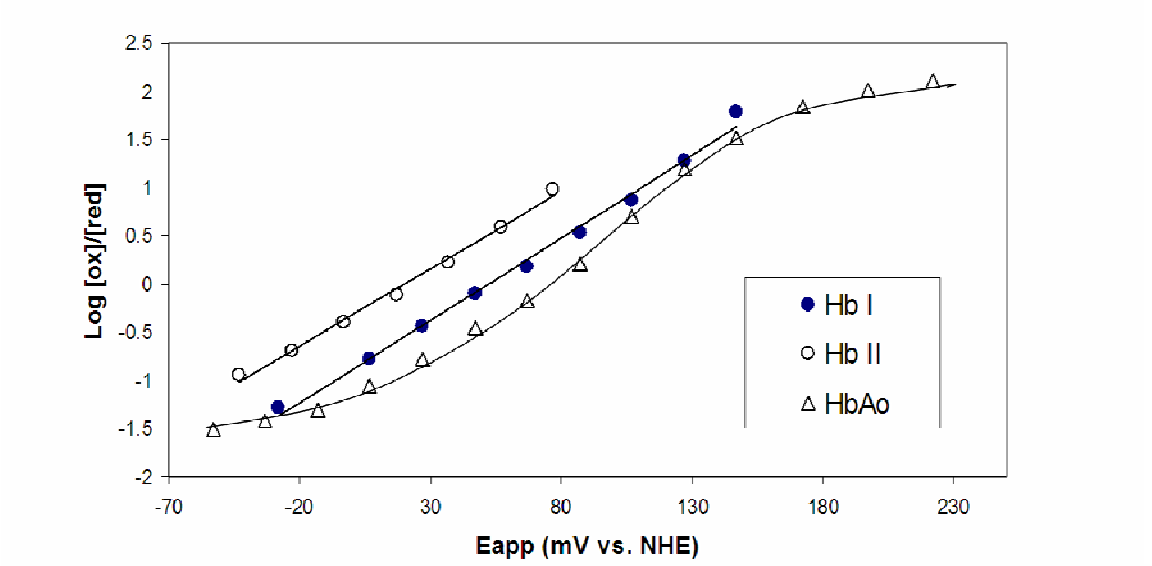

Figure 2.22: Representative Nernst plots of *Lucina* Hb I, *Lucina*, Hb II, and HbA$_o$. Conditions for *Lucina* Hbs: 0.1 mM Hb, 50 mM Bis-Tris buffer, no additional salt, pH 7.5, at 20^{o}C with 0.1 M KCl salt bridges. Data shown for Hb I was collected at 434 nm, while data for Hb II were collected at 407 nm. Conditions for HbA$_o$: 0.12 mM Hb, 50 mM MOPS buffer, 0.2 M KCl, pH 7.1, at 20^{o}C with 0.2 M KCl salt bridges. Data shown for HbA$_o$ was collected at 430 nm.

Each Hb sample was tested twice. Two wavelengths per experiment were used to calculate the average $E_{1/2}$ and n-value. The reduction potentials and n-values reported in Table 2.5 are the averages of the four calculated values for each sample.

Table 2.5: Electrochemical properties of *Lucina Hbs*. Conditions: 0.1 mM Hb, 50 mM Bis-Tris buffer, no additional salt, pH 7.5, at 20°C with 0.1 M KCl salt bridges. Average and standard deviations calculated from the $E_{1/2}$ and n-values calculated two wavelengths (407 and 430 nm).

Sample	$E_{1/2}$ (mV vs. NHE)		n-value	
	ave	sd	ave	sd
Hb I	52	5	0.96	0.08
Hb I mutant	25	8	1.0	0.2
Hb II	8	14	0.8	0.1

Surprisingly, although cooperativity was observed in the initial stages of the Hill plots for oxygen binding to *Lucina* Hb II, significant deviations from linearity are not apparent in the corresponding Nernst plots. The presence of an electrochemical mediator may have altered the extent of aggregation of *Lucina* Hb II, and thus its ability to show cooperative-like interactions in its oxidation curves.

Nernst plots obtained for the genetically engineered form of *Lucina* Hb I with Phe(B10)→Tyr(B10) indicate a shift in the redox potential to a value intermediate between that of *Lucina* Hb I and *Lucina* Hb II (Table 2.5).

Small differences in the redox potential results reported here relative to earlier studies, done under other conditions and with different methods [45], are attributable to the anion-dependence of Hb's redox behavior. The reducing agent/mediators used in

previous studies included some anions that may have shifted the measured reduction potentials positive relative to intrinsic (anion-free) values. The SEC technique employed in this study involved a cationic mediator, which ensures no anionic effects are introduced by the measurement itself.[13, 31]

2.4.1.3 Summary of Results

Results of the oxygen binding studies and the SEC investigations of the *Lucina pectinata* Hbs under the same experimental conditions are summarized in Table 2.6. The corresponding thermodynamic data for HbA_o in the presence and absence of allosteric effectors and for a cell free Hb blood substitute are also catalogued in Table 2.6. For ease of comparison, a kinetic parameter of the nitrite-induced oxidation of each Hb (the time, in minutes, required to oxidize half of the sample) is also listed in Table 2.6.

Table 2.6: Comparison of LogP_{50}, $E_{1/2}$ (mV vs. NHE), and time required for nitrite-induced oxidation (min) of air-equilibrated Hb solutions (60 μM in heme) by 100-fold excess nitrite of various Hbs and engineered hemoglobins. Except as otherwise indicated, Hbs were in 0.05 M Bis-Tris buffer, pH 7.5, 20°C.

Hemoglobin		Log P_{50}	$E_{1/2}$	Mins required for 50% oxidation by nitrite
Lucina pectinata	HbI	-0.9[$]	52	<2[$]
	HbI-B10Tyr	-1.7[$]	25	4[$]
	HbII	-1.0[$]	8	>200[$]
HbA_0	No effector	-0.2[$]	83[#]	28[$]
	0.2 M Cl	0.3[$]	122[#]	18[$]
	0.7 M Cl	0.6[$]	85[#]	18[$]
	150 μM IHP	1.6[#]	135[#]	50[#]
Crosslinked	Hb-DBBF:α99	0.8[*]	125[*]	18[*]

(#) From reference [81]

(*) From reference [19]

($) From reference [80]

2.4.2 Discussion

Our collaborators have shown that *Lucina* Hbs I and II exhibit extreme differences in their propensities for nitrite-induced oxidation.[80] Air-equilibrated *Lucina* Hb I is rapidly oxidized by nitrite. In striking contrast, air-equilibrated *Lucina* Hb II exhibits an unprecedented ability to resist nitrite-induced oxidation. Although oxy-

Hbs from varied organisms show variations in their rates of nitrite oxidation [72], none previously studied has shown a rate of nitrite oxidation as fast as that of *Lucina* Hb I or as slow as that of *Lucina* Hb II.

In order to explain this unusual behavior of the *Lucina* Hbs, an emerging theory regarding the role of heme accessibility in the control of heme reactivity has been invoked. Here we discuss this emerging theory and demonstrate that the traditional view of controlling Hb reactivity does not apply in the case of the *Lucina* Hbs.

2.4.2.1 Heme Accessibility Determines Hemoglobin Reactivity

The accessibility of the heme pocket for molecules such as O_2 or nitrite is beginning to be appreciated as a determining factor in the reactivity of a particular Hb structure with potential ligands.[19] Structural analysis performed by our collaborators [46], shows that the sterically hindered heme pocket of *Lucina* Hb II may explain the protein's unusual resistance to nitrite-induced oxidation. As shown in Figure 2.23, oxygen bound at the active site of Hb II, participates in a hydrogen-bonding network connecting it to the Tyr and Gln on the distal side of the heme pocket residues.[46] This hydrogen-bonding network adds steric hindrance to the narrow heme pocket of *Lucina* Hb II that was documented in previous studies [44, 46-48], and creates an Hb structure that is essentially resistant to nitrite-induced oxidation.

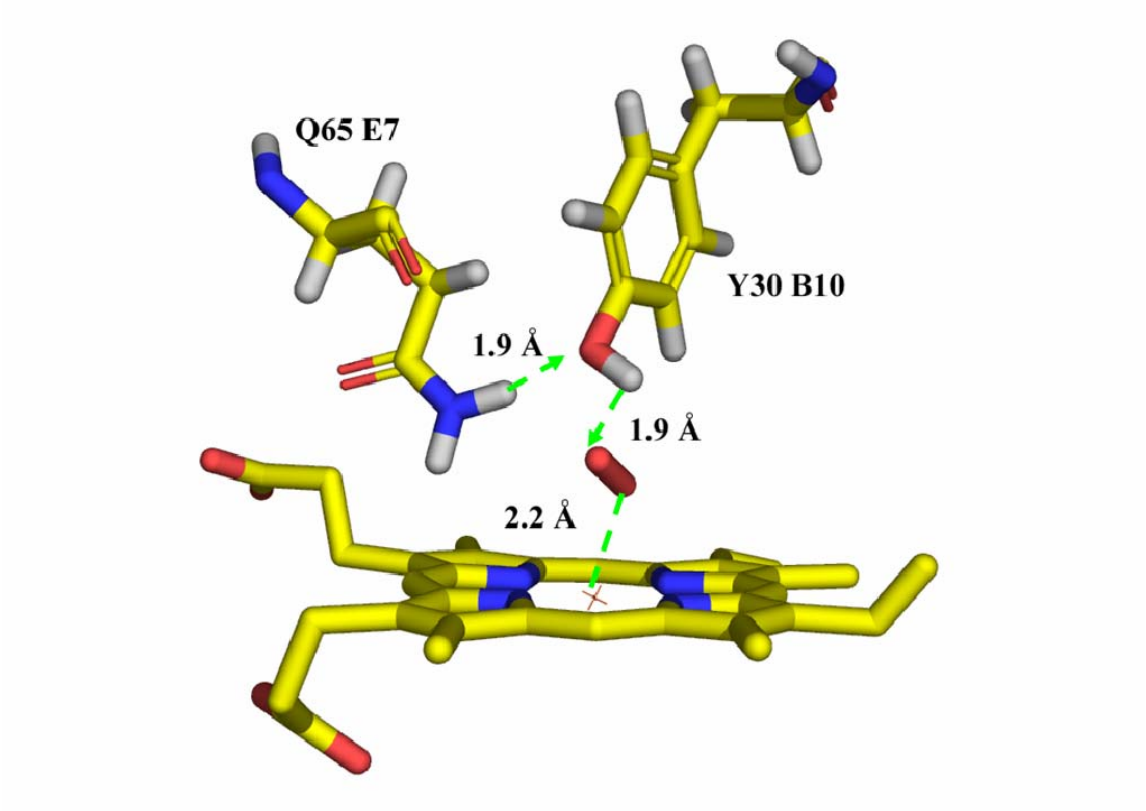

Figure 2.23: Molecular oxygen transported by Hb II, participates in a hydrogen bonding network with the amino acids present in the heme pocket. Figure reproduced from reference [80].

In addition to explaining the resistance of Hb II to nitrite-induced oxidation, the functional differences between Hb I and Hb II can be explained by heme accessibility arguments. The difference in volume of the heme pockets of Hbs I and II suggests a difference in heme accessibility for the incoming reactant (Figure 2.6). This difference in accessibility is consistent with the large differences the Hbs exhibit in their reactions with hydrogen sulfide, peroxide, nitric oxide, and nitrite.[44-46]

In addition to active site volume, heme accessibility is determined by the identity of the amino acids present in the pocket. Unlike most mammalian Hbs, both Hbs I and

Hb II have a Gln residue on the distal side of the heme. Without the distal His that normally forms a protective 'gate', *Lucina* Hb I is more accessible to incoming reactants than most vertebrate Mbs and Hbs.[30, 46-48] Increased heme accessibility is thus a reasonable explanation for the higher rate of nitrite-induced heme oxidation observed for air-equilibrated *Lucina* Hb I. In contrast, the resistance of air-equilibrated *Lucina* Hb II to incoming reactants can be explained by decreased heme accessibility. The distal Gln participates in a hydrogen bonding network (Figure 2.23) further decreasing the accessibility of this tightly packed heme pocket (Figure 2.6).

Further, as shown in Figure 2.23, Tyr(B10) plays a particularly important role in "clamming-up" the active site of *Lucina* Hb II by forming a hydrogen bond to heme-bound oxygen. In contrast, *Lucina* Hb I does not have a tyrosine at this location. An engineered form of *Lucina* Hb I was created by substituting the Phe at position B10 in *Lucina* Hb I with Tyr. The mutant exhibited modified thermodynamic properties, but failed to reproduce the unusual nitrite-resistant properties of oxygenated *Lucina* Hb II. Therefore, factors in addition to the presence of Tyr at B10 contribute to the sterically restricted active site of *Lucina* Hb II and its resistance to nitrite-induced oxidation. We suggest here that the volume of the active site and the solvent accessibility of the heme pocket are also important factors determining the reactivity of a Hb.

The heme accessibility arguments do however depend on a static view of a particular protein structure. Proteins are not static macromolecules with tightly packed

amino acids in fixed positions. Rather proteins are constantly folding and unfolding both locally and globally. Therefore, the designation of a more open or more closed/narrow active site only represents a snap shot of the possible conformations a particular protein may occupy. Further, the degree to which an active site is solvent exposed may not completely describe the path an incoming ligand must take to reach the active site. Therefore, distinguishing between the architecture of one protein and another, and correlating those differences with reactivity towards a particular incoming ligand is difficult. Finally, the heme accesbility argument is ultimately limited by the quality of the refinement of the crystal structure used to define the protein geometry. It is beyond the scope of this dissertation to analyze the crystal structures of the *Lucina* Hbs in detail. However, the author acknowledges that the heme accessibility argument is only a hypothesis that is consistant with the observed kinetic data.

2.4.2.2 Thermodynamics Do Not Completely Account for Hemoglobin Reactivity

Traditionally, thermodynamics have been implicated in the control of Hb reactivity with potential ligands and reactants. The effects of conformational change(s) on the oxygen affinity of a particular Hb have long been the focus of investigation and the goal of engineering new Hbs. For example, the reactivity of human HbA_o with nitrite has typically been discussed in terms of the protein's R- and T-state conformations, a thermodynamic argument. The high O_2 affinity R-state conformation

is normally expected to react quickly with nitrite because that form is easily oxidized. This prediction is based on the correlation between the decrease in oxygen affinity of HbA_o (T-stabilization) caused by IHP (another allosteric effector) and the decreased rate of reaction of HbA_o with nitrite in the presence if IHP. The low O_2 affinity T-state conformation is expected to react slowly with nitrite because it is difficult to oxidize. As well, studies of Hb embedded in sol-gels which are stabilized in the R-state conformation show a faster reaction between Hb and nitrite.[82]

We note several difficulties with assigning differences in rates of nitrite-induced Hb oxidation solely to shifts between R and T states. As shown in Table 2.6 there are many examples in which the oxygen affinity of a given Hb does not provide a good prediction of the nitrite reactivity. HbA_o in the presence of IHP and inorganic effectors, both of which stabilize the T-state (lower O_2 affinity), and Hbs stabilized in the T-state by chemical cross-linking (Hb-DBBF) have different effects on the reactivity of HbA_o with nitrite. IHP decreases the reactivity of HbA_o as shown by a longer reaction time. Conversely, chloride and chemical cross linking make HbA_o more reactive towards nitrite. These data suggest therefore that the effectors and cross linker causes multiple changes in the protein. Some changes shift the thermodynamic propensity for oxygen binding, such as a conformational shift, while some changes influence the ability of an incoming nitrite molecule to oxidize the heme-bound iron.

Including the *Lucina* Hbs in this comparison we see that all three *Lucina* Hbs have a higher affinity for oxygen compared to HbA_o (with no effectors). However, Hb I reacts significantly faster with nitrite than HbA_o, while Hb II requires more than 10 times the number of minutes than does HbA_o. It is evident therefore that the thermodynamic propensity of a Hb to bind oxygen can not predict the rate of a particular Hb reacting with nitrite.

2.4.2.3 Electrochemical Analysis of *Lucina* Hemoglobins

The anaerobic oxidation of Hb mimics the thermodynamic changes seen upon oxygen binding. However, in anaerobic oxidation no ligand enters the heme pocket. Therefore, SEC studies can give insight into the thermodynamic properties of a heme-protein without the complication of ligand access issues.

In our SEC investigations, both Hb I and Hb II showed linear Nernst plots with n-values near unity at 50% oxidation. This is consistent with the monomeric nature of *Lucina* Hb I, the unity slopes observed in its Hill plots of oxygen binding for Hb I and the predominantly linear Hill plot for Hb II. Although some deviation from linearity was observed for Hb II binding to oxygen at very low oxygen concentrations (indicating possible cooperativity), the Nernst plot showed no sign of cooperativity or heterogeneity. The presence of a mediator in the electrochemical studies may have prevented aggregation of the protein in the electrochemical study, precluding detection

of the small amount of cooperativity. Regardless of this minor discrepancy, the Nernst plots (anaerobic oxidation) of the *Lucina* Hbs correlate well with the respective Hill plots (oxygenation). Comparison of the *Lucina* Hbs and HbA_o shows that the *Lucina* Hbs have lower Log P_{50} values, indicating oxygenation is easier than HbA_o, and lower $E_{1/2}$ values, indicating oxidation is easier than HbA_o (Table 2.6). Taken together, this is strong evidence that anaerobic oxidation is a good model for the thermodynamics of oxygenation in the case of the *Lucina* Hbs, as has been shown for many other species.

The anaerobic oxidation potential is also a measure of how easy the heme-bound iron can be oxidized. This thermodynamic parameter is controlled not only by the first coordination shell surrounding the iron (which is the same in all Hbs studied here as provided by the heme and the proximal histidine), but also by the second coordination shell which varies depending on the architecture of the heme pocket. Under the experimental conditions of this study, *Lucina* Hb II was more easily oxidized than *Lucina* Hb I, consistent with *Lucina* Hb II having a more polar distal heme pocket. Nernst plots obtained for the genetically engineered form of *Lucina* Hb I with Phe(B10)→Tyr(B10) indicated a shift in the redox potential to a value intermediate between that of *Lucina* Hb I and *Lucina* Hb II (Table 2.6). This result is consistent with an increase in the polarity of the heme cavity in the engineered form.

Turning back to the biophysical explanation of how the *Lucina* Hbs can have such different and extreme reactions with nitrite, we can use the anaerobic oxidation

data as a probe for protein thermodynamics that eliminates the effect of the entering ligand. Table 2.6 shows that $E_{1/2}$ similar to Log P_{50} is NOT correlated to nitrite-induced oxidation kinetics. Specifically, SEC studies reveal that Hb II has an $E_{1/2}$ of 8 mV vs. NHE and is the most easily oxidized Hb reported here. However, Hb II shows significant resistance to nitrite-induced oxidation, requiring the longest time for a sample to be half oxidized. Conversely, Hb I is the most difficult to oxidize of the three *Lucina* Hbs according to the $E_{1/2}$ values, but is the most reactive towards nitrite.

Part of the heme accessibility argument is that O_2 bound to the heme participates in a hydrogen-bonding network that "clams-up" the active site of Hb II (Figure 2.23). When oxygen is removed, Hb II reacts quickly with nitrite. The small difference in Log P_{50} values determined by oxygenation studies (-0.9 for Hb I and -1.0 for Hb II) indicates that thermodynamics can not explain this difference in nitrite reactivity. However, the hydrogen bonding network in which the oxygen participates may skew our understanding of R- to T-state transitions by affecting the local affinity for oxygen, but not the global shift to a high affinity conformer. Anaerobic oxidation studies can therefore probe the protein thermodynamics without this complication of ligand binding. The difference in $E_{1/2}$ values for Hb I (52 mV) and Hb II (8 mV) indicates a larger difference in the thermodynamic propensities of the two Hbs than the oxygenation studies do. However, this difference is still not large enough to explain the drastically different rates of reaction with nitrite. Further, the $E_{1/2}$ values actually

indicate that the propensity of the iron to be oxidized is inversely correlated to the rate of nitrite-induced oxidation. Taken together, neither the thermodynamic measurement of oxygen affinity nor the thermodynamic propensity of the *Lucina* Hbs to be oxidized can explain the extreme differences observed when the Hbs are exposed to nitrite.

Further comparison of the *Lucina* Hbs with various forms of human Hb provides a context the thermodynamic and kinetic data and supports the proposal that thermodynamic arguments can not explain the reactivity of Hb and nitrite. HbA_o in the absence of effectors has an $E_{1/2}$ value of 83 mV and is harder to anaerobically oxidize than the *Lucina* Hbs (Table 2.6). However, a sample of HbA_o is half oxidized by nitrite in 28 min, an intermediate time between Hb I and Hb II. Within the set of HbA_o samples (in the presence and absence of effectors), the anaerobic oxidation potential also does not correlate with nitrite reactivity. The extreme case of HbA_o in the presence IHP, which stabilizes the T-state, shows an increase in $E_{1/2}$ to 135 mV, indicating the protein is harder to oxidize. HbA_o required 50 min to be half oxidized by nitrite. The opposite effect was observed for the crosslinked Hb, which also stabilizes the T-state. The $E_{1/2}$ value of 125 mV indicated the protein is harder to oxidize compared to HbA_o (83 mV), but the cross linked Hb reacted with nitrite in 18 min, a shorter time than HbA_o (28 min).

Anaerobic oxidation studies allow the investigation of the thermodynamic propensities of Hbs with the complication of an entering ligand. Here we have shown that anaerobic oxidation potentials, in addition to oxygenation affinities do not correlate

with the observed reactivity of Hbs with nitrite. Therefore, the R- to T- state conformation thermodynamics and the thermodynamic propensity toward iron oxidation can not fully predict the reaction between a heme and the entering ligand. Our thermodynamic investigations support the hypothesis that steric hindrance and heme accessibility are key parameters determining the reactivity of a Hb protein.

2.4.2.4 Implications for Protein Engineering

The role of bound oxygen in the inhibition of nitrite-oxidation of Hb may be transferable across species. O_2 bound in the active site of *Lucina* Hb II essentially prevented reaction with nitrite by participating in a hydrogen-bond network. However, when oxygen was removed deoxy-Hb II reacted quickly with nitrite. O_2 has also been shown to slow the reaction of human HbA_o with nitrite.[49] Previous reports have shown that high pressures of oxygen can also inhibit HbA_o oxidation by ethyl or butyl nitrite, ferricyanide, hydroxylamine, chlorate, hydrogen peroxide and quinines.[58, 69, 72] Although the full story of how inhibition by O_2 occurs in each of these instances is debated, it is clear that oxygen binding to both human and *Lucina* Hbs can provide protection against chemical oxidation.

The extreme differences in nitrite reactivity exhibited by the *Lucina* Hbs suggest heme accessibility is an important primary variable in determining heme oxidation by small molecules. The complex reactions of HbA_o with nitrite are under intense

investigation, but are still not well understood. Future studies regarding the interaction of HbA_o and nitrite should include examination of heme architecture and solvent accessibility as a function of experimental conditions and time. Further, details such as whether other polar residues at B10 and E7 can build a hydrogen bonding network with the heme-bound oxygen and such as the volume of the distal heme pocket should be considered when designing new cell free Hb substitutes.

2.5 Conclusions

In this chapter we have explored two cases studies in which the structure of a particular Hb dictates a physiologically important function for the organism that has adapted to its environment. For the Root Effect fish, the heightened sensitivity of the ligand binding properties of the Hb provides an oxygen pump used to fill the eyes and swim bladders of the fish against very high oxygen concentrations. For *Lucina pectinata*, Hb I and Hb II transport different molecules required for symbiosis and react in extreme and opposite ways with nitrite.

In both cases, we have probed the thermodynamic properties of heme-bound iron using SEC, in an effort to identify the underlying factors that control Hb reactivity. For the Hbs of fish exhibiting the Root Effect, the sensitivities of the redox reaction towards changes in pH are similar to those of non-Root Effect Hbs, i.e. there is no Redox Root Effect. Therefore the thermodynamic properties of the metalloprotein, observed by

monitoring the metal do not fully explain the Root Effect. For the Hbs of *Lucina pectinata* the thermodynamic propensity of the metalloprotein to be oxidized (i.e. the reduction potential) did not correlate with the unusual reactivity of these Hbs with the chemical oxidant nitrite. Therefore, the thermodynamic properties of the metalloprotein, observed by monitoring the metal do not fully explain the reactivity of these Hbs. We conclude that factors other than the thermodynamic balance between conformers and the thermodynamic properties of the metal, determineof the reactivity for the Hbs under investigation. We assert that heme accessibility and steric hindrance towards the entering reactant are responsible for the physiological function of the Hbs studied here and should be considered during the design of new structures of Hbs.

3. Electrochemical Investigations of Titanium-Transferrin and Active Site Mimics

In this chapter we have elected again to use the metal as our probe for the thermodynamic investigations of a metalloprotein. In this case we also utilize the extreme case of "removing" the protein from our investigations by studying small molecule metal complexes that mimic the active site of the protein. Using this metal-centric perspective, we draw conclusions regarding the metal-protein interactions and the mode of action of this metalloprotein in a biological setting.

During revison and defense of this dissertation, the manuscript reporting some of the work disccused in this chapter was accepted for publication in the Journal of Inorganic Biochemistry.[83]

3.1 Background

3.1.1 Transferrin-Mediated Iron Transport

The biological function of human Tf is to tightly sequester ferric ions for three fundamental purposes: to enable iron transport through plasma from storage to utilization site; to act as a bacteriostatic agent by preventing bacterial cells from acquiring the essential nutrient iron; to prevent iron catalyzed toxic free radical formation via Fenton reactions.[5, 84, 85] Tf is an 80 kDa protein that binds two ferric ions. Sequestration is made possible through two chemically identical iron binding sites

containing donor moieties from aspartate, histidine, and two tyrosine amino acid side chains. The first coordination shell around each iron is completed by a bidentate exogenous carbonate anion. Tf binds ferric iron tightly with a K_d ~10^{-20} M.[86]

The process of Tf-mediated iron uptake by human cells is depicted in Figure 3.1. Fe_2-Tf binds to the human Tf receptor (TfR) on the cell surface and the Fe_2-Tf/TfR assembly is endocytosed.[87] The pH of the fully formed endosome is decreased to 5.5 and iron is thought to be released from Tf via reduction of the ferric iron cargo. The ferrous ion is then transported into the cytosol through DMT1.[84] The receptor/apo-Tf complex is subsequently recycled to the surface of the cell and apo-Tf is released.

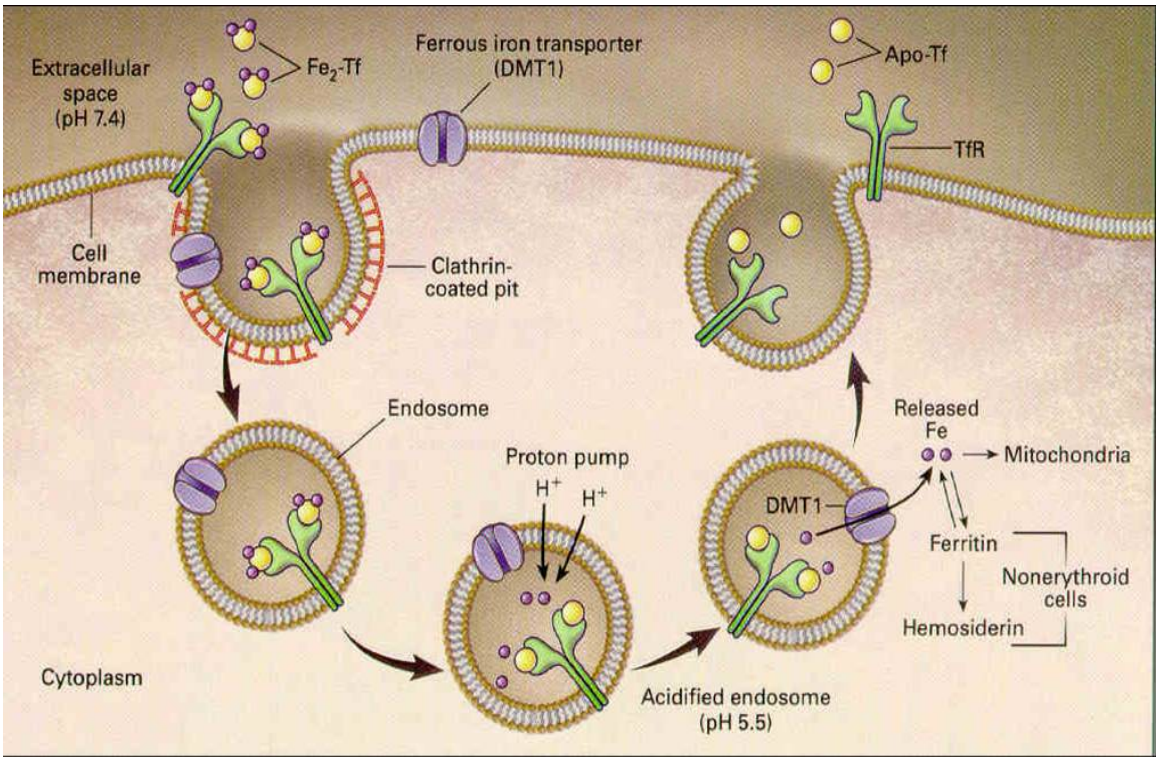

Figure 3.1: Iron loaded Tf binds to the human Tf receptor. The protein-receptor complex is brought into the cell by endocytosis. Inside the endosome (pH 5.5), iron is released from Tf, possibly facilitated by reduction. The protein-receptor complex is recycled back the to surface of the cell and apo-Tf is released into the serum.[84] Figure reprinted from reference [84] with permission.

It remains an open question as to whether reduction of the iron(III) in the endosome occurs prior to dissociation from Tf in the Fe_2-Tf/TfR assembly, or subsequent to dissociation from Tf. A redox mediated release of iron is an attractive hypothesis because the binding constant of Tf with Fe(II) is 17 orders of magnitude lower than that with Fe(III), and Fe(II) exchanges its first coordination shell at a much faster rate than Fe(III).[88, 89] The very negative reduction potential of Fe(III) in Fe_2-Tf at the conditions of the endosome (-526 mV vs. NHE) suggests that reduction to Fe(II) is energetically

unfavorable.[78] However, when bound to the receptor, Fe_2-Tf has a reduction potential of -300 mV and a redox mediated release mechanism is plausible.[12, 90, 91] Further details regarding the interaction of iron with Tf will be discussed in Chapter 4.

3.1.2 Transferrin-Mediated Titanium Transport

The Tf binding site is suitable for sequestration of a number of different metal ions.[92-94] Ti(IV) binds to Tf more tightly than Fe(III), with a K_d of 10^{-26} M.[95] The high affinity expressed by Tf for Fe(III) and Ti(IV) can be rationalized in that both are high charge-density, hard metal ions. Transport of Ti(IV) in the body via Tf is of great interest as the exposure of humans to titanium is increasing with the prevalence of titanium alloy implants, titanium-based imaging agents, titanium-based food additives, and the potential future use of titanium-based anti-cancer drugs.[92, 96-102] Further, the mode of action of titanium-based cancer drugs such as titanocene dichloride remains unclear, although binding to Tf is hypothesized to be involved.[93, 103, 104] However, once bound to human Tf the fate of Ti(IV) has not been identified, other than the binding of Ti_2-Tf to TfR.[105]

3.1.3 Statement of Objectives

Our objective was to identify the redox potential of Ti_2-Tf and to determine if a redox-mediated release mechanism is plausible for the release of titanium(IV) from Tf.

Using discontinuous spectroelectrochemistry (dSEC), we demonstrate for the first time that the reduction potential of Ti_2-Tf is lower than that of Fe_2-Tf. In a second approach, we used small molecule active site mimics to model the first coordination shell of the metal in the protein. We present a linear free energy relationship (LFER) between these low molecular weight Fe(III) and Ti(IV) complexes to estimate the very negative reduction potential of Ti_2-Tf. These studies provide insight into the biodistribution of titanium. They also address whether the reduction-initiated release from transferrin hypothesized for iron [12] may be applicable to titanium transport.

3.2 Materials and Methods

3.2.1 Identification of Appropriate Model Complexes

The metal binding site of human Tf and the ligands used to model that site are depicted in Figure 3.2. Each ligand has oxygen or nitrogen moieties that can act as Lewis bases in a similar manner as the oxygens and nitrogen of the protein active site. See Section 3.3.5.1 for further discussion of this topic.

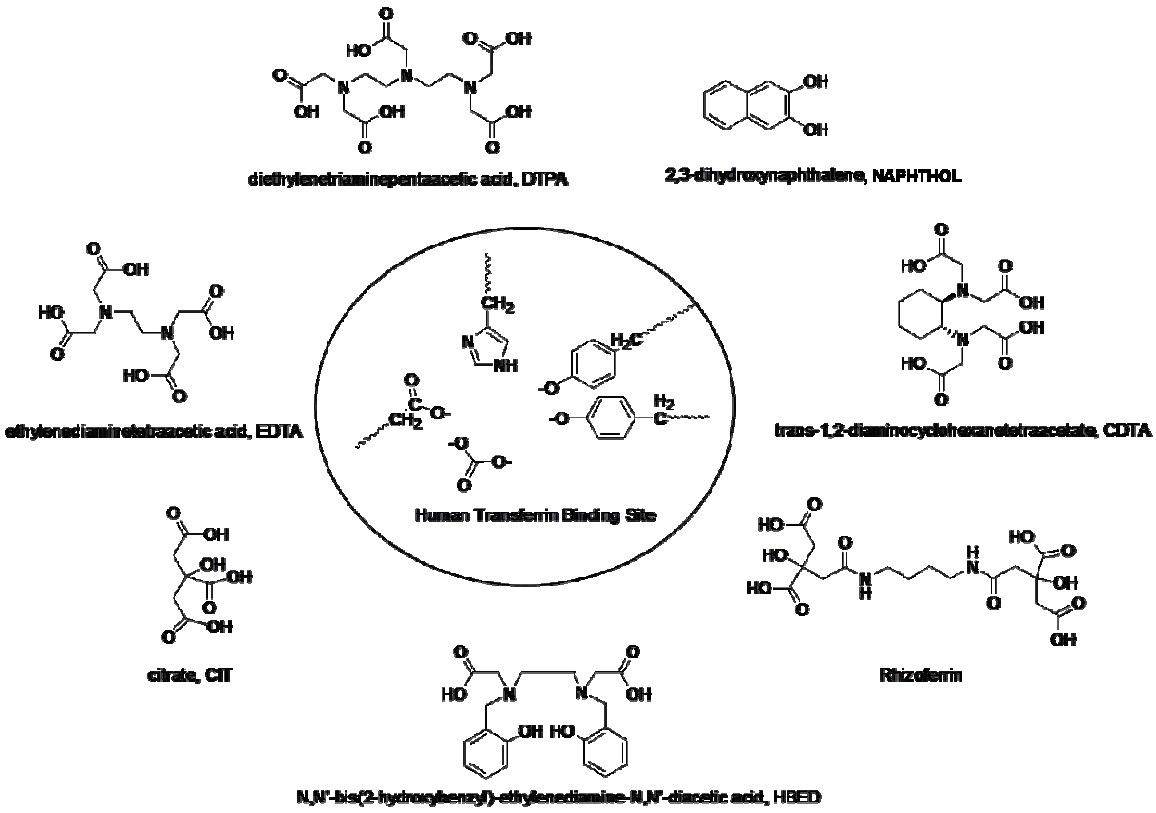

Figure 3.2: Tf binding site and model ligands.

3.2.2 Synthesis of TiCIT

TiCIT was prepared according to procedures from Tinoco and Valentine, and Zhou, et al.[95, 106] De-ionized water (20 mL) was purged of oxygen in a round bottom flask with argon and simultaneously cooled in an ice bath. $TiCl_4$ (Alfa Aesar; 1.2 mL) was transferred to the flask, and the resulting white solution was left to stir for 30 minutes under a blanket of Ar. A 1 M citric acid (Sigma) solution (32.8 mL) was prepared in a separate round bottom flask and degassed using Ar. The citric acid

solution was added to the $TiCl_4$ solution using a cannula, and the mixture, which remained white, was stirred for 2 hr on ice and under an Ar environment. The pH was then increased to approximately 2 using 3M KOH at ambient conditions and monitored with a Oaklon pH 510 series pH meter. The white mixture was left stirring on ice. The resulting white precipitate was filtered. Additional product was collected after the filtrate was allowed to form white needle-like crystals. The product was re-crystallized using minimal DI H_2O. Elemental analysis by Atlantic Microlabs (calculation for $K_2[Ti(H_2citrate)_3]$ in parentheses): C - 30.89% (31.0), H - 3.24% (2.6), O - 48.43% (48.3). TiCIT was used as a starting material for the preparation of the other titanium complexes described below. Sara Jane Brandt and Emily Lin are acknowledged for their technical assistance with the syntheses of TiCIT, TiCDTA, TiDTPA, and FeNAPHTHOL.

3.2.3 Preparation of TiCDTA and TiDTPA

Aqueous TiCDTA and TiDTPA (25 mM) solutions were prepared *in situ* by adding 1, 5 and 10 molar equivalents of 1,2-cyclohexylenedinitrilotetraacetic acid (CDTA; Aldrich) or diethylenetriaminepentaacetic acid (DTPA; Fluka Analytical) to 25 mM TiCIT in aqueous solution. Sonication, heating, and stirring were used to aid the dissolution of the respective ligand. The pH of the mixture was adjusted using minimal amounts of NaOH. Confirmation of *in situ* preparation was verified by obtaining cyclic

voltammograms of solutions containing variable ratios of TiCIT and CDTA or DTPA. Alternative syntheses for TiCDTA and TiDTPA have been reported previously.[107]

3.2.4 Preparation of FeHBED

A solution of 2 mM FeHBED was prepared *in situ* by dissolving 1.1 equivalents of solid N,N'-di(2-hydroxybenzyl)-ethylenediamine-N,N'-diacetic acid (HBED; Strem Chemical) in a standardized solution of $FeCl_3$ in HCl with concomitant change in color to reddish-purple. The pH of the mixture was adjusted using minimal amounts of NaOH.

3.2.5 Preparation of FeNAPHTHOL

A solution of $[Fe(2,3\text{-dihydroxynaphthlene})_3]^{3-}$ was prepared *in situ* by combing appropriate volumes of standardized $FeCl_3$ (in 1 M HCl) with 40 mM 2,3-dihydroxynaphthlene (Sigma) dissolved in 0.08 M KNO_3 in 20% methanol. The amount of iron added to each solution was altered in order to vary the ligand to metal ratio. The pH was raised to 8 with 3 M KOH.

3.2.6 Spectrophotometric Characterization of FeNAPHTHOL

Solutions of 10 to 1 ligand to metal ratio and 5 to 1 ligand to metal ratio at different pH values were allowed to come to equilibrium over night. The absorbance

spectrum of each solution was measured with a Cary 50 spectrophotometer (data not shown).

3.2.7 Preparation of Ti_2-Tf and Mediators

Titanium loaded Tf was prepared as previously published [95] and provided by Dr. Valentine, Yale University. Once loaded, Ti_2-Tf was dialyzed into two working buffers (50 mM MOPS, 500 mM KCl, pH 7.4 and 50 mM MES, 500 mM KCl, pH 5.76). 1,1'-propylene-2,2'-bipyridylium dichloride (triquat), synthesized in house by Katherine D. Weaver, and 1,1'-dimethyl-4,4'-bipyridylium dichloride (methyl viologen or paraquat), from Aldrich Chem. Co. were analyzed and used as mediators (small molecule electron shuttles in the SEC cell) without further purification.[36, 108-113] All other reagents (buffers, electrolytes, etc.) used were of the highest purity commercially available.

3.2.8 Cyclic Voltammetry

A Cypress Systems 1R and 2R potentiostats were used to control the applied potential for CV analyses. An Ag/AgCl/3M KCl reference electrode (BioAnalytical Systems) was used, in addition to an 18-gauge platinum wire auxiliary electrode and either a glassy carbon (for TiCDTA, triquat, and methyl viologen) or platinum button (for FeHBED and TiDTPA) working electrode. Between runs, working electrodes were

cleaned with a slurry of alumina and de-ionized water, the auxiliary electrode was cleaned with fine sandpaper, and the reference electrode was rinsed with de-ionized water. A BASi-CGME hanging drop mercury electrode (drop size corresponded to a surface area of 16 x 10^{-3} cm^2) was used to investigate FeNAPHTHOL. The Hg drop was replaced for each scan. N_2 was bubbled through the solutions between each trial for 15 minutes, and a N_2 blanket was maintained above the sample during each run. All reported potentials are versus NHE.

Redox potentials ($E_{1/2}$) were determined by taking the midpoint between the reduction and oxidation peaks of each voltammogram. Reversibility was monitored by observing the cathodic to anodic peak current ratio (I_c/I_a), the peak to peak separation (ΔE_p), and by comparing the diffusion coefficients calculated from the anodic and cathodic peaks using the Randles-Sevcik equation,

$$D = \left[\frac{m}{2.687x10^3 n^{3/2} AC} \right]^2 \qquad (3.1)$$

where m = slope of peak current vs. square root of scan rate, n = number of electrons, A = area of the electrode, and C = concentration of analyte. Sara Jane Brandt and Emily Lin are acknowledged for their technical assistance with the electrochemical characterization of TiCIT, TiCDTA, TiDTPA, and FeNAPHTHOL. Kirsten Bazemore is acknowledged for her technical assistance in characterizing potential mediators for SEC.

3.2.9 Metalloprotein Spectroelectrochemistry

As described in Chapter 2, SEC is a technique used to study the redox behavior of a metalloprotein. In brief, SEC utilizes a short optical pathlength, created by an optically transparent thin layer electrode (OTTLE) cell. The variations in UV-vis spectra of the protein-metal complex are measured, while applying an increasingly negative potential.[32] The change in absorbance corresponds to a change in concentration of oxidized and reduced species.[13] Following the Nernst equation (Equation 3.2), the absorbance data can be plotted as a function of the applied potential, E_{app}, to determine both the midpoint potential, $E_{1/2}$, and the number of electrons, n, transferred during a redox reaction.

$$E_{app} = E_{1/2} + \frac{RT}{nF}\log\left(\frac{[ox]}{[red]}\right) \qquad (3.2)$$

The heterogeneous reaction between a soluble metalloprotein and the solid optically transparent mesh electrode is complicated because the metal redox site is buried in the protein and the protein diffuses slowly to the electrode surface. Mediators are used to shuttle electrons between the metalloprotein analyte and the electrode. The solution is allowed to reach equilibrium at each E_{app}, as determined by stabilization of the absorbance spectrum.[13, 78, 108] Triquat and methyl viologen were used as mediators for the investigation of Ti_2-Tf. The electrochemical and spectroscopic properties of each mediator were characterized using CV and SEC.

All UV-vis spectra were measured on a CARY BIO 100 UV-vis spectrophotometer. Applied potentials in SEC experiments were controlled with a EG & G Princeton Applied Research model 263 potentiostat. The same Ag/AgCl reference electrode (BAS MW-2030) was used for all electrochemical experiments. All reported potentials are versus NHE.

3.2.9.1 Spectroelectrochemistry

Anaerobic OTTLE cells were assembled and solutions were prepared for SEC as previously described.[32] The pathlength of the OTTLE cell was determined to be ~0.04 cm using a standard solution of $K_3Fe(CN)_6$. The SEC equipment and methodology were calibrated using 1.5 mM methyl viologen, 50 mM MES (pH 5.6, adjusted with KOH), and 500 mM KCl. A gold mesh working electrode and a platinum wire auxiliary electrode were used. In a continuous experiment (one sample and one OTTLE cell), the E_{app} was decreased step-wise from -103 mV to -503 mV, allowing the system to come to equilibrium at each potential as determine by a stable absorbance spectrum. The modified Nernst equation used to analyze SEC data is shown below:

$$E_{app} = E_{1/2} + \frac{RT}{nF}\log\left(\frac{[A - A_r]}{[A_o - A]}\right) \qquad (3.3)$$

where A is the equilibrium absorbance at an applied potential, A_r is the absorbance of fully reduced species, and A_o is the absorbance of the fully oxidized species.

3.2.9.2 Discontinuous Spectroelectrochemistry

In order to investigate the redox chemistry of protein bound metals with very negative reduction potentials we developed the method of dSEC. Development of this method was begun by Daniel Kraiter [78] and Katherine Weaver is acknowledged for her technical assistance.

dSEC enables the use of Hg-Au amalgam working electrodes, which are required in the case of very negative potentials such as those utilized in this study. At such low potentials, it is necessary to avoid solvent reduction. The choice of a Hg-Au amalgam as a working electrode material was based on its over-potential with respect to water solvent breakdown. However, the Hg-Au amalgam mesh electrode is not robust and the Hg must be re-deposited once equilibrium is reached at each potential. This requires discontinuous experiments involving a series of OTTLE cells, each with a freshly prepared working electrode and a new protein solution. Only one potential was applied to each cell and after equilibrium was achieved the cell was disassembled.

Electrode cleaning consisted of soaking the Au gauze electrode (25x25 mm mesh, 0.102 mm diameter, Alfa Aesar) in 4 M HNO_3 for 1 hr, followed by 30 min sonication in ethanol. Electrochemical cleaning consisted of applying a potential of -173 mV vs. NHE in 1 M H_2SO_4 for ~15 min and repeating for another 15 min with fresh solution. The potential was then scanned between +1897 mV and +447 mV vs. NHE in 1 M H_2SO_4 until the voltammogram stabilized. For electrodes that have been previously plated, any

remaining Hg was removed prior to cleaning (Hg removal: E_{app} = +857 mV vs. NHE in 0.05 M $Hg(NO_3)_2$ and 2 M HNO_3 for 1 hr). Hg plating consisted of holding a clean Au electrode at a deposition potential of +537 mV vs NHE in a solution of 0.05 M $Hg(NO_3)_2$ and 2 M HNO_3 for $\leq$ 15 min until shiny. Cleaning and plating potentials were controlled with a BAS Voltamograph CV-27.

The dSEC method was calibrated by performing dSEC on triquat using 2.38 mM TQ, 500 mM KCl, at pH 7.4 (50 mM MOPS) and pH 5.6 (50 mM MES). The dSEC results were then compared to the results obtained using CV. Subsequently, dSEC was performed on the protein sample in the presence of triquat at each pH value (0.476 mM Ti_2-Tf, 2.38 mM TQ, 500 mM KCl, 50 mM MOPS or MES).

In SEC, the change in absorbance of a molecule is measured as a function of the external potential applied to the system.[13] The change in absorbance corresponds to a change in concentration of oxidized and reduced species (Equation 3.3). In order to calculate the concentration of the oxidized and reduced species at a particular E_{app}, one must know the absorbance of the fully oxidized and fully reduced systems. For dSEC we assume for the systems under investigation here that each analyte is fully oxidized at -300mV. Alternatively, the absorbance of the fully reduced species is calculated it using Beer's Law, since full reduction cannot be achieved in the dSEC experiment:

$$[red] = \frac{Abs}{\varepsilon b} \tag{3.4}$$

We calculated the absorbance (at 600 nm) of fully reduced methyl viologen to be 0.7792, using a molar absorptivity of 13000 M^{-1} cm^{-1}, a concentration of 0.0015 M, and a path length of 0.04 cm.[114] The absorbance of the fully oxidized solution is 0.0 at 600 nm (data not shown). The absorbance of the fully reduced triquat sample was calculated to be 1.5, using a molar absorptivity (385 nm) of 15,000 M^{-1} cm^{-1}, a concentration of 0.00238 M, and pathlength of 0.04 cm.[108]

Using the conservation relationship,

$$[total] = [ox] + [red] \tag{3.5}$$

the Nernst equation can be modified to relate the experimental absorbance to the applied potential:

$$\log\left(\frac{\varepsilon b[total]}{Abs} - 1\right) = \frac{nF}{RT}(E_{app}) - E_{1/2}\left(\frac{nF}{RT}\right) \tag{3.6}$$

For dSEC experiments, each cell was allowed to equilibrate at -303 mV, in order to obtain the absorbance which is assumed to be of the fully oxidized system. Equilibrium was determined by stabilization of the absorbance spectrum. The external potential was decreased to the applied potential (E_{app}). Sequential spectra (700 nm – 300 nm) were obtained as the solution was allowed to equilibrate at the new potential. The equilibrium absorbance at -303 mV was subtracted from the equilibrium absorbance at E_{app}.

$$\Delta A = A_{E_{app}} - A_{-303\,mV} \tag{3.7}$$

Using only the change in absorbance between the two potentials (ΔA), we eliminated differences in absorbance caused by variations in path length or junction potential that might occur during reconstruction of the OTTLE cell between each E_{app}. The change in absorbance (ΔA) at the λ_{max}, instead of actual absorbance, was used to create the Nernst plots for the dSEC experiments.

For experiments in which both the protein and the mediator absorb visible light, the change in absorbance due to mediator (ΔA_m) was subtracted from the overall change in absorbance (ΔA_{pm}). This procedure allowed determination of the change in absorbance due to just the protein (ΔA_p) (Equation 3.8).

$$\Delta A_p = \Delta A_{pm} - \Delta A_m \tag{3.8}$$

Due to side reactions, the system can not reach equilibrium at lower potentials. Care must be taken to account for variations in absorbance due to time, specifically the time between when the E_{app} was applied and when the spectrum was taken. The prime notation in the following equation (a modification of Equation 3.8) signifies that the A_{Eapp} is not the equilibrium absorbance:

$$\Delta A'_p = \Delta A'_{pm} - \Delta A'_m \tag{3.9}$$

To minimize the discrepancy between spectra due to time, we chose between the spectra taken at sequential times after the potential was applied. The criteria used for this decision was the comparison between the $\Delta A'_m$ of the mediator alone and the $\Delta A'_{pm}$

of the protein mediator mixture at the two wavelengths where the protein does not absorb.

3.3 Results

3.3.1 Characterization of Mediators using Cyclic Voltammetry

As shown in Figure 3.3, the first reduction (Equation 3.10) of methyl viologen is reversible based on three criteria: peak to peak separation, diffusion coefficients, and the ratio of peak heights.

$$MV^{2+} + 1e^{-} \leftrightarrow MV^{\cdot 1+} \qquad (3.10)$$

The peak separation of the resulting voltammogram is 69 mV and the ratio of cathodic to anodic peak heights (I_c/I_a) is 0.910 (Figure 3.3). The cathodic and anodic diffusion coefficients were calculated to be 1.7×10^{-6} cm^2s^{-1} and 1.1×10^{-6} cm^2s^{-1} respectively and are consistent with the literature (Figure 3.3 Inset).[108, 109] The $E_{1/2}$ of methyl viologen is -460.7 mV vs. NHE.

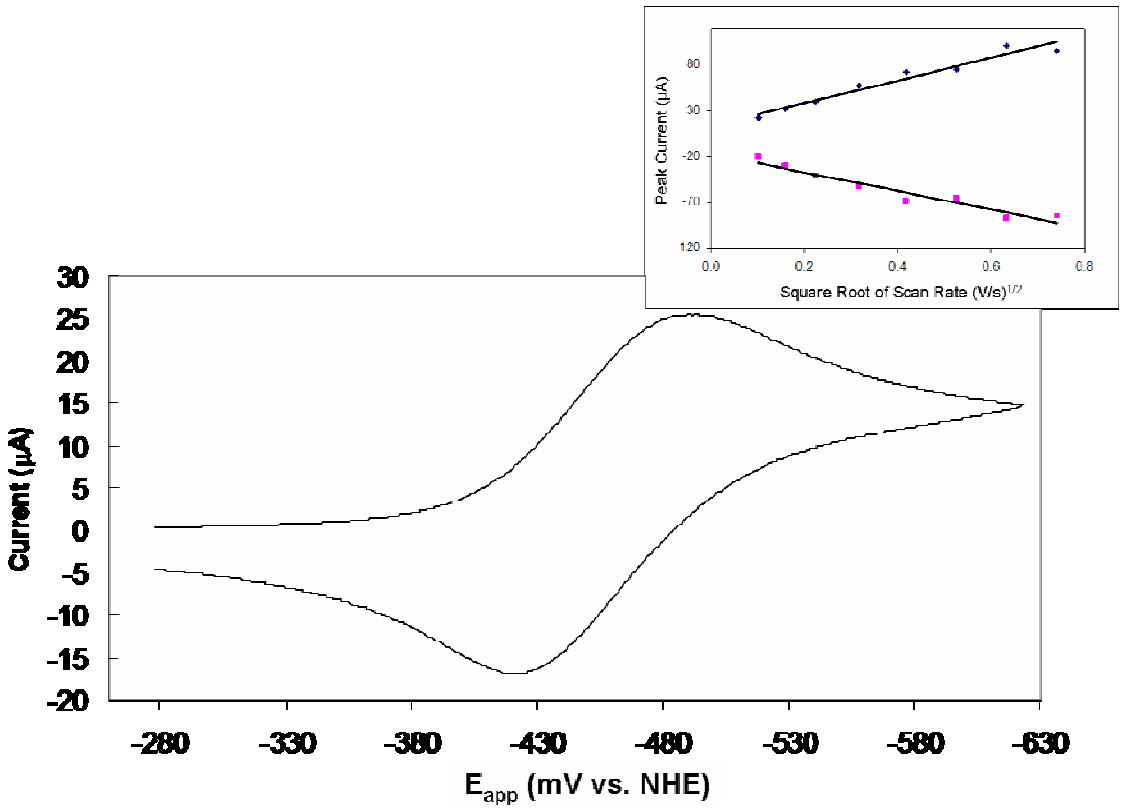

Figure 3.3: Representative voltammogram of 5 mM methyl viologen in 200 mM KCl scanning at 10 mV/s. $E_{1/2}$ is -460.7 mV vs. NHE and the peak separation is 69 mV. Glassy carbon button served as the working electrode and a Pt wire as the auxiliary electrode. Inset: Linear dependence of peak current on the square root of scan rate. Solid lines represent the least squares analysis of cathodic (top) and anodic (bottom) data. The slope of each line was used to calculate the respective diffusion coefficient.

For the first reduction of triquat (Equation 3.11), the cathodic and anodic diffusion coefficients were calculated to be 1.8x 10^{-6} cm^2s^{-1} and 6.2 x 10^{-7} cm^2s^{-1} (Figure 3.4 Inset), respectively. Both are consistent with the literature and with a reversible reduction.[108] When scanning 10 mV/s, the peak separation is 73 mV, indicating a one electron transfer, and the ratio of peak heights (I_c/I_a) is 0.913 (Figure 3.4).

$$TQ^{2+} + 1e^- \leftrightarrow TQ^{1+} \qquad (3.11)$$

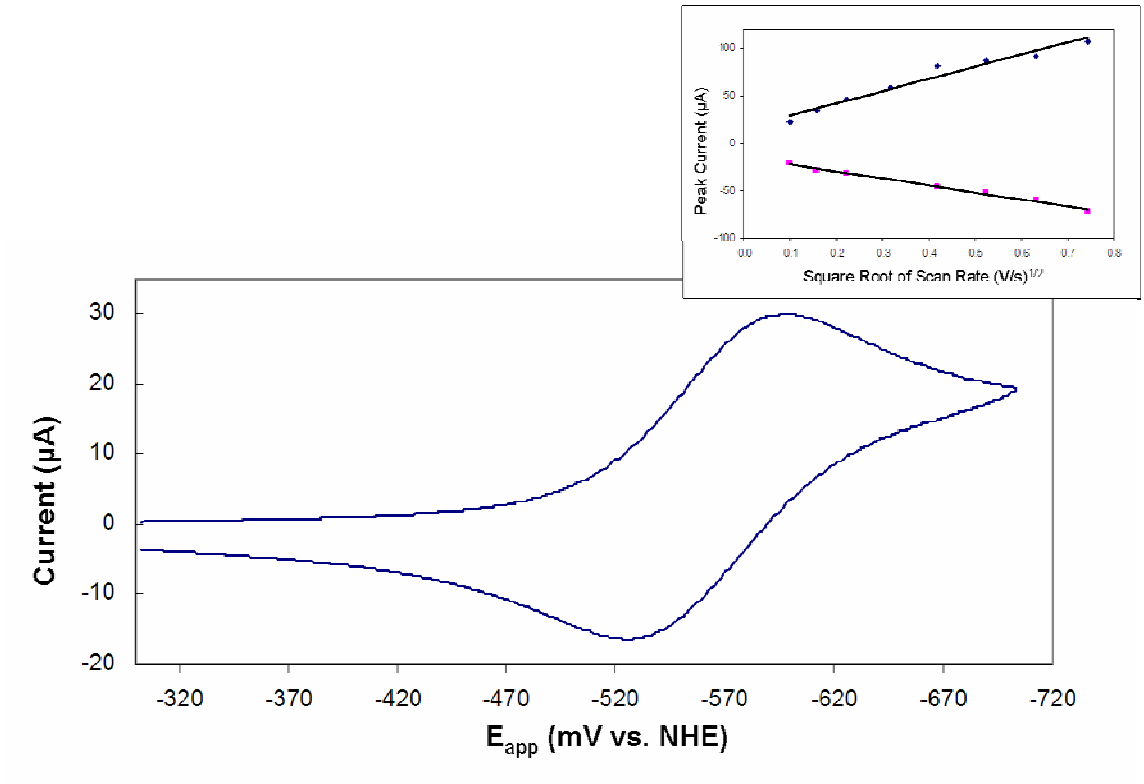

Figure 3.4: Representative voltammogram of 5 mM triquat in 200 mM KCl scanning at 10 mV/s. The $E_{1/2}$ is -568.8 mV vs. NHE and the peak separation is 73 mV. Glassy carbon button served as the working electrode and a Pt wire as the auxiliary electrode. Inset: Linear dependence of peak current on the square root of scan rate. Solid lines represent the least squares analysis of cathodic (top) and anodic (bottom) data. The slope of each line was used to calculate the respective diffusion coefficient.

3.3.2 Characterization of Mediators using Spectroelectrochemistry and Discontinuous Spectroelectrochemistry

Methyl viologen was characterized using a combination of SEC and dSEC. A Nernst plot (Figure 3.5) was created from data collected at 600 nm. An $E_{1/2}$ of -501 mV and a n-value of 1.03 electrons were calculated from the least squares fit of the data.

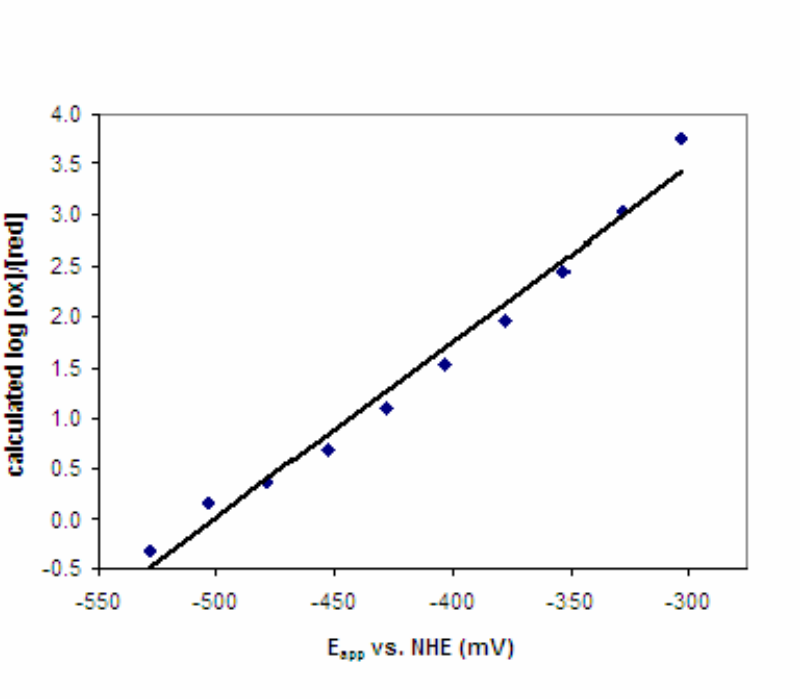

Figure 3.5: Nernst plot of 1.5 mM methyl viologen in 50 mM MES buffer and 500 mM KCl at pH 5.6. The data point at -528 mV was collected from an independent discontinuous experiment. The solid line represents the least squares analysis of all data points from which the $E_{1/2}$ was calculated to be -501 mV with an n-value of 1.03.

The electrochemical and spectral behaviors of triquat at low potentials were characterized using dSEC (Figure 3.6).

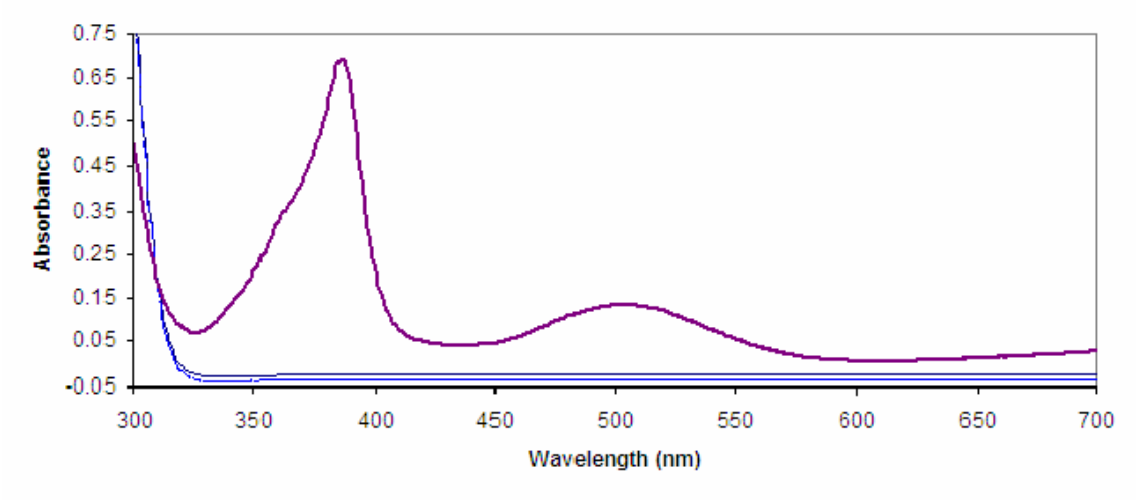

Figure 3.6: Representative plot of a single datum of a dSEC experiment of triquat (2.38 mM TQ, 50 mM MOPS, 500 mM KCl, pH 7.4) at E_{app} = -603 mV (purple line). Hg-Au amalgam served as the working and auxiliary electrodes. No absorbance is observed at -303 mV (blue lines).

The corresponding Nernst plot for triquat (Figure 3.7) was used to calculate an $E_{1/2}$ of -629 mV vs. NHE and a transfer of 0.48 electrons. The transfer of ~0.5 electrons is not consistent with the number of transferred electrons calculated using CV. This inconsistency might be caused by a difference in the interaction of the analyte and two different electrode materials.

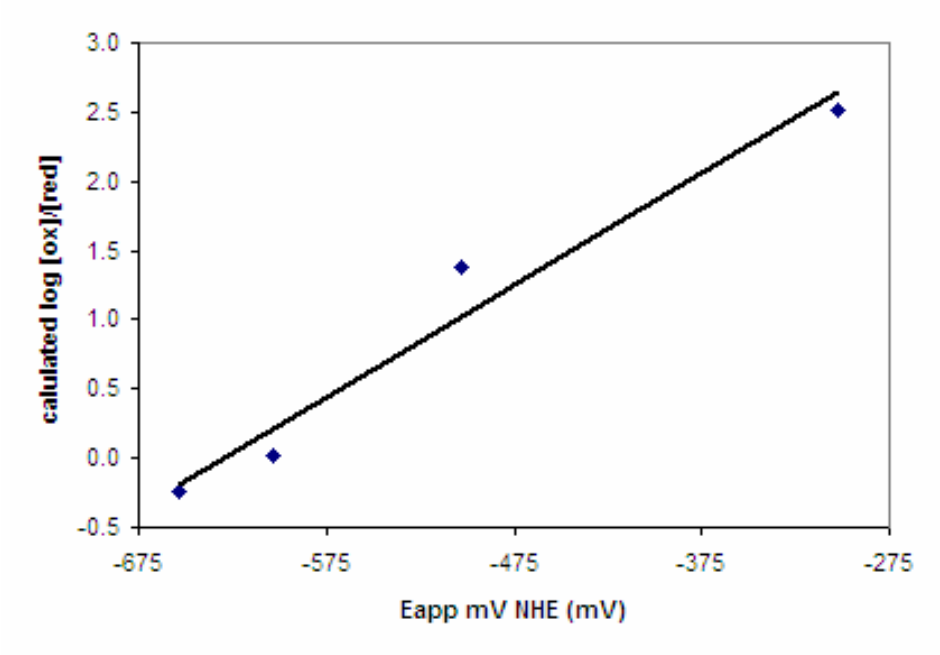

Figure 3.7: Nernst plot of 2.38 mM Triquat in 50 mM MOPS and 500 mM KCl at pH 7.4. The calculated $E_{1/2}$ is -629 mV and number of electrons transferred is 0.48. The solid line represents the least squares analysis of the data points from four separate experiments using amalgamated working and auxiliary electrodes.

3.3.3 Discontinuous Spectroelectrochemistry of Ti_2-Tf

Ti_2-Tf was studied using dSEC to reach very negative reduction potentials. Triquat served as an electrochemical mediator to facilitate the biphasic interaction between the solution-phase metalloprotein and the solid electrode surface. Figure 3.8 depicts the change in the observed spectrum of the fully oxidized protein-mediator solution (E_{app} = -303 mV) after the applied potential is decreased to -603 mV vs. NHE.

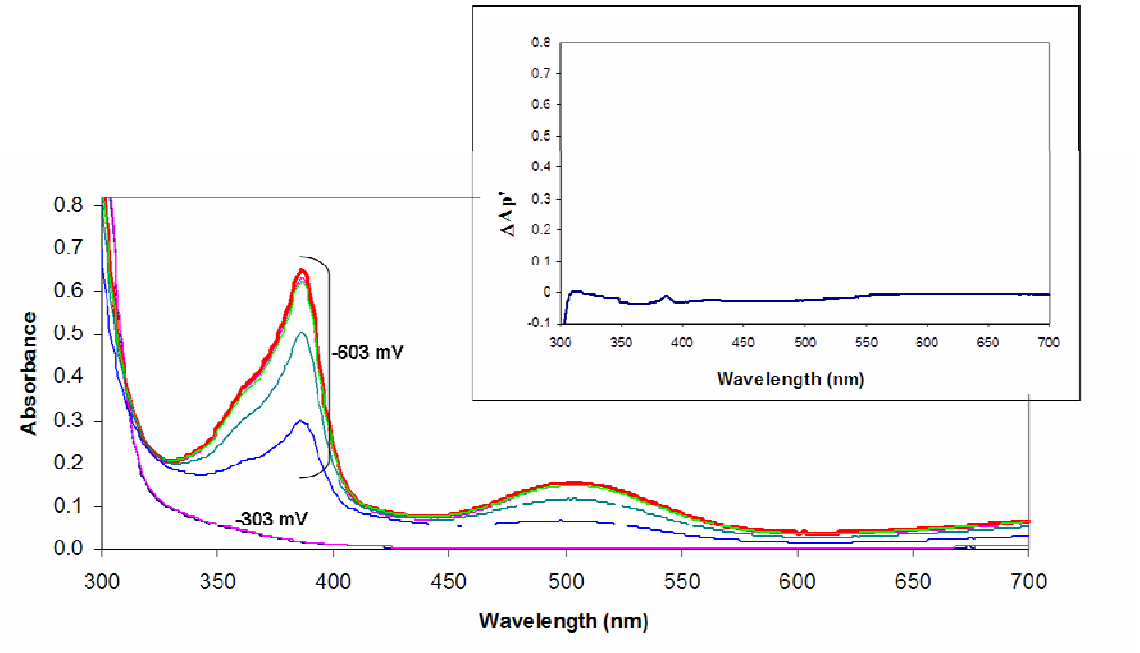

Figure 3.8: Spectra of a solution of Ti_2-Tf and triquat when an applied potential of -303 mV is decreased to -603 mV during a dSEC experiment. The bracket indicates the set of spectra taken over time after the potential is decreased until equilibrium in achieved. Inset: Subtraction of $\Delta A'_m$ from $\Delta A'_{pm}$ yields the change in absorbance due to protein alone ($\Delta A'_p$), after the potential was decreased from -303 mV to -603 mV. Conditions: 0.476 mM Ti_2-Tf and 2.38 mM triquat, 50 mM MES, 500 mM KCl at pH 5.6. Hg-Au amalgam served as the working and auxiliary electrodes.

The change in absorbance caused solely by the mediator ($\Delta A'_m$) was subtracted from the total change in absorbance ($\Delta A'_{pm}$) (Equation 3.9). The absorbance change due to the protein is shown in the inset of Figure 3.8. No reduction of Ti_2-Tf was observed at or above -600 mV vs. NHE under these conditions. The same result is seen at pH 7.4 (data not shown).

3.3.4 Electrochemical Characterization of Ti and Fe Complexes

We characterized the electrochemical behavior of Ti and Fe complexes of low molecular weight chelators that mimic the active site of human Tf. Using this binding site model approach, we constructed a LFER in order to estimate the reduction potential of Ti_2-Tf. EDTA, CDTA, and DTPA, are amine carboxylic acids, as is HBED that also includes two phenol groups (Figure 3.2), which chelate Fe(III) and Ti(IV) in a similar manner to the amino acids and synergistic anion involved in the metal-protein interaction of human transferrin. NAPHTHOL, which contains catechol oxygen donors (Figure 3.2) is used to help define the LFER. Citrate, an α-hydroxy carboxylic acid, is included in our plot, but for reasons described in Section 3.3.5.2 is not used in the linear least squares analysis. The interactions of these common metal chelators with Fe(III) are well understood and the reduction potentials of many of the corresponding complexes are available in the literature.[115-119] However, few electrochemical data are available for the corresponding Ti(IV) complexes.[120-122] We report here the preparation and electrochemical characterization of FeHBED, FeNAPHTHOL, TiCDTA, and TiDTPA.

3.3.4.1 TiCDTA[1]

A representative voltammogram of TiCDTA is shown in Figure 3.9. Although the peak to peak separation is large, the cathodic and anodic diffusion coefficients are within the same order of magnitude. This quasi-reversible system has an $E_{1/2}$ of -20 mV at pH 3.5. The electrochemical behavior of TiCDTA was studied as function of pH, electrode material, and ligand to metal ratio (data not shown).

[1] The electrochemical properties of TiCDTA have been reported previously.[123, 124] However, these references can not be used for our purposes as each either failed to describe to which scale the reported potentials are referenced or did not include sufficient information regarding pH, electrode material, or ligand/metal ratio.

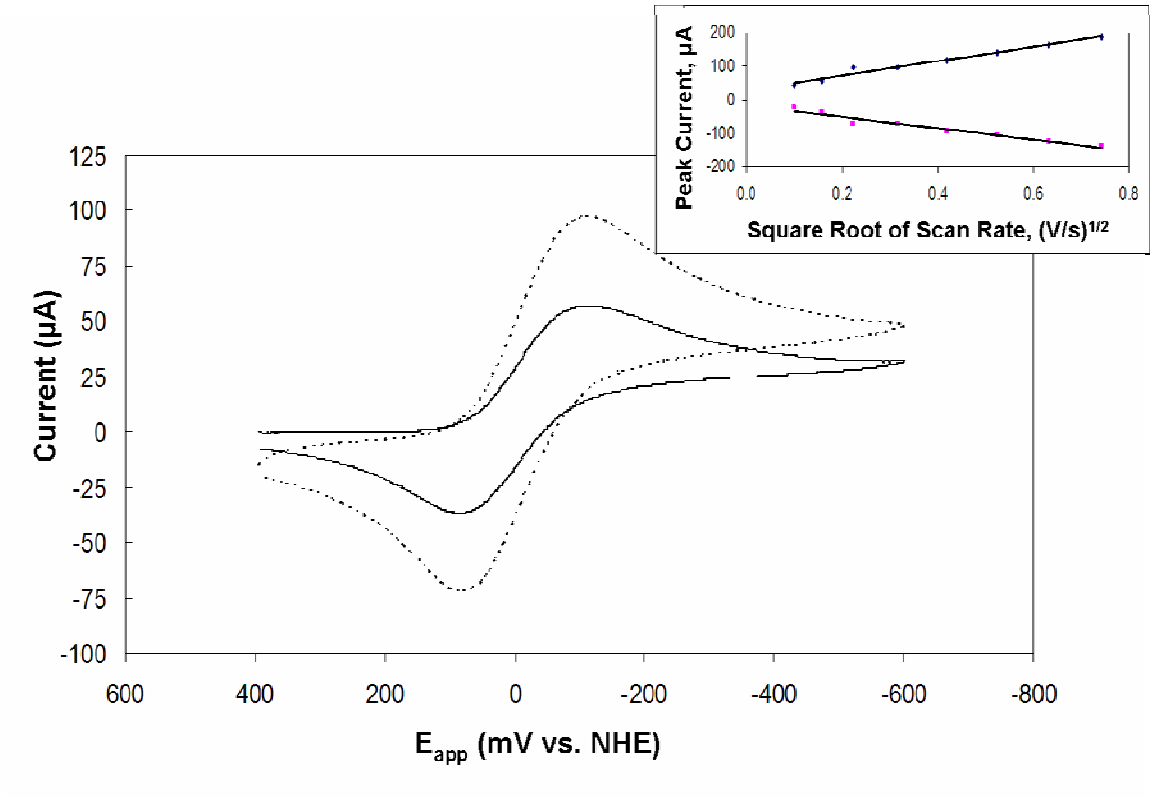

Figure 3.9: Representative cyclic voltammograms of TiCDTA with varying scan rates. Conditions: 25 mM TiCDTA (1/5 metal/ligand ratio), 0.1 M KCl, pH 3.5, glassy carbon working electrode, Ag/AgCl reference electrode, scan rates 25 mV/s (solid line) and 50 mV/s (dotted line). $E_{1/2}$ = -20 ± 6 mV vs. NHE. Inset: Peak currents plotted as a function of the square root of the scan rates where $D_{ano} = 0.8 \times 10^{-6}$ cm²/s and $D_{cat} = 1.3 \times 10^{-6}$ cm²/s. Peak to peak separation was ca. 200 mV over the scan rates 25 - 50 mV/s.

3.3.4.2 TiDPTA[2]

The electrochemical behavior of TiDPTA was studied using CV. The effects of pH, ligand to metal ratio, and working electrode material were investigated (data not shown). The representative voltammogram shown in Figure 3.10 depicts the quasi-reversible reduction of TiDTPA, which is independent of changes in pH between 2.5 and 4.5. The peak to peak separation is quite large and the calculated diffusion coefficients are more than an order of magnitude different. However, a re-oxidation peak is apparent.

[2] The electrochemical properties of TiDTPA have been reported previously.[125] However, this reference can not be used for our purposes as the authors failed to describe to which scale the reported potentials are referenced and did not include sufficient information regarding pH, electrode material, or ligand/metal ratio.

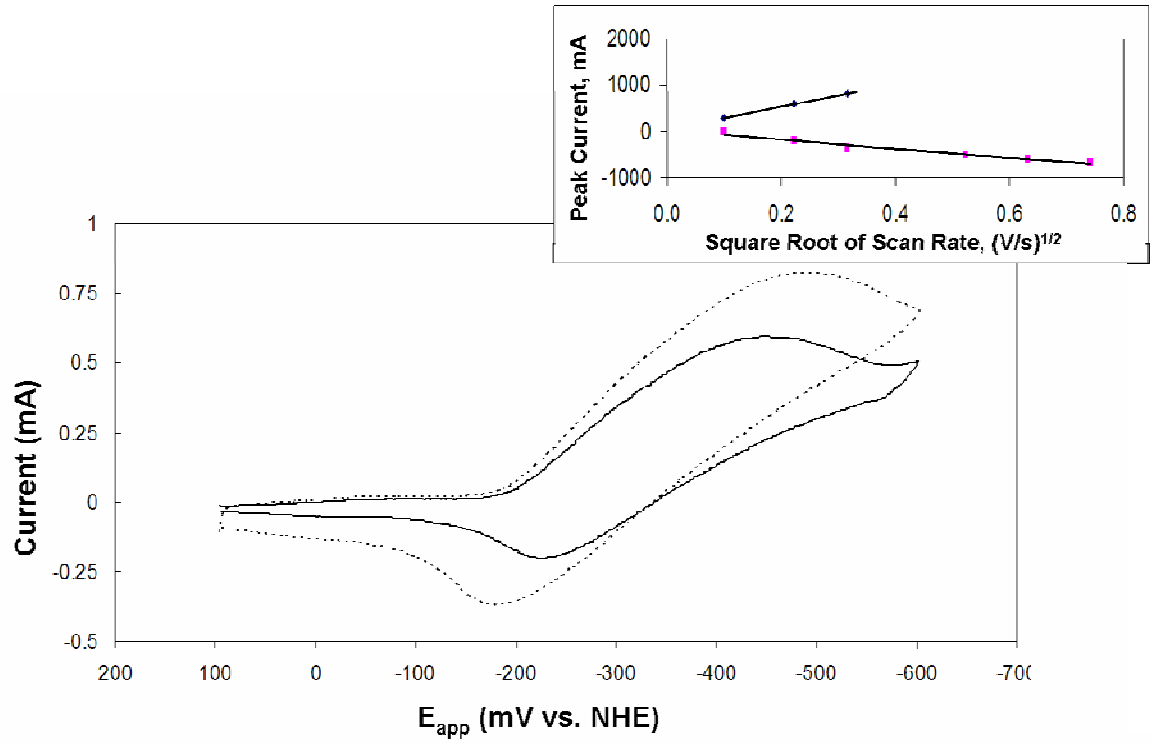

Figure 3.10: Cyclic voltammograms of TiDTPA with varying scan rates. Conditions: 25 mM TiDTPA (1/5 metal/ligand ratio), 0.1 M KCl, pH 3.5, platinum working electrode, Ag/AgCl reference electrode, scan rates 50 mV/s (solid line) and 100 mV/s (dotted line). $E_{½}$ = -332 ± 4 mV vs. NHE. Inset: Peak currents plotted as function of the square root of the scan rates where $D_{ano} = 3.3 \times 10^{-4}$ cm²/s and $D_{cat} = 2.0 \times 10^{-3}$ cm²/s. Peak to peak separation was 220 mV for the 50 mV/s scan and 308 mV for the 100 mV/s scan.

3.3.4.3 FeHBED

The electrochemical behavior of FeHBED was studied using CV. The effects of background electrolyte, and working electrode material were investigated (data not shown). The voltammogram shown in Figure 3.11 represents the reversible reduction of FeHBED, centered around an $E_{1/2}$ value of -365 mV vs. NHE.

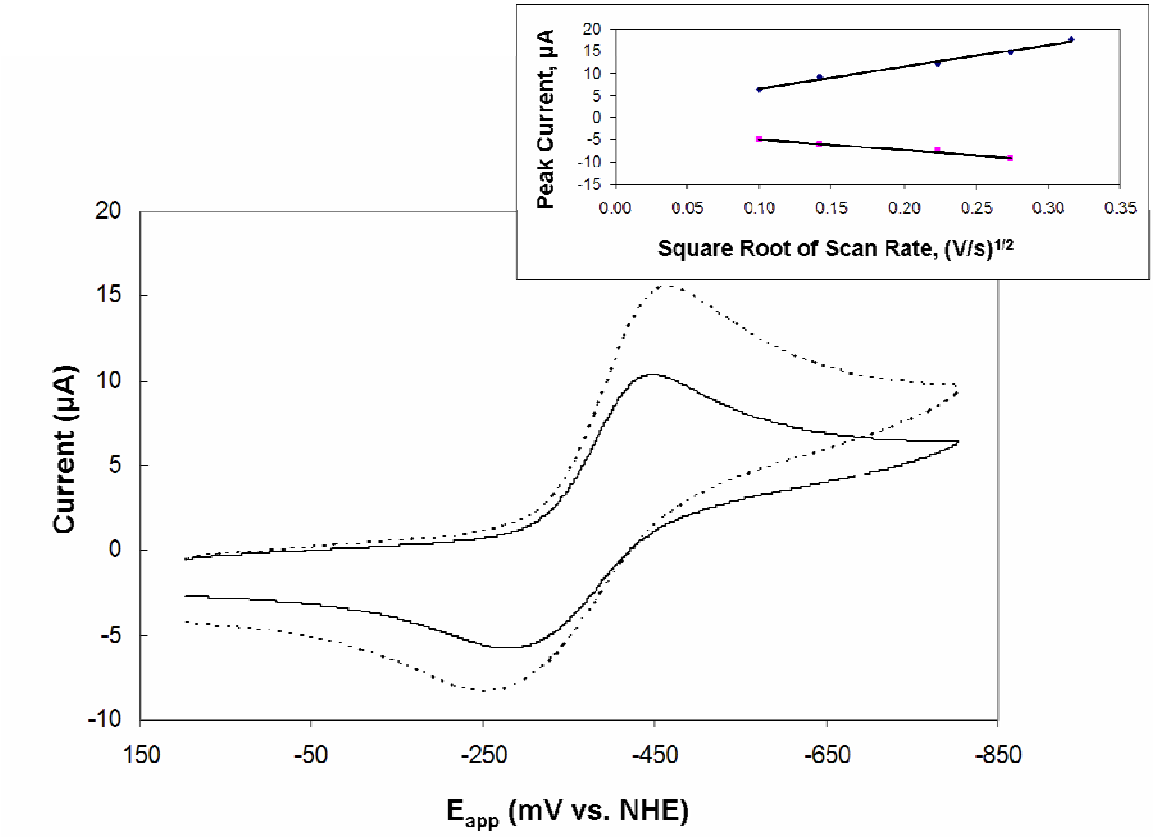

Figure 3.11: Cyclic voltammograms of FeHBED with varying scan rates. Conditions: 2 mM FeHBED (1/1.1 metal/ligand ratio), 0.1 M $NaNO_3$, pH 8, glassy carbon working electrode, Ag/AgCl reference electrode, scan rates 20 mV/s (solid line) and 50 mV/s (dotted line). $E_{½}$ = -365 ± 5 mV vs. NHE. Inset: Peak currents plotted as function of the square root of the scan rates where $D_{ano} = 1.6 \times 10^{-8}$ cm²/s and $D_{cat} = 6.7 \times 10^{-8}$ cm²/s. Peak to peak separation was 92 mV for the 2 mV/s scan (data not shown). Peak to peak separation was 157 mV for the 20 mV/s scan and 208 mV for the 50 mV/s scan.

3.3.4.4 FeNAPHTHOL

At the concentrations used for the electrochemical analysis, significant solubility issues were encountered. According to the speciation plot resulting from published equilibrium constants, the tris-complex should be the predominant species at pH 8.[126,

127] The presence of the tris-complex was visually confirmed by the change in color of the solution from ink blue to deep orange-maroon wine. This color change indicates a mixture of tris- and bis- species consistent with the absorbance spectrum for the tris-complex (λ_{max} = ~450 nm) and the bis-complex (λ_{max} = ~500 nm).

The electrochemical behavior of FeNAPHTHOL was studied using CV. The effects of pH and ligand to metal ratio were investigated. The voltammogram shown in Figure 3.12 represents the semi-reversible reduction of FeNAPHTHOL in solution.

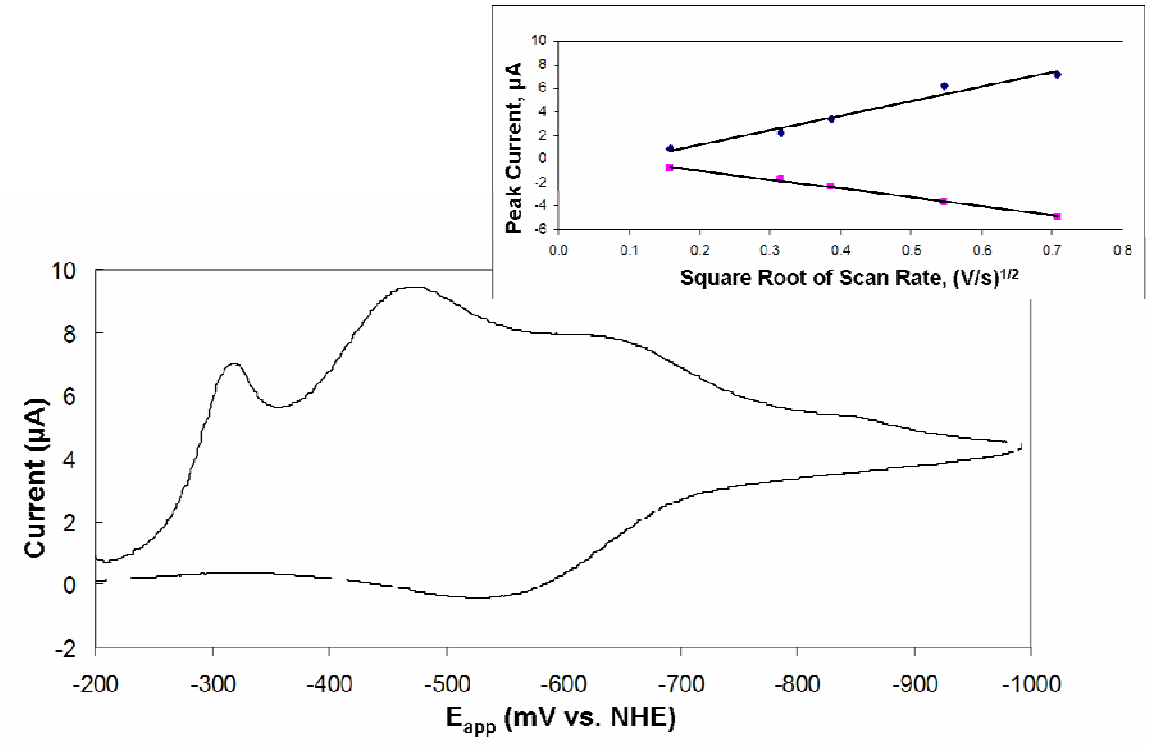

Figure 3.12: Cyclic voltammograms of FeNAPHTHOL with varying scan rates. Conditions: 38.5 mM 2,3-dihydroxynaphthalene, 4 mM $FeCl_3$ (9.6/1 ligand to metal ratio), 0.08 M KNO_3 in 20% methanol, pH 7.6, hanging drop Hg electrode, Ag/AgCl reference, and Pt wire auxiliary. Applied potentials are vs. NHE. Inset: Peak currents plotted as function of the square root of the scan rates where $D_{ano} = 3.2 \times 10^{-8}$ cm²/s and $D_{cat} = 8.3 \times 10^{-8}$ cm²/s. Peak to peak separation was 94 mV for the 300 mV/s scan (data not shown) and 118 mV for the 500 mV/s scan.

Two separate solutions were prepared and analyzed at various scan rates and times after preparation. The average $E_{1/2}$ value corresponding to the tris-complex $[Fe(2,3\text{-dihydroxynaphthlene})_3]^{3-}$ was -575 ± 11 mV vs. NHE. 2,3-dihydroxynaphthlene under the same experimental conditions does not show significant redox behavior. The diffusion coefficient calculated from the cathodic peak currents for the tris-complex is 8 x 10^{-8} cm² s^{-1} and from the anodic peak currents is 3 x 10^{-8} cm² s^{-1}.

In addition to the redox couple we attribute to the tris-complex, two other reduction peaks were consistently observed at pH 8 for a solution with a ligand to metal ratio of 10 to 1. When the pH is lowered to pH 4, where the speciation plot predicts the bis-complex should dominate, the redox couple we attribute to the tris-complex disappears (data not shown).

In order to confirm the assignment of the most negative reduction peak at $E_{1/2}$ = -575 mV vs. NHE to the tris-complex, the spectrophotometric and electrochemical behavior of very dilute solutions (10/1 ligand to metal ratio and 5/1 ligand to metal ratio) were investigated. The dilute concentration prevented the precipitation observed at higher concentrations. At pH 12.5, the solution with a 10 to 1 ligand to metal ratio the absorbance spectra has an absorbance maximum at ~450 nm, similar to tris-complexes of other similar iron ligands.[128-130] For the same solution, a single irreversible reduction peak at ~600 mV vs NHE confirms our assignment of the redox couple with a $E_{1/2}$ of -575 mV as corresponding to the presence of the tris-complex in the saturated solution.

3.3.5 Iron and Titanium Complexes Mimic the Protein Active Site

3.3.5.1 Speciation and Redox Potentials of Model Complexes

For each metal-ligand complex, the species that most closely mimics the active site of the metal-loaded Tf at biological pH was identified using reported literature structures, stability constants, and species distribution plots.[121, 126, 127, 131-134] As

well, the effects of changes in pH on the E½ for each complex characterized here (FeHBED, FeNAPHTHOL, TiDTPA, and TiCDTA) were investigated (data not shown). In general, the reduction potential decreased as pH increased (data not shown).

Table 3.1 summarizes the species, pH, and structure that correspond to the redox potentials used to construct the LFER discussed in Section 3.3.5.3.

Table 3.1: Redox potentials used to construct LFER and complex structures

Complex	$E_{1/2}$ (mV vs. NHE)	pH	Species	Structure (L/M)
FeEDTA[a]	120	3-7	$(FeEDTA)^-$	hexadentate/ 6 or 7 coordinate
TiEDTA[b]	22	0-3	TiEDTA or $Ti(EDTA)H_2O$	hexadentate/ 6 or 7 coordinate
FeCDTA[c]	41	4-7	$(FeCDTA)^-$	hexadentate/ hexacoordinate
TiCDTA[d]	-20	3.5	TiCDTA	hexadentate/ hexacoordinate
FeDTPA[e]	80	7	$(FeDTPA)^-$	hexadentate/ hexacoordinate
TiDTPA[f]	-332	3.5	TiDTPA	hexadentate/ hexacoordinate
FeCIT[g]	-82	7	$(FeL)^{3-}$ L = Rhizoferrin	hexadentate/ hexacoordinate
TiCIT[h]	-312	3	$Ti(H_2cit)_3^{2-}$	3 bidentate/ hexacoordinate
FeHBED[i]	-365	8	$(FeHBED)^-$	hexadentate/ hexacoordinate
TiHBED[j]	-641	3-4	TiHBED	hexadentate/ hexacoordinate
FeNAPHTHOL[k]	-575	8	$[Fe(L)_3]^{3-}$	bidentate/ Hexacoordinate
TiNAPHTHOL[l]	-1122	7	$[Ti(L)_3]^{2-}$	bidentate/ Hexacoordinate

a. FeEDTA - Hexadentate chelation with possible water coordination at seventh site.[115, 116, 135]

b. TiEDTA - Hexadentate chelation with possible water coordination at seventh site.[120, 136]

c. FeCDTA - [115, 116, 118, 119]

d. TiCDTA - Redox potential determined herein. Redox potential is independent of pH study until 3.5 (data not shown). Structure assumed to be similar to FeCDTA.

e. FeDTPA - Small variations in $E_{1/2}$ values reported literature due to varying L/M ratio.[115, 117]

f. TiDTPA - Redox potential reported herein. Redox potential is independent of pH between pH 2.5 and 5 (data not shown). Structure discussed previously.[125]

g. FeCIT - Rhizoferrin model used. See Section 3.3.5.3.

h. TiCIT - [122] [137]

i. FeHBED - Redox potential determined herein. Structure reported previously.[131, 132, 138]

j. TiHBED - [121]

k. FeNAPHTHOL - Redox potential determined in this work. Speciation determined using references [126, 127].

l. TiNAPHTHOL - [139]

3.3.5.2 Treatment of Published Electrochemical Data for FeCIT

The redox behavior of Fe(III)citrate is under intense electrochemical investigation and numerous conflicting results have been published.[140-144] The wide variety of values reported for the reduction potential of Fe(III)citrate is certainly due to the complex speciation of Fe(III)citrate complexes in aqueous solution and the difficulty therefore associated with such measurements. Values have been reported as high as +372 mV vs. NHE [140] and we have measured reduction potentials as low as -350 mV vs. NHE (data not shown). Therefore, we elected to use the well defined reduction potential of iron-Rhizoferrin (-82 mV vs. NHE at pH 7, $[FeL]^{3-}$), a fungal siderophore, as an estimate of the $[Fe(citrate)_2]^{5-}$ reduction potential.[145] Rhizoferrin is composed of two citric acid molecules and is therefore a good model for the $[Fe(citrate)_2]^{5-}$ complex of interest (see Figure 3.2).

3.3.5.3 Linear Free Energy Relationship

In Figure 3.13, the reduction potentials of several Ti(IV) complexes are plotted as a function of the reduction potentials of the corresponding Fe(III) complexes and a linear relationship is apparent. $E_{1/2}$ is related to the free energy associated with the reduction of the metal complex. Therefore, the trend shown in Figure 3.13 is called a LFER.

pH affects metal-ligand complex speciation in solution and changes in the first coordination shell modulate reduction potentials. We therefore investigated the change

in reduction potential for each metal-ligand mixture as a function of pH. In general, the reduction potential decreased as pH increased (data not shown). For each complex, the species that most closely mimics the active site of the metal-loaded transferrin at biological pH was identified. Therefore, the reduction potentials used in the construction of our LFER were obtained at various pH values. The citrate data point poses a particular problem with respect to pH and speciation. Consequently, although the (Fe/Ti)CIT data point is shown in Figure 3.13, it was not included in the least squares analysis of either line shown.

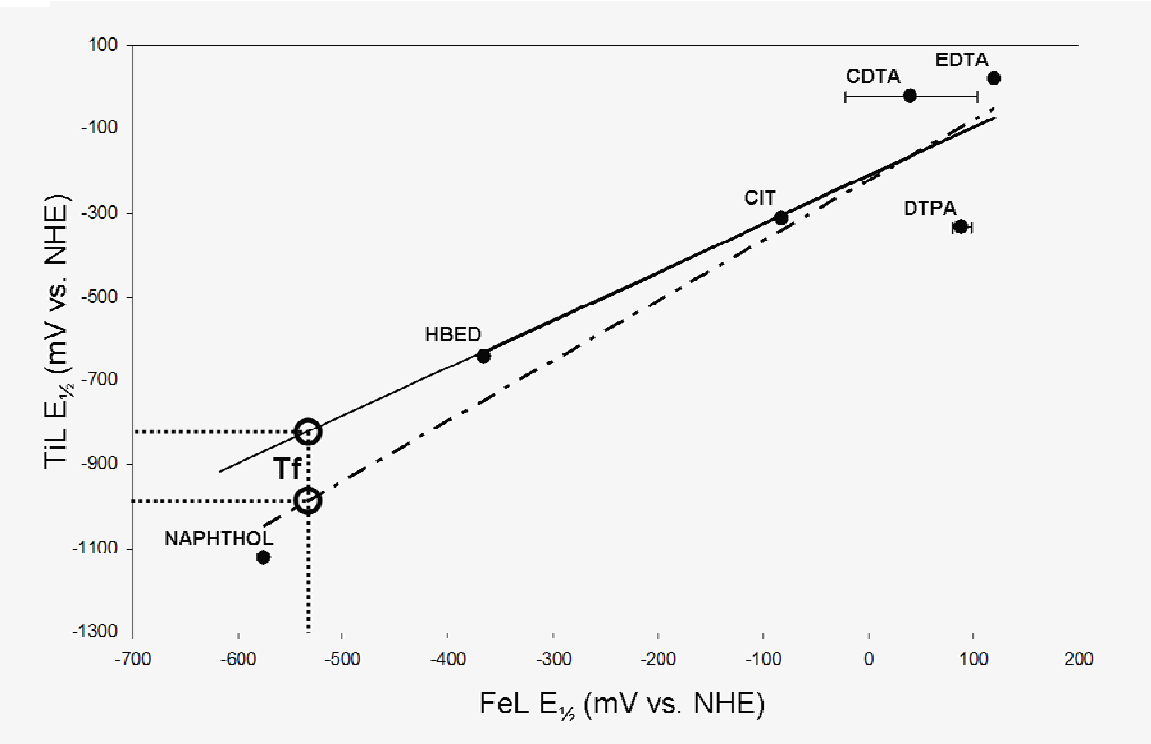

Figure 3.13: Plot of measured $E_{1/2}$ values for Ti(IV) complexes as a function of measured $E_{1/2}$ values for the corresponding Fe(III) complexes. Data for FeEDTA (pH 3-7)[115, 116], TiEDTA (pH 0-3)[120], TiHBED (pH 3-4)[121], FeDTPA (pH 7)[115, 117], FeCDTA (pH 3-7)[115, 116, 118, 119], TiCIT (pH 3)[122], TiNAPHTHOL (pH 7)[139], and FeCIT (estimated value-see Section 3.3.5.2) were taken from the literature, while data for FeHBED (pH 8), TiDTPA (pH 3.5), FeNAPHTHOL (pH 8), and TiCDTA (pH 3.5) were determined in this work. Data points represent the $E_{1/2}$ value for the form of complex where the inner coordination shell most closely models the Tf binding site. For complexes for which a range of redox potentials were reported in the literature for a given species, the datum point represents the average of the reported values. Solid line represents a linear least squares fit to data points for complexes containing amine carboxylic acids (HBED, CDTA, EDTA, and DTPA), for which the slope = 1.2 $\pm$ 0.5 and intercept = -200 $\pm$ 100 mV. The dashed line represents linear least squares fit to data points for complexes containing NAPHTHOL and amine carboxylic acids (HBED, CDTA, EDTA, and DTPA), for which the slope = 1.4 $\pm$ 0.3 and intercept = -220 $\pm$ 90 mV. The datum point representing the $E_{1/2}$ of TiCIT and the estimated $E_{1/2}$ of FeCIT ($E_{1/2}$ for FeRhizoferrin) was not included in either least squares analysis due to uncertainties in complex speciation. Vertical and horizontal dotted lines intersect (open circles) at the measured $E_{1/2}$ value for Fe_2-Tf at endosomal conditions [78] and the predicted $E_{1/2}$ values for Ti_2-Tf.

3.4 Discussion

3.4.1 Method Development

A discontinuous SEC method was developed to investigate metalloproteins with very negative reduction potentials. We used methyl viologen to calibrate the spectroelectrochemical experiments. Using CV we measured an $E_{1/2}$ of -460.7 mV (NHE), while SEC yielded an $E_{1/2}$ value of -501 mV for methyl viologen. The literature value for the $E_{1/2}$ of methyl viologen is -450 mV.[77] This 40 mV difference could be due to an ohmic drop caused by differences in electrode composition and surface area, ionic strength, the presence of buffer in the SEC solution, and junction potentials as compared to the CV set up. The method and equipment of dSEC produced reasonable values for the $E_{1/2}$ and the number of electrons transferred for this analyte.

Triquat appeared to be an appropriate mediator based on CV data. The first reduction of triquat was shown to be reversible and the measured $E_{1/2}$ value (-569 mV) was within experimental error of the literature value (-540 mV).[146] However, the dSEC experiment yielded significantly different results. The $E_{1/2}$ value (-629 mV) was more than 60 mV lower than expected and the n-value calculated from the dSEC data was half the ideal value of one. This may be evidence that the mediator does not interact productively with the Hg-Au electrode.

Additionally, the radical cation of triquat (Equation 3.11) absorbs light in the visible spectrum, significantly complicating the data analysis. In an ideal situation, the

re-oxidation of the visible radical cation (reduced mediator) is coupled to the reduction of the analyte (Ti_2-Tf) as shown in Figure 3.14. In this case the absorbance of the mediator should be minimal.

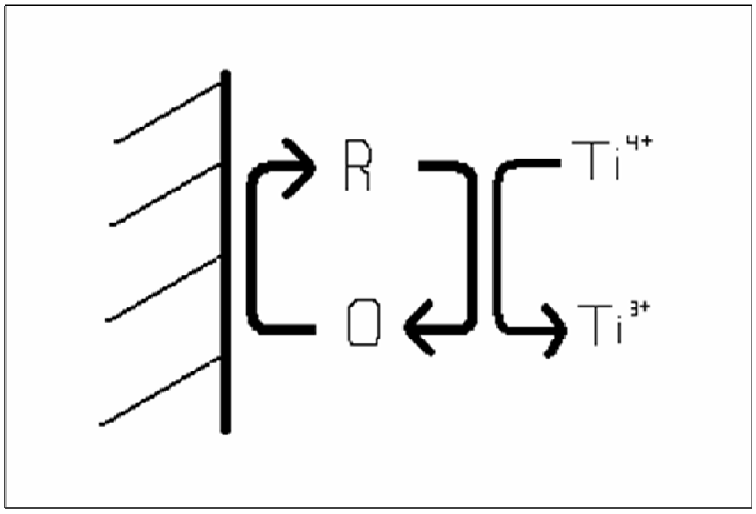

Figure 3.14: Depiction of the redox coupling between the solid electrode, the mediator, and the analyte in an electrochemical experiment.

However, our dSEC studies show that triquat strongly absorbs UV-visible light at low potentials, indicating the mediator is not being reoxidized by the protein. Two explanations are possible: 1) a second irreversible reduction of the mediator may occur at low potentials, or 2) the reduction potential of Ti^{4+} is too low to be reduced by the mediator. In both cases, the mediator would be trapped as the intensely colored, reduced species.

An ideal mediator should: 1) have a known $E_{1/2}$ within the potential range of the analyte, 2) have fast homo- and heterogeneous electron transfer rates with known stoichiometry, 3) be stable in both redox forms, and 4) not interfere optically or

physically with the analyte.[36] Without an appropriate re-oxidizing agent, it is evident that triquat does not meet these criteria. Therefore, another mediator with a more negative reduction potential and a more stable reduced species should be explored in order to optimize this protocol for general use.

3.4.2 Electrochemical Behavior of Ti_2-Tf

Although this method of dSEC is not yet appropriate for general use, important information can be gleaned from these studies regarding the electrochemical behavior of Ti_2-Tf. No reduction of Ti_2-Tf was observed at or above -600 mV vs. NHE. We conclude that the reduction potential of Ti_2-Tf therefore is more negative than -600 mV and not detectable given the limits of the dSEC experiment at our conditions. One piece of evidence that the reduction potential of Ti_2-Tf is lower than -600 mV (the most negative applied potential) is the fact that the protein spectrum remained constant (Figure 3.8 Inset). Another confirmation is that the spectral change of the mediator (as a function of the applied potential) was not affected by the presence of the protein. Both indicate that the oxidizing power (or ability to be reduced) of Ti_2-Tf is not strong enough (high enough $E_{1/2}$ value) to re-oxidize the reduced form of the mediator. Said another way, the reduction potential ($E_{1/2}$) of Ti_2-Tf is so low the protein does not interact with the reduced form of the triquat and the mediator/electrode cycle is broken.

3.4.3 Predicted Reduction Potential of Ti_2-Tf

In plotting the reduction potentials of our series of Ti(IV) complexes that mimic that active site of the Tf as a function of the reduction potentials of the corresponding Fe(III) complexes, a LFER is apparent (Figure 3.13). Two linear least squares analyses are shown, with and without the NAPHTHOL ligand, which is least representative of the transferrin binding site due to being bidentate and having only –OH donor groups. Using these trends we predict the redox potential of Ti_2-Tf to be around -900 mV vs. NHE. The first coordination shell surrounding each metal exerts a similar effect on both metals, yielding a slope in Figure 3.13 close to one. Consideration of each TiL/FeL pair and the scaling factor (Figure 3.13 intercept) shows that while the $E_{1/2}$ for TiL is consistently lower than FeL the difference in redox potentials is significantly smaller than the 570 mV difference in the aquo couple redox potentials [3]. It is likely that this reduction in scaling factor is due to differences in metal-ligand bond strength in the oxidized and reduced forms of the titanium and iron complexes, and hydration energy effects.

3.4.4 Transferrin-Mediated Titanium Transport

Our data support the general trend that Ti(IV) complexes have lower reduction potentials than the corresponding Fe(III) complexes and we predict the reduction potential of Ti_2-Tf to be ca. -900 mV (NHE) (see Figure 3.13). This finding corresponds

with the fact that we did not observe any reduction of Ti_2-Tf above -600 mV using dSEC. By analogy to iron we may anticipate an approximate 200 mV positive shift in the reduction potential of Ti_2-Tf upon binding to the receptor. However, that shift would not be sufficient to move the reduction potential into the biologically accessible range. Therefore, the extremely negative reduction potential of Ti_2-Tf precludes a Ti(IV) →Ti(III) reduction-induced transferrin release mechanism for titanium transport.

3.5 Conclusions

In order to investigate the metalloprotein titantium transferrin, we have elected to use the metal as our probe. Using dSEC, we have shown that the reduction potential of Ti_2-Tf is lower than the reduction potential of the mediator triquat. As well, we have utilized the LFER between Fe(III) complexes that mimic the active site of Tf and the corresponding Ti(IV) complexes, to predict the reduction potential of Ti_2-Tf. Given that the reduction potential of Ti_2-Tf is predicted to be at least 200 mV more negative than Fe_2-Tf, we propose that the release of titanium from Tf within a cell will follow a non-redox process (Figure 3.15). These studies further suggest that the Tf-mediated transport of titanium is dissimilar to iron transport and deserves further scrutiny as the fate of titanium has implications in many facets of biology.

During revison and defense of this dissertation, the manuscript reporting some of the work disccused in this chapter was accepted for publication in the Journal of

Inorganic Biochemistry.[83] Figure 3.15 was submitted to the journal as the Table of Content image for the manuscript.

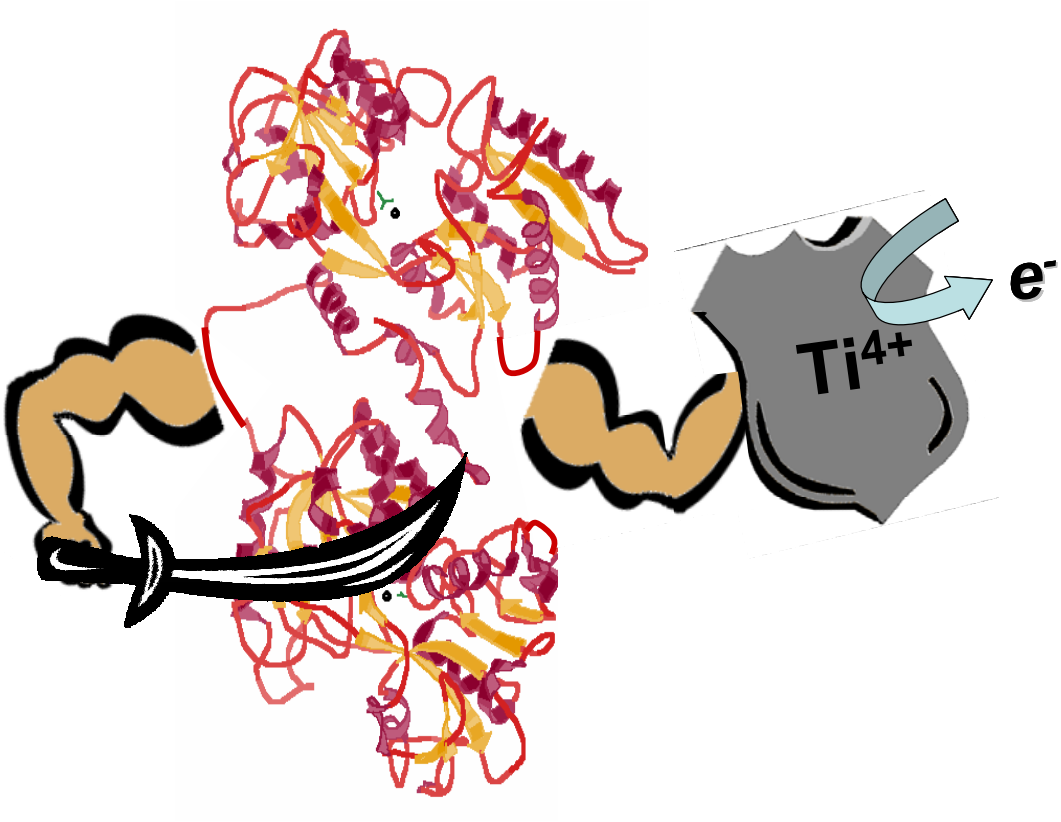

Figure 3.15: The protein shield, which comprises the first and second coordination shells of Ti(IV), repels a reducing electron from attack.

4. Hijacking Transferrin Bound Iron: Protein-Receptor Interactions Involved in Iron Transport in *N. gonorrhoeae*

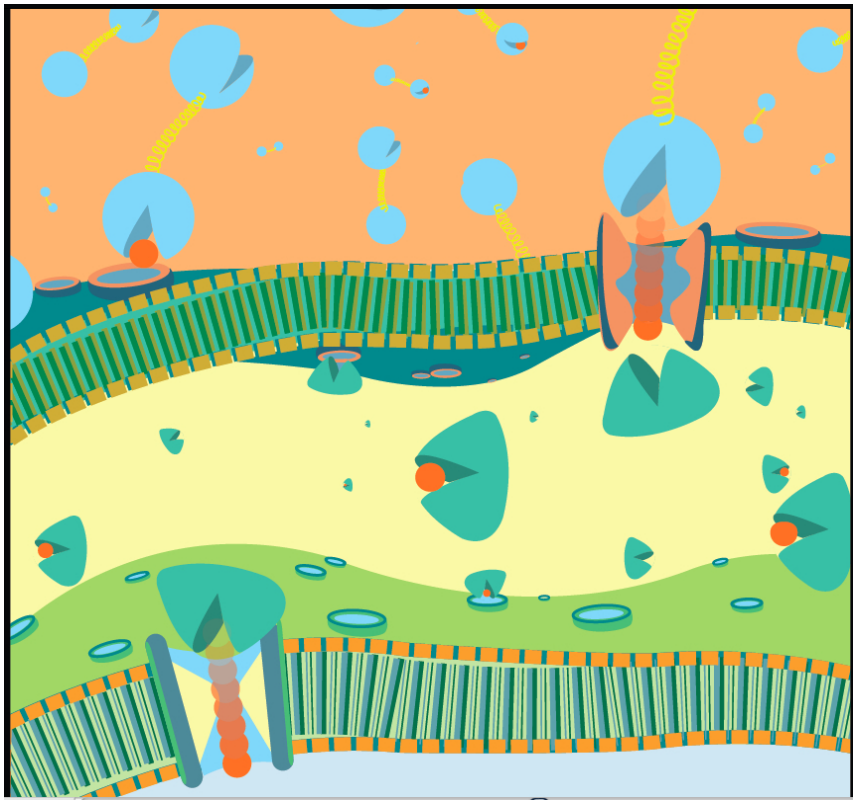

Figure 4.1: The major findings of this study were published in and featured on the cover of the journal Metallomics.[147] Artwork by S. Grant Shuler.

Dr. Petra L. Roulhac, Dr. Katherine D. Weaver, and the author contributed equally to this collaborative work. The author's predominant role in this collaboration was to interpret the experimental results, discern the significance of this work in the context of this rapidly growing sub-field of microbiology, facilitate the collaboration between multiple laboratories, and communicate the findings through publication. The author is grateful to all those involved for their hard work and cooperation.

4.1 Introduction

In this Chapter, we shift our focus to the thermodynamic properties of the protein. We have elected to use the protein as the probe in order to investigate the protein-protein interactions involved in the iron transport pathway of *N. gonorrhoeae*.

4.1.1 Background

Almost all living organisms must acquire iron from their environment. *Neisseria gonorrhoeae* employ a complex system of proteins to strip iron from the human host protein transferrin (Tf) and transport iron across its membranes. Transferrin binding protein A (TbpA), a 100 kDa outer membrane protein, is required for utilization of transferrin-bound iron and functions synergistically with Transferrin binding protein B (TbpB).[148-150] While the surface-exposed lipoprotein TbpB is not absolutely required for *in vitro* growth by *N. gonorrhoeae* on Tf as a sole iron source, TbpB makes iron utilization more efficient.[149] In the periplasm, Ferric binding protein A (FbpA) binds iron with a synergistic anion and delivers it to the cytoplasmic membrane.[6, 151-155] Although the important components of this transport process have been identified, the contributions of TbpA and TbpB to removal of iron from Tf have not been individually evaluated and the biological process of how FbpA acquires transferrin-derived iron in intact cells remains unclear.

4.1.2 Component Proteins

4.1.2.1 TbpA

The mechanisms of iron transport in other Gram-negative bacteria have been extensively studied [156-165] and the crystal structures of several key proteins have been described.[151, 166-168] Iron acquisition can be accomplished by hijacking the iron bound by host heme proteins or metalloproteins, as is the case for *N. gonorrhoeae* discussed here, or by incorporating extracellularly chelated iron in the form of ferric siderophores. Acquisition of siderophore bound iron involves binding to and passage through integral outer membrane proteins called TonB-dependent transporters.[169-173] These transporters share a similar architecture, being comprised of a 22-stranded β-barrel and an amino-terminal plug domain, which is sequestered within the lumen of the β-barrel.[166, 174] The receptor proteins in *Neisseria* (TbpA/TbpB), which acquire iron from the human metalloprotein Tf, have not yet been crystallized. However, by analogy with the other TonB-dependent transporters, it is expected that the integral membrane, TonB-dependent protein TbpA forms a β-barrel, which is periplasmically-occluded by a plug domain.[148, 175, 176] Dislocation or extraction of the plug from within the β-barrel of the transporter and subsequent presentation of transported ligand to the periplasmic binding protein is thought to be the general mechanism of transport by TonB-dependent outer membrane receptors.[177]

Specific parts of the structure of TbpA have been shown to be surface exposed and/or important for functioning. Hemagglutinin epitope tags were used to identify

surface exposed regions the proposed eleven loops of the protein.[178] As well, insertions in the proposed plug domain of TbpA revealed partial surface exposure of the plug.[178] Insertions in the plug and loop 3 decreased Tf binding and retarded growth. However, while mutants with insertions in loops 2, 9, and 11 were still able to bind Tf, these altered forms of TbpA could not transport iron.[178] Interestingly, TbpB was able to compensate for these mutation in TbpA, restoring utilization of iron from Tf.[178]

4.1.2.2 TbpB

The iron uptake machinery of *N. gonorrhoeae* is unique in that it involves an auxiliary protein in addition to the Ton-B dependent transporter. The auxiliary protein, TbpB, varies in size from 64 to 85 kDa depending on the strain of bacteria.[149] TbpB is not required for iron acquisition from Fe_2-Tf in the wild-type bacteria, but is thought to make iron utilization more efficient. TbpB is able to discriminate between apo- and holo-Tf and in terms of binding constant can compete with the mammalian transferrin receptor for binding the iron transport protein.[150]

The structure and location of TbpB has also been investigated using epitope tags. TbpB is proposed to consist of two lobes that can each bind Fe_2-Tf.[179] As well, epitope insertions were used to demonstrate that TbpB is completely surface exposed.[179] It is thought that a lipid moiety anchors TbpB to the surface of the outer membrane.

As discussed in the previous section, TbpB is able to restore the action of Fe_2-Tf utilization in some bacterial mutants that have specific defects in TbpA. For example, a mutation in loop 9 of TbpA is able to bind Fe_2-Tf, but is not able to acquire iron. TbpB can compensate for this defect, restoring the utilization of Fe_2-Tf as the iron source.[179] The ability of TbpB to compensate for defects in TbpA requires both lobes of TbpB and both lobes have been shown to contribute to Tf binding.[179]

4.1.2.3 TonB

TonB-dependent transporters require TonB and metabolic energy to accomplish transport across the outer membrane. TonB, in a complex with ExbB and ExbD, is energized by the proton motive force across the cytoplasmic membrane.[180] TonB-derived energy is then conveyed to the outer membrane transporter proteins to accomplish iron internalization.[181] The mechanism through which TonB conveys energy across the periplasm is under intense investigation.[172, 180, 181]

Energy transduction from TonB to accomplish vectorial transport of the ligand into the periplasm involves an interaction between the carboxy-terminal domain of TonB and a short amino acid sequence near the amino-terminus of TonB-dependent transporters, known as the TonB-box.[182] The TonB box of gonococcal TbpA has been defined and has been shown to be required for interaction with TonB and iron internalization from Tf.[183] Some TonB-dependent transporters such as FpvA, the β-

barrel transporter for iron-pyoverdine in *P. aeruginosa*, are hypothesized to only bind TonB when the cargo is bound to the receptor.[170] However, another unique feature of TbpA is that Tf does not have to be bound in order for TonB to interact with TbpA.[183]

Since TbpA is in general similar to other TonB-dependent transporters, it is thought that TonB is required to move the plug (out of the barrel or around inside the barrel) to facilitate cargo transport. However in *N. gonorrhoeae*, TonB-derived energy is also required for efficient release of Tf from the gonococcal cell surface, as Tf dissociation from intact gonococci is dramatically inhibited in the absence of TonB.[184, 185] It is also possible that the energy derived from TonB is involved in other steps of the transport process.

4.1.2.4 FbpA

FbpA, which is required for bacterial growth, is 34 kDa periplasmic binding protein that acquires iron after iron is stripped from Tf and crosses the outer membrane. Once loaded with iron, FbpA transports the cargo across periplasm and delivers it to the cytoplasmic membrane receptor FbpB/C.[152, 186, 187] FbpA/B/C constitute an ABC (ATP-binding cassette) transporter that utilizes energy derived from ATP to move iron across the cytoplasmic membrane and into the cytosol where it can be metabolized.[152] The reader is referred to two reviews for a complete understanding of ATP-binding cassettes.[188, 189]

The structure of FbpA is depicted in Figure 4.2. On the right is a ribbon diagram of the crystal structure of holo-FbpA (PDB code ID9Y) and on the left is a cartoon diagram of the active site of the protein.[190]

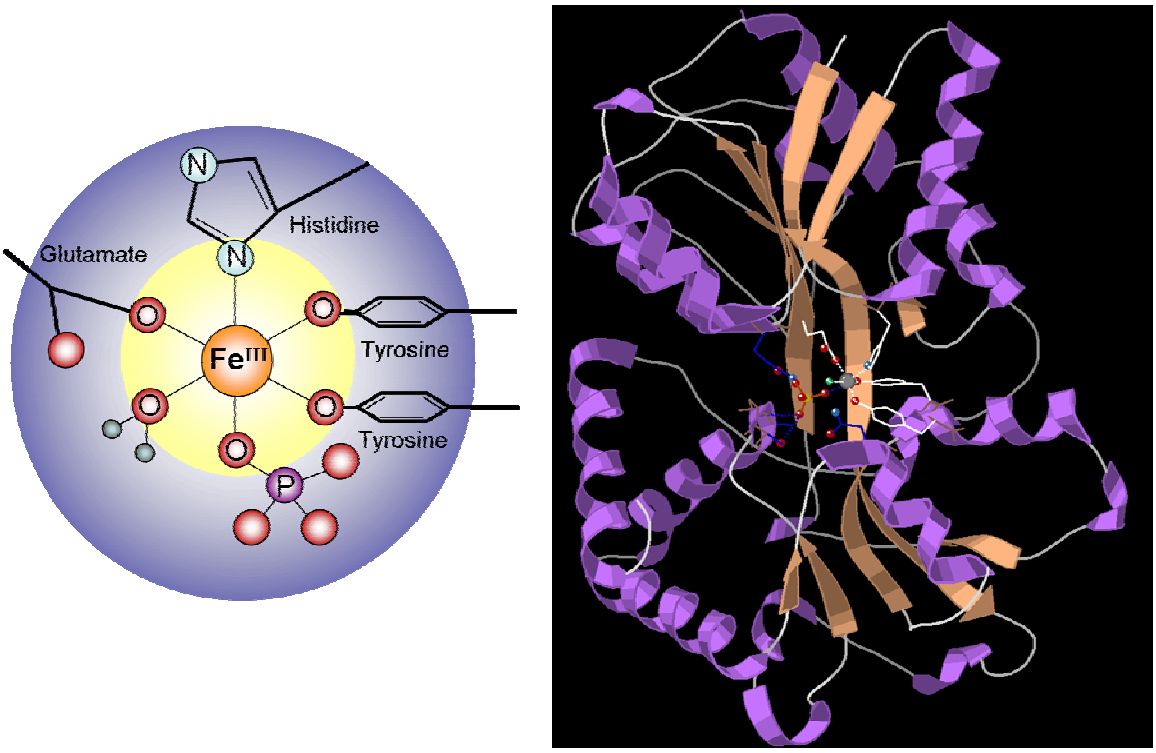

Figure 4.2: FbpA tightly binds Fe^{3+} at the cleft between two lobes of the monomeric protein (shown on the right). Four amino acids bind the iron ion, while the first coordination shell is completed by a labile phosphate anion and a water molecule.[190]

FbpA binds iron with four amino acids (glutamate, histidine, and two tyrosines). Specifically the nitrogen atom of the histidine and the oxygen atoms of glutamate and the two tyrosines, all of which are relatively hard Lewis bases, bind strongly to the hard Fe^{3+} ion.[155] The first coordination shell of the iron ion is completed by a synergistic

anion, which *in vivo* is expected to be phosphate (Figure 4.2).[153] The synergistic anion is labile can exchange *in vitro* with many other anions such as citrate. In the case of a monodentate synergistic anion like phosphate, a water molecule serves as the sixth ligand as shown in Figure 4.2).

FbpA is a member of the periplasmic binding protein family and binds iron in the cleft between two globular lobes. The lobes are connected by a hinge which, in the case of FbpA, is comprised of a β-sheet.[151, 154] The members of the periplasmic binding protein family are categorized by the type of hinge connecting the two lobes. When iron is bound to FbpA the protein is in the closed conformation, binding the cargo like a clamp. Apo-FbpA, on the other hand, has a more open conformation.

The chemistry surrounding the loading and unloading of iron into and out of FbpA has been intensely investigated. The synergistic anion has been shown to modulate the thermodynamics properties of this metalloprotein. Specifically, the binding constant, the protein folding stability, and the redox potential of the metalloprotein are affected by a change in the synergistic anion.[6, 191, 192] The modulation of the redox potential is particularly important as reduction of Fe^{3+} to Fe^{2+} has been shown to decrease the protein affinity for the metal by 12 orders of magnitude and is thought to trigger iron release at the cytoplasmic membrane.[6, 193]

The kinetics of iron loading and unloading and the kinetics of anion exchange have also been investigated in detail. For the purposes for this chapter it is sufficient to

state a brief list of some of the major findings reported in the literature. First, the synergistic anion has been shown to be promiscuous and given the pool of anions present in the periplasm fluctuates during the life of a bacterium, the labile anion may serve as a control system for regulating iron uptake.[192, 194] Second, the synergistic anion is thought to preorganize the iron binding site of apo-Fbp and has been shown to be essential for iron binding.[195] Third, the synergistic anion is also important for iron release at the cytoplasmic membrane.[196, 197]

FbpA serves as our experimental handle in this chapter as we seek to further understand the iron uptake pathway of *N. gonorrhoeae.* By focusing on the thermodynamic properties of the FbpA, we use the protein as the probe to investigate the multiple protein-protein interactions and protein-metal interactions required for iron transport.

The thermodynamic properties of FbpA, specifically of the protein folding and unfolding behaviors, have been well characterized using SUPREX (Stability of Unpurified Proteins from Rates of H/D EXchange). An introduction to the SUPREX technique appears in Section 4.2.3. Here we will only briefly describe the major findings of the prior investigations to set the stage for our use of FbpA as the thermodynamic probe in the studies reported here. Previously, SUPREX was used to demonstrate that phosphate serves as a synergistic anion in the FeFbpA-PO_4 complex *in vivo.*[153] As well, SUPREX, was used to investigate the change in protein folding stability as the

synergistic anion is varied.[191] As shown in Figure 4.3, a dramatic difference in SUPREX data is observed when FbpA is ferrated or not.

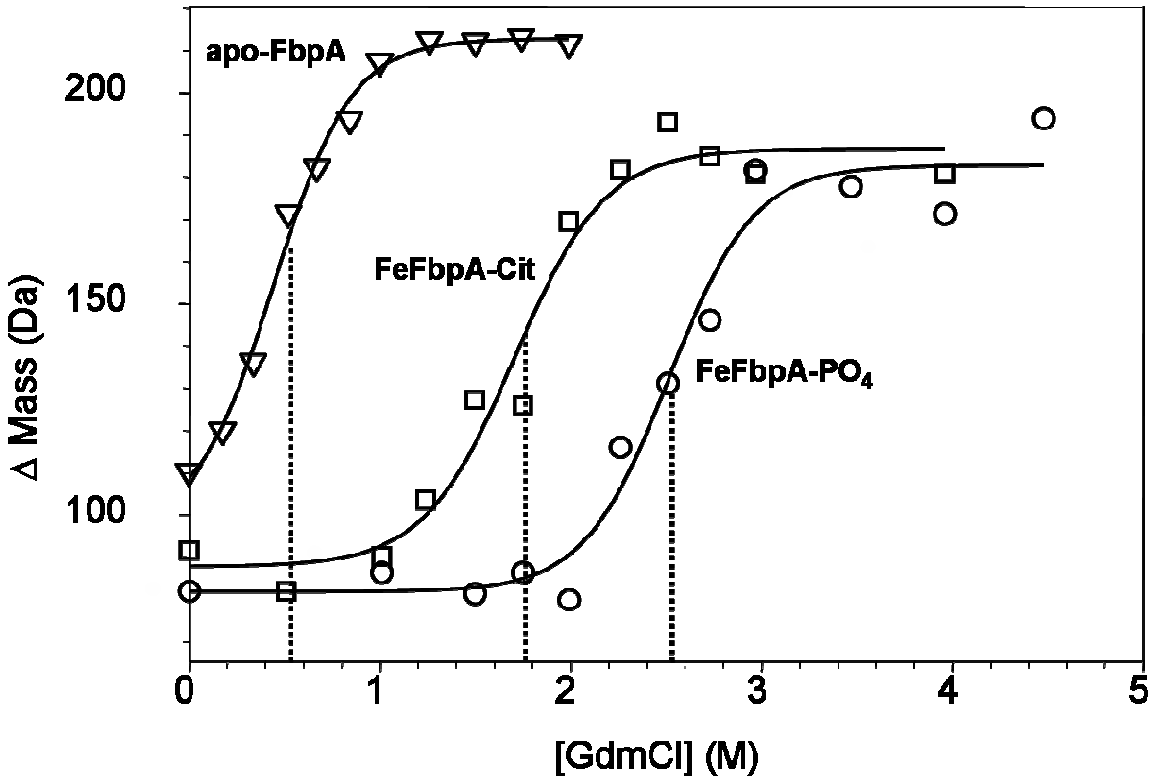

Figure 4.3: Generalized SUPREX data demonstrating a dramatic difference in the folding behavior of FbpA when iron is present or absent and depending on the identity of the synergistic anion present. This general trend is reported in detail in reference [191].

A difference in the SUPREX data was also observed as a function of the identity of the synergistic anion present in the active site of holo-FbpA. Therefore, SUPREX is sensitive enough to monitor the iron loaded status of FbpA and the synergistic anion present. Here we extend our use of SUPREX to investigate the protein-protein interactions in which FbpA participates in order to acquire and deliver iron through the transport process.

4.1.2.5 Transferrin

As discussed in Section 3.1.1, Tf is the human iron transport protein, which sequesters iron with a K_d ~10^{-20} M.[5, 84-86] With this strong iron chelation ability, Tf serves a bacteriostatic function gathering essentially all of the free iron in the human blood serum and preventing iron acquisition by pathogens living in the human host. The exclusive human pathogen *N. gonorrhoeae*, under investigation here, is one of the few types of bacteria is that has developed a mechanism to hijack iron from transferrin.[148] The mechanism through which humans utilize transferrin-bound iron was discussed in detail in Section 3.1.1. Here we will focus on the structure of transferrin and the iron-protein interactions that have important implications for iron acquisition by *N. gonorrhoeae*.

The structure of human Tf is similar to FbpA, which is sometimes called a "bacterial transferrin". Both proteins are part of the transferrin superfamily of proteins that all have structural and functional similarities. All proteins in this family require an anion for tight iron sequestration all are designed to transport iron. Figure 4.4 presents a ribbon diagram of the bilobal structure of the 80 kDa human Tf. Each lobe, named the N-lobe and the C-lobe, forms an iron binding site that is similar to FbpA.

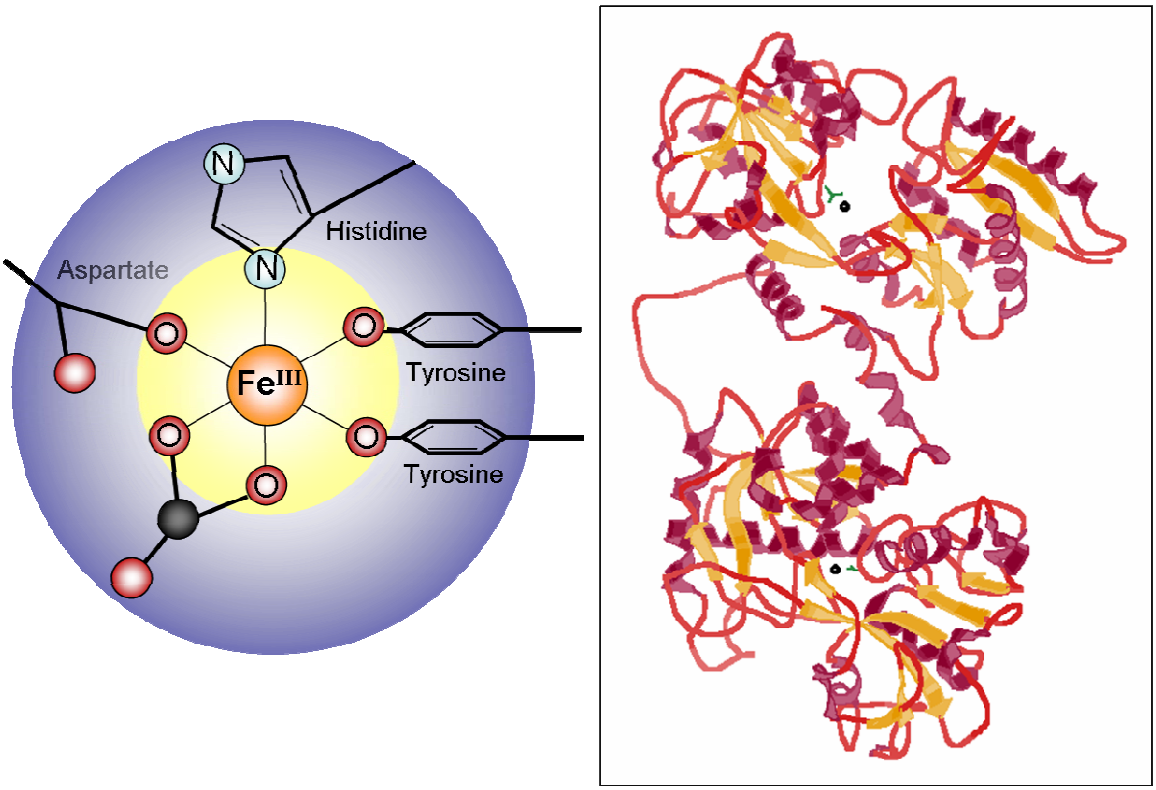

Figure 4.4: Kinemage created by Dr. Katherine Weaver depicts the ribbon diagram of Fe_2-Tf (shown on the right). The active site of one lobe of Tf is shown as a cartoon on the left. Similar to FbpA, Tf provides four amino acids and binds iron in the cleft between two globular domains. Aspartate, histidine, and two tyrosines provide four ligands to the iron, while a synergistic anion carbonate completes the first coordination shell.

As shown on the left side of Figure 4.4, each active site of Tf is comprised of four amino acids: aspartate, histidine, and two tyrosines. This combination of iron binding ligands is identical to FbpA expect that aspartate is substituted for glutamate. In Tf, the first coordination shell around the iron is completed again by a synergistic anion, in this case carbonate. Similar to FbpA, each active site of Tf is located between two globular domains that are hinged and clamp the iron in place.[198]

A rich body of literature is available regarding the structure-function relationships important for iron removal from Tf in the context of human iron regulation diseases. Here we will focus on the findings that may have implications for how bacteria hijack iron from Tf. Changes in protein conformation, induced either by protonation of allosteric sites or by another mechanism, are thought to be important for the release of iron from Tf.[199, 200] Further, Mason et al. have demonstrated that conformational changes in one lobe are communicated to the other.[201] A reasonable hypothesis follows that conformational changes are induced in Tf when Tf is bound by the bacterial receptor TbpA/TbpB. Further communication between the lobes of Tf may facilitate the removal of both iron atoms upon binding to the bacterial receptor. Such hypotheses have not yet been investigated, but are an important for a complete understanding of the pathogenic iron uptake system. Finally, Boukhalfa et al. have demonstrated the importance of the synergistic anion in the release of iron from Tf with parallel mechanistic studies of FbpA and Tf.[196] The role of the synergistic anion as iron is hijacked from Tf and transported across the bacterial outer membrane remains an open question.

4.1.3 Iron Transport in *N. gonorrhoeae*

A model, as depicted conceptually in Figure 4.5, for the transport of iron in *N. gonorrhoeae* involves several protein-protein interactions and is likely to follow these

steps: 1) holo-Tf interaction with the TbpA/B receptor, 2) iron release from holo-Tf, 3) iron movement across the outer membrane, 4) apo-Tf dissociation from the TbpA/B receptor, and 5) iron insertion into apo-FbpA.[178, 187] Since iron hydrolysis/precipitation and redox reactions that produce toxic radicals must be prevented in a biological system, it is a reasonable assumption that the first coordination shell of iron is always controlled by sequestration in protein binding sites. Therefore, we hypothesize additional steps are involved in the above model: i) TbpA/B receptor interacts with apo-FbpA and ii) holo-FbpA dissociates from the TbpA/B receptor. The exact role(s) of TbpA and TbpB in each of these steps, especially i) and ii), remain unclear. In addition, the point(s) at which the energy requirement fulfilled by TonB is imposed on this step-wise process has not been completely defined.[184] Conceptually, the seven steps outlined above can be treated separately in order to investigate the proteins and detailed mechanism involved in iron transport.

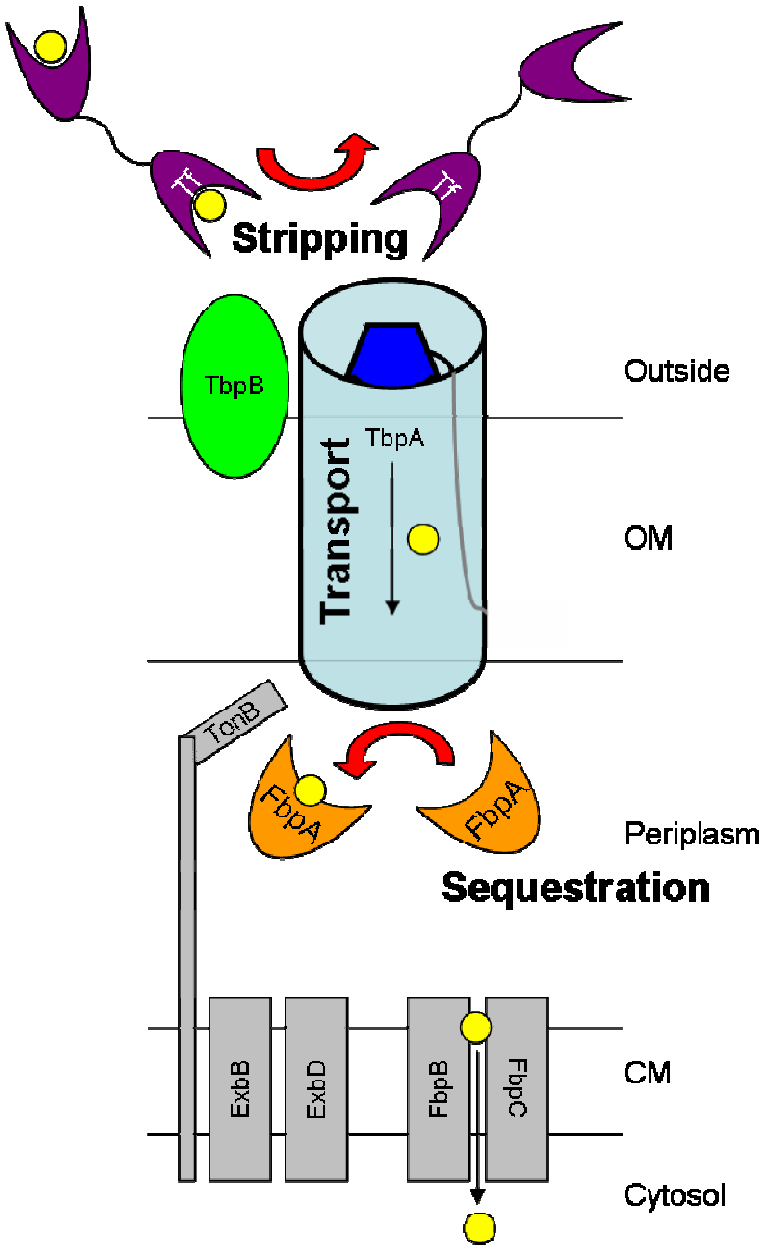

Figure 4.5: Utilization of transferrin-bound iron by live, wild-type *Neisseria gonorrhoeae* involves many proteins. TbpA and TbpB constitute the outer membrane receptor complex responsible for binding Tf, stripping the tightly-bound iron from the host-derived molecule, and transporting iron into the periplasmic space. In the periplasm, iron is sequestered by FbpA, which delivers it to the cytoplasmic membrane. After crossing the cytoplasmic membrane, iron is metabolized according to the needs of the cell. Energy derived from TonB, ExbB, and ExbD is required for utilization of transferrin-bound iron. Figure reproduced with permission.[147]

4.1.4 Statement of Objectives

Our main objective was to use the well-characterized SUPREX behaviors of apo-FbpA and FeFbpA-PO_4 as probes to investigate the transferrin-iron transport system of *N. gonorrhoeae*. Here we report the first direct detection and analysis of the apo-FbpA binding interaction with TbpA. We also show that TbpA can discriminate between apo- and holo-FbpA. We demonstrate that TbpB does not bind either apo- or holo-FbpA. Finally, these studies help to delineate the functions of TbpA and TbpB by showing that either TbpA or TbpB can facilitate the release of iron from holo-Tf without the participation of TonB. These studies illustrate the power of SUPREX to probe protein-protein interactions and receptor-substrate binding in the presence of other proteins and in crude membrane preparations. As well, this investigation provides key experimental data that significantly extend our understanding of the distinctive roles that TbpA and TbpB play and provide insight into the point at which energy requirements are imposed on this multi-step iron transport process across the outer membrane.

4.2 Materials and Methods

4.2.1 Materials

Human apo- and holo-Tf were purchased from Sigma Aldrich. Recombinant FbpA (*N. gonorrhoeae*) was expressed in *E. coli* and purified as previously reported.[186, 193] Holo-FbpA was reconstituted in either the phosphate or citrate form as reported

previously.[6] Horseradish peroxidase labeled transferrin (HRP-Tf) (Jackson ImmunoResearch) was used in competitive solid-phase, transferrin-binding assays as described previously.[150]

4.2.2 Membrane Preparations

4.2.2.1 Collection of Membrane Preparations

Total membrane preparations were kindly provided by Dr. Cindi Cornellissen's laboratory at Virginia Commonwealth University. Briefly, total membrane preparations were isolated from gonococcal strains FA19 ($TbpA^+/TbpB^+$), FA6905 ($TbpA^+/TbpB^-$), FA6747 ($TbpA^-/TbpB^+$), and FA6815 ($TbpA^-/TbpB^-$). Gonococcal strains were subjected to iron-stressed growth to promote maximal expression of the iron-regulated proteins, including transferrin binding proteins. Following growth, cells were harvested and bacterial pellets were resuspended in 10 mM Hepes buffer at pH 7.4 and subjected to French Press at 16,000 psi. The resulting lysate was centrifuged to remove cellular debris. The supernatant was collected and then subjected to ultracentrifugation at 140,000 x *g* to isolate total membrane fractions. Total membranes were suspended in 10 mM Hepes buffer and BCA (bicinchoninic acid) assays (Pierce Biochemicals) were performed to quantify total protein concentration. TbpA and TbpB were estimated to comprise approximately 1% of the total membrane protein concentration.[202]

4.2.2.2 Composition of Membrane Preparations

The *N. gonorrhoeae* membrane preparations used in our experiments consisted of both inner and outer membranes and contained many different proteins. Membrane vesicles, generated by French Press of intact, iron-starved gonococci, were heterogeneous with respect to protein orientation and possibly dynamic in solution. Some vesicles were oriented with the periplasmic face of the outer membrane exposed to the solution. This means that the extracellular face of the receptor (TbpA and TbpB) and the periplasmic face of TbpA were exposed to the solvent. Additionally, the stoichiometry of TbpA and TbpB required for a functioning receptor complex has not been unequivocally resolved.[150, 203-206] Consequently, the interpretations of the experiments reported here are complicated by the heterogeneity of protein orientation in any observed binding event.

In addition to sample heterogeneity, the membrane potential of the inner membrane is not preserved in the total membrane preparations. Therefore, TonB was not functional in the total membrane preparations because it had been uncoupled from its energy source. We are careful not to draw any conclusions regarding the movement of iron through the membrane or regarding any conformational change of TbpA. However, the uncoupling of TonB from its energy source does allow us to separate various stages of the transport process as will be discussed in detail in the following sections.

4.2.3 SUPREX

SUPREX is a mass spectrometry analysis that provides information about the folding stability of a protein or mixture of proteins.[17] The analysis can be performed in the presence of many other biological molecules and requires relatively small amounts of sample. The following description of SUPREX is a general explanation meant to prepare the reader for the qualitative interpretations of SUPREX data that follow in this chapter. For a more detailed explanation of SUPREX protocols and a thorough analysis of the SUPREX behavior of FbpA (independent of other proteins), the reader is referred to Dr. Petra L. Rouhac's dissertation and the papers the Crumbliss and Fitzgerald groups have published previously.[153, 191, 207, 208]

In general, SUPREX allows one to monitor the equilibrium between the folded and unfolded forms of the protein of interest. This equilibrium is related to the folding free energy (ΔG_f) of a protein, which is a relative measure of the folding stability of a protein. For ideal proteins (which FbpA is not) SUPREX can be used to calculate ΔG_f and changes in ΔG_f caused by ligand binding or protein-protein interactions.

No matter the extent of the folding stability (ΔG_f), proteins are constantly folding and unfolding either globally or locally or both. As well, the protons of the amino acid side chains and of the peptide backbone are constantly exchanging with protons from the solvent. In SUPREX the protein is exposed to deuterated buffers for a certain length of time and the protons exchange for deuterons. As the protein is folding and

unfolding, the number protons that are exposed to the solvent is decreased or increased respectively. Therefore, a relatively unfolded protein will exchange more protons for deuterons and the mass of the protein will increase a larger amount than a relatively folded protein exposed to D_2O over a set amount of time. This concept is depicted in Figure 4.6, panel A. The mass of the protein is monitored using MALDI mass spectrometry. As shown schematically in Figure 4.6, panel B, the change in mass (ΔMass) of the protein can be calculated by subtracting the mass of the protein after the proton/deuteron exchange from the mass of the native protein.

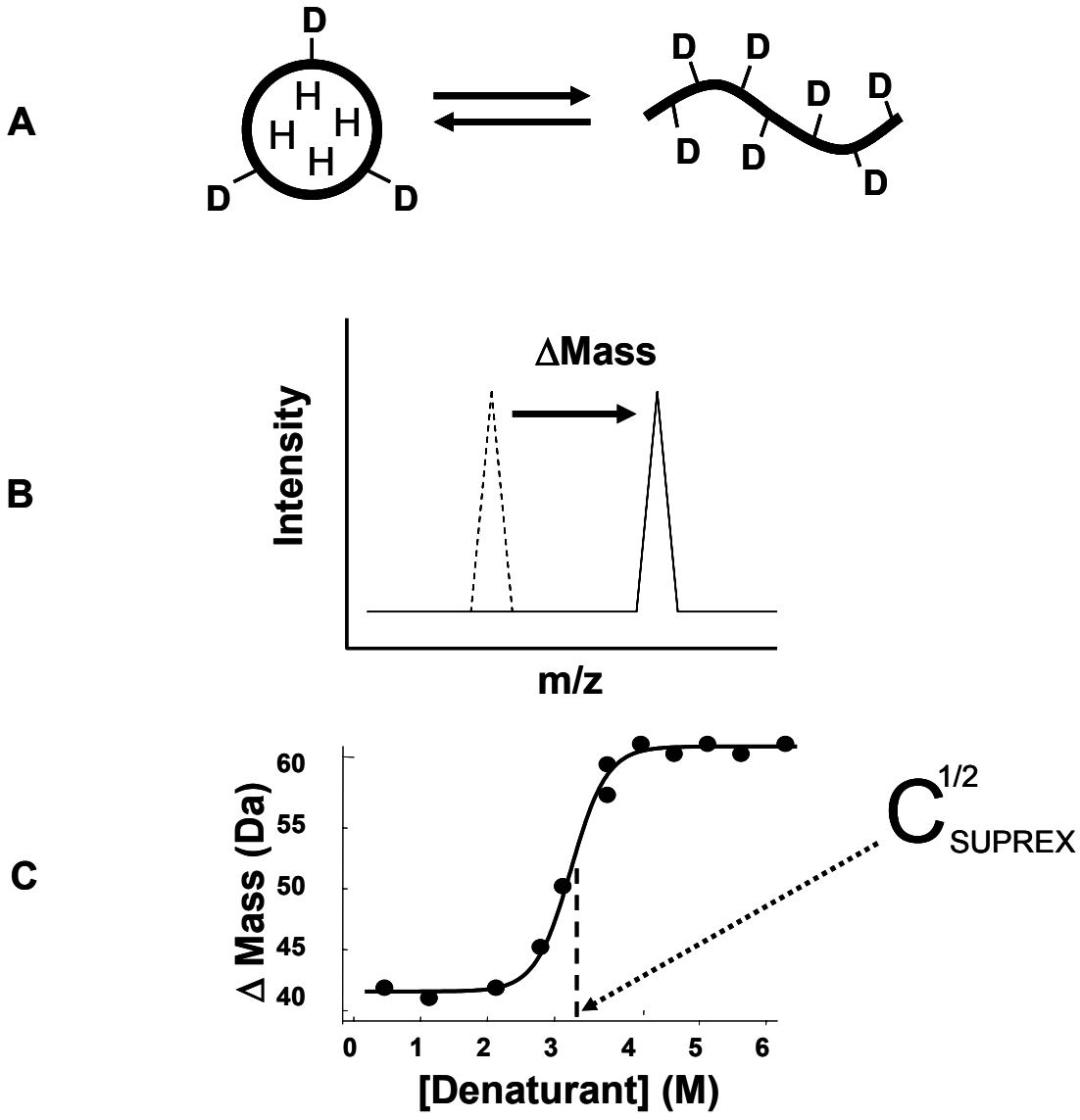

Figure 4.6: Depiction of the SUPREX analysis. A) Proteins are in equilibrium between the folded and unfolded states. The protons on the surface of the protein at any given time are exposed to the SURPEX solvent and exchange for deuterons. B) The mass of the protein is detected using MALDI -MS. The change in mass from the fully protonated form is calculated and denoted as ΔMass. C) A SUPREX curve is constructed by plotting the ΔMass as a function of denaturant concentration. The concentration at which the transition from low ΔMass to high ΔMass occurs is termed the $C^{1/2}_{SUPREX}$ value.

The SUPREX analysis involves a series of denaturant concentrations prepared in the deuterated buffer to probe the folding stability of a protein. As the denaturant concentration is increased the folding equilibrium is shifted towards a higher proportion of unfolded proteins. Therefore when ΔMass is plotted as a function of denaturant concentration, as seen in Figure 4.6, panel C, a characteristic "s" shaped curve is observed. This "SUPREX behavior" corresponds to: a small number of deuterons exchanged at low denaturant concentrations (called the pre-transition phase), a transition phase, and a so called post-transition phase where a large number of deuterons were exchanged at high concentrations of denaturant. The concentration (of denaturant) at which the transition occurs is called the $C^{1/2}_{SUPREX}$ value. The position of the $C^{1/2}_{SUPREX}$ value depends on the time the protein is exposed to D_2O and the whether the protein unfolds following the EX1 or EX2 regime. For ideal proteins the $C^{1/2}_{SUPREX}$ value can be related to ΔG_f. FbpA is not an ideal protein as has been discussed previously.[191] Therefore, we will use the $C^{1/2}_{SUPREX}$ value and the shape of the SUPREX curve for qualitative comparisons only.

The SUPREX protocol is depicted in Figure 4.7. The SUPREX analyses of FbpA in the absence and presence of transferrin and/or membrane preparations were initiated by 10-fold dilution into a series of deuterated H/D exchange buffers. The deuterated exchange buffers contained 50 mM MES, 200 mM KCl (pD = 6.5), and concentrations of deuterated GdmCl that ranged from 0 to 6 M. The concentration of FbpA in the

exchange buffers was 0.3 μM. A high-sensitivity SUPREX protocol was used on these complex mixtures.[17] SUPREX curves were generated using an H/D exchange time of 1 hr. The H/D exchange reactions in each SUPREX experiment were quenched with the addition of TFA (final concentration 0.3% v/v). Protein samples were concentrated and desalted using C4 ZipTips™ (Millipore, Inc.) and subsequently mixed with 5 μL of a saturated aqueous solution of sinapinic acid. Data analyses were performed as described previously for FbpA.[191]

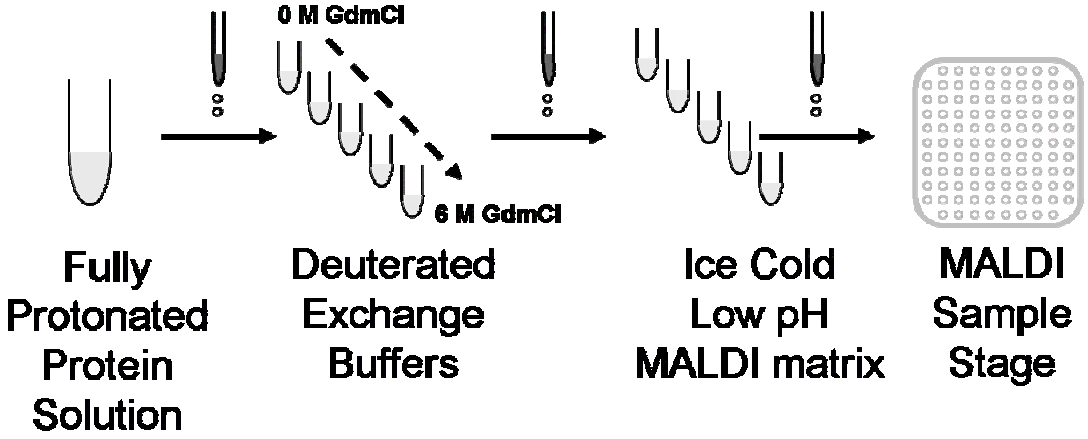

Figure 4.7: Scheme of SUPREX protocol. A protein (with or without ligand present) is exposed to a series of D_2O solutions that contain a varied amount of denaturant. The protons (of the protein) that are exposed to the solvent exchange for deuterons and consequently the mass of the protein increases. The exchange process is slowed by quickly decreasing the temperature of the solution and decreasing the pH. The sample is then analyzed using MALDI mass spectrometry and the change in mass from the fully protonated protein is calculated.

4.2.4 Whole Bacteria Experiments

To evaluate surface binding by FbpA, whole iron-stressed gonococci were applied to nitrocellulose membranes as previously described.[148, 178] After blocking, membranes were probed with his-tagged, recombinant FbpA. Specifically bound apo- or holo-FbpA was detected with his-tag specific antibodies, followed by a secondary antibody conjugated to either alkaline phosphatase or HRP. In an indirect assay, we also tested whether recombinant FbpA (apo or holo) interfered with binding of Tf to intact gonococci. As described previously,[148, 150] whole, iron-stressed gonococci were applied to nitrocellulose and then probed with a mixture of HRP-labeled Tf and unlabeled competitor apo- or holo-FbpA. Tf that remained bound in the presence of excess competitor was detected by development with the commercially-available substrate for HRP, Opti-4CN (Bio-Rad). The author thanks Heather Strange, VCU, for her excellent technical contributions in collecting this data.

4.3 Results[1]

4.3.1 SUPREX Analysis of apo-FbpA in the Presence of Membrane Bound Receptor

SUPREX analysis of apo-FbpA corresponds to a predominantly unfolded protein that is fully denatured in minimal concentration of denaturant and a large portion of the

[1] Dr. Petra L. Roulhac and Dr. Jennifer Noto were the lead scientists in the collection of the data presented here. Some of the figures published here are modifications of figures presented in Dr. Roulhac's dissertation [208] and some have been previously published in the journal Metallomics [147].

peptidic protons are exposed in the native state. As depicted in Figure 4.8, the SUPREX behavior of apo-FbpA is altered by the presence of membranes with either $TbpA^{+}/TbpB^{+}$ or $TbpA^{+}/TbpB^{-}$. A higher concentration of denaturant is required to denature apo-FbpA and fewer peptidic protons are exchanged when the protein is in its native state. A shift in $C^{1/2}_{SUPREX}$ of ~0.5 M corresponds to a $\Delta\Delta G$ value of ~1 kcal/mol using a m-value of 2.4.[17] The limit of detection for this experiment is 0.5 kcal/mol.

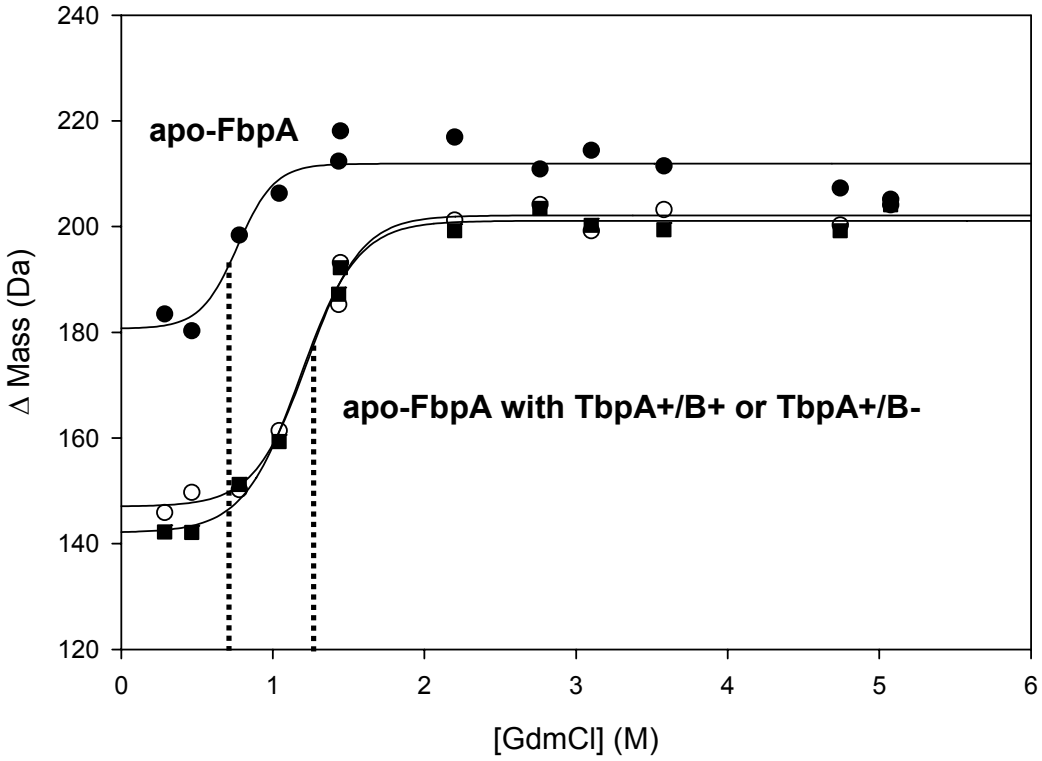

Figure 4.8: SUPREX analysis of apo-FbpA (closed circles) alone or in the presence of (open circles) $TbpA^{+}/B^{+}$ or (dark squares) $TbpA^{+}/B^{-}$ membrane preparations. Dotted lines indicate the $C^{1/2}_{SUPREX}$ values for each curve. All data were collected using an H/D exchange time of 1 hr at pD 6.5. Figure reproduced with permission.[147]

The presence of membranes with only TbpB ($TbpA^-/TbpB^+$) does not affect the SUPREX behavior of apo-FbpA (Figure 4.9). The SUPREX behavior of apo-FbpA (data not shown) in the presence of membranes containing $TbpA^-/TbpB^-$ also has same midpoint as apo-FbpA alone.

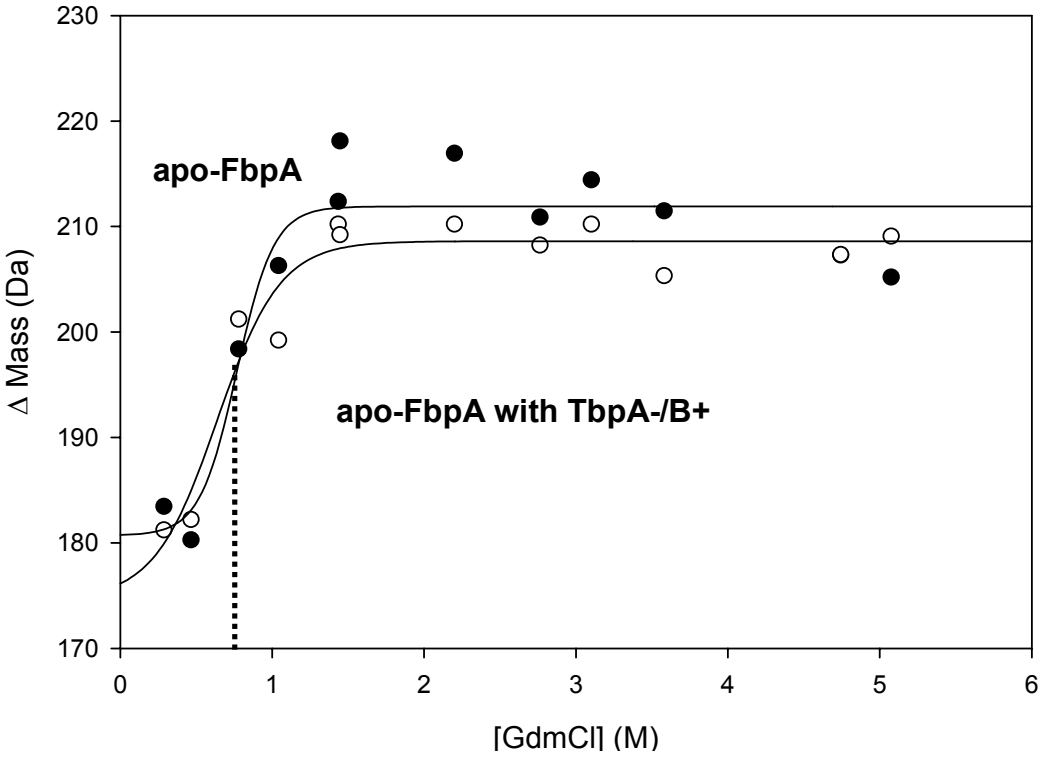

Figure 4.9: SUPREX analysis of apo-FbpA in the presence of (open circles) $TbpA^-/B^+$. The data for apo-FbpA (closed circles) alone is reprinted for ease of comparison. The dotted line indicates the $C^{1/2}_{SUPREX}$ value. Notice the scale of Figures 4.8 and 4.9 are different. All data were collected using an H/D exchange time of 1 hr at pD 6.5. Figure reproduced with permission.[147]

All data shown in Figures 4.8 and 4.9 were collected in the presence of phosphate. Similar results are obtained in the presence of citrate rather than phosphate:

apo-FbpA-citrate requires very little denaturant to be fully unfolded and the presence of membranes with $TbpA^+/TbpB^+$ causes a shift in the SUPREX curve of apo-FbpA-citrate, indicating a more folded protein with more globally protected protons in the native state (Figure 4.10).

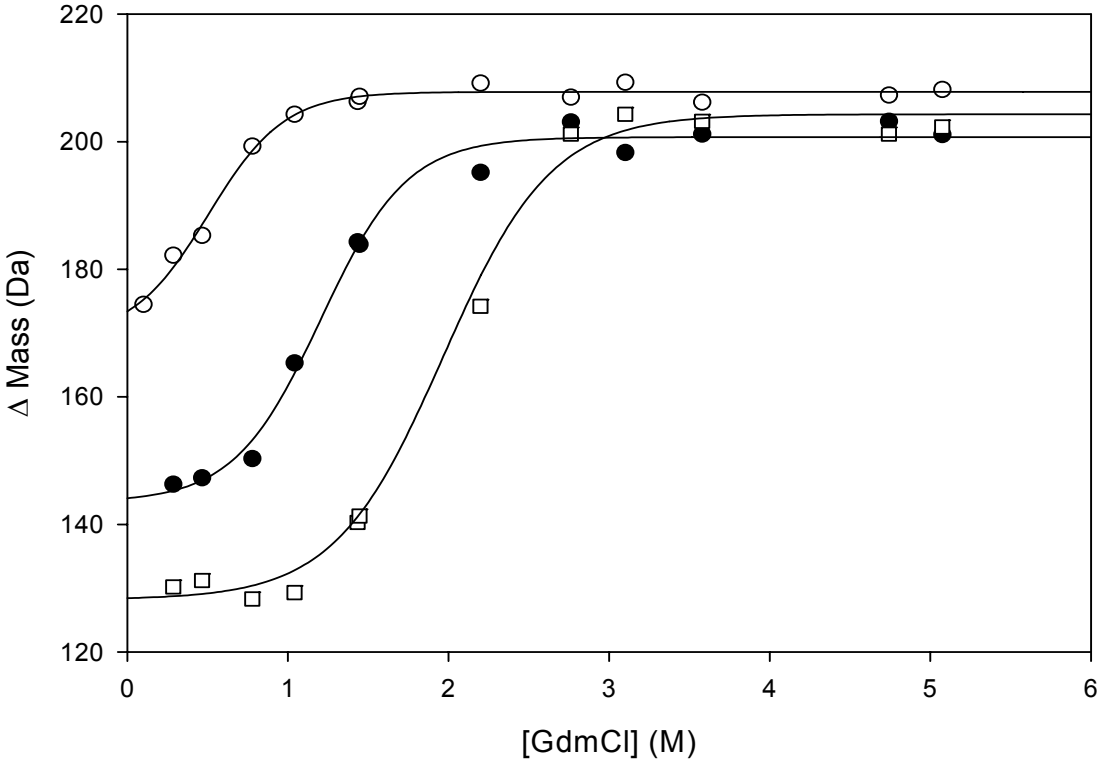

Figure 4.10: SUPREX behavior for apo-FbpA-Cit in the absence (open circles) and in the presence of $TbpA^+/B^+$ (closed circles). FeFbpA-Cit (open squares) is included for comparison. All data were collected using an H/D exchange time of 1 hr at ph 6.5. Figure reproduced with permission.[147]

4.3.2 SUPREX Analysis of holo-FbpA in the Presence of Membrane Bound Receptor

As shown in Figure 4.11, the presence of membranes alone or membranes containing the receptor ($TbpA^+/TbpB^+$) do not affect the SUPREX behavior of FeFbpA-PO_4.

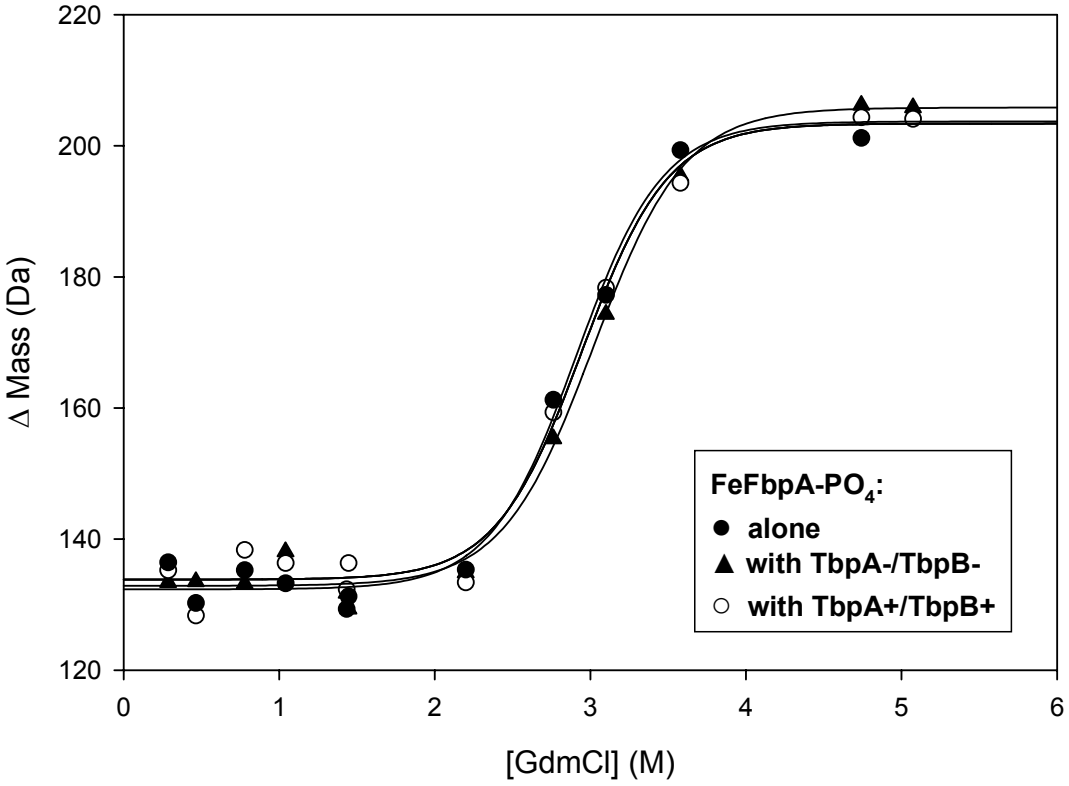

Figure 4.11: SUPREX analysis of FeFbpA-PO_4 (closed circles) alone, (open circles) in the presence of $TbpA^+/B^+$ and (dark triangles) in the presence of null ($TbpA^-/B^-$) membrane preparations using an H/D exchange time of 1 hour at pD 6.5. Figure reproduced with permission.[147]

4.3.3 SUPREX Analysis of FbpA in the Presence of holo-Tf and Membrane Bound Receptor

The SUPREX behavior of apo-FbpA-PO_4 was investigated in the presence of holo-Tf. When only apo-FbpA and holo-Tf are mixed together the SUPREX data of apo-FbpA are coincident with data for apo-FbpA alone (data not shown). Similarly, when apo-FbpA and holo-Tf are mixed in the presence of null membrane preparations ($TbpA^-$/$TbpB^-$), there is no apparent change in the SUPREX behavior of apo-FbpA (data not shown). However, as shown in Figure 4.12 when apo-FbpA is exposed to holo-Tf in the presence of membranes containing TbpA, TbpB, or both ($TbpA^+$/$TbpB^+$, $TbpA^+$/$TbpB^-$, $TbpA^-$/$TbpB^+$), the SUPREX behavior of Fbp is coincident with FeFbpA-PO_4. The SUPREX curves of apo-FbpA alone, apo-FbpA in the presence of $TbpA^+$/$TbpB^+$ membranes (no holo-Tf) , and FeFbpA-PO_4 alone are included in Figure 4.12 for ease of comparison.

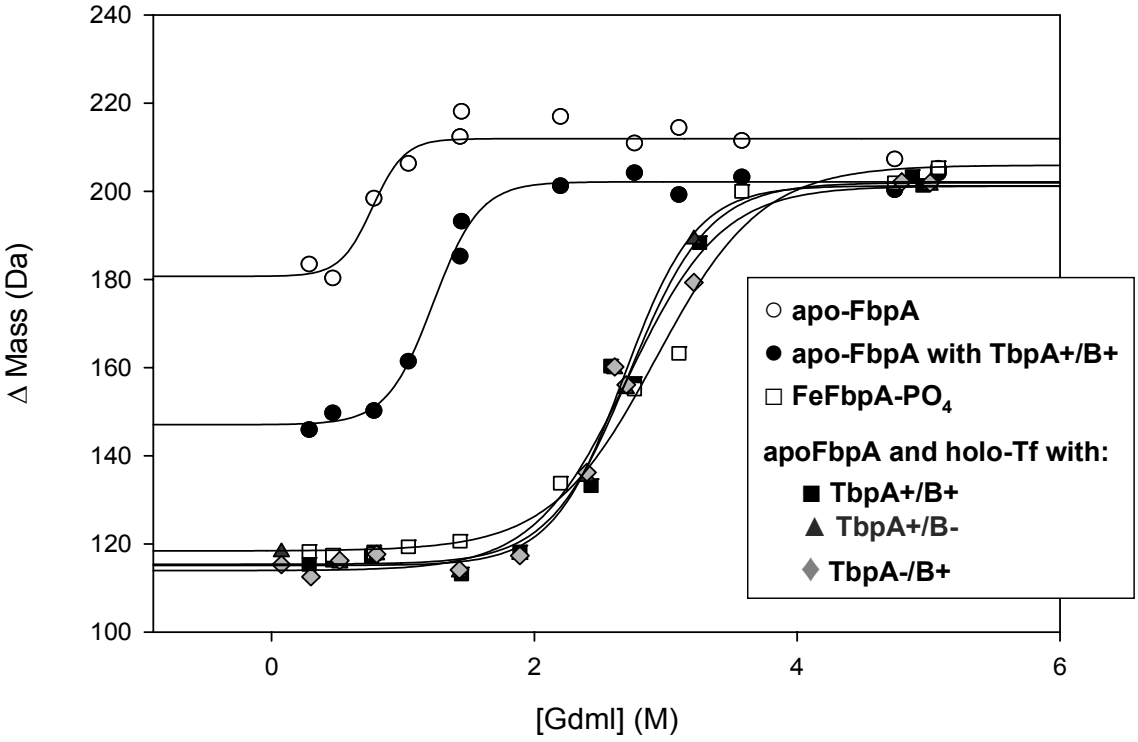

Figure 4.12: Exchange of iron between Tf and FbpA. SUPREX analysis of apo-FbpA in the presence and absence of holo-Tf and Tbp receptor membrane constructs. SUPREX data obtained for (open circles) apo-FbpA, (closed circles) apo-FbpA/TbpA$^+$/TbpB$^+$, (dark squares) apo-FbpA/TbpA$^+$/TbpB$^+$/holo-Tf, (dark triangles) apo-FbpA/TbpA$^+$/TbpB$^-$/holo-Tf, (dark diamonds) apo-FbpA/TbpA$^-$/TbpB$^+$/holo-Tf and (open squares) FeFbpA-PO$_4$ using an H/D exchange time of 1 hr at pD 6.5. Data are not shown for apo-FbpA with null membrane preparations; however, data are coincident with data for apo-FbpA alone. Figure reproduced with permission.[147]

Similar results are observed when apo-FbpA-citrate is exposed to holo-Tf in the presence of the membrane bound receptor (Figure 4.13).

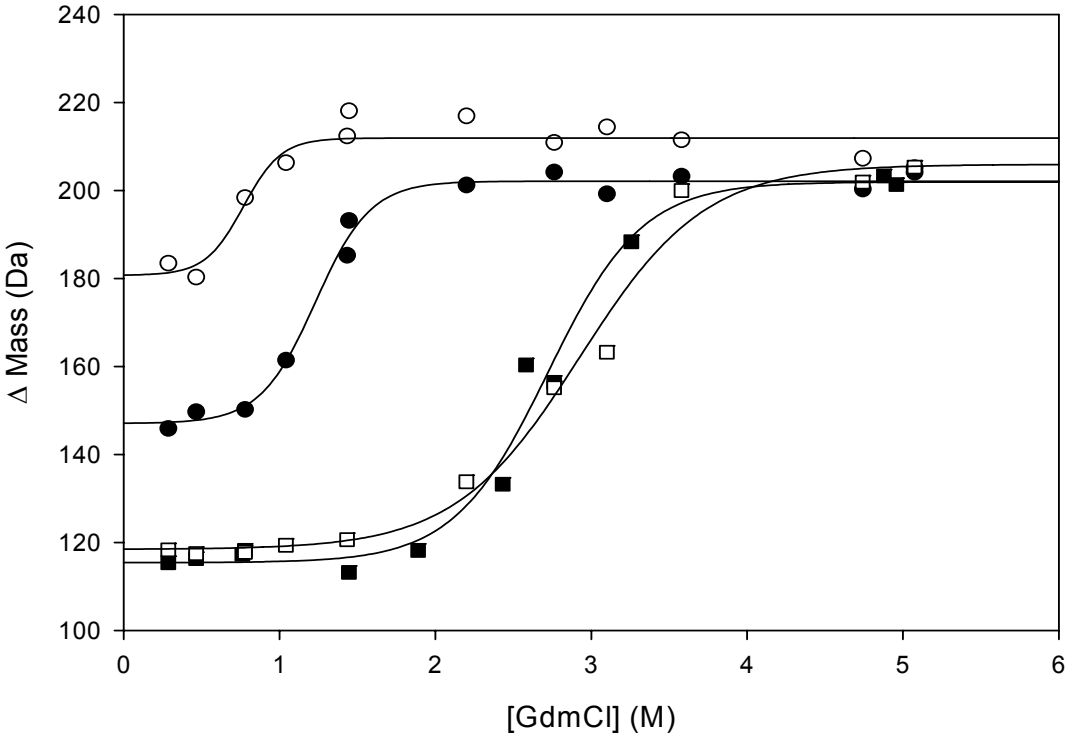

Figure 4.13: SUPREX data obtained for apo-FbpA-Cit (open circles), apo-FbpA-Cit in the presence of $TbpA^+/B^+$ (closed circles), apo-FbpA-Cit in the presence of $TbpA^+/B^+$ and holo-Tf (closed squares), and Fe-FbpA-Cit (open squares) using an H/D exchange time of 1 hr. Figure reproduced with permission.[147]

4.3.4 Interaction of FbpA with Intact Bacterial Cells

Figure 4.14 is a digital image of a representative binding assay performed on whole gonococcal cells. When either apo- or holo-FbpA is introduced to the cells no increase in signal (denoting anti-body binding) is observed.

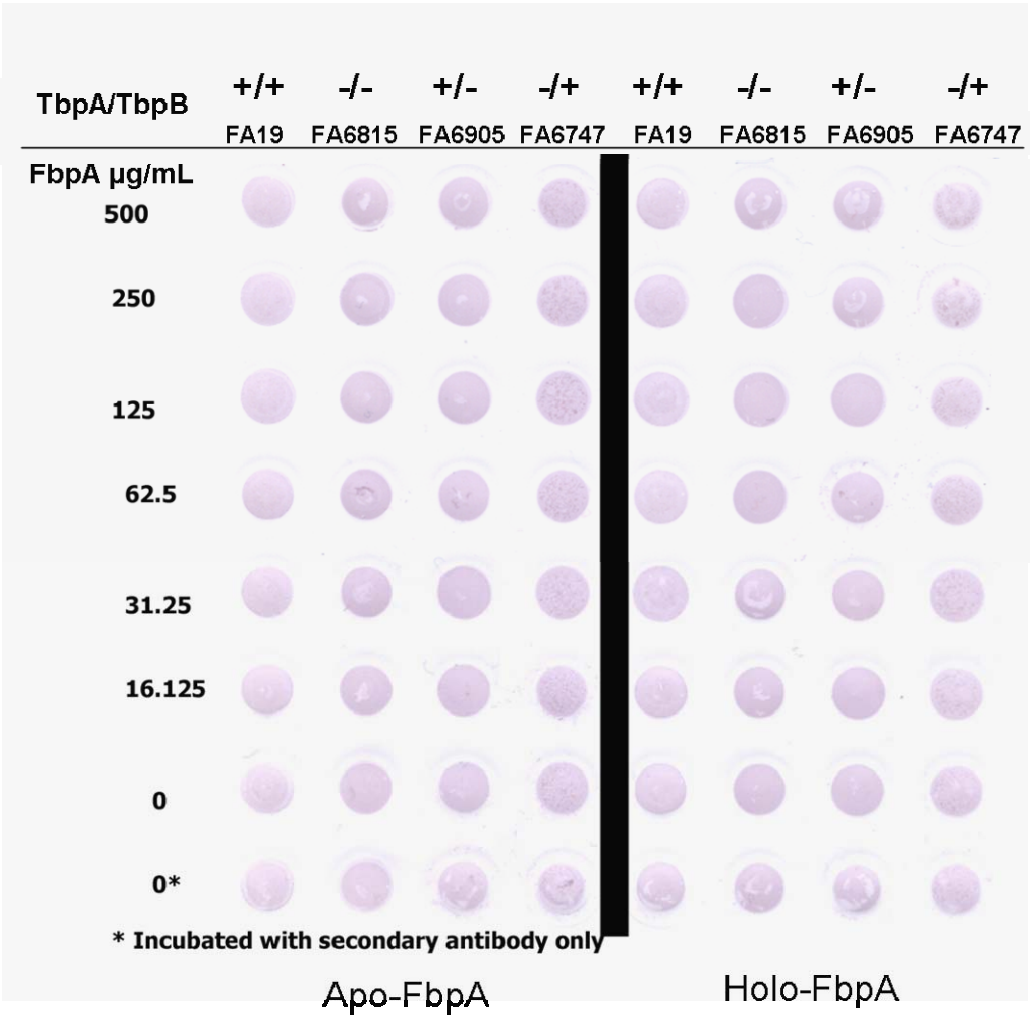

Figure 4.14: Dot blot assay to determine if FbpA binds to the surface of whole gonococcal cells of various strains (with respect to TbpA and TbpB). Both apo- and holo-FbpA were tested at varying concentrations. The bottom two rows are negative controls. No significant increase in signal is observed for either apo- or holo-FbpA for any of the bacterial strains.

Similarly, when Tf is introduced to the cells and subsequently FbpA is introduced, there is no decrease in the signal due to Tf binding (Figure 4.15).

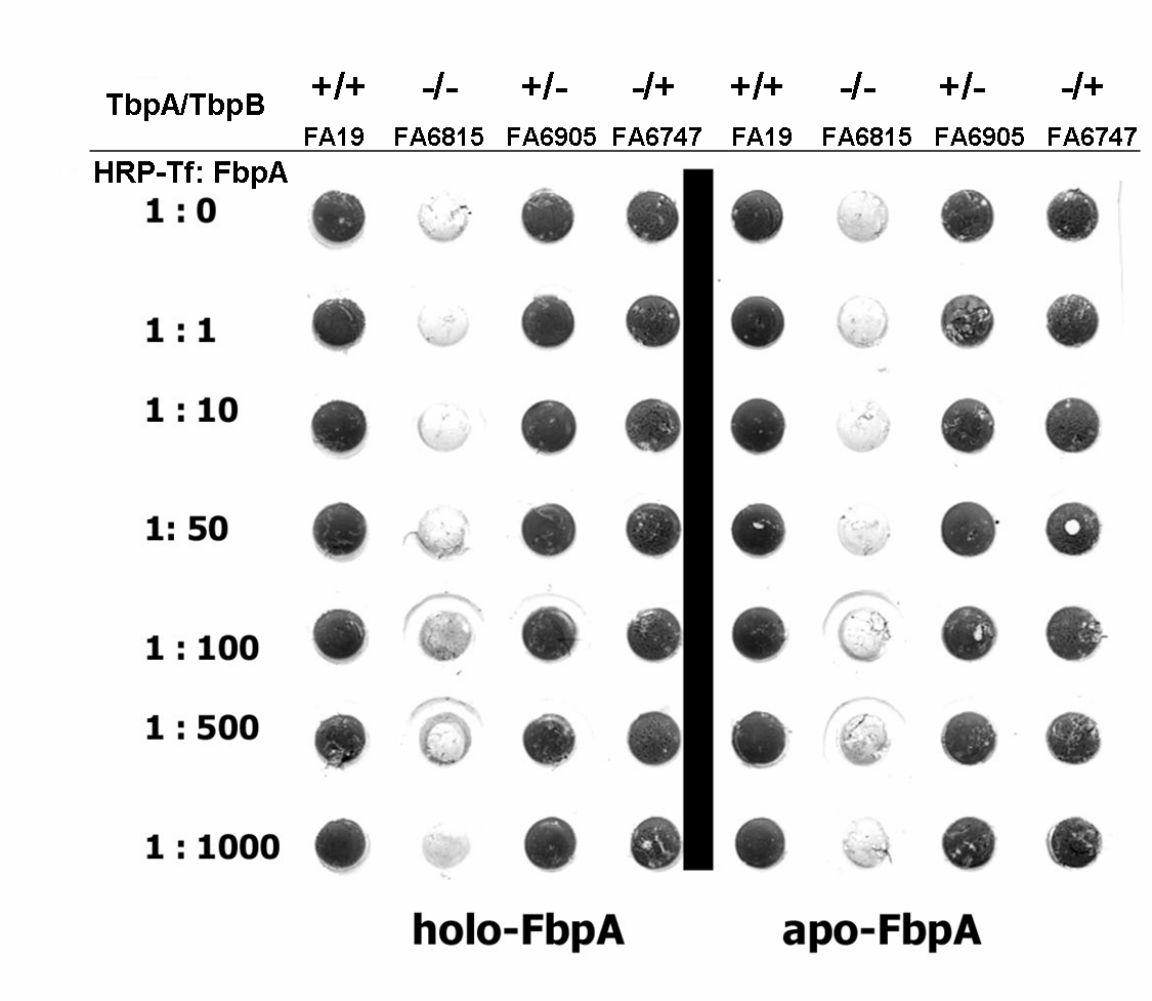

Figure 4.15: Dot blot assay to determine whether or not either apo- or holo-FbpA can compete with Tf for binding to the surface of whole gonococcal cells of various strains (with respect to TbpA and TbpB). Both apo- and holo-FbpA were tested at varying concentrations relative to a constant HRP-Tf concentration. The top row is a positive control. No significant decrease in signal due to Tf binding is observed for either apo- or holo-FbpA for any of the bacterial strains.

4.4 Discussion

4.4.1 TbpA Directly Binds apo-FbpA

Upon exposure of apo-FbpA to membranes containing TbpA and TbpB ($TbpA^+/TbpB^+$), the SUPREX curve transition midpoint (i.e. $C^{1/2}$ value) of apo-FbpA is shifted to a higher concentration of denaturant and the pre-transition baseline is lowered to a smaller ΔMass (Figure 4.8). This change in SUPREX behavior indicated an increase in the folding stability of apo-FbpA. The shift in the pre-transition baseline is consistent with a larger population of globally protected amide protons in the apo-FbpA/$TbpA^+/TbpB^+$ complex compared to that of apo-FbpA alone. As expected, the post-transition regions of the two experiments are within the uncertainty of ΔMass values that are typically 10 Da. The SUPREX behavior of apo-FbpA in the presence of membranes containing only TbpA ($TbpA^+/TbpB^-$) is similar to that observed for membranes containing TbpA and TbpB ($TbpA^+/TbpB^+$; Figure 4.8).

In contrast, the SUPREX behavior of apo-FbpA in the presence of membranes containing only TbpB ($TbpA^-/TbpB^+$) is unchanged from that of apo-FbpA alone (Figure 4.9). As well, apo-FbpA in the presence of null membrane preparations ($TbpA^-/TbpB^-$) exhibits the same behavior as purified apo-FbpA (data not shown). These data suggest that within the limits of our binding assay, which is expected to detect binding events with binding free energies >0.5 kcal/mol, there is no evidence of a binding interaction between apo-FbpA and TbpB. Taken together, these data suggest that apo-FbpA is

stabilized by TbpA and not TbpB. We therefore conclude that apo-FbpA only binds to TbpA.

We hypothesize that apo-FbpA interacts with TbpA on the periplasmic face of the outer membrane in intact cells. In our SUPREX experiments however, due to the heterogeneity of the membrane vesicle orientation, exogenously added FbpA may be exposed to both extracellular and periplasmic faces of the outer membrane. To determine whether FbpA could interact with the extracellular face of TbpA- or TbpB-containing membranes, we measured direct binding of FbpA to whole cells (Figure 4.14). His-tagged FbpA (both apo and holo) were applied to whole cells and an anti-his antibody was utilized to visualize binding to the cell surface. The results for holo-FbpA and apo-FbpA are identical. Neither apo- nor holo-FbpA bound to the surface of gonococcal cells in a specific manner. Background levels of reactivity were detected in all strains tested, regardless of whether TbpA was expressed or not. This result indicates that FbpA does not bind to surface exposed epitopes of TbpA, at least to an extent that is detectable in this assay format. Therefore, we conclude that any binding event detected between FbpA and TbpA-containing membrane preparations using SUPREX likely occurs at the periplasmic interface.

We also tested whether recombinant apo- or holo-FbpA could compete with HRP-Tf for binding to the gonococcal Tbps on whole cells (Figure 4.15). The concentration of HRP-Tf remained constant, while the concentration of FbpA was varied

from a molar ratio of 0:1 (Fbp: HRP-Tf) to a molar ratio of 1000:1. Binding of HRP-Tf to the Tbp receptor was not diminished in the presence of either excess apo-FbpA or holo-FbpA. This result strengthens our conclusion that FbpA does not bind to the external surface of TbpA directly, nor does it interfere with the interaction between TbpA and Tf.

Our SUPREX results show that apo-FbpA is stabilized by the presence of TbpA and that apo-FbpA is not affected by the presence of TbpB or membranes lacking both of these proteins. Using SUPREX we have demonstrated a direct binding event between apo-FbpA and TbpA. These data support our model in which apo-FbpA interacts in intact cells with the periplasmic face of TbpA and is separated from TbpB by the outer membrane.

4.4.2 TbpA Discriminates Between apo- and holo-FbpA

FbpA is more stable when it is in the FeFbpA-PO_4 form rather than the apo-FbpA form with respect to protein folding.[191] Evidence for this stabilization comes from the observed changes in SUPREX behavior: relative to apo-FbpA, FbpA in the FeFbpA-PO_4 form has lower ΔMass baseline and the $C^{1/2}_{SUPREX}$ value for FbpA in the FeFbpA-PO_4 form is shifted to the right of the $C^{1/2}_{SUPREX}$ value of apo-FbpA.[191] This characteristic SUPREX behavior of FeFbpA-PO_4 can be used to probe the protein-protein interactions in which FeFbpA-PO_4 participates.

Upon exposure of FeFbpA-PO_4 to gonococcal membrane preparations, whether devoid of Tbp receptor complex ($TbpA^-/TbpB^-$) or containing the complete Tbp receptor complex ($TbpA^+/TbpB^+$), the SUPREX behavior is the same as FeFbpA-PO_4 alone (Figure 4.11). The presence of TbpA- or TbpB-containing membranes neither increases nor decreases the thermodynamic stability of FbpA in the FeFbpA-PO_4 form with respect to protein folding, to a degree which can be detected within the limits of our experimental system.

We hypothesize that in a living bacterium TbpA would have a higher binding affinity for apo-FbpA than for holo-FbpA, ensuring the vectorial transport of iron through the outer membrane into the periplasm. The observed change in SUPREX behavior of apo-FbpA in the presence of TbpA (Figure 4.8) and the lack of any observed change in SUPREX behavior of FeFbpA-PO_4 in the presence of TbpA containing membranes (Figure 4.11) provide the first direct experimental evidence for the ability of TbpA to discriminate between apo- and holo-FbpA. Further, this discriminatory binding may indicate a thermodynamic sink that imposes directional transport of iron across the outer membrane.

Our conclusion that TbpA can discriminate between apo- and holo-FbpA, corresponds well with the seven-step transport process described in Section 4.1.3, in which holo-Tf binds to the receptor, iron is released and apo-Tf dissociates, while apo-FbpA binds to TbpA, iron is inserted into apo-FbpA, and holo-FbpA dissociates.

4.4.3 TbpA and TbpB Facilitate Iron Transfer Between Transferrin and FbpA

When apo-FbpA and holo-Tf are mixed together, no exchange of iron is observed between the two protein binding sites. The SUPREX curve resulting from the mixture of apo-FbpA and holo-Tf is coincident with that of purified apo-FbpA (data not shown). This is not surprising given that the iron binding constant for FbpA is 10^{-18}, while transferrin binds iron more tightly with a binding constant of 10^{-20}.[86, 198] Therefore, there is no thermodynamic driving force for the transfer of iron from Tf to FbpA when the two proteins are mixed *in vitro*. The same result is also observed when apo-FbpA, holo-Tf, and $TbpA^-/B^-$ membranes are mixed together (data not shown). However, when the mixture of apo-FbpA and holo-Tf is combined with membrane preparations containing TbpA and TbpB ($TbpA^+/TbpB^+$), the resulting SUPREX curve matches that of purified FeFbpA-PO_4 (Figure 4.12). These data suggest that the Tbp receptor complex facilitates the transfer of iron from holo-Tf to apo-FbpA.

Interestingly, when apo-FbpA and holo-Tf are reacted in the presence of either $TbpA^+/TbpB^-$ or $TbpA^-/TbpB^+$ membranes, the SUPREX curves also resemble FeFbpA-PO_4 (Figure 4.12). These further findings suggest that either TbpA or TbpB, individually or together can facilitate the transfer of iron from holo-Tf to apo-FbpA. It is important to note that this transfer of iron can be facilitated by TbpB even though we cannot detect a binding event between TbpB and FbpA.

Previous studies with the closely related *N. meningitidis* (an organism that is nearly 80% identical by genetic sequence to *N. gonorrhoeae*),[209, 210] indicate the Tbp complex is able to facilitate the transfer of iron from holo-Tf to apo-FbpA.[211, 212] Here using different techniques, we confirm that in the presence of membranes derived from *N. gonorrhoeae*, iron is transferred from holo-Tf to apo-FbpA in the presence of TbpA or TbpB or both. From these data, we cannot discern whether or not iron is transported through the receptor barrel during our experiments. We cannot state what exact mechanism of iron transfer occurs as many possibilities exist. For example, FbpA may be acting as an exogenous iron chelator. However, we are able to conclude that either TbpA or TbpB can facilitate the stripping of iron from holo-Tf in an energy independent process.

4.4.4 Equivalent Behavior of the Phosphate and Citrate Forms of FbpA

Citrate and phosphate act as synergisitic anions *in vitro*.[6, 191] *In vitro* the synergistic anion is labile and the identity of the anion affects the thermodynamic properties of FbpA.[6, 196] Although it has been shown that phosphate is present in the iron binding site of FbpA in crude cell lysates, it is important to understand the protein-protein interactions in which the citrate form of FbpA participates, since the anion is labile and may change during the life of a bacterium.[153]

We observed parallel behavior, with respect to protein-protein interactions, when citrate was the synergistic anion rather than phosphate. These observations are illustrated by data presented in Figures 4.10 and 4.13. In the presence of $TbpA^+/TbpB^+$ apo-FbpA-citrate is stabilized in the SUPREX experiment, indicating a binding event between apo-FbpA-citrate and the bacterial receptor. As well, when apo-FbpA-citrate, $TbpA^+/TbpB^+$, and holo-Tf are combined, the SUPREX behavior observed matches that of holo-FbpA-citrate. This later observation is consistent with the bacterial receptor stripping the iron from holo-Tf and apo-FbpA-citrate acting as the iron chelator. We conclude therefore that both the phosphate and citrate forms of apo-FbpA bind to the bacterial receptor. Further, both the phosphate and citrate forms of apo-FbpA are able to chelate iron when it is released from holo-Tf by TbpA and TbpB.

4.4.5 The Roles of TbpA, TbpB, and TonB

TonB derived energy is required for utilization of iron derived from Tf in intact cells.[183] When considering the role of TonB, we regard the mechanistic steps of deferrating holo-Tf, releasing apo-Tf from the receptor, and transporting iron across the membrane as separate functions. Each function may have different energy requirements. Cornelissen et al. have shown previously that energy supplied from TonB is required to release apo-Tf from the Tbp complex.[184] However, iron-utilization studies with live, intact bacteria do not allow differentiation between the separate

activities of stripping iron from holo-Tf and transporting iron through the membrane. The data shown here allow us to separate the functions of stripping iron from transferrin and transporting iron across the membrane. We report here that either TbpA or TbpB can facilitate the release of iron from holo-Tf without energy supplied by TonB. Further studies are necessary to define the energy requirement and the role of TonB in the separate step of transporting iron across the gonococcal outer membrane.

In addition to the TonB literature, a significant body of knowledge has been published about the role(s) of TbpA and TbpB in transferrin bound iron acquisition. It has been shown previously that the Tbp receptor is required for initiation of infection *in vivo*, and *in vitro* studies have shown that only TbpA is required for iron utilization.[148, 213] We specifically show here that TbpA can independently facilitate the release of iron from holo-Tf, an individual mechanistic step required for iron utilization. It has also been shown previously, that amino acids located in the proposed plug domain of TbpA are required for iron utilization.[214] Consequently, when those amino acids are replaced with alanines, the ability of gonococci to acquire transferrin bound iron via TbpA (in a $TbpB^-$ construct) is lost. Similarly, the presence of small epitope insertions in putative loops 2, 9, or 11 also render TbpA incapable of iron utilization from transferrin in the absence of a functional TbpB protein.[178] However, the presence of TbpB can compensate for these defects in TbpA and restore the ability of gonococci to utilize Tf derived iron.[178, 214]

Although not required and not able to sustain iron utilization alone, we demonstrate here that TbpB can remove the iron from Tf in the absence of TbpA. Therefore, we propose that while the separate step of iron transport through the membrane requires TbpA, stripping of iron from transferrin can occur independently of TbpA. More studies are necessary to identify how the various structural domains of TbpA (the plug and the β-barrel) are involved in each step of the iron transport model proposed here. However, our SUPREX results suggest that both TbpA and TbpB can interact with holo-Tf and strip the iron from Tf independently of one another or in concert.

Further, TbpA and TbpB each play a specific discriminatory role, with respect to protein-protein interactions essential to our hypothesized multi-step transport process. It has been shown previously that only TbpB discriminates between apo-Tf and holo-Tf, preferentially binding holo-Tf.[150, 215-217] Herein we demonstrate that only TbpA is able to discriminate the iron status of FbpA, preferentially binding apo-FbpA.

4.5 Conclusion

While the proteins required for the transport of iron from human transferrin to the bacterial periplasmic binding protein FbpA have been identified, questions have remained regarding how the tightly-bound iron is released from Tf via the membrane-bound receptor complex and how iron is transferred to FbpA. The SUPREX studies

described here allowed us to explore the protein-protein interactions involved in iron transport by *N. gonorrhoeae* and to address these questions by using the thermodynamic properties of the protein as our probe. In the current study, we have shown that 1) TbpA binds to apo-FbpA, 2) TbpA can discriminate between apo- and holo-FbpA, 3) TbpB does not interact with apo- or holo-FbpA, and 4) both TbpA and TbpB can facilitate the release of iron from holo-Tf in an energy-independent fashion resulting in sequestration by apo-FbpA. These studies help to clarify the role(s) that each protein plays in our expanded hypothesis for the multi-step transferrin-mediated iron transport mechanism in *N. gonorrhoeae.*

5. Characterization of the TbpA-plug and Thermodynamic Investigations of Fe_2-Tf in the Presence of TbpA and TbpB

In this chapter we investigate the mode of action of TbpA (and TbpB) using the metal as the probe in one line of inquiry and focusing on the protein as the probe in another line of inquiry. In *N. gonorrhoeae*, TbpA and TbpB comprise the outer membrane receptor responsible for hijacking iron from human Tf. These investigations illustrate the multiple modes of inquiry necessary to fully develop a complete understanding of the role of a metalloprotein in a metal transport pathway.

5.1 Introduction

5.1.1 Background

N. gonorrhoeae, like many pathogenic Gram-negative bacteria require iron to grow and to cause disease. Bacteria must acquire this necessary nutrient from their environment, which in the case of *N. gonorrhoeae* is the human host. The human iron transport protein transferrin (Tf) is hijacked for its iron by the bacterial receptor proteins transferrin binding protein A (TbpA) and transferrin binding protein B (TbpB).[148-150] As discussed in Chapter 4, TbpA, an integral membrane protein, is required for growth and is presumably required for iron release from Tf and iron transport across the outer membrane.[147-150] TbpB on the other hand, is not required for growth, but makes the iron acquisition process more efficient.[149]

Significant progress has been made in determining the specific function and structure of both TbpA and TbpB. The current model of the structure of TbpA is a β-barrel with an N-terminus plug domain occluding the porin, while TbpB is proposed to be surface exposed and composed of two lobes.[148, 175, 176, 179] Both TbpA and TbpB can bind Tf and, as reported in Chapter 4, both can facilitate the release of iron from Tf.[147, 178, 214] Figure 5.1 (also shown in section 4.1.3) depicts the current conceptual understanding of the *N. gonorrhoeae* iron transport process.

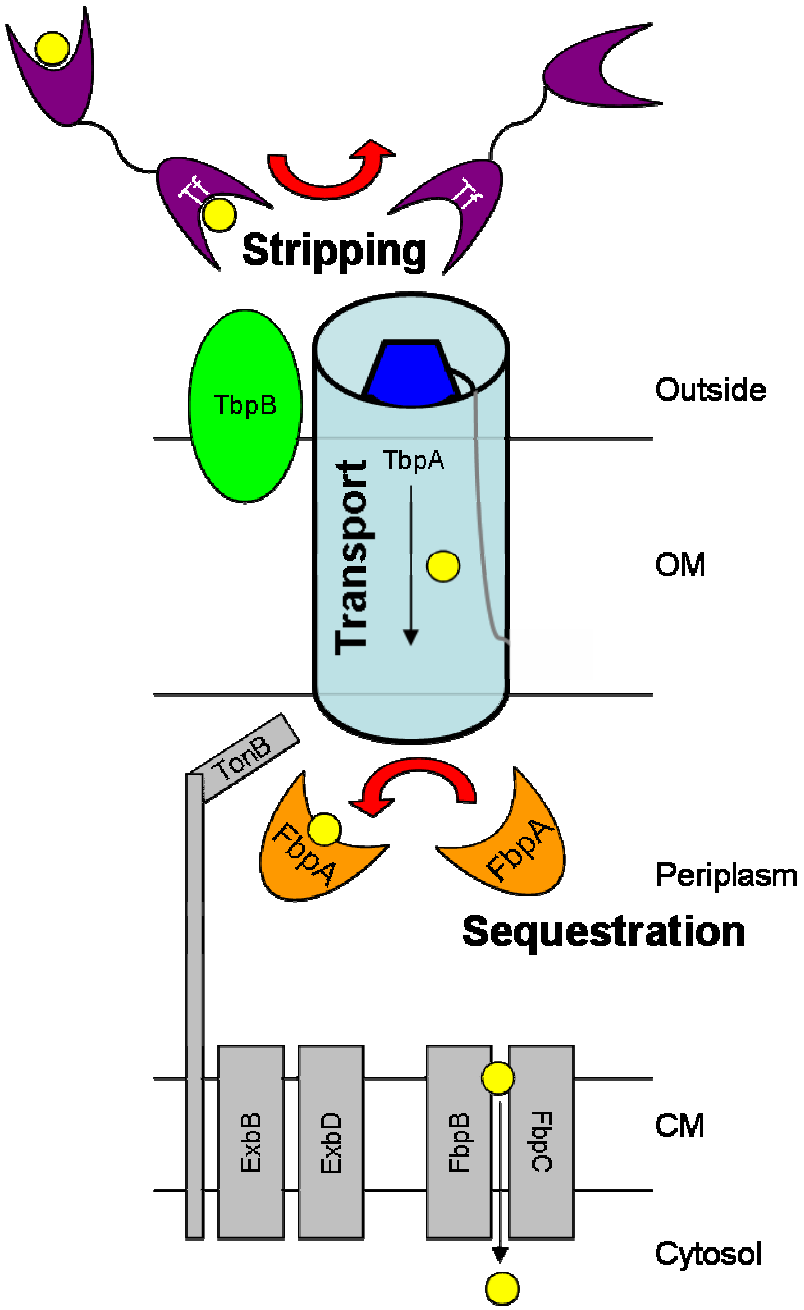

Figure 5.1: Utilization of transferrin-bound iron by live, wild-type *N. gonorrhoeae* involves many proteins. TbpA and TbpB bind human Tf and steal its iron. Iron is transported through TbpA into the periplasmic space. In the periplasm, iron is sequestered by ferric binding protein A (FbpA), which delivers it to the cytoplasmic membrane. Figure reprinted with permission from reference [147].

Many questions about the transport process remain. How do TbpA and TbpB facilitate the release of iron from Tf? How does iron move through the barrel of TbpA and into the periplasm? What is the role of the plug-domain of TbpA as iron is hijacked from Tf, moved across the outer membrane, and inserted into the periplasmic iron binding protein FbpA? In the present chapter, we first explore the potential role(s) of the TbpA-plug. Second, we report the development of a specific equilibrium dialysis technique that makes possible the investigation of how TbpA and TbpB affect iron release from Tf.

5.1.2 Current Understanding of the Structure and Function of TbpA

Although progress has been made in understanding the structure of TbpA and what role it serves in the iron acquisition process, the specifics of how TbpA functions are unclear. As discussed and referenced in Chapter 4, insertion and deletion analysis yielded significant insight into the structure of TbpA and identified functionally important epitopes. However, those studies only hint at the chemical mechanism at play during transport. The current hypothesis of how iron is hijacked from Tf and delivered to FbpA was developed in the context of what is known about similar outer membrane transporters. Here we briefly review the literature regarding β-barrel transporters in order to develop a context for our work on TbpA reported in this chapter.

5.1.2.1 β-Barrel Transporters

No crystal structure of TbpA has been solved. However, crystal structures of homologous β-barrel transporters provide a working model for the structure of TbpA.[178] Several β-barrel transporters have been crystallized to date.[172, 181] The two transporters discussed here, FepA and FhuA, both bind specific siderophores and are expressed by *E. coli*. Siderophores are small iron chelators that extracellularly sequester iron, preparing the necessary nutrient to be taken up by the bacteria. The *E. coli* outer membrane transporter FepA binds the cognate siderophore enterobactin, while FhuA transports ferrichrome.[166, 168] Both FepA and FhuA are composed of a β-barrel with loops projecting into the extracellular environment and a N-terminal plug domain, which occludes the lumen of the barrel (Figure 5.2).[166, 168]

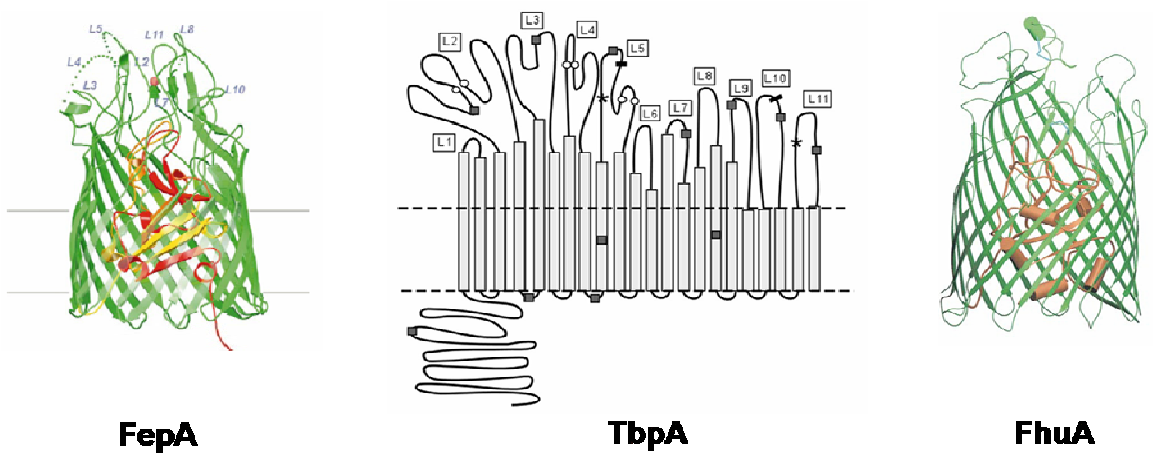

Figure 5.2: The crystal structures of FepA and FhuA serve as models for the proposed structure of TbpA. The green ribbon diagrams depicted the β-barrels of FepA and FhuA, while the transmembrane portions of TbpA are shown as gray rectangles. The plug domain of FepA is colored in red and yellow, while the plug domain of FhuA is shown in khaki. The proposed plug domain of TbpA is denoted with a black line. Figure adapted from references [166, 168, 178].

During transport, it is unclear whether the plug domain of each of these transporters is fully or partially removed from the lumen of the barrel. Another option to make the passage of the respective cargo possible is movement of the plug within the barrel. There is some evidence that in the case of large cargos such as the protein toxin colicin B, which can enter an *E. coli* bacterium through FepA, the plug is at least partially removed from the barrel.[172] Interestingly, when the plug and the barrel are expressed as two separate proteins, transport is still accomplished. This result suggests that the relationship between the location and/or movement of the plug with respect to the β-barrel may not be as straight forward as first proposed.[218, 219] Intense investigation of how the plug moves during transport is ongoing.

In addition to just blocking the passage of cargo through the barrel, other roles for the plug domain have been proposed. Binding of ferrichrome to FhuA has been shown to cause conformation changes in the FhuA-plug. It is hypothesized that these changes may serve a signaling function such as transmitting information (i.e. the presence of the iron-complex) to periplasmic side of membrane.[168] The plug domain of FepA has been recombinately expressed in the absence of the barrel and has been shown to be predominantly unfolded when expressed alone.[220] Further, the recombinant FepA-plug was shown to bind enterobactin two orders of magnitude less tightly than the wild-type transporter. It has been proposed that this result may indicate a thermodynamic sink for cargo release in the periplasm.[220, 221] Finally, the plug domain has also been hypothesized to bind to the periplasmic binding protein prior to cargo transfer.[172] Each of these possible roles for the plug domain is feasible. Given that the sequence corresponding to the plug domain is well conserved across many transporters, it is likely that this soluble globular domain is integral to the efficient transport of the respective cargo.[166]

It should be noted here that while FhuA and FepA are good models for the structure for homologous β-barrel transporters, there is an important difference between these models and TbpA. FhuA and FepA transport Fe-siderophore complexes. TbpA interacts with an iron transport protein Tf and is expected to transport "naked iron". It is unclear at this point whether the "naked" iron is transported with an anion such as

phosphate, but it is clear that no siderophore is present. The importance of this distinction between TbpA and the other β-barrel transporters is discussed throughout this chapter.

5.1.2.2 What is the Role of the TbpA-Plug?

Using the crystal structure of FepA, Yost-Dalijev and Cornelissen developed a model for the structure of the plug of TbpA shown in Figure 5.3.[178]

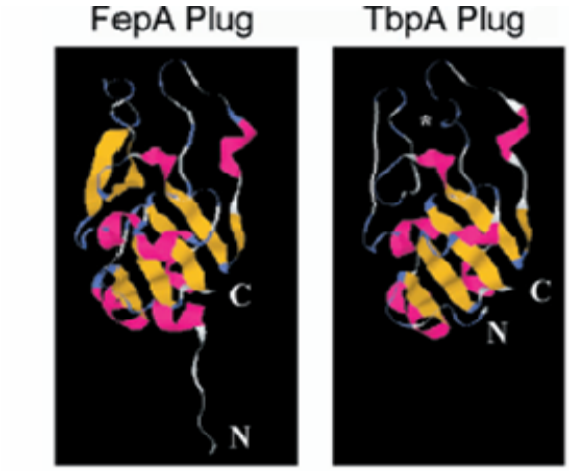

Figure 5.3: Proposed model of the TbpA-plug based on the crystal structure of FepA a homologousn TonB-dependent transporter. Figure reprinted with permission from reference [178].

Given the context that the plug domains of other transporters (e.g. FepA and FhuA) may participate in binding their respective cargo, Noto and Cornelissen recently proposed and investigated the hypothesis that the TbpA-plug binds iron.[214] Mutagenesis of the plug showed that specific residues are required for iron utilization. Noto and

Cornelissen created single, double, and triple alanine substitutions in the highly conserved region of the plug corresponding to amino acids 118 through 122. Importantly, these residues, EIEYE, have the potential to bind iron.[214] All of the mutants were able to bind Tf. However, iron uptake was decreased in the double mutants and the triple mutant was not able to utilize Tf as its iron source.[214] These data strongly suggest that the plug of TbpA binds iron.

However, Noto and Cornelissen also showed that TbpB could compensate for these mutations.[214] Given that the TbpA-plug was previously shown to be partially surface exposed using hemagglutinin analysis [178] and that TbpB was able to compensate for the plug mutations, an alternative interpretation of the data is that the plug is involved in iron removal from Tf and the alanine substitutions in the EIEYE region cause a conformational change that disrupts this proposed function.

The two functions of the TbpA-plug proposed above (to bind iron and to remove iron from Fe_2-Tf) are not mutually exclusive. The TbpA-plug may participate in the release of iron from Tf and the EIEYE residues may in fact form an iron binding site. It is also possible that the plug has multiple iron binding sites. Here we propose an additional role for the plug of TbpA: binding to FbpA.

As reported in Chapter 4, TbpA binds to apo-FbpA and is able to discriminate between apo-FbpA and holo-FbpA. Here we extend this proposed transport mechanism, asserting the possibility that the plug domain of TbpA is responsible for

interacting with apo-FbpA. A modified version of our working transport scheme is shown in Figure 5.4. Using SUPREX to probe the thermodynamic properties of protein structure and protein-protein interactions, we set out to investigate the ability of recombinant TbpA-plug (provided by Dr. Cornelissen) to bind iron and to interact with FbpA.

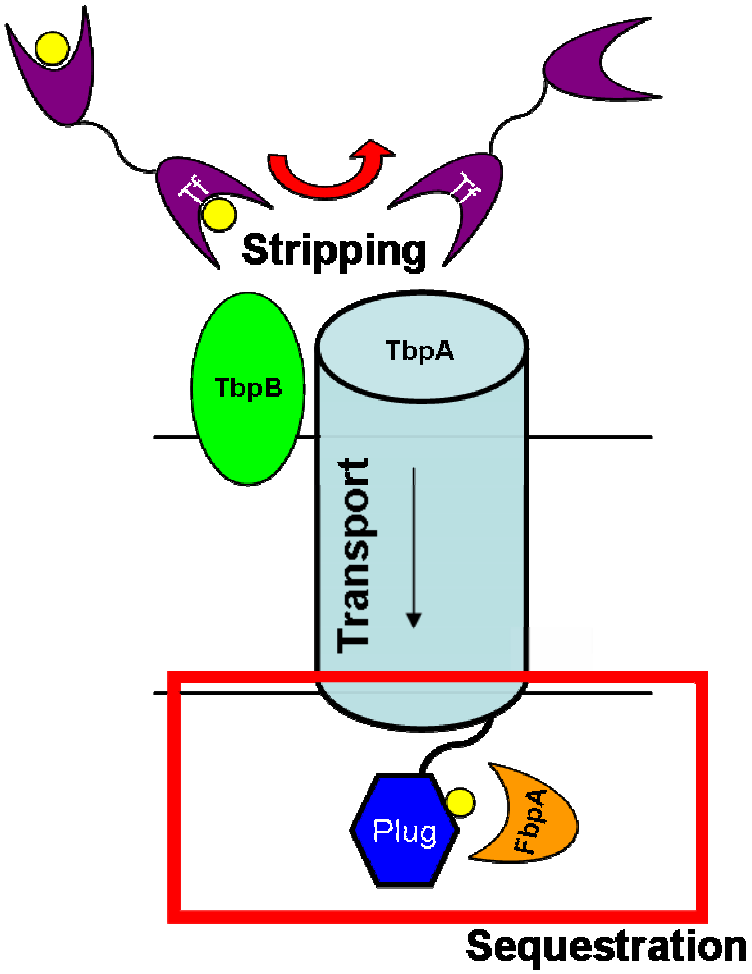

Figure 5.4: Modified transport scheme (see Figure 5.1) depicts the hypothesis that the plug domain of TbpA binds iron and interacts directly with FbpA.

5.1.3 How do TbpA and TbpB Facilitate the Release of Iron From Tf?

Another outlying question regarding the process by which bacteria acquire iron from Tf is how iron is removed from Tf. In Chapter 4, we reported that both TbpA and TbpB are able to facilitate the release of iron from Tf.[147] Here we seek to extend our understanding of this characteristic of TbpA and TbpB. Is the method through which TbpA and TbpB each facilitate the release of iron the same? Does the interaction of Tf with the receptor component(s) cause a thermodynamic or kinetic change in the iron dissociation reaction? These questions are integral to our understanding of how *N. gonorrhoeae* is able to compete with the human transferrin receptor and how this pathogenic bacteria has overcome the bacteriostatic efforts of the human host.

5.1.3.1 Goals of Method Development

Our objective here was to develop a method with which we can investigate the ability of TbpA and TbpB to induce a thermodynamic change in the iron release reaction of Tf. Additionally, we set out to measure the effect of the receptor on the iron release reaction isolated from the incorporation of iron into FbpA. Figure 5.5 depicts a modified version of the transport scheme that focuses on the stripping of iron from Tf.

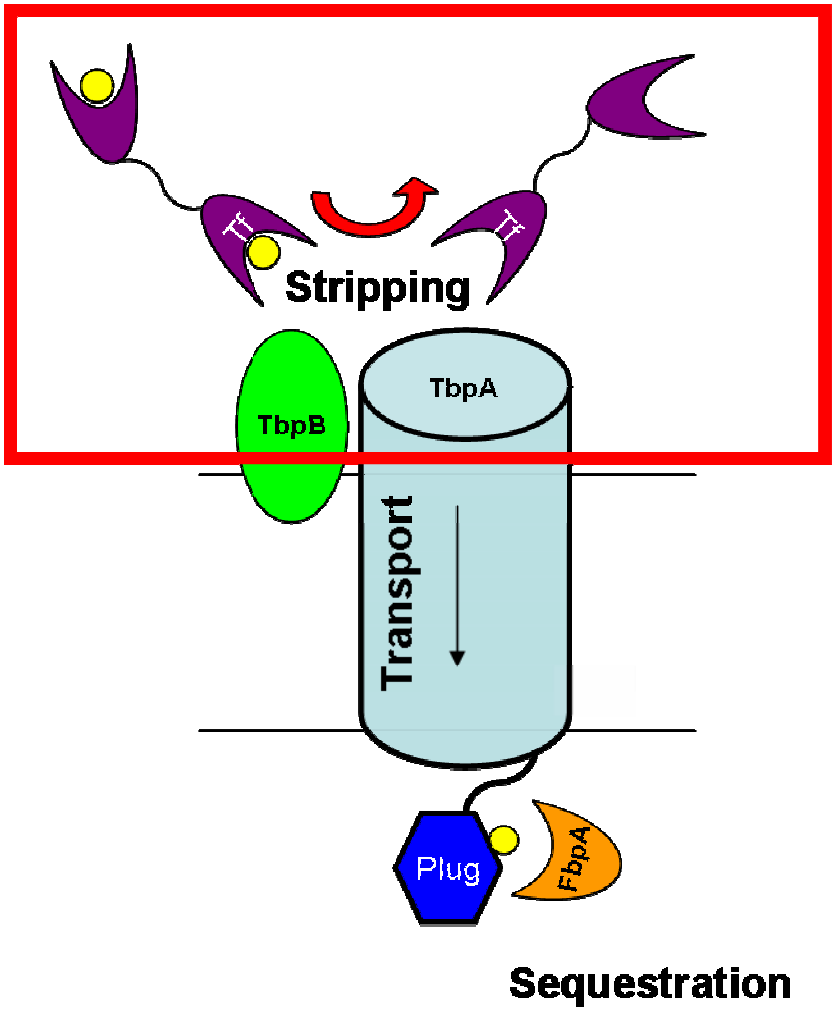

Figure 5.5: Modified transport scheme (see Figure 5.1) emphasizes the ability of TbpA and TbpB to strip iron from Tf. The specific effect(s) of the receptor on the iron release process is unknown.

The technique chosen to accomplish these two goals is equilibrium dialysis. Although equilibrium dialysis is a well known technique and many dialysis products are commercially available, the development of a quantitative and reproducible method used to investigate a reaction system with many complex variables required significant

effort. The challenging and detailed work reported here was performed by Michael MacIntyre under the guidance of the author.

5.1.3.2 Requirements for Equilibrium Dialysis Method

One advantage of using equilibrium dialysis rather than the SUPREX experiment reported previously [147], is that the effect of the receptor components on Tf can be monitored without the presence of FbpA. The equilibrium dialysis method developed here utilizes the well known iron chelator Tiron (1,2-dihydroxybenzene-3,5-disulfonic acid) as a thermodynamic sink and as the spectroscopic handle to monitor how much iron is released from Tf. The competitive reaction between Tiron and Fe_2-Tf is shown in Equation 5.1, where T represents the bidentate chelator Tiron.

$$Fe_2\text{-Tf} + 6T^{-4} \leftrightarrows 2(FeT_3)^{-9} + Tf \qquad (5.1)$$

Tiron was chosen because this small molecule has been shown to efficiently remove iron from Tf at a reasonable rate.[199-201] As well, the spectroscopic properties of Tiron and the speciation of the FeT_x complexes are well understood. Under the conditions used in our equilibrium dialysis method, the $Fe(Tiron)_3^{9-}$ complex, which absorbs light at 480 nm, is the dominant species.[222-224]

In addition to eliminating FbpA from the system under investigation, another initial goal was to develop a technique that is more specific and more quantitative than the SUPREX experiment described in Chapter 4. Our expectation was that the

equilibrium dialysis method would be sensitive enough to detect potentially different thermodynamic effects caused by TbpA compared to TbpB or the mutants of each receptor protein. As discussed in Section 4.1.2, TbpB is able to compensate for TbpA mutants that are incapable of binding Tf or utilizing bound Tf.[179] As well, TbpB can facilitate the release of iron from Tf without TbpA present.[147] We hypothesize that the function supplied by TbpB in these TbpA mutants is that of stripping iron from Tf. A variety of mutants of both TbpA and TbpB are available to us from Dr. Cornelissen, Medical College of Virginia. It is of great interest to understand on the molecular level, what effect each of these mutants has on the iron transport process.

The use of equilibrium dialysis for a complex biological system of Tf interacting with receptor containing bacterial membrane preparations (see Section 4.2.2.2) provides a possible experimental method to investigate the thermodynamic properties of the dissociation reaction in which iron is released from Tf. However, the effect of the bacterial receptor on the iron release reaction may not be thermodynamic in nature. The effect might be kinetic, if the receptor acts as a catalyst, changing the mechanism or pathway the reaction follows. It is important to consider both the possible kinetic and thermodynamic role(s) the receptor may play, in order to fully understand how this pathogenic bacteria hijacks iron from Tf.

5.1.4 Statement of Objectives

The objective of this chapter is to extend our understanding of the iron transport process in *N. gonorrhoeae* in two areas, as depicted in Figure 5.6: Lower box) the ability of the TbpA-plug to bind iron and interact with FbpA and Upper box) how TbpA and TbpB facilitate the release of iron from Tf.

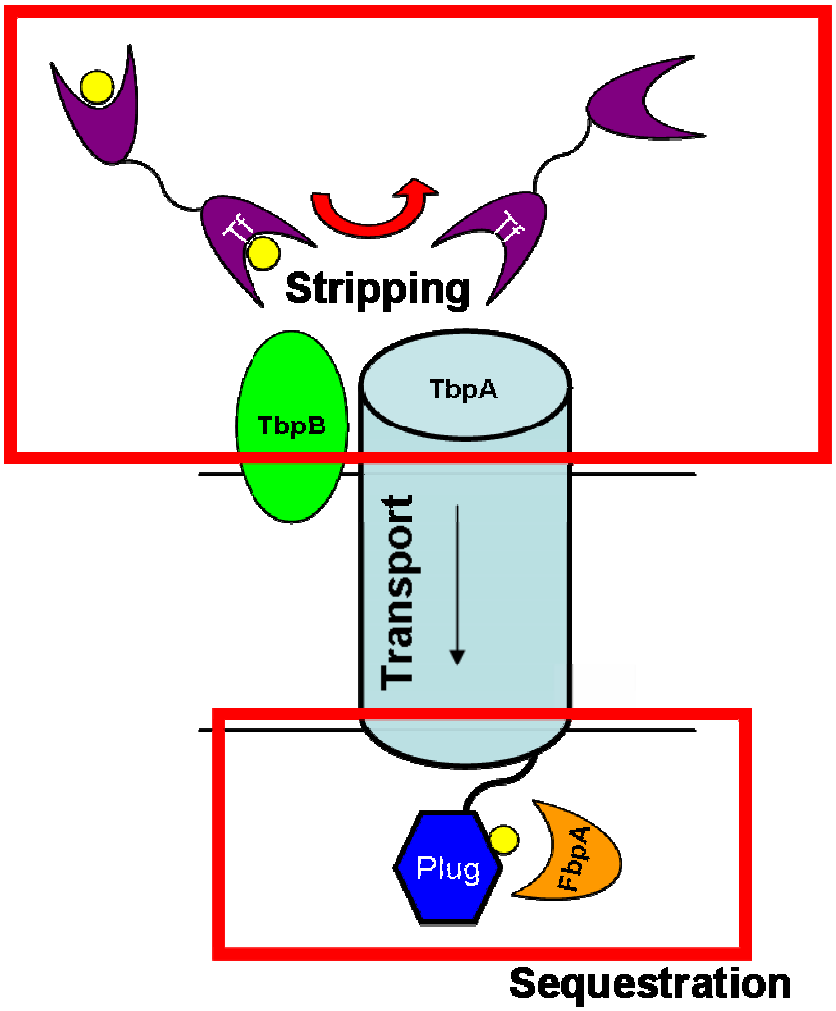

Figure 5.6: Modified version of the iron transport process. Red boxes highlight the two areas under investigation in this chapter: upper box illustrates the release of iron from Tf facilitated by TbpA and TbpB; lower box illustrates the proposed roles of the TbpA-plug, specifically binding to naked iron and interacting directly with FbpA.

In both cases we use thermodynamic measurements to better understand the biological system. For the TbpA-plug (Figure 5.6 lower box) we focus on the thermodynamics of protein folding, while for Tf (Figure 5.6 upper box) we focus on how protein-protein interactions affect the competition of two iron chelators (Tf and Tiron) for binding iron.

5.2 Methods and Materials

5.2.1 Materials

All chemicals were purchased from Fischer (MES, phosphate, and NaCl) or Sigma Aldrich (Hepes, KCl, NTA, and Tiron) and were of high quality. All buffer solutions were exposed to CHELEX-100 (Bio-Rad) overnight to remove trace amounts of iron and stored in acid washed glassware in the dark. A stock solution of Fe(III)NTA was made in 50 mM MES, 200 mM KCl, pH 6.5 and allowed to equilibrate overnight. Using a one to one ligand to metal ratio, the speciation of the solution at this pH is 50% $FeNTAH_{-1}$ and 50% $FeNTAH_{-2}$.

5.2.2 Protein Preparation

Human apo- and holo-Tf were purchased from Sigma Aldrich. To ensure that holo-Tf was fully loaded with iron, holo-Tf was dissolved in DI-H_2O and one small crystal of ferrous chloride was added with a small amount of bicarbonate. The solution

was allowed to sit over night. Any solids were filtered out with a 0.2 μm filter (Corning) and the then the protein solution was dialyzed against a series of buffers (0.1 M $NaClO_4$, DI H_2O, 0.1 M NaCl, and finally 50 mM Hepes buffer/200 mM KCl/20 mM $KHCO_3$/pH 7.4). Complete saturation was determined by comparing the concentrations of Fe_2-Tf determined using the absorbance at 280 nm (ϵ = 114,000 M^{-1} cm^{-1}) and the absorbance at 465 nm (ϵ = 4800 M^{-1} cm^{-1}).

Recombinant FbpA (*N. gonorrhoeae*) provided by Dr. Timothy Meitzner, was expressed in *E. coli* and purified as previously reported.[186, 193] Holo-FbpA was reconstituted in the phosphate form as reported previously.[6] The absence of iron in apo-FbpA samples was ensured by dialysis against 100 mM EDTA in 50 mM MES, 200 mM NaCl at pH 8 overnight. The buffer was then exchanged for 50 mM MES, 200 mM KCl, pH 6.5 using a chelexed buffer solution and acid washed glassware. Following dialysis, the sample did not absorb light in the visible region and yielded a SURPEX curve characteristic of previously analyzed samples of apo-FbpA.

The membrane preparations used in the experiments reported in this chapter were kindly provided by Dr. Cynthia N. Cornelissen. See Section 4.2.2.1 and 4.2.2.2 for a discussion of preparation and components of these membrane preparations. Recombinant plug domain of TbpA was also provided by Dr. Cornelissen. The plug domain was expressed using the pET22b(+) expression construct and included a 6xHis-tag at the C-terminus.[225]

5.2.3 SUPREX

A thorough explanation of the SUPREX protocol can be found in Section 4.2.3. Here we report the experimental details specific to the experiments reported in this chapter. FbpA was allowed to react with each ligand for at least 30 min prior to starting the SUPREX experiment. The SUPREX analyses of FbpA in the absence and presence of the TbpA-plug were initiated by 10-fold dilution into a series of deuterated H/D exchange buffers. The deuterated exchange buffers contained 50 mM MES, 200 mM KCl (pD = 6.5), and concentrations of deuterated GdmCl that ranged from 0 to 6 M. The H/D exchange reactions were allowed to proceed for 1 hr and then were quenched by adding 1 μL of the reaction solution to 9 μL saturated aqueous solution of sinapinic acid. Data analyses were performed as described previously for FbpA.[191] Aldolase was used as an internal standard.

For SUPREX analysis of the Tbp-plug in the presence and absence of excess ligand, a high-sensitivity SUPREX protocol was utilized.[17] The plug was allowed to react with the ligand for at least 15 min prior to SUPREX analysis. The deuterated exchange buffers contained either 50 mM MES and 200 mM KCl (pD = 6.5) or 20 mM phosphate (pD=7.4). Concentrations of deuterated GdmCl ranged from 0 to 6 M. Protein samples were exposed to the deuterated exchange buffer for 5 min. Exchange reactions were quenched with 0.1% TFA and then concentrated and desalted using C4 ZipTips™ (Millipore, Inc.). Deuterated protein was eluted with a 2 μL saturated

solution of sinapinic acid containing 0.1% TFA. Trypsin inhibitor was used as an internal standard. Patrick DeArmond, Duke University is acknowledged for his tireless efforts and helpful discussions regarding this aspect of the work described here.

5.2.4 Equilibrium Dialysis

As is the usual practice for equilibrium determinations, we monitored the reaction shown in Equation 5.1 with a series of reaction mixtures in which we maintained the concentration of Fe_2-Tf constant and varied the concentration of Tiron in a series of separate reaction vessels. However, because we also wanted to introduce opaque, semi-soluble bacterial membrane preparations making light transmission spectroscopy difficult, we utilized dialysis cassettes to contain the Fe_2-Tf and membranes. In each reaction vessel, the Tiron was added to the dialysis solution and diffused into the cassette. Inside the dialysis cassette the Tiron reacted with the Fe_2-Tf (Equation 5.1) and the $Fe(Tiron)_3^{9-}$ complex diffused out of the cassette. Figure 5.7 displays a schematic of the dialysis apparatus. The appropriate volume of the 0.01 M stock solution of Tiron in 50 mM Hepes buffer and 200 mM KCl at pH 7.4 was added to each acid washed 150 mL beaker. We specify the size of the 150 mL beaker because this particular size provided the appropriate depth to ensure the dialysis cassette was completely submerged in the small volume of Tiron solution used. Buffer was added to each beaker to make the total volume 20 mL.

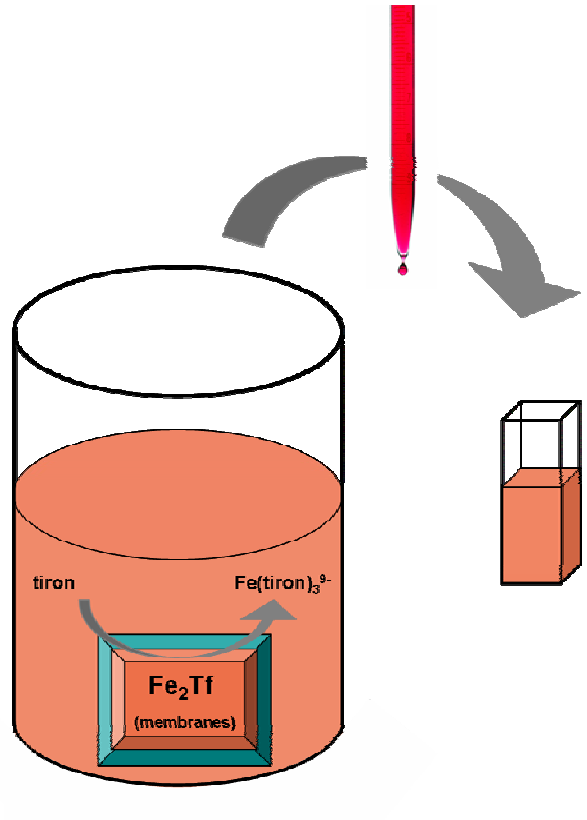

Figure 5.7: Schematic of dialysis apparatus for one Tiron concentration in a series of reaction vessels.

A 1 mL pipette was used to measure 0.4 mL of protein solution, either stock Fe_2-Tf in the same buffer or a pre-mixed sample of Fe_2-Tf and membrane preparations. Then a Luer-lock needle and syringe were used to withdraw the liquid directly from the tip of the pipette. The protein solution was then injected into the dialysis cassette. This modification of the standard procedure was used to control the amount of protein solution added to each dialysis cassette ensuring that each Fe_2-Tf sample was as uniform as possible.

Each cassette was placed on its side at the bottom of the beaker so that it was completely submerged in the Tiron solution. Each beaker was covered and placed in a dark environment for the duration of the experiment. After 24, 48, and 72 hours, ~1 mL was removed from the dialysis solution, a UV-vis absorption spectrum was measured. Then the sample of dialysis solution was returned to the dialysis apparatus (Figure 5.7).

5.2.5 UV-Visible Spectroscopy

UV-vis spectroscopy was used to monitor the equilibrium dialysis experiments and to investigate the interaction of proteins with various reactants discussed herein. For all analytes observed with UV-vis spectroscopy, a Cary 50 spectrophotometer was used and the corresponding background solution of buffer and salt were subtracted as a baseline. A baseline solution of Tiron and buffer were subtracted from all dialysis experiments except those including membrane preparations (see Section 5.3.2.3).

5.3 Results

5.3.1 Thermodynamic Investigations of the Possible Roles of TbpA-plug

5.3.1.1 TbpA-Plug

The mass of the recombinant TbpA-plug, measured using MALDI-MS and using trypsin inhibitor protein as an internal standard, was calculated to be 18282 Da $\pm$ 3 Da.

The SUPREX behavior of the TbpA-plug was characterized at pH 6.5 and 7.4 and as shown in Figure 5.8, does not appear to be affected by the variation in pH tested.

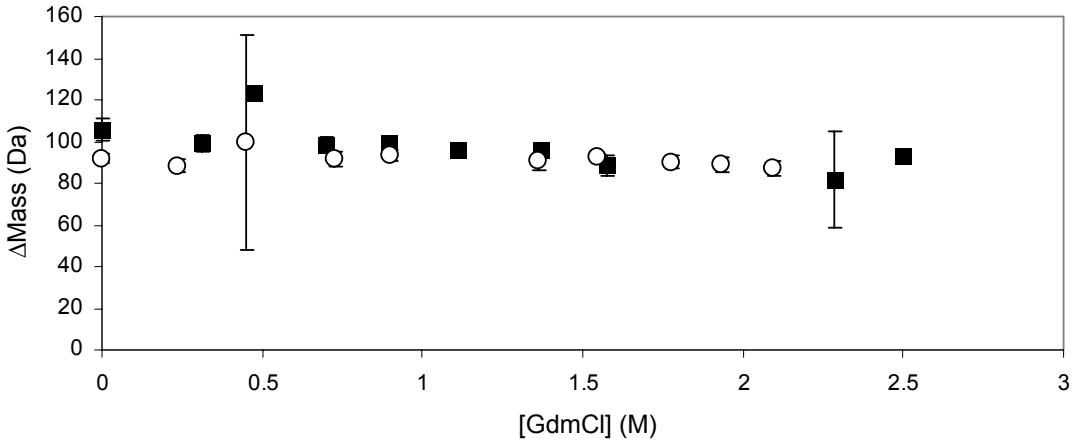

Figure 5.8: SUPREX behavior of TbpA-plug at pH 7.4 (dark squares) and pH 6.5 (open circles). Conditions: exchange time 5 min, Trypsin inhibitor used as the internal standard, 50 mM MES buffer/200 mM KCl/pD 6.5 or 20 mM phosphate buffer/pD 7.4. Error bars indicate the variation between the 10 mass spectra collected for each denaturant concentration. When error bars are not visible the mass variation is smaller than the symbol designating the datum point.

Given that the TbpA-plug consists of 160 amino acids, a ΔMass of around 100 Da means that a majority of the peptidic protons are exchanged for deuterons at all denaturant concentrations when allowed to exchange for 5 minutes.

5.3.1.2 TbpA-Plug in the Presence of Iron

The interaction between the TbpA-plug and FeNTA at pH 6.5 was measured using SUPREX. Figure 5.9 shows the SUPREX behavior of the TbpA-plug is not changed by the presence of excess FeNTA.

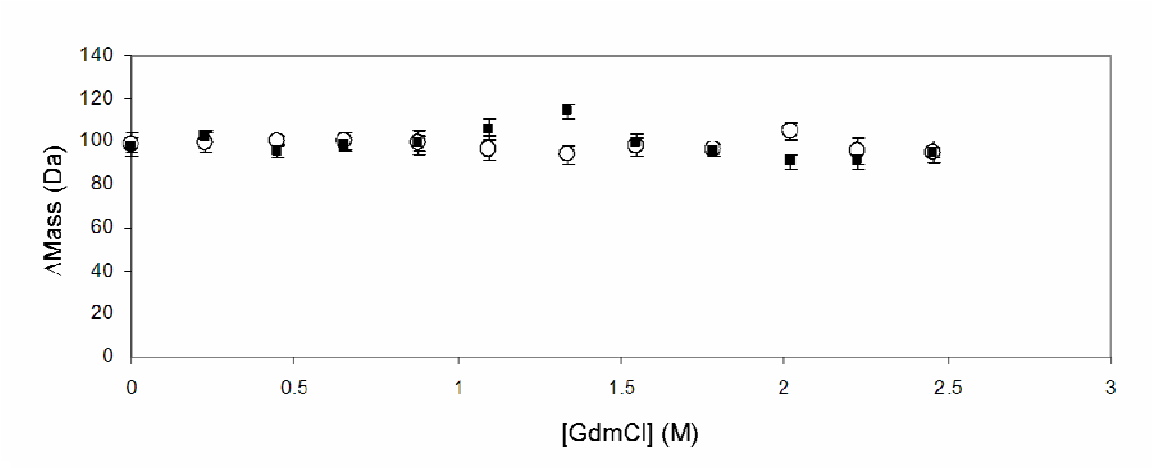

Figure 5.9: SUPREX on the TbpA-plug alone (open circles) and in the presence of excess FeNTA (black squares). Conditions: pH 6.5, exchange time 5 min, Trypsin inhibitor used as the internal standard, 50 mM MES buffer, 200 mM KCl, 0.0013 M TbpA-plug and 10-fold excess FeNTA in the mixture prior to deuterium exchange. Error bars indicate the variation between the 10 mass spectra collected for each denaturant concentration. When error bars are not visible the mass variation is smaller than the symbol designating the datum point.

Similar results were observed for the reaction of the TbpA-plug and FeNTA at pH 7.4 (data not shown).

5.3.1.3 TbpA-plug and FbpA

SUPREX can be used to investigate the unfolding of both FbpA and the plug of TbpA. With this technique we can monitor the stability of each individual protein participating in the reaction. Stated in a different way, we can investigate possible FbpA-TbpA interactions using either FbpA or TbpA as the probe using SUPREX. However, the SUPREX experiment requires the "ligand" to be in excess of the protein under investigation. Therefore, the reaction between apo-FbpA and the TbpA-plug was investigated with an excess of one over the other and vice versa. Figure 5.10 shows the SUPREX behavior of apo-FbpA alone and in the presence of excess Tbp-plug.

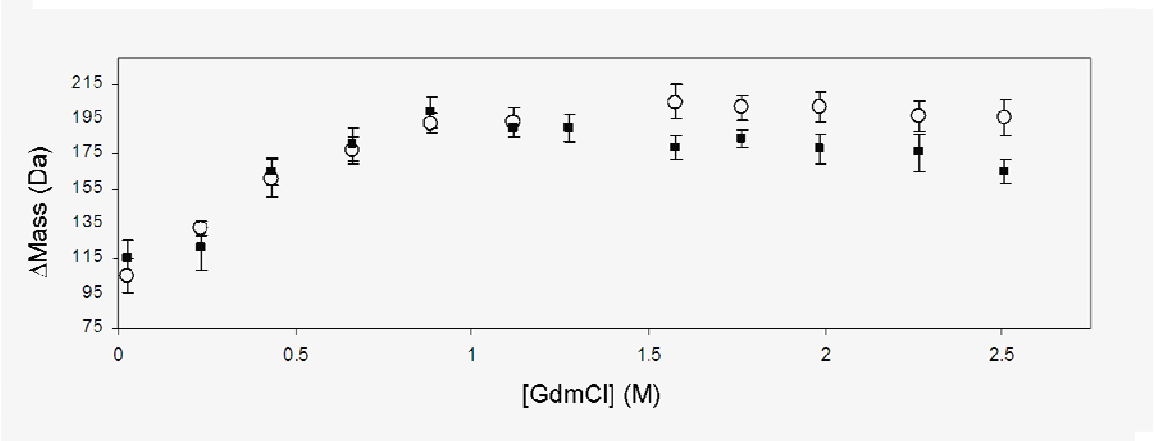

Figure 5.10: SUPREX on apo-FbpA alone (open circles) and in the presence of excess Tbp-plug (black squares). Conditions: pH 6.5, 50 mM MES buffer, 200 mM KCl, and exchange time 1hr. Aldolase was used as an internal standard. During the reaction the protein concentrations were 600 μM TbpA-plug and 50 μM apo-FbpA.

Conversely, Figure 5.11 shows the SUPREX behavior of the TbpA-plug in the presence and absence of excess apo-FbpA.

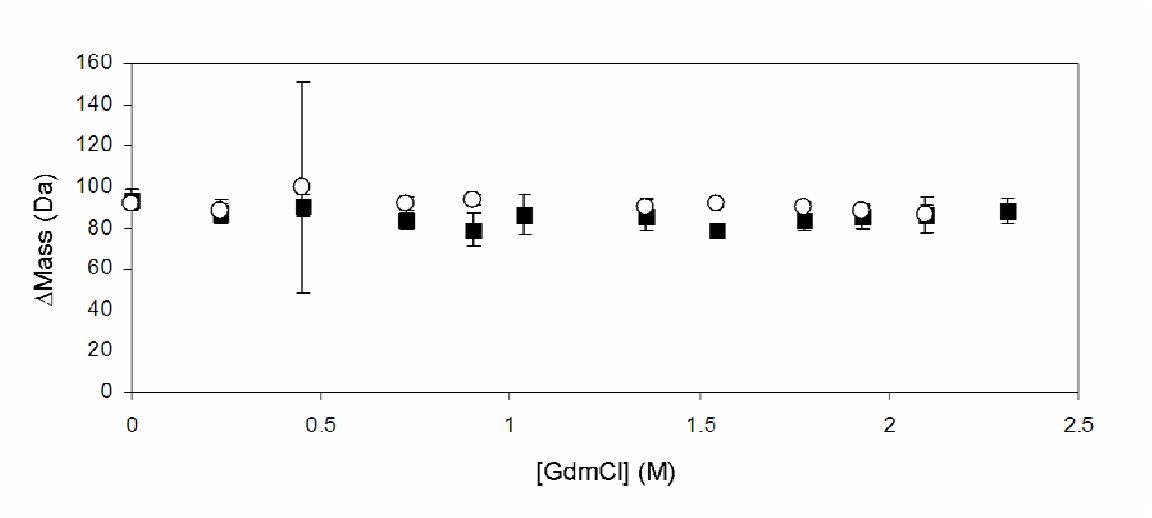

Figure 5.11: SUPREX on the TbpA-plug in the presence (black squares) and absence (open circles) of excess apo-FbpA. Conditions: pH 6.5, 50 mM MES buffer , 200 mM KCl, and exchange time of 5 min. Trypsin inhibitor was used as an internal standard. During the exchange reaction the protein concentrations were 33.6 μM apo-FbpA and 4.5 μM TbpA-plug.

The interaction between the TbpA-plug and apo-FbpA at pH 7.4 (data not shown) yielded similar results as seen for pH 6.5 in Figure 5.11. Additionally, the interactions of the Tbp-plug with holo-FbpA at pH 6.5 and 7.4 were investigated by monitoring the SUPREX behavior of the TbpA-plug. Similar to the results depicted in Figure 5.11, ΔMass values of around 100 Da were observed for all denaturant concentrations independent of the presence of holo-FbpA and independent of pH (data not shown).

In theory, shorter exchange times might enable the observation of the classic sigmoidal SUPREX curve, if the TbpA-plug does have some weakly protected protons.

However, an exchange time of five minutes (utilized in this study) is the minimum time required to manipulate the samples and shorter exchange time can not be achieved.

5.3.2 Thermodynamic Investigations of the Effect of TbpA/TbpB on Fe_2-Tf

5.3.2.1 Method Development

5.3.2.1.1 Tiron Stability in Dialysis Apparatus

As preparation for the dialysis experiment to investigate the reaction shown in Equation 5.1, the stability of Tiron and any possible interactions between Tiron and the dialysis cassette were monitored over time. The dialysis apparatus was prepared following the exact procedure used for each protein trial. The maximum concentration of Tiron used in the protein dialysis experiments was placed on the outside and inside of the dialysis cassette. After 72 hours, the solution began to absorb around 430 nm, however the absorbance value remained negligible until 96 hours. We attribute this increase in absorbance to degradation of the Tiron over time and/or the leaching of metals or other colored molecules from the dialysis cassette over time. Given this limitation of the apparatus, all protein dialysis experiments were stopped after 72 hours.

5.3.2.1.2 Reaction of Iron and Tiron

The reaction of Fe^{3+} and Tiron is well characterized, with the spectral properties, protonation constants, and equilibrium constants available in the literature.[128, 222-

224] A speciation plot (Figure 5.12) for a ligand to metal ratio of 10 to 1 was constructed using the equilibrium constants listed in the Critical Stability Constant Database and HySS 2006.[226] Under our conditions (50 mM Hepes buffer, 200 mM KCl, pH 7.4), any iron released from Tf will form $Fe(Tiron)_3^{9-}$ once it is localized in the bulk Tiron solution on the outside of the dialysis bag. The λ_{max} of the $Fe(Tiron)_3^{9-}$ complex is 480 nm and the ϵ is 3700 M^{-1} cm^{-1}.[128]

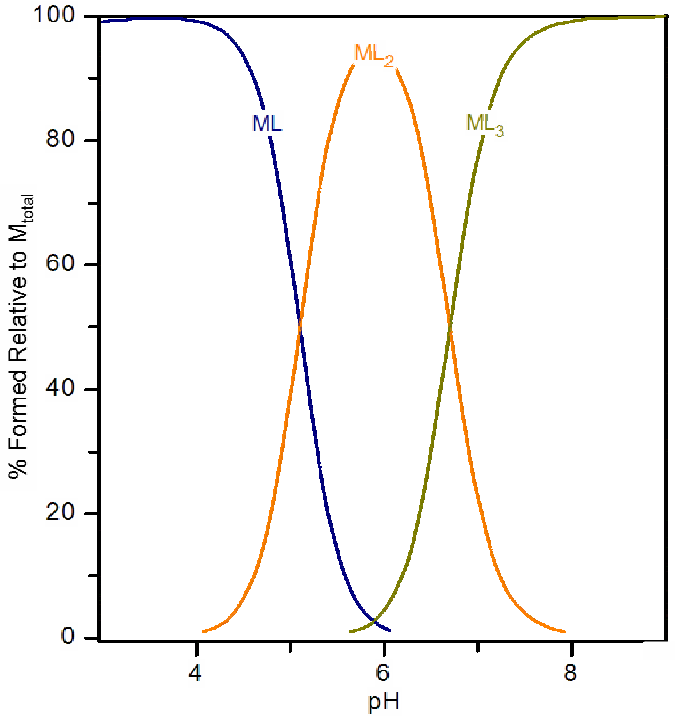

Figure 5.12: Speciation plot of iron and Tiron calculated using a 10 to 1 ligand to metal ratio and concentrations representative of those used in our equilibrium dialysis experiments. Conditions: 1.2 x 10^{-5} M iron, 1.2 x 10^{-4} M Tiron, 25°C, and 0.1 ionic strength.

In order to characterize the reaction of Fe_2-Tf and Tiron (Equation 5.1) under our conditions without the complication of the dialysis apparatus, a series of solutions

containing a constant Fe_2-Tf concentration and varied concentrations of Tiron were analyzed using UV-vis spectroscopy. The molar ratio of Tiron to Fe_2-Tf ranged from 0:1 to 200:1. Figure 5.13 shows the absorbance spectrum of each reaction and equilibrium.

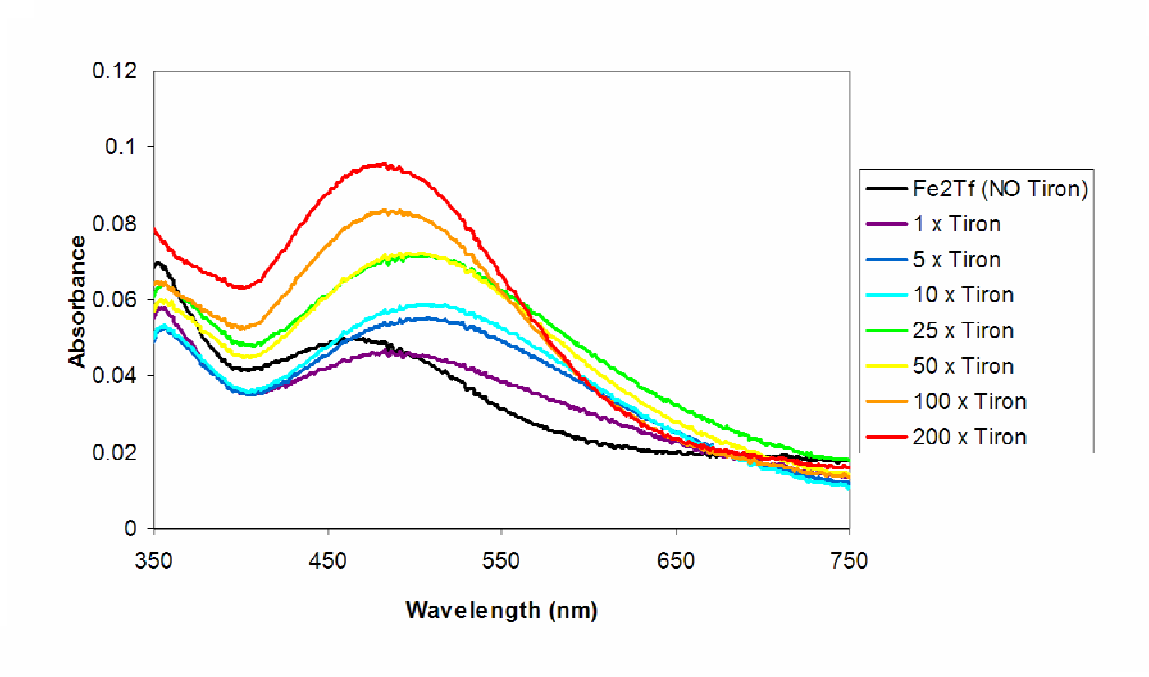

Figure 5.13: Absorbance spectra of the reaction of Fe_2-Tf with varying concentrations of Tiron. Conditions: 6.45×10^{-5} M Fe_2Tf, 50 mM Hepes buffer, pH 7.4, reaction measured after 48 hours. Data collected in collaboration with Michael MacIntyre.

5.3.2.2 Equilibrium Dialysis Experiment: Fe_2-Tf

The reaction of Tiron and Fe_2-Tf (Equation 5.1) was investigated using the dialysis method reported herein. Fe_2Tf was placed inside the cassette and dialyzed against varying concentrations of Tiron. The absorbance of the $Fe(Tiron)_3^{9-}$ outside the

bag was measured after 24, 48, and 72 hours. A representative plot of absorbance at 480 nm (72 hours) as a function of added Tiron concentration is shown in Figure 5.14.

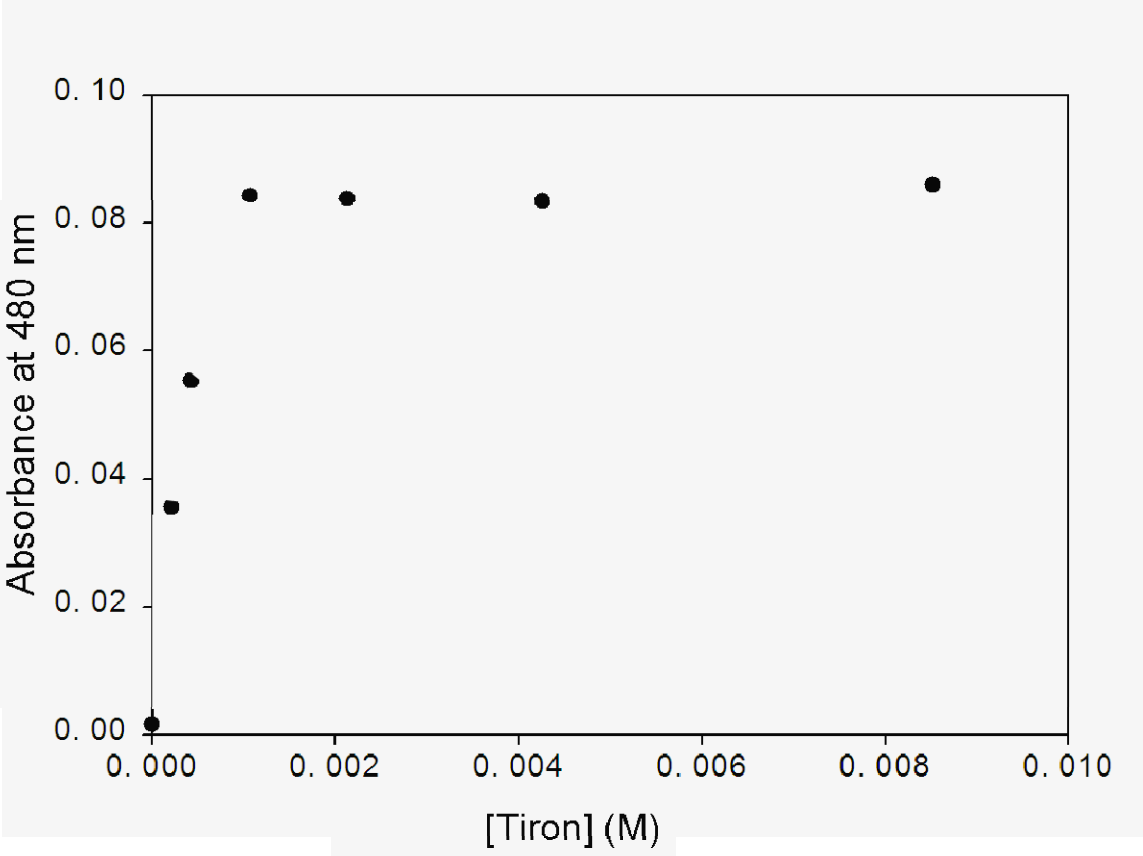

Figure 5.14: Absorbance at 480 nm outside the dialysis bag as a function of Tiron concentration at equilibrium. Conditions: $1.09 \cdot 10^{-3}$ M Fe_2Tf inside the bag, 50 mM Hepes buffer, 200 mM KCl, and pH 7.4.

5.3.2.3 Equilibrium Dialysis Experiment: Membrane Preparations

As discussed in Section 4.2.2.2, the TbpA/TbpB receptor protein samples consist of membrane preparations including many other proteins. The interaction between Tiron and the membrane preparations without Fe_2-Tf present, was investigated to

determine if the membrane preparations contained exogenous iron and if any side reactions affected the optical and diffusion properties of the Tiron. Membrane preparations (FA6815 $TbpA^-/TbpB^-$) that lacked the TbpA/TbpB receptor were placed inside the dialysis cassettes and reacted with a range of Tiron concentrations. After three days, only minimal absorbance at 480 nm was detected outside the dialysis cassettes. However, the plot of absorbance at 480 nm as a function of Tiron concentration (data not shown) did exhibit saturation behavior. This result indicates that although small, there is an amount of iron in the membrane preparations, which is available for chelation by Tiron. In all trials involving membrane preparations, a set of identical dialysis reactions containing membrane preparation but lacking Fe_2-Tf, were also measured. Any absorbance due to exogenous iron in the membrane was subtracted as a baseline prior to analysis. Concurrent background reactions are required because the iron content of each membrane preparation may vary.

5.3.2.4 Equilibrium Dialysis Experiment: Fe_2-Tf in the Presence of TbpA/TbpB Containing Membrane Preparations

The effect of membrane preparations containing TbpA and TbpB (FA19 $TbpA^+/TbpB^+$) on the reaction between Fe_2-Tf and Tiron was investigated using the dialysis techniques described herein. A mixture of membrane preparation and Fe_2-Tf was placed inside the cassette and dialyzed against varying concentrations of Tiron. The absorbance of the $Fe(Tiron)_3^{9-}$ outside the bag after dialysis was measured after 24, 48,

and 72 hours. A representative plot of absorbance at 480 nm (72 hours) as a function of added Tiron concentration is shown in Figure 5.15.

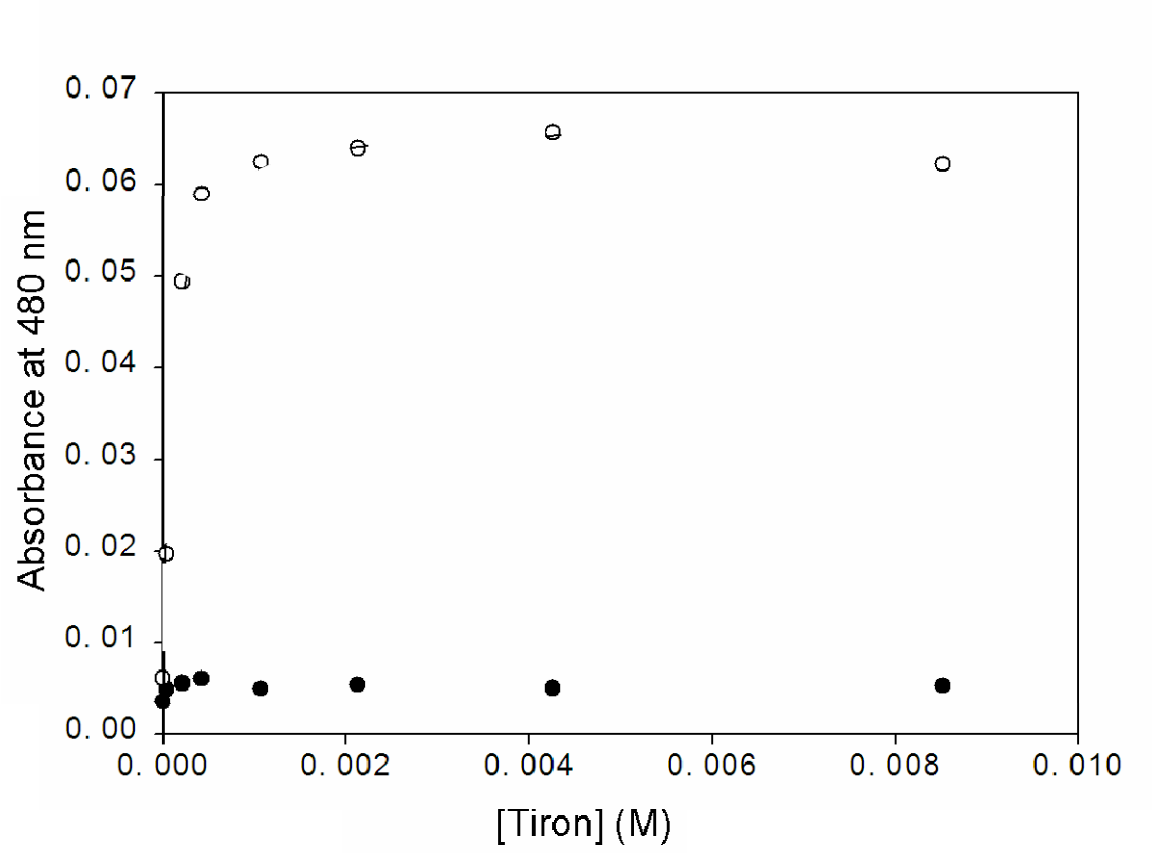

Figure 5.15: Absorbance at 480 nm outside the dialysis bag as a function of Tiron concentration, when Fe_2-Tf in the presence of membrane preparations containing TbpA and TbpB (open circles) and for membrane preparations alone (dark circles). Conditions: 0.3 mL of 5 x 10^{-4} M Fe_2-Tf and 0.2 mL of $TbpA^+/TbpB^+$ membrane preparation inside the bag, 50 mM Hepes buffer, 200 mM KCl, and pH 7.4.

5.4 Discussion

5.4.1 TbpA-Plug

The structure of TbpA consists of a β-barrel and a N-terminus plug domain, which we hypothesize is used to bind the iron during iron transport through TbpA (Figure 5.4). TbpA, an integral membrane protein located in the outer membrane of *N. gonorrhoeae*, has been shown to interact preferentially with apo-Fbp rather than holo-Fbp (Chapter 4). Using the plug domain of TbpA, expressed by our collaborators, we set out to characterize the ability of the TbpA-plug to bind iron and interact with FbpA.

SUPREX was utilized to examine the unfolding behavior of the TbpA-plug. As shown in Figure 5.8, the plug is deuterated to the same extent at all denaturant concentrations after a 5 min exchange time at either pH 6.5 and 7.4. This indicates there are only a few globally protected protons and that the number of globally protected protons does not change when the pH is varied from 6.5 (the pH of the periplasm) to 7.4 the pH of environment surrounding the bacteria. These data are consistent with a predominantly unfolded protein, or a protein that does not contain a detectable amount of secondary or tertiary structure at these pH values. These results are not surprising given the protein is quite small compared to other proteins studied with SUPREX and the predominantly unfolded structure of similar plug domains previously characterized.[220]

The ability of the TbpA-plug to bind iron was investigated by monitoring the effect of FeNTA on the SUPREX behavior of the TbpA-plug. As shown in Figure 5.9, the presence of excess FeNTA does not exert a detectable effect on the structure of the TbpA-plug at either pH 6.5 of 7.4. Therefore, using SUPREX there is no detectable binding event between the TbpA-plug and FeNTA.

These results neither confirm nor disprove the hypothesis that the TbpA-plug binds iron temporarily during the transport mechanism. The binding constant between the TbpA-plug and iron may be weak. If this is the situation, NTA may be too strong of an iron chelator, precluding any competitive binding by the TbpA-plug in our experimental conditions. In a similar vein, the TbpA-plug may only be able to bind iron inside the core of the β-barrel. Due to differences in dielectric constant, hydrophobic environment, or changes in protein structure, the interaction between the recombinant TbpA-plug and FeNTA in an aqueous environment that mimics the periplasm, may not be a good model for the hypothesized iron-protein interaction. Both of the above scenarios would yield a SUPREX curve for the plug that is unchanged in the presence of FeNTA. It is also possible that iron does not bind to the plug specifically. Rather the plug could either be moved within or be removed from the β-barrel prior to iron crossing the membrane. This situation would also yield SUPREX behavior that is unchanged by the presence of FeNTA. In the future, techniques which are more

sensitive to small and/or local changes in protein structure should be used to investigate the possible interactions between iron and the TbpA-plug.

Independent of the TbpA-plug interacting directly with iron, the possibility that the TbpA-plug interacts with FbpA is hypothesized to be an important step in the mechanism of TbpA-dependent iron transport. TbpA has been shown to preferentially interact with apo-Fbp (Chapter 4). However, the studies reported in Chapter 4 do not identify the structural location of this interaction on TbpA.

The TbpA-plug is hypothesized to be a globular domain that is linked to the barrel through a loop at the periplasmic face of the barrel. The TbpA-plug is expected to fit inside the barrel precluding passage through the transporter. It is unclear whether the plug is completely or partially moved into the periplasm during iron transport. Therefore, the accessibility of both the plug and the periplasmic face of the barrel may affect the ability of TbpA to interact with FbpA. Here we explored the possibility that FbpA interacts directly with the TbpA-plug domain.

Using apo-FbpA as the probe there is no detectable binding between apo-FbpA and TbpA-plug. Figure 5.10 shows that there is no difference in the SUPREX behavior of apo-FbpA in the presence or absence of the TbpA-plug at pH 6.5. Previous SUPREX investigations of apo-Fbp have been able to detect binding events with small binding constants for apo-Fbp.[191] Therefore, the results presented here strongly suggest that apo-Fbp does not bind to TbpA by interacting directly with the plug.

Given that the recombinant plug of TbpA is much smaller than apo-Fbp, and therefore a possible binding event may only cause a local change the unfolding behavior of apo-Fbp (not detectable with SUPREX), we also used SUPREX to analyze the effect of apo-Fbp on the TbpA-plug. Using the TbpA-plug as our probe, we did not detect any binding event between the TbpA-plug and apo-FbpA at either pH 6.5 or 7.4 (Figure 5.11). Further, we did not detect any binding event between holo-Fbp and the TbpA-plug at pH 6.5 or 7.4.

Although the limitations of interpreting SUPREX data for the TbpA-plug as discussed previously are applicable here as well, the SUPREX analysis of TbpA-plug is consistent with the SUPREX analysis of apo-Fbp. Under the conditions studied, no interaction between apo-Fbp and the plug domain of TbpA was observed.

5.4.2 Method Development for Thermodynamic Investigations of TbpA/TbpB

The intended use of the equilibrium dialysis method developed here was to characterize the *effect* of protein-protein interactions (Tf binding to the bacterial receptor TbpA/TbpB as shown in Figure 5.5) on the equilibrium position of the reaction described in Equation 5.1, the competition between Tf and Tiron for the binding of iron. Equation 5.1 is reprinted here for the convenience of the reader.

$$Fe_2\text{-Tf} + 6(T) \leftrightarrows 2(FeT_3) + Tf \qquad (5.1)$$

We are therefore interested in changes in the apparent equilibrium constant (K_{app}) of Equation 5.1, rather than the exact K_{eq}. The exact K_{eq} is difficult to accurately determine, because of the complicated reaction stoichiometry, the difference in the two Tf binding sites, the possible kinetic limitations of the reaction, and the speciation of $Fe(Tiron)_x$ complexes. For the purpose of our experiment, we have chosen to regard Fe_2-Tf as a uniform iron source. Therefore, the reaction described in Equation 5.2 sufficiently represents the apparent reaction in which we are interested:

$$M + 3T \leftrightarrows MT_3 \tag{5.2}$$

where M represents the concentration of metal available to bind to Tiron, T represents the concentration of free Tiron, and MT_3 represents the $Fe(Tiron)_3^{9-}$ complex. The following equilibrium expression describes the reaction:

$$K_{app} = \frac{[MT_3]_{eq}}{[T]_{eq}^3 \times [M]_{eq}} \tag{5.3}$$

where K_{app} represents the equilibrium constant for the forward reaction shown in Equation 5.2, and the subscript "eq" denotes concentrations at equilibrium.

In our dialysis experiment we monitor the absorbance at 480 nm of the $Fe(Tiron)_3^{9-}$ complex outside the dialysis cassette. The Fe_2-Tf and Tf remain inside the dialysis bag at all times (Figure 5.7). One advantage of this dialysis method is that the absorbance of Fe_2-Tf which also absorbs light at 480 nm, does not complicate our spectroscopic handle, because it is isolated from the compartment from which the

samples used for spectroscopic measurement are derived. Therefore, the concentration of MT_3 can be calculated directly from the absorbance of $Fe(Tiron)_3^{9-}$.

In order to compare equilibrium dialysis data for Equation 5.1 in the presence (Figure 5.15) and absence (Figure 5.14) of membrane preparations containing TbpA and TbpB, it is necessary to account for differences in initial amounts of metal (variable amounts of Fe_2-Tf added) in our data analysis. Figure 5.16 presents a generic diagram describing how we treated the data. The ratio of the concentration of MT_3 that is formed over the concentration total metal is plotted as a function of the ratio of total ligand over total metal.

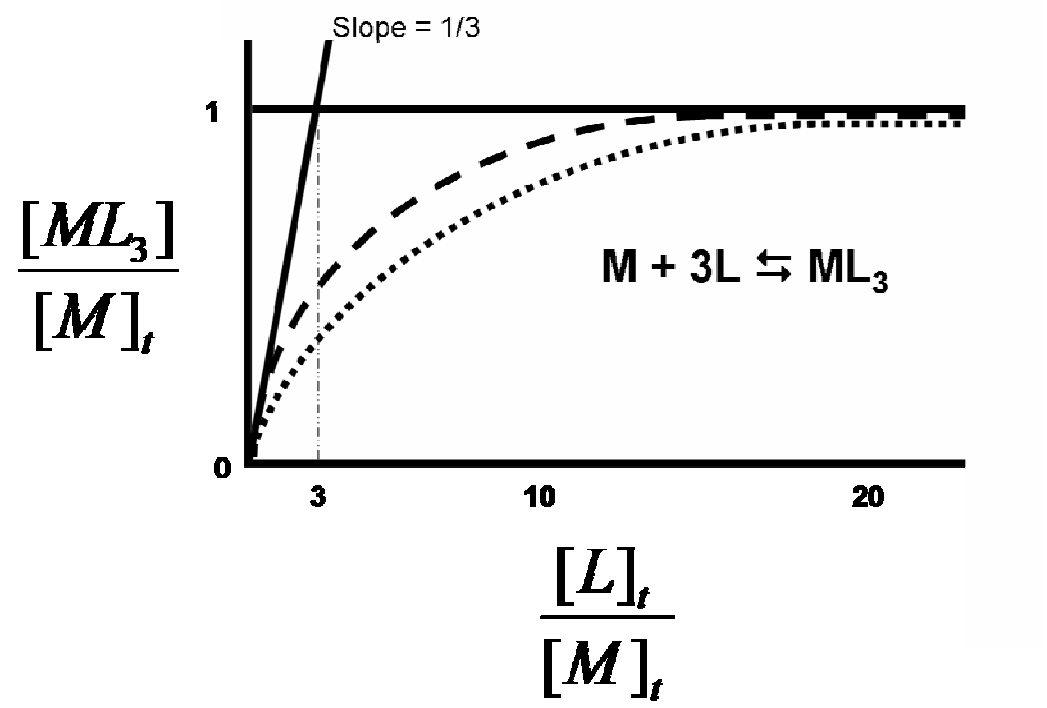

Figure 5.16: Generic plot of $[ML_3]/[M]_t$ as a function of $[L]_t/[M]_t$ for a complex formation reaction with a ligand to metal ratio of 3 to 1. Solid lines denoted the theoretical stoichiometric addition reaction, while the dashed and dotted lines represent reactions with different equilibrium constants.

In our generic plot, L represents an unspecified ligand and M represents an unspecified metal. On the x-axis the ratio of ligand to metal can extend indefinitely. Practically, data points are gathered at varying ligand to metal ratios until saturation is achieved. On the y-axis the ratio of product (ML_3) to limiting reagent (M), cannot exceed the value of one. This axis can also be described as the percent of M that has reacted. The solid black lines represent the theoretical case of a stoichiometric addition reaction. As the ligand to metal ratio is increased, stoichiometric amounts of product are produced. Therefore the slope of the increasing solid line is 1/3 for this reaction.

Saturation is achieved when all of the metal has reacted and the maximal amount of ML_3 has been produced.

Reversible chemical reactions do not follow this theoretical stoichiometric behavior because at equilibrium there is both product and reactant remaining. The extent to which a reversible chemical reaction approaches the theoretical stoichiometric behavior depicted in Figure 5.16 is determined by the characteristic equilibrium constant of the reaction. The reaction represented by the dashed curve has a larger equilibrium constant compared to the reaction described by the dotted curve. Said another way, the dashed curve corresponds to a reaction which has an equilibrium position which lies further towards product formation, in this case MT_3, relative to the reaction corresponding to the dotted line.

In our equilibrium dialysis experiments, we hypothesized that the presence of membrane preparations containing receptor components TbpA and TbpB would alter the thermodynamic behavior of the reaction between Fe_2-Tf and Tiron (Equation 5.1). Figure 5.17 displays the thermodynamic data described in Section 5.3.2 using the analysis described above.

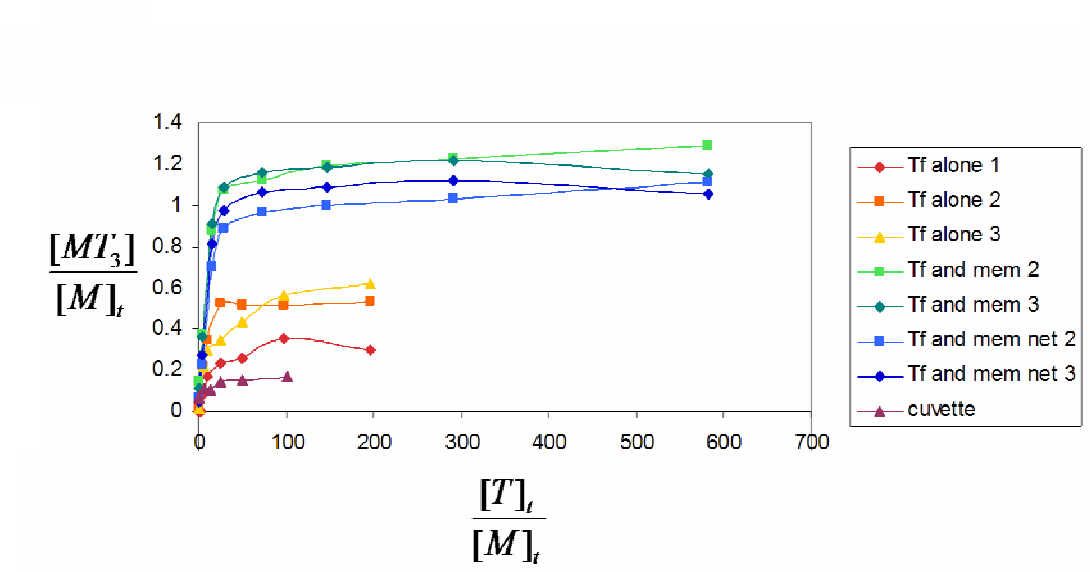

Figure 5.17: Ratio of $Fe[(Tiron)_3]^{9-}$ to total iron as a function of the ratio total Tiron added to total iron. "Tf alone" denotes trials where purified Tf was placed inside a dialysis cassette. "Tf and mem" denotes the total MT_3 measured for trials in which Tf and membranes were placed in the cassette. "Tf and mem net" denotes the net amount of iron released by Tf after the contribution of the membrane was subtracted. "Cuvette" denotes the reaction of Tf and Tiron observed in the absence of the dialysis apparatus.

The data shown in light green ("Tf and mem 2") and dark green ("Tf and mem 3") represent the total metal chelated by Tiron in the equilibrium dialysis experiment in which membrane preparation containing TbpA and TbpB were present. The values of MT_3/M_t larger than one indicate that additional iron was present in the membrane preparations. As discussed in Section 5.3.2, the absorbance due to iron present in the membrane preparations was subtracted from the total absorbance in order to determine the amount of iron removed from Tf. The corrected data corresponding to the light

green and dark green data sets are colored in light blue ("Tf and mem 2 net") and dark blue ("Tf and mem 3 net") respectively. These data describe the amount of metal removed from Tf and chelated by Tiron in the presence of membrane preparations containing TbpA and TbpB and indicate that saturation is reached when all of the iron is removed from Tf.

The red, orange, and yellow data sets represent three separate trials in which only Fe_2-Tf was placed in the dialysis cassette (no membrane preparations). Under the conditions studied, it appears that Tiron was not able to remove all of the iron from Tf or that the $Fe(Tiron)_3^{9-}$ complex did not diffuse back into the bulk dialysis solution in the absence of the membrane preparations. Similar iron complexes binding to the dialysis membrane itself have been mentioned in the literature [227], but this does not seem plausible given the ability to observe the maximum $Fe(Tiron)_3^{9-}$ concentrations when the membrane preparations are present.

The final data set presented in Figure 5.17 (shown in purple), represents the reaction of Fe_2-Tf and Tiron in a cuvette rather than the dialysis apparatus. This data set shows that under the conditions studied, Tiron is not able to remove all of the iron from Tf. Quantitative measurements of the effect of the TbpA/TbpB receptor on the dissociation reaction of iron from Tf are therefore precluded because a baseline apparent equilibrium was obtained. However, using the specific equilibrium dialysis method developed here, we have observed a change in the thermodynamics of iron release from

Tf to Tiron in the presence membrane preparations containing TbpA and TbpB. Membrane preparations containing TbpA and TbpB enhance the formation of $Fe(Tiron)_3^{9-}$.

5.5 Future Directions

5.5.1 Characterization of the TbpA-Plug

Further SUPREX experiments on the TbpA-plug are not recommended, as this technique is not sensitive enough to monitor small changes in the structure of the plug domain. However, characterization of the Tbp-plug is still of significant interest. Two techniques which could be employed in the future are circular dichroism (CD) and fluorescence. The secondary structures of the plug domains of other TonB-transporters have been characterized using CD previously.[220] This technique can provide insight as to the amount and type of secondary structure in various conditions. Monitoring the fluorescence of the TbpA-plug may also prove useful as the interactions between many proteins and iron have been elucidated using this technique.

5.5.2 The Thermodynamic Influence of TbpA/TbpB of Iron Release from Transferrin

Further development of the equilibrium dialysis method is not warranted for several reasons. The method as reported here requires large amounts of protein and is cumbersome to set up due to the larger number of reaction vessels required.

Additionally, the number of dialysis cassettes required for each experiment is financially prohibitive.

Although another iron chelator, which can fully remove iron from Tf at a reasonable rate and easily diffuse in and out of the dialysis cassette may be available, two factors that limit our ability to quantify the effect of any specific protein/receptor interaction remain. First, the stoichiometry of the biologically active receptor is not known and second the number of TbpA and TbpB proteins present in any given membrane preparation is unclear. Therefore, any observed change in the equilibrium constant could only be attributed to the presence of a particular component. The interpretation that a specific binding event between Fe_2-Tf and a particular receptor component is responsible for that effect can not be made. Further, only a minimum estimate for the extent or energetic contribution of an observed effect is possible. It is impossible to know if the entire population of Tf molecules reacting with the iron chelator and producing the observed signal, are in fact influenced by the receptor or if the observed signal represents only an average of the affected and unaffected populations of Tf molecules.

Finally, it is possible that the interaction of Tf and the receptor has a catalytic effect (kinetic) and provides a new mechanism of iron release rather than having a thermodynamic effect. In this situation, the equilibrium constant of the reaction would be expected to remain the same in the presence and absence of receptor. However,

given the limitations discussed above, caution should be used when interpreting two similar equilibrium constants measured using this method.

References

[1] Boukhalfa, H., and Crumbliss, A. L., *Chemical aspects of siderophore mediated iron transport*, BioMetals 15 (2002) 325-339.

[2] Dhungana, S., and Crumbliss, A. L., *Coordination chemistry and redox processes in siderophore mediated iron transport*, Geomicrobiology Journal 22 (2005) 87-98.

[3] Cotton, F. A., Wilkinson, G., Murillo, C. A., and Bouchmann, M. Advances in Inorganic Chemistry, 6th Edition, Wiley-Interscience, New York, 1999.

[4] Haber, F., and Weiss, J., Proc. R. Soc. Lond. A 147 (1934) 332-337.

[5] Crichton, R. Iron metabolism: From molecular mechanism to clinical consequences, 3rd ed., John Wiley and Sons, West Sussex, 2009.

[6] Dhungana, S., Taboy, C. H., Anderson, D. S., Vaughan, K. G., Aisen, P., Mietzner, T. A., and Crumbliss, A. L., *The influence of the synergisitic anion on iron chelation by ferric binding protein, a bacterial transferrin*, PNAS 100 (2003) 3659-3664.

[7] Meis, K. A., Wirgau, J. I., and Crumbliss, A. L., *Ternary complex formation facilitates a redox mechanism for iron release from a siderophore*, BioMetals 19 (2006) 115-126.

[8] Taboy, C. H., Bonaventura, C., and Crumbliss, A. L., *Spectroelectrochemistry of heme proteins: effects of active-site heterogeneity on Nernst plots*, Bioelectrochem. and Bioenerg. 48 (1999) 79-86.

[9] Harrington, J. M., and Crumbliss, A. L., *The redox hypothesis in siderophore-mediated iron uptake*, Biometals 22 (2009) 679-689.

[10] Harrington, J. M., and Crumbliss, A. L. in: (Eds.), Advances in Inorganic Chemistry, Elsevier Academic Press Inc., San Diego, 2009, pp. 179-250.

[11] Pearson, R. G., *Hard and Soft Acids and Bases*, J. Am. Chem. Soc. 85 (1963) 3533.

[12] Dhungana, S., Taboy, C. H., Zak, O., Larvie, M., Crumbliss, A. L., and Aisen, P., *Redox Properties of Human Transferrin Bound to Its Receptor*, Biochem. 43 (2004) 205-209.

[13] Taboy, C. H., Bonaventura, C., and Crumbliss, A. L. in: Sen, C. K., and Packer, L. (Eds.), Methods in Enzymology: Redox Cell Biology and Genetics Part B, Academic Press, Elsevier Science, 2002, pp. 187-209.

[14] Branden, C., and Tooze, J. Introduction to Protein Structure, 2 Ed., Garland Publishing, Inc., New York, 1999.

[15] Lakowicz, J. R. Principles of fluoresecence spectroscopy, 2nd Ed., Springer, New York, 1999.

[16] Kelly, S. M., and Price, N. C. in: (Eds.), Current Protocols in Protein Science, John Wiley and Sons, Inc, 2006.

[17] Powell, K. D., and Fitzgerald, M. C., *Measurements of protein stability by H/D exchange and matrix-assisted laser desorption/ionization mass spectrometry using picomoles of material*, Anal. Chem. 73 (2001) 3300-3304.

[18] Kosmachevskaya, O. V., and Topunov, A. F., *Hemoglobins: Diversity of structures and functions*, Applied Biochemistry and Microbiology 45 (2009) 563-587.

[19] Bonaventura, C., Henkens, R., Weaver, K. D., Alayash, A. I., and Crumbliss, A. L. in: Bolognesi, M., di Prisco, G., and Verde, C. (Eds.), Protein Reviews Springer, Verlag, 2008.

[20] Dimino, M. L., and Palmer, A. F., *High O2 affinity hemoglobin-based oxygen carriers synthesized via polymerization of hemoglobin with ring-opened 2-chloroethyl-B-D-Fructopyranoside and 1-o-Octyl-B-D-Glucopyranoside*, Biotechnology and Bioengineering 97 (2006) 462-472.

[21] Nagababu, E., Ramasamy, S., and Rifkind, J. M., *Site-specific cross-linking of human and bovine hemoglobins differentially alters oxygen binding and redox side readtions producing rhombic heme and heme degradation*, Biochem. 41 (2002) 7407-7415.

[22] Everts, S. (2009) Artificial Blood: Poor clinical trial results and controversy stymie attempts to create alternatives to donated blood, in *C and E News*, pp 52-55, Berlin.

[23] Monod, J. J., Wymann, J., and Changeux, J. P., J. Mol. Biol. 12 (1965) 88.

[24] Hill, A. V., J. Physiol. 40 (1910) 4.

[25] Antonini, E., and Brunori, M. Hemoglobin and myoglobin in their interactions with ligands, North Holland Publishing Co., Amsterdam, 1971.

[26] Adair, G. S., J. Biol. Chem. 63 (1925) 529.

[27] Koshland, D. E., Nemethy, G., and Filmer, D., Biochem. 5 (1966) 365.

[28] Perutz, M. F. Mechanism of cooperativity and allosteric regulation in proteins, Cambridge University Press, Cambridge, 1991.

[29] Taboy, C. H., Faulkner, K. M., Kraiter, D. C., Bonaventura, C., and Crumbliss, A. L., *Concentration -dependent Effects of Anions on the Anaerobic Oxidation of Hemoglobin and Myoglobin*, Journal of Biological Chemistry 275 (2000) 39048 - 39054.

[30] Esquera, R. M., Jensen, R. A., Bhaskaran, S., Pillsbury, M. L., Mandoza, J. L., Lintner, B. W., Kliger, D. S., and Goldbeck, R. A., *The pH dependence of heme pocket hydration and ligand rebinding kinetics in photodissociated carbonmonoxymyoglobin,* Journal of Biological Chemistry (2008).

[31] Faulkner, K. M., Bonaventura, C., and Crumbliss, A. L., *A spectroelectrochemical method for evaluating factors which regulate the redox potential of hemoglobins.*, Inorganica Chemica Acta 226 (1994) 187-194.

[32] Dhungana, S., and Crumbliss, A. L. in: Kaim, W., and Klein, A. (Eds.), Spectroelectrochemistry, Royal Society of Chemistry, London, 2008.

[33] Bonaventura, C., Crumbliss, A. L., and Weber, R. E., *New Insights into the proton-dependent oxygen affinity of Root Effect haemoglobins*, Acta Physiol. Scand. 182 (2004) 245-258.

[34] Remington, N., Stevens, R. D., Wells, R. S., Holm, A., Dhungana, S., Taboy, C. H., Crumbliss, A. L., Henkens, R., and Bonaventura, C., *Genetic Diversity of coastal bottlenose dolphins revealed by structurally and functionally diverse hemoglobins*. Gene 398 (2007) 123-131.

[35] Van Dyke, B. R., Saltman, P., and Armstrong, F. A., *Control of Myoglobin Electron-Transfer Rates by the Distal (Nonbound) Histidine Residue*, J. Am. Chem. Soc. 118 (1996) 3490-3492.

[36] Fultz, M. L., and Durst, R. A., *Mediator compounds for the electrochemical study of biological redox systems: a compilation*, Ana. Chim. Acta 140 (1982) 1-18.

[37] Hoffman, B. M., and Bull, C., *Linearity of the hemoglobin oxidation Bohr effect*, PNAS 73 (1976) 800-803.

[38] Bonaventura, C., and Bonaventura, J., Amer. Zool. 20 (1980) 131-138.

[39] Root, R. W., *The respiratory function of the blood of marine fishes*, Bio. Bull. 61 (1931) 427-465.

[40] Coletta, M., Santucci, R., Focesi Jr., A., Ascoli, F., and Brunori, M., *Redox properties of components I and IV of trout hemoglobins: kinetic and potentiometric studies*, Biochim. Biophys. Acta 915 (1987) 415-419.

[41] Parkhurst, L. J., Goss, D. J., and Perutz, M. F., *Kinetic and equilibrium studies on the role of beta-147 histidine in the Root Effect and cooperativity in carp hemoglobin*, Biochem. 22 (1983) 5401-5409.

[42] Mylvaganam, S. E., Bonaventura, C., Bonaventura, J., and Getzoff, E. D., *Structural basis for the Root Effect in haemolglobin*, Nature Structural Biology 3 (1996) 275-283.

[43] Kraiter, D. C., Crumbliss, A. L., Doctoral Dissertation, Department of Chemistry, Duke University, 1998.

[44] De Jesus-Bonilla, W., Jia, Y., Alayash, A. I., and Lopez-Garriga, J., *The Heme Pocket Geometry of Lucina pectinata Hemoglobind II Restricts Nitric Oxide and Peroxide Entry: Model of Ligand Control for the Design of a Stable Oxygen Carrier*, Biochem. 46 (2007) 10451-10460.

[45] Kraus, D. W., and Wittenberg, J. B., *Hemoglobin of the Lucina pectinata/bacteria symbiosis*, J. Biol. Chem. 265 (1990) 16043-16053.

[46] Gavira, J. A., Camara-Artigas, A., De Jesus-Bonilla, W., Lopez-Garriga, J., Lewis, A., Pietri, R., Yeh, S.-R., Cadilla, C. L., and Garcia-Ruiz, J. M., *Structure and Ligand Selection of Hemoglobin II from Lucina pectinata*, Journal of Biological Chemistry 283 (2008) 9414-9423.

[47] Rizzi, M., Wittenberg, J. B., Coda, A., Ascenzi, P., and Bolognesi, M., *Structural bases for sulfide recognition in Lucina pectinata hemoglobin*, J. Mol. Biol. 258 (1996) 1-5.

[48] Pietri, R., Granell, L., Cruz, A., De Jesus-Bonilla, W., Lewis, A., Leon, R., Cadilla, C. L., and Lopez-Garriga, J., *Tyrosine B10 and heme-ligand interactions of Lucina pectinata hemoglobin II: control of heme reactivity* Biochim. Biophys. Acta 1747 (2005) 195-203.

[49] Bonaventura, C., personal communication with Crumbliss, A. L.

[50] Weber, R. E., and Vinogradov, S. N., *Non-vertebrate hemoglobins: functions and molecular adaptations*, Physiol. Rev. 81 (2001) 596-628.

[51] see Reference [19].

[52] Keszler, A., Piknova, B., Schechter, A. N., and Hogg, N., *The reaction between nitrite and oxyhemoglobin: a mechanistic study*, J. Biol. Chem. 283 (2008) 9615-9622.

[53] Kosaka, H., Imaizumi, K., and Tyuma, I., *Mechanism of autocatalytic oxidation of oxyhemoglobin by nitrite. An intermediate detected by electron spin resonance*, Biochim. Biophys. Acta 702 (1982) 237-241.

[54] Kosaka, H., and Tyuma, I., *Production of superoxide anion by N,N-bis(2-hydroxyethyl)-iminotris(hydroxymethyl)methane buffer during oxidation of oxyhemoglobin by nitrite and effect of inositol hexaphosphate on the oxidation*, Biochim. Biophys. Acta 709 (1982) 187-193.

[55] Doyle, M. P., Pickering, R. A., Dykstra, R. L., Nelson, C. L., and Boyer, R. F., *Involvement of peroxide and superoxide in the oxidation of hemoglobin by nitrite*, Biochim. Biophys. Res. Commun. 105 (1982) 127-132.

[56] Lissi, E., *Autocatalytic oxidation of hemoglobin by nitrite: a possible mechanism*, Free Radical Biology & Medicine 24 (1988) 1535-1536.

[57] Brooks, J., *Action of nitrite on hemoglobin in the absence of oxygen*, Proc. R. Soc. Med. 123 (1937) 368-382.

[58] Doyle, M. P., Pickering, R. A., DeWeert, T. M., Hoekstra, J. W., and Pater, D., *Kinetics and mechanism of the oxidation of human deoxyhemoglobin by nitrites*, J. Biol. Chem. 256 (1981) 12393-12398.

[59] Allen, B. W., Stamler, J. S., and Piantadosi, C., *Hemoglobin, nitric oxide and molecular mechanism of hypoxic vasodilation*, Trends in Molecular Medicine 15 (2009) 452-460.

[60] Gladwin, M. T., Schechter, A. N., Kim-Shapiro, D. B., Patel, R. P., Hogg, N., Shiva, S., Cannon III, R. O., Kelm, M., Wink, D. A., Espey, M. G., Oldfield, E. H., Pluta, R. M., Freeman, B. A., Lancaster Jr, J. R., Feelisch, M., and Lundberg, J. O., *The emerging biology of the nitrite anion*, Nat. Chem. Biol. 1 (2005) 308-314.

[61] Crawford, J. T., Scott, I. T., Huang, Z., Shiva, S., Chacko, B., Schechter, A. N., Darley-Usmar, V., Kerby, J., Lang, J., Kraus, D., Ho, C., Gladwin, M. T., and Patel,

R., *Hypoxia, red blood cells, and nitrite regulate NO-dependent hypoxic vasodilation*, Blood 107 (2006) 566-574.

[62] Cosby, K., Partovi, K. S., Crawford, J. H., Patel, R. P., Reiter, C. D., Martyr, S., Yang, B. K., Waclawiw, G., Zalos, G., Xu, X., Huang, K. T., Shields, H., Kim-Shapiro, D. B., Schechter, A. N., Cannon III, R. O., and Gladwin, M. T., *Nitrite reduction to nitric oxide by deoxyhemoglobin vasodilates the human circulation*, Nat. Med. 9 (2003) 1498-1505.

[63] Angelo, M., Singel, D. J., and Stamler, J. S., *An S-nitrosothiol (SNO) synthase function of hemoglobin that utilizes nitrite as a substrate*, PNAS 103 (2006) 8366-8371.

[64] van Faassen, E. E., Bahrami, S., Feelisch, M., Hogg, N., Kelm, M., Kim-Shapiro, D. B., Kozlov, A. V., Li, H., Lundberg, J. O., Mason, R., Nohl, H., Rassaf, T., Samouilov, A., Slama-Schwok, A., Shiva, S., Vanin, A. F., Weitzberg, E., Zweier, J., and Gladwin, M. T., *Nitrite as regulator of hypoxic signaling in mammalian physiology*, Med. Res. Reviews 29 (2009) 683-741.

[65] Nagababu, E., Ramasamy, S., Abernethy, D. R., and Rifkind, J. M., *Active nitric oxide produced in the red cell under hypoxic conditions by deoxyhemoglobin-mediated nitrite reduction*, J. Biol. Chem. 278 (2003) 46349-46356.

[66] Salgado, M. T., Nagababu, E., and Rifkind, J. M., *Quantification of intermediates formed during the reduction of nitrite by deoxyhemoglobin*, J. Biol. Chem. 284 (2009) 12710-12718.

[67] Bonaventura, C., Fago, A., Henkens, R., and Crumbliss, A. L., *Critical redox and allosteric aspects of nitrix oxide interaction with hemoglobin*, Antioxidants and Redox Signaling 6 (2004) 979-991.

[68] Bonaventura, C., Taboy, C. H., Low, P. S., Stevens, R. D., Lafon, C., and Crumbliss, A. L., *Heme redox properties of S-nitrosated hemoglobin Ao and hemoglobin S*, J. Biol. Chem. 277 (2002) 14557-14563.

[69] Doyle, M. P., Lepoire, D. M., and Pickering, R. A., *Oxidation of hemoglobin and myoglobin by alkyl nitrites inhibition by oxygen*, J. Biol. Chem. 256 (1981) 12399-12404.

[70] Yi, J., Safo, M. K., and Richter-Aldo, B., *The nitrite anion binds to human hemoglobin via the uncommon o-nitrito mode*, Biochem. 47 (2008) 8247-8249.

[71] Grubina, R., Basu, S., Tiso, M., Kim-Shapiro, D. B., and Gladwin, M. T., *Nitrite reductase activity of hemoglobin S (Sickle) provides insight into contributions of heme redox potential versus ligand affinity*, J. Biol. Chem. 283 (2008) 3628-3638.

[72] Kiese, M. Methemoglobinemias: a comprehensive treatise, CRC Press, Inc., Cleveland, 1974.

[73] Bonaventura, C., Ferruzzi, G., Tesh, S., and Stevens, R. D., *Effects of s-nitrosation on oxygen binding by normal and sickle cell hemoglobin*, J. Biol. Chem. 274 (1999) 24742-24748.

[74] Leon, R. G., Munier-Lehmann, H., Barzu, O., Baudin-Creuza, V., Pietri, R., Lopez-Garriga, J., and Cadilla, C. L., *High-level production of recombinant sulfide-reactive hemoglobin I from Lucina pectinata in Escherichia coli*, Protein Expression and Purification 38 (2004) 184-195.

[75] Weaver, K. D., Crumbliss, A. L., Doctoral Dissertation, Department of Chemistry, Duke University (2008).

[76] see Reference [32].

[77] Steckhan, E., and Kuwana, T., *Spectroelectrochemical Study of Mediators I. Bipyridylium Salts and Thier Electron Transfer Rates to Cytochrome c.*, Berichte der Bunsen-Gesellschaft fur physikalische chemie 78 (1974) 253-259.

[78] Kraiter, D. C., Zak, O., Aisen, P., and Crumbliss, A. L., Inorg. Chem. 37 (1998) 964-968.

[79] Riggs, A. F., and Wolbach, R. A., *Sulfhydryl groups and the structure of hemoglobin*, J. Gen. Physiol. 39 (1956) 585-605.

[80] Bonaventura, C., Henkens, R., De Jesus-Boniila, W., Lopez-Garriga, J., Jia, Y., Alayash, A. I., Parker Siburt, C. J., Crumbliss, A. L., submitted for publication (2010).

[81] Bonaventura, C., Henkens, R., Alayash, A. I., and Crumbliss, A. L., *Allosteric effects on oxidative and nitrosative reaction of cell-free hemoglobins*, IUBMB Life 59 (2007) 498-506.

[82] Roche, C. J., Guo, F., and Friedman, J. M., *Molecular level probing of prefential hydration and its modulation by osmolytes through the use of pyranine complexed to hemoglobin*, J. Biol. Chem. 281 (2006) 38757-38768.

[83] Parker Siburt, C. J., Lin, E. M., Brandt, S. J., Tinoco, A. D., Valentine, A. M., and Crumbliss, A. L., *Redox potentials of Ti(IV) and Fe(III) complexes provide insights into titanium biodistribution mechanisms*, J. Inorg. Biochem. Accepted for publication (2010) 10.1016/j.jinorgbio.2010.1004.1004.

[84] Andrews, N. C., N. Engl. J. Med. 341 (1999) 1986-1995.

[85] Garrick, M. D., and Garrick, L. M., *Cellular iron transport*, Biochim. Biophys. Acta 1790 (2009) 309-325.

[86] Aisen, P., Leibman, A., and Zweier, J., *Stoichiometric and Site Characteristics of the Binding of Iron to Human Transferrin*, The Journal of Biological Chemistry 253 (1978) 1930-1937.

[87] Aisen, P., Wessling-Resnick, M., and Leibold, E. A., *Iron metabolism*, Curr. Opin. Chem. Biol. 3 (1999) 200-206.

[88] Harris, W. R., *Estimation of the Ferrous-Transferrin Binding Constants Based on Thermodynamic Studies of Nickel(II)-Transferrin*, J. Inorg. Biochem. 27 (1986) 41-52.

[89] Wilkins, R. G. Kinetics and mechanism of reaction of transition metal complexes, 2nd ed., VCH Publishers, New York, 1991.

[90] Ohgami, R. S., Campagna, D. R., Greer, E. L., Antiochos, B., McDonald, A., Chen, J., Sharp, J. J., Fujiwara, Y., Barker, J. E., and Fleming, M. D., *Identification of a ferrireductase required for efficient transferrin-dependent iron uptake in erythroid cells*, Nat. Genet. 37 (2005) 1264-1269.

[91] McKie, A. T., *A ferrireductase fills the gap in the transferrin cycle*, Nature Genetics 37 (2005) 1159-1160.

[92] Li, H., Sun, H., and Qian, Z. M., *The role of the transferrin-transferrin-receptor system in drug delivery and targeting*, Trends Pharmacol. Sci. 23 (2002) 206-209.

[93] Guo, M., Sun, H., McArdle, H. J., Gambling, L., and Sadler, P. J., *Ti(IV) Uptake and Release by Human Serum Transferrin and Recognition of Ti(IV)-Transferrin by Cancer Cells: Understanding the Mechanism of Action of the Anticancer Drug Titanocene Dichloride*, Biochem. 39 (2000) 10023-10033.

[94] Sun, H., Cox, M. C., Li, H., and Sadler, P. J. in: Hill, H. A. O., Sadler, P. J., and Thomsom, A. J. (Eds.), Metal sites in proteins and models, Springer, Verlag, 1999, pp. 71-102.

[95] Tinoco, A. D., and Valentine, A. M., *Ti(IV) binds to Human Serum Transferrin More Tightly Than Does Fe(III)*, J. Am. Chem. Soc. 127 (2005) 11218-11219.

[96] Kefalas, E. T., Panagiotidis, P., Raptopoulou, C. P., Terzis, A., Mavromoustakos, T., and Salifoglou, A., *Mononuclear titanium(IV)-citrate complexes from aqueous solutions: pH-specific synthesis and structural and spectroscopic studies in relevance to aqueous titanium(IV)-citrate speciation*, Inorg. Chem. 44 (2005) 2596-2605.

[97] Sarmiento-Gonzalez, A., Encinar, J. R., Cantarero-Roldan, A., Marchante-Gayon, J. M., and Sanz-Medel, A., *HPLC-ICPMS and stable isotope-labeled approaches to assess quantitatively Ti(IV) uptade by transferrin in human blood serum*, Anal. Chem. 80 (2008) 8702-8711.

[98] Hallab, N. J., Skipor, A., and Jacobs, J. J., *Interfacial kinetics of titanium- and cobalt-based implant alloys in human serum: Metal release and biofilm formation*, J. Biomed. Mater. Res. 65A (2003) 311-318.

[99] Ishiwata, K., Ido, T., Monma, M., Murakami, M., Fukuda, H., Kameyama, M., Yamada, K., Endo, S., Yoshioka, S., Sato, T., and Matsuzawa, T., *Potential Radiopharmaceuticals Labeled with Titanium -45*, Appl. Radiat. Isot. 42 (1991) 707-712.

[100] Clarke, M. J., Zhu, F., and Frasca, D. R., *Non-Platinum Chemotherapeutic Metallopharmaceuticals*, Chem. Rev. 99 (1999) 2511-2533.

[101] Messori, L., Orioli, P., Banholzer, V., Pais, I., and Zatta, P., *Formation of titanium(IV) transferrin by reaction of human serum apotransferrin with titanium complexes*, FEBS Lett. 442 (1999) 157-161.

[102] Guo, M., Harvey, I., Campopiano, D. J., and Sadler, P. J., *Short Oxo-Titanium(IV) Bond in Bacterial Transferrin: A Protein Target for Metalloantibiotics*, Angew. Chem., Int. Ed. 45 (2006) 2758-2761.

[103] Guo, M., Guo, Z., and Sadler, P. J., *Titanium(IV) targets phosphoesters on nucleotides: implication for the mechanism of action of the anticancer drug titanocene dichloride*, J. Biol. Inorg. Chem. 6 (2001) 698-707.

[104] Guo, M., Sun, H., Bihari, S., Parkison, J. A., Gould, R. O., Parsons, S., and Sadler, P. J., *Stereoselective Formation of Seven-Coordinate Titanium(IV) Monomer and Dimer Complexes of Ethylenebis(o-hydroxyphenyl)glycine*, Inorg. Chem. 39 (2000) 206 -215.

[105] Tinoco, A. D., Eames, E. V., and Valentine, A. M., *Reconsideration of serum Ti(IV) transport: Albumin and transferrin trafficking of Ti(IV) and its complexes*, J. Am. Chem. Soc. 130 (2008) 2262-2270.

[106] Zhou, Z.-H., Deng, Y.-F., Jiang, Y.-Q., Wan, H.-L., and Ng, S.-W., *The first structural examples of tricitratotitanate [Ti(H2cit)3]2- dianions*, Dalton Trans. (2003) 3636-3638.

[107] Paradies, J., Crudaa, J., MacKay, F., Yellowless, L., Montgomery, J., Parsons, S., Oswald, I., Robertson, N., and Sadler, P. J., *Photogeneration of titanium(III) from titanium(IV) citrate in aqueous solution*, J. Inorg. Biochem. 100 (2006) 1260-1264.

[108] Steckhan, E., and Kuwana, T., *Spectroelectrochemical Study of Mediators I. Bipyridylium Salts and Thier Electron Transfer Rates to Cytochrome c.*, Ber. Bunsenges. Phys. Chem. 78 (1974) 253-259.

[109] Salmon, R. T., and Hawkridge, F. M., *The electrochemical properties of three dipryidinium salts as mediators*, J. Electroanal. Chem. 112 (1980) 253-264.

[110] Thorneley, R. N. F., *A Convenient electrochemical preparation of reduced methyl viologen and a kinetic study of the reaction with oxygen using an anaerobic stopped-flow apparatus.*, Biochim. Biophys. Acta 333 (1974) 487-496.

[111] Bird, C. L., and Kuhn, A. T., *Electrochemistry of the Viologens*, Chem. Soc. Rev. 10 (1981) 49-82.

[112] Farrington, J. A., *Bipyridylium Quaternary Salts and Related Compounds*, Journal of the Chemical Society Faraday Transactions, I 74 (1978) 665-675.

[113] Homer, R. F., and Tominson, T. E., *The Stereochemistry of the Bridged Quaternary Salts of 2,2'-Bipyridyl.*, J. Chem. Soc. (1960) 2498-2503.

[114] Thorneley, R. N. F., *A Convenient electrochemical preparation of reduced methyl viologen and a kinetic study of the reaction with oxygen using an anaerobic stopped-flow apparatus.*, Biochimica et Biophysica Acta 333 (1974) 487-496.

[115] Bond, J., and Jones, T. I., *Iron Chelates of Polyaminocarboxylic Acids*, Trans. Faraday Soc. 55 (1959) 1310-1318.

[116] Ogino, H., Nagata, T., and Ogino, K., *Redox potentials and related thermodynamic parameters of (Diamino polycarboxylato)metal(III/II) redox couples*, Inorg. Chem. 28 (1989) 3656-3659.

[117] Engelmann, M. D., Bobier, R. T., Hiatt, T., and Cheng, I. F., *Variability of the Fenton reaction characteristics of the EDTA, DTPA, and citrate complexes of iron*, BioMetals 16 (2003) 519-527.

[118] Seibig, S., and van Eldik, R., *Structural information on trans-1,2-diaminocyclohexane-N,N'-tetraacetateferrate(III) in the solid and aqueous phase*, Inorg. Chim. Acta 279 (1998) 37-43.

[119] Taylor, S. W., Luther III, G. W., and Waite, J. H., *Polargraphic and Spectrophotometric Investigation of Iron(III) Complexation to 3,4-Dihydroxyphenylalanine-Containing Peptides and Proteins from Mytilus edulis*, Inorg. Chem. 33 (1994) 5819-5824.

[120] Pecsok, R. L., and Maverick, E. F., *A Polarographic Study of the Titanium-Ethylenediaminetetraacetate Complexes*, J. Am. Chem. Soc. 76 (1954) 358-362.

[121] Tinoco, A. D., Incarvito, C. D., and Valentine, A. M., *Calorimetric, Spectroscopic, and Model Studies Provide New Insight into the Transport of Ti(IV) by Human Serum Transferrin*, J. Am. Chem. Soc. 129 (2007) 3445-3454.

[122] Uppal, R., Incarvito, C. D., Lakshmi, K. V., and Valentine, A. M., *Aqueous Spectrocopy and Redox Properties of Carboxylate-Bound Titanium*, Inorg. Chem. 45 (2006) 1795-1804.

[123] Susic, M. V., and Dojcinovic, M. M., *Electrochemical behaviour of Ti(IV) in presence of EGTA and CyDTA*, Glasnik Hemijskog Drustva Beograd 41 (1976) 359-369.

[124] Kaneko, H., and Kaneko, K., *Polargraphic determination of titanium. II. Polargraphic determination of titanium in nickel, copper, and iron-chromium-alunminum alloys using CyDTA.*, Bunseki kagaku 18 (1969) 1494-1497.

[125] Susic, M. V., and Ghonaim, A. K., *Polargraphic behaviour of titanium IV in the presence of diethylenetriaminepentaacetic acid, (DTPA)*, Glasnik Hemijskog Drustva Beograd 34 (1969) 481-487.

[126] Bartusek, M., Coll. Czech. Chem. Comm. 32 (1967) 757.

[127] Zemcikova, M., and Sommer, L., Spisy. Prir. Fak. Univ. Purk. Brne. E37 (1969) 199.

[128] Sever, M. J., and Wilker, J. J., *Visible absorption spectra of metal-catecholate and metal-tironate complexes*, Dalton Trans. (2004) 1061-1072.

[129] Manku, G. S., *2,3-Dihydroxynaphthalene as indicator for complexometric titration of iron(III) with EDTA*, Fresenius J. Anal. Chem. 263 (1973) 335-335.

[130] Garrett, T. M., Miller, P. W., and Raymond, K. N., *2,3-Dihydroxyterephthalamides: Highly efficient iron(III)-chelating agents*, Inorg. Chem. 28 (1989) 128-133.

[131] Larson, S. K., Jenkins, B. G., Memon, N. G., and Lauffer, R. B., *Structure-Affinity Relationships in the Binding of Unsubstituted Iron Phenolate Complexes to Human Serum Albumin. Molecular Structre of Iron(III) N,N'-Bis(2-hydroxybenzyl)ethylemediamine-N,N'-diacetate*, Inorg. Chem. 29 (1990) 1147-1152.

[132] L'Eplattenier, F., Murase, I., and Martell, A. E., *New multidentate ligands. VI. Chelating tendencies of N,N'-Di(2-hydroxybenzyl)ethylenediamine-N,N'-diacetic acid*, J. Am. Chem. Soc. 89 (1967) 837-843.

[133] Kaneko, H., and Ozawa, T., *Polargraphic catalytic waves of titanium(IV) chelates of EDTA and related compounds*, Bull. Chem. Soc. Jpn. 45 (1972) 140-145.

[134] Uppal, R., Israel, H., Incarvito, C. D., and Valentine, A. M., *Titanium(IV) complexes with N,N'-dialkyl-2,3,-dihydroxyterepthalamides and 1-hydroxy-2(IH)-pyridinone as siderophore and tunichrome analogues*, Inorg. Chem. 48 (2009) 10769-10779.

[135] Lind, M. D., and Hoard, J. L., *Stereochemistry of ethylenediaminetetraacetato complexes. II. The structure of crystalline Rb[Fe(OH$_2$)YH$_2$O$^{1-3}$*, Inorg. Chem. 3 (1964) 34-43.

[136] Fackler, J. P., Kristine, F. J., Mazany, A. M., Moyer, T. J., and Shepherd, R. E., *The Absence of a Titanyl Oxygen in the Ti(IV)-edta4- Complex: [Ti(edta)(H2O)*, Inorg. Chem. 24 (1985) 1857-1860.

[137] Collins, J. M., Uppal, R., Incarvito, C. D., and Valentine, A. M., *Titanium(IV) Citrate Speciation and Structure under Environmentally and Biologically Relevant Conditions*, Inorg. Chem. 44 (2005) 3431-3440.

[138] Ma, R., Motekaitis, R. J., and Martell, A. E., *Stability of metal ion complexes of N,N'-bis(2-hydroxybenzyl)ethylenediamine-N,N'-diacetic acid*, Inorg. Chemica Acta 224 (1994) 151-155.

[139] Tinoco, A. D., Eames, E. V., Incarvito, C. D., and Valentine, A. M., *Hydrolytic metal with a hydrophobic periphery: Titanium(IV) complexes of naphthalene-2,3-diolate and interactions with serum albumin*, Inorg. Chem. 47 (2008) 8380-8390.

[140] Bauer, I., and Kappler, A., *Rates and extent of reduction of Fe(III) compounds and O2 by humic substances*, Environ. Sci. Technol. 43 (2009) 4902-4908.

[141] Field, T. B., McCourt, J. L., and McBryde, A. E., *Composition and stability of iron and copper citrate complexes in aqueous solution*, Can. J. Chem. 52 (1974) 3119-3124.

[142] Cox, J., and Cummings, T. E., *A cyclic voltammetric investigation of the iron(III)/(II) coupld in citrate and phosphate media*, J. Electroanal. Chem. Interfacial Electrochem. 42 (1973) 153-157.

[143] Stulikova, M., and Vydra, F., *Voltammetry with disk electrodes and its analytical application V. The voltammetry of iron(III) at the glassy carbon disk electrode in complexing media*, J. Electroanal. Chem. Interfacial Electrochem. 39 (1972) 229-231.

[144] Silva, A. M. N., Kong, X., Parkin, M. C., Cammack, R., and Hider, R. C., *Iron(III) citrate speciation in aqueous solution*, Dalton Trans. (2009) 8616-8625.

[145] Pierre, J. L., and Gautier-Luneau, I., *Iron and citric acid: A fuzzy chemistry of ubiquitous biological relevance*, BioMetals 13 (2000) 91-96.

[146] Homer, R. F., and Tominson, T. E., *The Stereochemistry of the Bridged Quaternary Salts of 2,2'-Bipyridyl.*, Journal of the Chemical Society (1960) 2498-2503.

[147] Parker Siburt, C. J., Roulhac, P. L., Weaver, K. D., Noto, J. L. M., Mietzner, T. A., Cornelissen, C. N., Fitzgerald, M. C., and Crumbliss, A. L., *Hijacking transferrin bound iron: protein-receptor interactions involved in iron transport in N. gonorrhoeae*, Metallomics 1 (2009) 249-255.

[148] Cornelissen, C. N., Biswas, G. D., Tsai, J., Paruchuri, D. K., Thompson, S. A., and Sparling, P. F., *Gonococcal transferrin-binding protein 1 is required for transferrin utilization and is homologous to TonB-dependent outer membrane receptors*, J. Bacteriol. 174 (1992) 5788-5797.

[149] Anderson, J. E., Sparling, P. F., and Cornelissen, C. N., *Gonococcal transferrin-binding protein 2 facilitates but is not essential for transferrin utilization.*, J. Bacteriol. 176 (1994) 3126-3170.

[150] Cornelissen, C. N., and Sparling, P. F., *Binding and surface exposure characteristics of the gonococcal transferrin receptor are dependent on both transferrin-binding proteins*, J. Bacteriol. 178 (1996) 1437-1444.

[151] Bruns, C. M., Nowalk, A. J., Arvai, A. S., McTigue, M. A., Vaughan, K. G., Meitzner, T. A., and McRee, D. E., *Structure of Haemophilus influenzae Fe^{3+} binding protein reveals convergent evolution within a suprefamily*, Nat. Struc. Biol. 4 (1997) 919-924.

[152] Mietzner, T. A., Tencza, S. B., Adhikari, P., Vaughan, K. G., and Nowalk, A. J. in: Vogt, P. K., and Maham, M. J. (Eds.), Current Topic in Microbiology and Immunology, Vol. 225 Bacterial Infection: Close Encounters at the Host Pathogen Interface, Springer - Verlag Berlin Heidelberg, Germany, 1998.

[153] Roulhac, P. L., Weaver, K. D., Adhikari, P., Anderson, D. S., DeArmond, P. D., Mietzner, T. A., Crumbliss, A. L., and Fitzgerald, M. C., *Ex vivo analysis of synergistic anion binding to FbpA in Gram-negative bacteria*, Biochem. 47 (2008) 4298-4305.

[154] Bruns, C. M., Anderson, D. S., Vaughan, K. G., Williams, P. A., Nowalk, A. J., McRee, D. E., and Mietzner, T. A., *Crystallographic and biochemical analyses of the metal-free Haemophilus influenzae Fe^{3+}-binding protein.*, Biochem. 40 (2001) 15631-15637.

[155] Guo, M., Harvey, I., Yang, W., Coghill, L., Campopiano, D. J., Parkinson, J. A., MacGillivary, R. T. A., Harris, W. R., and Sadler, P. J., *Synergisitic anion and metal binding to the ferric ion-binding protein from Neisseria gonorrhoeae*, J. Biol. Chem. 278 (2003) 2490-2502.

[156] Brickman, T. J., Anderson, M. T., and Armstrong, S. K., *Bordetella iron transport and virulence.*, Biometals 20 (2007) 303-320.

[157] Perkins-Balding, D., Ratliff-Griffin, M., and Stojiljkovic, I., *Iron transport systems in Neisseria meningitidis*, Microbiol. Mol. Biol. Rev. 68 (2004) 154-171.

[158] Wyckoff, E. E., Mey, A. R., and Payne, S. M., *Iron acquisition in Vibrio cholerae*, Biometals 20 (2007) 405-416.

[159] Krewulak, K. D., and Vogel, H. J., *Structural biology of bacterial iron uptake*, Biochim. Biophys. Acta 1778 (2008) 1781-1804.

[160] Boulton, I. C., Gorringe, A. R., Gorinsky, B., Retzner, M. D., Schryvers, A. B., Joannou, C. L., and Evans, R. W., *Purified meningococcal transferrin-binding protein B interacts with a secondary, strain-specific, binding site in the N-terminal lobe of human transferrin*, Biochem. J. 339 (1999) 143-149.

[161] Khan, A. G., Shouldice, S. R., Kirby, S. D., Yu, R.-h., Tari, L. W., and Schryvers, A. B., *High affinity binding by the periplasmic iron binding protein from Haemophilus influenzae is required for acquiring iron from transferrin*, Biochem. J. 404 (2007) 217-225.

[162] Krell, T., Renauld-Mongenie, G., Nicolai, M.-C., Fraysse, S., Chevalier, M., Berard, Y., Oakhill, J. S., Evans, R. W., Gorringe, A., and Lissolo, L., *Insight into the structure and function of the transferrin receptor from Niesseria memingitidis using microcalorimetric techniques*, J. Biol. Chem. 278 (2003) 14712-14722.

[163] Oakhill, J. S., Joannou, C. L., Buchanan, S. K., Gorringe, A., and Evans, R. W., *Expression and purification of functional recombinant meningococcal transferrin-binding protein A*, Biochem. J. 364 (2002) 613-616.

[164] Ekins, A., Khan, A. G., Shouldice, S. R., and Schryvers, A. B., *Lactoferrin receptors in Gram-negative bacteria: Insights into the iron acquisition process*, BioMetals 17 (2004) 235-243.

[165] Letoffe, S., Wecker, K., Delepelaire, M., Delepelaire, P., and Wandersman, C., *Activities of the Serratia marcescens heme receptor HasR and isolated plug and β-barrel domains: the β-barrel forms a heme-specific channel*, J. Bacter. 187 (2005) 4637-4645.

[166] Buchanan, S. K., Smith, B. S., Venkatramani, L., Xia, D., Esser, L., Palnitka, M., Chakraborty, R., van der Helm, D., and Deisenhofer, J., *Crystal structure of the outer membrane active transporter FepA from Escheria coli*, Nat. Struc. Biol. 6 (1999) 56-63.

[167] Ferguson, A. D., Charkraborty, R., Smith, B. S., Esser, L., van der Helm, D., and Deisenhofer, J., *Structural basis of gating by the outer membrane transporter FecA*, Science 295 (2002) 1715-1719.

[168] Locher, K. P., Rees, B., Koebnik, R., Mitschler, A., Moulinier, L., Rosenbusch, J. P., and Moras, D., *Transmembrane signaling across the ligand-gated FhuA receptor: Crystal structures of free and ferrichrome-bound states reveal allosteric changes*, Cell 95 (1998) 771-778.

[169] Wandersman, C., and Delepelaire, P., *Bacterial iron sources: from siderophores to hemophores*, Annu. Rev. Microbiol. 58 (2004) 611-647.

[170] Moeck, G. S., and Coulton, J. W., *TonB-dependent iron acquisition: mechanisms of siderophore-mediated active transport*, Molecular Microbiology 28 (1998) 675-681.

[171] Brillet, K., Journett, L., Celia, H., Paulus, L., Stahl, A., Pattus, F., and Cobessi, D., *A β-strand lock-exchange for signal transduction in TonB-dependent transducers on the basis of a common structural motif*, Structure 15 (2007) 1383-1391.

[172] Devanathan, S., and Postle, K., *Studies on colicin B translocation: FepA is gated by TonB*, Mol. Microbiol. 65 (2007) 441-453.

[173] Schalk, I. J., Kyslik, P., Prome, D., van Dorsselaer, A., Poole, K., Abdallah, M. A., and Pattus, F., *Copurification of the FpvA Ferric Pyoverdine Receptor of Pseudomonas aeruginosa with Its Iron-Free Ligand: Implications for Siderophore-Mediated Iron Transport*, Biochem. 38 (1999) 9357-9365.

[174] Ferguson, A. D., and Deisenhofer, J., *TonB-dependent receptors - structural perspectives*, Biochim. Biophys. Acta 1565 (2002) 318-332.

[175] Cornelissen, C. N., and Sparling, P. F., *Iron piracy: acquisition of transferrin-bound iron by bacterial pathogens*, Mol. Microbiol. 14 (1994) 843-850.

[176] Boulton, I. C., Yost, M. K., Anderson, J. E., and Cornelissen, C. N., *Identification of discrete domains withitn gonococcal transferrin-binding protein A that are necessary for ligand binding and iron uptake functions*, Infect. Immun. 68 (2000) 6988-6996.

[177] Gumbart, J., Wiener, M. C., and Tajkhorshid, E., *Mechanics of force propagation in TonB-dependent outer membrane transport*, Biophys. J. 93 (2007) 496-504.

[178] Yost-Daljev, M. K., and Cornelissen, C. N., *Determination of surface-exposed, functional domains of gonococcal transferrin-binding protein A*, Infect. Immun. 72 (2004) 1774-1785.

[179] DeRocco, A. J., and Cornelissen, C. N., *Identification of Transferrin-Binding Domains in TbpB Expressed by Neisseria gonorrhoeae*, Infection and Immunity 75 (2007) 3220-3232.

[180] Braun, V., *Energy Transfer between Biological Membranes*, ACS Chem. Biol. 1 (2006) 352-354.

[181] Postle, K., and Larsen, R. A., *TonB-dependent energy transduction between outer and cytoplasmic membranes*, Biometals 20 (2007) 453-465.

[182] Shultis, D. D., Purdy, M. D., Banchs, C. N., and Wiener, M. C., *Outer membrane active transport: structure of the BtuB: TonB complex*, Science 312 (2006) 1396-1399.

[183] Kenney, C. D., and Cornelissen, C. N., *Demonstration and characterization of a specific interaction between gonococcal transferrin binding protein A and TonB*, J. Bacteriol. 184 (2002) 6138-6145.

[184] Cornelissen, C. N., Anderson, J. E., and Sparling, P. F., *Energy-dependent changes in the gonococcal transferrin receptor*, Mol. Microbiol. 26 (1997) 25-36.

[185] DeRocco, A. J., Yost-Daljev, M. K., Kenney, C. D., and Cornelissen, C. N., *Kinetic Analysis of Ligand Interaction with the Gonococcal Transferrin-Iron Acquisition System*, Biometals 22 (2009) 439-451.

[186] Mietzner, T. A., Bolan, G., Schoolnik, G. K., and Morse, S. A., *Purification and characterization of the major iron-regulated protein expressed by pathogenic Neisseriae*, J. Exp. Med. 165 (1987) 1041-1057.

[187] Chen, C.-Y., Berish, S. A., Morse, S. A., and Mietzner, T. A., *The ferric iron-binding protein of pathogenic Neisseria spp. functions as a periplasmic transport protein in iron acquisition from human transferrin*, Mol. Microbiol. 10 (1993) 311-318.

[188] Davidson, A. L., and Chen, J., *ATP-Binding Cassette Transporters in Bacteria*, Annu. Rev. Biochem. 73 (2004) 241-268.

[189] Jones, P. M., and George, A. M., *The ABC transporter structure and mechanism: perspectives on recent research*, Cell. Mol. Life Sci. 61 (2004) 682-699.

[190] McRee, D. E., Bruns, C. M., Williams, P. A., Mietzner, T. A., and Nunn, R., *Neisseria gonorrhoeae ferric binding protein*, PDB ID9Y (1999).

[191] Roulhac, P. L., Powell, K. D., Dhungana, S., Weaver, K. D., Mietzner, T. A., Crumbliss, A. L., and Fitzgerald, M. C., *SUPREX (Stability of Unpurified Proteins from Rates of H/D Exchange) analysis of the thermodynamics of synergistic anion binding by ferric-binding protein (FbpA), a bacterial transferrin*, Biochem. 43 (2004) 15767-15774.

[192] Heymann, J. J., Weaver, K. D., Mietzner, T. A., and Crumbliss, A. L., *Sulfate as a Synergistic Anion Facilitating Iron Binding by the Bacterial Transferrin FbpA: The Origins and Effects of Anion Promiscuity*, J. Am. Chem. Soc. (2007).

[193] Taboy, C. H., Vaughan, K. G., Mietzner, T. A., Aisen, P., and Crumbliss, A. L., *Fe^{3+} coordination and redox properties of a bacterial transferrin*, J. Biol. Chem. 276 (2001) 2719-2724.

[194] Heymann, J. J., Gabricevic, M., Mietzner, T. A., and Crumbliss, A. L., *Kinetics and mechanism of exogenous anion exchange in FeFpbA-NTA: significance of periplasmic anion lability and anion binding activity of ferric binding protein A*, J. Biol. Inorg. Chem. 15 (2010) 237-248.

[195] Gabricevic, M., Anderson, D. S., Mietzner, T. A., and Crumbliss, A. L., *Kinetics and Mechanism of Iron(III) Complexation by Ferric Binding Protein: The Role of Phosphate.*, Biochemistry 43 (2004) 5811-5819.

[196] Boukhalfa, H., Anderson, D. S., Mietzner, T. A., and Crumbliss, A. L., *Kinetics and mechanism of iron release from the bacterial ferric binding protein nFbp: exogenous anion influence and comparison with mammalian transferrin*, J. Biol. Inorg. Chem. 8 (2003) 881-892.

[197] Dhungana, S., Anderson, D. S., Mietzner, T. A., and Crumbliss, A. L., *Kinetics of Iron Release from Ferric Binding Protein (FbpA): Mechanistic Implications in Bacterial Periplasm-to-Cytosol Fe^{3+} Transport*, Biochemistry 44 (2005) 9606-9618.

[198] MacGillivary, R. T. A., Moore, S., A., Chen, J., Anderson, B., Baker, H., Luo, Y., Bewley, M., Smith, C. A., Murphy, M. E. P., Wang, Y., Mason, A. B., Woodworth, R. C., Brayer, G. D., and Baker, E. N., *Two high-resolution crystal structures of the recombinant N-lobe of human transferrin reveal a structural change implicated in iron release*, Biochem. 37 (1998) 7919-7928.

[199] Kretchmar Nguyen, S. A., Craig, A., and Raymond, K. N., *Transferrin: The Role of Conformational Changes in Iron Removal by Chelators*, J. Am. Chem. Soc. 115 (1993) 6758-6764.

[200] Halbrooks, P. J., He, Q.-Y., Briggs, S. K., Everse, S. J., Smith, V. C., MacGillivary, R. T. A., and Mason, A. B., *Investigation of the Mechanism of Iron Release from the C-Lobe of Human Serum Transferrin: Mutational Analysis of the Role of a pH Sensitive Triad*, Biochemistry 42 (2003) 3701-3707.

[201] Mason, A. B., He, Q.-Y., Halbrooks, P. J., Everse, S. J., Gumerov, D. R., Kaltashov, I. A., Smith, V. C., Hewitt, J., and MacGillivary, R. T. A., *Differential effect of a his tap at the N- and C-termini: functional studies with recombinant human serum transferrin*, Biochem. 41 (2002) 9448-9454.

[202] Mietzner, T. A., and Morse, S. A. (1985) Iron-regulated membrane proteins of *Neisseria gonorrhoeae*: purification and partial characterization of a 37,000-dalton protein, in *Pathog. Neisseriae. Proc. Int. Symp., 4th*, Washington, D. C.

[203] Boulton, I. C., Gorringe, A. R., Carr, R. J. G., Gorinsky, B., Joannou, C. L., and Evans, R. W., *Characterization of the meningococcal transferrin binding protein complex by photon correlation spectroscopy*, FEBS 414 (1997) 409-413.

[204] Powell, N. B. L., Bishop, K., Palmer, H. M., Ala'aldeen, D. A., Gorringe, A. R., and Borriello, S. P., *Differential binding of apo and holo human transferrin to meningococci and co-localization of the transferrin-binding proteins (TbpA and TbpB)*, J. Med. Microbiol. 47 (1998) 257-264.

[205] Ronpirin, C., Jerse, A. E., and Cornelissen, C. N., *Gonococcal genes encoding transferrin-binding proteins A and B are arranged in a bicistronic operon but are subject to differential expression*, Infect. Immun. 69 (2001) 6336-6347.

[206] Boulton, I. C., Gorringe, A. R., Shergill, J. K., Joannou, C. L., and Evans, R. W., *A dynamic model of the meningococcal transferrin receptor*, J. Thero. Biol. 198 (1999) 497-505.

[207] Weaver, K. D., Heymann, J. J., Mehta, A., Roulhac, P. L., Anderson, D. S., Nowalk, A. J., Adhikari, P., Meitzner, T. A., Fitzgerald, M. C., and Crumbliss, A. L., *Ga^{3+} as a mechanistic probe in Fe^{3+} transport: Characterization of Ga^{3+} interaction with FbpA*, J. Biol. Inorg. Chem. 13 (2008) 887-898.

[208] Roulhac, P. L., Fitzgerald, M. C., Doctoral Dissertation, Department of Chemistry, Duke University, 2007.

[209] Cornelissen, C. N., Anderson, J. E., Boulton, I. C., and Sparling, P. F., *Antigenic and sequence diversity in gonococcal transferrin-binding protein A*, Infect. Immun. 68 (2000) 4725-4735.

[210] Cornelissen, C. N., Anderson, J. E., and Sparling, P. F., *Characterization of the diversity and the transferrin-binding domain of gonococcal transferrin-binding protein 2*, Infect. Immun. 65 (1997) 822-828.

[211] Gomez, J. A., Criado, M. T., and Ferreiros, C., *Cooperation between the components of the meningococcal transferrin receptor, TbpA and TbpB, in the uptake of transferrin iron by the 37-kDa ferric-binding protein (FbpA)*, Res. Microbiol. 149 (1998) 381-387.

[212] Irwin, S. W., Averil, N., Cheng, C. Y., and Schryvers, A. B., *Preparation and analysis of isogenic mutants in the transferrin receptor protein genes, tbpA and tbpB, from Neisseria meningitidis*, Mol. Microbiol. 8 (1993) 1125-1133.

[213] Cornelissen, C. N., Kelley, M., Hobbs, M. M., Anderson, J. E., Cannon, J. G., Cohen, M. S., and Sparling, P. F., *The transferrin receptor expressed by gonococcal strain FA1090 is required for the experimental infection of human male volunteers*, Mol. Microbiol. 27 (1998) 611-616.

[214] Noto, J. M., and Cornelissen, C. N., *Identification of TbpA residues required for transferrin-iron utilization by Neisseria gonorrhoeae*, Infect. Immun. 76 (2008) 1960-1969.

[215] Renauld-Mongenie, G., Latour, M., Poncet, D., Naville, S., and Quentin-Millet, M.-J., *Both the full-length and the N-terminal domain of the meningococcal transferrin-binding protein B discriminate between human iron-loaded and apo-transferrin*, FEMS 169 (1998) 171-177.

[216] Boulton, I. C., Gorringe, A. R., Allison, N., Robinson, A., Gorinsky, B., Joannou, C. L., and Evans, R. W., *Transferrin-binding protein B isolated from Neisseria meningitidis discriminates between apo and diferric human transferrin*, Biochem. J. 334 (1998) 269-273.

[217] Retzer, M. D., Yu, R.-H., Zhang, Y., Gonzalez, G. C., and Schryvers, A. B., *Discrimination between apo and iron-loaded forms of transferrin by transferrin binding protein B and its N-terminal subfragment*, Microb. Path. 25 (1998) 175-180.

[218] Braun, M., Endriss, F., and Killmann, H., *In vivo reconstruction of the FhuA transporter protein of Escherichia coli K-12.*, J. Bacter. 185 (2003) 5508-5518.

[219] Ma, L., Kaserer, W., Annamalai, R., Scott, D. C., Jin, B., and Jiang, X., *Evidence of ball-and-chain transport of ferric enterobactin through FepA.*, J. Biol. Chem. 282 (2007) 397-406.

[220] Usher, K. C., Ozkan, E., Gardner, K. H., and Deisenhofer, J., *The plug domain of FepA, a TonB-dependent transport protein from Escherichia coli, blinds its siderophore in the absence of the transmembrane barrel domain*, PNAS 98 (2001) 10676-10681.

[221] Peacock, R. S., Andrushchenko, V. V., Demcoe, A. R., Gehmlich, M., Lu, L. S., Herrero, A. G., and Vogel, H. J., *Characterization of TonB interactions with the FepA cork domain and FecA N-terminal signaling domain.*, BioMetals 19 (2006) 127-142.

[222] Ozutsumi, K., Uchima, Y., and Kawashima, T., *Structure of iron(III)-tiron complexes in aqueous solution*, Analytical Sciences 6 (1990) 573-577.

[223] Elhabiri, M., Carrer, C., Marmolle, F., and Traboulsi, H., *Complexation of iron(III) by catecholate-type polyphenols*, Inorganica Chemica Acta 360 (2007) 353-359.

[224] McBryde, W. A. E., *A spectrophotometric reexamination of the spectra and stabilities of the iron (III) - tiron complexes*, Can. J. Chem. 42 (1964) 1917-1927.

[225] Cornelissen, C. N., personal communication with Crumbliss, A. L.

[226] Martell, A. E., and Smith Critical Stability Constant Database NIST, Gaithersburg, MD, 2001.

[227] Carrano, C. J., and Raymond, K. N., *Ferric Ion Sequestering Agents. 2. Kinetics and Mechanism of Iron Removal from Transferrin by Enterobactin and Synthetic Tricatechols*, J. Am. Chem. Soc. 101 (1979) 5401-5404

Biography

The author was born Claire Jarvis Parker on February 28, 1982 in Danville, KY. She grew up near Blacksburg, VA and in Asheville, NC. She attended Virginia Polytechnic Institute and State University and graduated with a B.S. in Biochemistry in 2004. In 2004, fellow Hokie, Michael T. Siburt and the author married and began their life together in the NC.

As a graduate student at Duke University, the author has been involved in many teaching and service activities. In collaboration with Dr. Richard MacPhail, the author designed and implemented a new approach to *General Chemistry* recitation. In collaboration with Sarah Crider, Graham West, and Esther Tristani, the author development and taught a freshman seminar course named *Digging Up Chemistry: The Chemistry of Art and Archeology*. Additionally, the author served as a teaching assistant for several courses including *Advanced General Chemistry* and *Analytical Chemistry*. In 2009, the author was honored for these efforts with the Duke University Graduate School Award for Excellence in Teaching.

The author was also very involved in the university community and the community at large during her five years at Duke. Serving as the Graduate and Professional Student Council's representative to the University Scheduling Committee, the author helped ensure that no classes are held on the Fourth of July and Memorial Day. As well, the author was an active participant in Preparing Future Faculty, the

Structural Biochemistry and Biophysics Program, Phi Lambda Upsilon, the Chemistry Department Demo Team, and the American Chemical Society. Finally, the author continues to serve as a regular volunteer at Craig Springs Camp and Retreat Center.

HONORS AND AWARDS

Graduate School Dean's Award for Excellence in Teaching, Duke University	2009
C. R. Hauser Research Fellowship, Chemistry Department, Duke University	2009
Departmental Recognition Award, Chemistry Department, Duke University	2009
Duke University Graduate School Travel Grant, Duke University	2009
Division of Inorganic Chemistry Travel Grant, American Chemical Society	2008
Phi Lambda Upsilon Travel Grant, PLU Duke University Chapter	2008
Duke University Graduate School Travel Grant, Duke University	2008
Pelham Wilder Teaching Award, Chemistry Department, Duke University	2007-8
John Herbert Pearson Teaching Award, Chemistry Department, Duke University	2008

PUBLICATIONS

Parker Siburt, C. J., Lin, E. M., Brandt, S. J., Tinoco, A. D., Valentine, A. M., and Crumbliss, A. L., *Redox potentials of Ti(IV) and Fe(III) complexes provide insights into titanium biodistribution mechanisms*, J. Inorg. Biochem. Accepted for publication (2010) 10.1016/j.jinorgbio.2010.1004.1004.

"Hijacking transferrin bound iron: protein-receptor interactions essential for iron transport in N. gonorrhoeae", C. J. Parker Siburt, P. L. Roulhac, K. D. Weaver, J. M. Noto, T. A. Mietzner, C. N. Cornelissen, M. C. Fitzgerald, and A. L. Crumbliss, Metallomics, 2009, 1, 249 (Featured on cover)

"Comparative studies of clam and human hemoglobins highlight the importance of heme accessibility in reactions with nitrite", C. Bonaventura, R. Henkens, W. De Jesus-Bonilla, J. Lopez-Garriga, Y. Jia, A. I. Alayash, C. J. Parker Siburt, and A. L. Crumbliss, submitted 2009

RESEARCH PRESENTATIONS

"Hijacking transferrin-bound iron: protein-receptor interactions involved in iron transport in pathogenic N. gonorrhoeae", C. J. Parker Siburt and A. L. Crumbliss, SBB Seminar Series, Duke University, Durham, NC, November 2009

"Redox potentials of Ti(IV) and Fe(III) complexes provide insights into titanium biodistribution mechanisms", C. J. Parker Siburt, E. M. Lin, S. J. Brandt, A. D. Tinoco, A. M. Valentine, and A. L. Crumbliss, 61st Southeastern Regional Meeting of the American Chemical Society, San Juan, Puerto Rico, October 2009

"Using SUPREX to investigate iron transport in N. gonorrhoeae", C. J. Parker Siburt, J. J. Heymann, K. D. Weaver, P. L. Roulhac, M. C. Fitzgerald, T. A. Mietzner, and A. L. Crumbliss, NC ACS Local Section Meeting, Research Triangle Park, NC, September 2009

"Spectroelectrochemical analysis confirms that steric hindrance dictates the extreme rates of nitrite-induced oxidation of the functionally distinct hemoglobins from Lucina pectinata", C. J. Parker Siburt, C. Bonaventura, A. I. Alayash, and A. L. Crumbliss, 238th ACS National Meeting, Washington, DC, August 2009

"Hijacking transferrin-bound iron: iron transport from outside the cell to the periplasm of pathogenic N. gonorrhoeae", C. J. Parker Siburt and A. L. Crumbliss, Gordon Research Conference on Bioinorganic Chemistry, Ventura, CA, January 2009

"Using SUPREX to investigate iron transport in N. gonorrhoeae", C. J. Parker Siburt, J. J. Heymann, K. D. Weaver, P. L. Roulhac, M. C. Fitzgerald, T. A. Mietzner, and A. L. Crumbliss, Gordon Research Conference on Bioinorganic Chemistry Biometals Poster Session, Ventura, CA, January 2009

"Clams, carp, and chemistry: protein structure-function relationships from the metal's perspective", C. J. Parker Siburt, A. L. Crumbliss, C. Bonaventura, SBB Seminar Series, Duke University, Durham, NC, November 2008

"Iron transport across the periplasm in Neisseria", A. L. Crumbliss, K. D. Weaver, J. J. Heymann, C. J. Parker Siburt, and T. A. Mietzner, 236th ACS National Meeting, Philadelphia, PA, August 2008

"Ferric binding protein: moving iron and anions across the periplasm", A. L. Crumbliss, J. J. Heymann, K. D. Weaver, C. J. Parker Siburt, P. L. Roulhac, P. D. DeArmond, M. C. Fitzgerald, J. M. Noto, C. N. Cornelissen, D. S. Anderson, and T. A. Mietzner, Biometals, Spain, July 2008

"Origin of the root effect in fish Hbs: moderate proton-dependence of redox potentials suggests steric hindrance dominance", C. J. Parker Siburt, C. Bonaventura, and A. L. Crumbliss, 235th ACS National Meeting, New Orleans, LA, April 2008

"A computational model for metal ion speciation in multiple component systems applied to gallium sequestration by a bacterial transferrin", A. Mehta, C. J. Parker Siburt, J. J. Heymann, K. D. Weaver, and A. L. Crumbliss, Beckman Scholars Poster Session, 235th National ACS Conference, New Orleans, LA, April 2008

"Bioinorganic investigation of transferrin mediated titanium ion transport", C. J. Parker Siburt and A. L. Crumbliss, 121st NC-ACS Sectional Conference, Durham, NC, April 2007

"Inorganic biochemistry of iron proteins", J. J. Heymann, C. J. Parker Siburt, K. D. Weaver, and A. L. Crumbliss, East Coast Iron Club Meeting, Winston-Salem, NC, November 2006

TEACHING PRESENTATIONS

"Chemistry, art, and archaeology: an engaging combination for a vibrant and relevant seminar", E. M. Tristani, C. J. Parker Siburt, G. M. West, and S. E. Crider, General Chemical Education Poster Session, 238th ACS National Meeting, Washington, DC, August 2009

"Digging up chemistry: chemistry of art and archeology", C. J. Parker Siburt, S. Crider, G. West, E. Tristani, and J. Bonk, ChemEd 2009, Radford, VA, August 2009

"An instructor, a graduate student, and an undergraduate", C. J. Parker Siburt, M. Siegel, and K. Lyle, Generation Symposium, ChemEd 2009, Radford, VA, August 2009

"Chemistry, art, and archeology: an engaging combination for a vibrant and relevant seminar", C. J. Parker Siburt, S. Crider, G. West, E. Tristani, and J. Bonk, Lilly Conference on College and University Teaching Poster Session, Greensboro, NC, February 2009

"Manipulating problems: a tool to connect with students", C. J. Parker Siburt, invited Tutor Inservice Workshop for the Peer Tutoring Program at Duke University, Durham, NC, February 2009

"Manipulating problems in the General Chemistry classroom: A metacognitive approach", C. J. Parker Siburt, A. N. Bissell, and R. MacPhail, Second Annual Round Table Conference on Learning Services at Highly Selective Colleges/Universities, presentation invited by Donna Hall, Director of Academic Resource Center of Duke University, Durham, NC, November 2008

“Teaching IDEAS: TA Survival Skills”, C. J. Parker Siburt, panel member invited by Dr. Doug James, Assistant Dean for Academic Affairs, Teaching IDEAS Workshop Series, Graduate School of Duke University, Durham, NC, September 2008

"Manipulating problems in the General Chemistry classroom: a metacognitive approach", C. J. Parker Siburt, A. N. Bissell, and R. MacPhail, 20th Biennial Conference on Chemical Education, Bloomington, IN, July 2008

“Chemical Demonstrations”, C. J. Parker Siburt, A. Kasper, and K. Lyle, Generation Symposium, 20th Biennial Conference on Chemical Education, Bloomington, IN, July 2008